ISBN 978-82-326-1786-9 (printed version)
ISBN 978-82-326-1787-6 (electronic version)
ISSN 1503-8181

Doctoral theses at NTNU, 2016:224

Wei Chai

Stochastic dynamic analysis and reliability evaluation of the roll motion for ships in random seas

NTNU
Norwegian University of
Science and Technology
Faculty of Engineering
Science and Technology
Department of MarineTechnology

NTNU
Norwegian University of
Science and Technology

Doctoral theses at NTNU, 2016:224

NTNU

NTNU
Norwegian University of
Science and Technology

Wei Chai

Stochastic dynamic analysis and reliability evaluation of the roll motion for ships in random seas

Thesis for the degree of Philosophiae Doctor

Trondheim, August 2016

Norwegian University of Science and Technology
Faculty of Engineering
Science and Technology
Department of MarineTechnology

NTNU
Norwegian University of
Science and Technology

NTNU
Norwegian University of Science and Technology

Thesis for the degree of Philosophiae Doctor

Faculty of Engineering
Science and Technology
Department of MarineTechnology

ISBN 978-82-326-1786-9 (printed version)
ISBN 978-82-326-1787-6 (electronic version)
ISSN 1503-8181

Doctoral theses at NTNU, 2016:224

Printed by Skipnes Kommunikasjon as

Dedicated to my dear parents and my family.

Abstract

Large amplitude roll motion in realistic seas is a serious threat to ship stability because it can lead to damage or even capsizing of the vessel. For the excessive roll motion in random seas, the nonlinear effects and dynamics associated with damping and restoring terms should be considered. Currently, the criteria of the International Maritime Organization (IMO) for evaluation of the intact stability are based on both hydrostatics and dynamics (IMO, 2008). However, due to the stochastic nature of the ocean environment and the randomness of the roll response, the assessment of extreme rolling should inevitably be based on dynamic considerations and probabilistic methods. With the awareness of the deficiencies of the current criteria for intact stability evaluation, the IMO is currently developing the next generation (also second generation) of such criteria with a certain consideration of the physics associated with the dynamics of nonlinear roll motion and the randomness of the ocean environment and roll response.

In this work, probabilistic methods are proposed for studying the nonlinear behavior of the random roll motion as well as for evaluating the dynamic stability of the vessel in random seas. The problems of dead ship condition in random beam seas and parametric roll in random head seas are studied. For the first problem, the Markov theory is applied in order to study the stochastic nonlinear roll response. Specifically, the rolling behavior is described by a single-degree-of-freedom (SDOF) model which incorporates the nonlinearities associated with the damping and restoring terms as well as the randomness of the wave excitation. The linear filter technique is employed to approximate the random external excitation and then the SDOF model is extended into a four-dimensional (4D) Markov system whose probabilistic properties are governed by the Fokker-Planck (FP) equation. Based on the Markov property of the coupled dynamic system, the 4D path integration (PI) method is introduced in order to solve the high-dimensional FP equation. The numerical robustness and high efficiency of the 4D PI method are evaluated by comparing with the results from Monte Carlo simulation (MCS).

Based on the PI method and the MCS method, the feasibility of applying the second-order linear filter and the Gaussian white noise to approximate the random external excitation are studied. The 4D dynamic system is shown to be an appropriate model for studying the stochastic roll response. With the assistance of the 4D PI method, the influence of ship parameters and wind excitation on the stochastic roll response are investigated. Furthermore, the reliability evaluation associated with high response levels is studied and long-term extreme response is predicted by combing the 4D PI method with the metocean description.

In the second part of the thesis, the Grim effective wave model is introduced in order

to approximate the variation of the restoring moment in random head seas. Based on the Grim effective wave approximation, the mathematical model for describing the rolling behavior is established. The linear filter technique and an efficient MCS method are applied to predict the extreme roll response of a vessel sailing in random head seas. It is demonstrated that the efficient MCS method is able to provide satisfactory estimation of the extreme roll response with a dramatic reduction of computation time, which is important for the subsequent long-term statistical evaluation.

The probabilistic methods mentioned above and the results and conclusions obtained in this work hopefully can provide a useful reference for the second generation IMO intact stability criteria which are currently being developed as well as for stochastic dynamic analysis of nonlinear systems.

Acknowledgements

First of all, my deepest gratitude goes to my supervisors Professor Arvid Næss and Professor Bernt Johan Leira for giving me the chance to pursue my PhD degree at the Department of Marine Technology, NTNU. During the past three years, Prof. Arvid helped me to overcome a number of scientific challenges. I have learned and experienced a lot during the discussions with him. His solid fundaments in mathematics and ocean engineering as well as his ability to grasp the advanced research trends impressed and helped me a lot. Without his assistance, I cannot imagine that my PhD study could be finished within three years.

I would also like to express my deepest appreciation to my co-supervisor, Professor Bernt Leira for his proofreading of all the scientific papers during the PhD study. He has proposed a wealth of advice for the research work and the scientific papers during our meetings. Besides that, he provided opportunities for me to serve as a teaching assistant for the courses TMR4235 Stochastic Theory of Sea Loads and MR8209 Structural Reliability. It is my great pleasure to be one of his PhD students.

My gratitude goes also to the committee members, Adjunct Professor Sverre Haver at NTNU, Professor Jeffrey Falzarano from Texas A&M University and Professor Jørgen Juncher Jensen from Technical University of Denmark, who have reviewed the thesis and provided valuable comments.

Profs. Torgeir Moan, Dag Myrhaug, Zhen Gao and Marilena Greco have given the lectures for my courses during the PhD study and special thanks are given to them. I am also grateful for my friends and colleagues at NTNU, many thanks to Dr. Zhengshun Cheng, Ling Wan, Dr. Xiaopeng Wu, Zhaolong Yu, Chenyu Luan, Wilson Guachamin Acero, to name a few. They are always helpful. Furthermore, I would like to thank Astrid Elisabeth Hansen and Jannike Gripp for their kind help.

I also wish to acknowledge the financial support from the China Scholarship Council (CSC). Grants from the Norwegian University Fund and the Anders Jahres Fund through Unifor in Oslo and grants from the Norwegian ship-owners' association fund at NTNU are gratefully acknowledged.

Finally, I want to give my special thanks to my parents and all of my family members in China. Their encouragements and love have been the main support to keep me going over the years.

Abbreviations

2D	Two-dimensional
4D	Four-dimensional
6D	Six-dimensional
6DOF	Six-degree-of-freedom
CDF	Cumulative distribution function
CI	Confidence interval
DOF	Degree-of-freedom
FP	Fokker-Planck
IMO	International Maritime Organization
LPCD	Linear-plus-cubic damping
LPQD	Linear-plus-quadratic damping
MCS	Monte Carlo simulation
NDBC	National Data Buoy Center
PDF	Probability density function
PI	Path integration
RK4	Fourth-order Runge-Kutta
RKM	Runge-Kutta-Muruyama
SDE	Stochastic differential equation
SDOF	Single-degree-of-freedom
TPD	Transition probability density

List of appended papers

This thesis consists of an introduction section, five journal papers and an additional work. The following five papers are reported in Appendix A:

Paper 1:
Stochastic dynamic analysis and reliability of a vessel rolling in random beam seas
Wei Chai, Arvid Naess and Bernt J. Leira
Published in *Journal of Ship Research* (2015), Vol. 59. (2), pp. 113-131.

Paper 2:
Filter models for prediction of stochastic ship roll response
Wei Chai, Arvid Naess and Bernt J. Leira
Published in *Probabilistic Engineering Mechanics* (2015), Vol. 41, pp. 104-114.

Paper 3:
Stochastic nonlinear ship rolling in random beam seas by the path integration method
Wei Chai, Arvid Naess and Bernt J. Leira
Published in *Probabilistic Engineering Mechanics* (2016), Vol. 44, pp. 43-52.

Paper 4:
Stochastic roll response for a vessel with nonlinear damping models and steady heeling angles in random beam seas
Wei Chai, Arvid Naess and Bernt J. Leira
Published in *Ocean Engineering* (2016), Vol. 120, pp. 202-211.

Paper 5:
Monte Carlo simulation and Grim effective wave model for predicting the extreme response of a vessel rolling in random head seas
Wei Chai, Arvid Naess, Bernt J. Leira and Gabriele Bulian
Published in *Ocean Engineering* (2016), Vol. 123, pp. 191-203.

Declaration of Authorship

I am the first author of the five papers included in this thesis. The main work of papers 1-5, including initiating ideas, establishing the numerical models, preparing the programs for numerical calculations and analysis, writing the papers, were planned and carried out by me. Prof. Arvid Naess and Prof. Bernt Leira are co-authors for all of these papers. They have discussed the work with me and provided critical comments for theses academic papers. In addition, Prof. Arvid Naess provided part of the initial ideas with respect to stochastic dynamics for papers 2-3. Dr. Gabriele Bulian at University of Trieste (Italy) provided written comments and suggestions which are important for paper 5.

Additional papers

The following papers are not reported as the Appendix in this thesis, but the main work in theses two papers will be included in Chapter 5 of this dissertation:

Additional paper 1:
Long-term extreme response and reliability of a vessel rolling in random seas
Wei Chai, Arvid Naess, Bernt J. Leira
Under review in *Journal of Offshore Mechanics and Arctic Engineering* (2016).

Additional paper 2:
Reliability evaluation of the roll motion under the wind and irregular beam waves
Wei Chai
Published in *Journal of Ocean Engineering and Science*, (2016), Vol. 2. (1), pp. 149-156.

Contents

1 Introduction

1.1 General Background

Ship stability is a fundamental requirement for naval engineers since it relates to ship safety and integrity. For intact vessels, there are two types of stability failures, i.e. total intact stability failure and partial stability failure (ITTC, 2014). Ship capsizing is classified as the first category and it can be defined as the transition from a position of equilibrium that is considered safe, or from periodic motions near such an equilibrium, to another position of equilibrium that is intrinsically unsafe (Belenky et al., 2008). The latter is associated with occurrence of large or extreme roll angles, which would impair the normal operations or even lead to damage of the ship. Basically, loss of ship stability in random seas is most frequently associated with excessive roll motion, which is nonlinear by nature and inherently random.

Even though the current criteria of the International Maritime Organization (IMO) for evaluation of the intact stability are based on both on hydrostatics and dynamics (IMO, 2008). There is not enough consideration with respect to the dynamics associated with the nonlinear roll motion as well as the randomness of the ocean environments and the roll response, which are important for stability assessment. The deficiencies of the current criteria for dynamic stability evaluation have been reflected by a considerable number of stability failure accidents every year (MAIB, 2014).

The IMO is currently developing the next (second) generation of intact stability criteria with a certain consideration of the nonlinear dynamic behavior in realistic seas. The second generation intact stability criteria apply a multi-tiered vulnerability criteria in three levels of complexity in order to assess the vessel's capacity to withstand different modes of stability failures, such as: dead ship condition (resonant roll in beam seas), parametric roll, pure loss of stability, broaching and excessive acceleration (SLF, 2011).

In this work, only the failure modes of the dead ship condition and the parametric roll are considered. The dead ship condition means that when a ship loses power or has maneuvering problems, the ship will be turned into beam wave scenario and large oscillations occurs if a resonance is encountered. On the other hand, parametric roll is caused by sufficient large oscillation of the roll restoring moment occurring within certain frequencies of wave encounter (nearly twice the natural roll frequency). Even though the mechanisms for these two failure modes are different, the excessive roll motion caused by these two failure modes will lead to damage or even capsizing of the vessel.

For the random wave scenario, the large amplitude roll motion, either caused by parametric roll or under dead ship condition, is a stochastic process and the dynamic stability should be evaluated by means of a probabilistic approach. However, assessing the stochastic responses of such nonlinear dynamic systems has been a demanding challenge in the past decades since elaborate theoretical model as well as appropriate mathematical techniques are required for such kinds of problems (Ellermann, 2009).

In this dissertation, the problem of dead ship condition in random beam seas and the parametric roll in random longitudinal seas will be studied separately. For each failure mode, relevant assumptions and simplifications will be made and dedicated mathematical techniques will be applied in order to estimate the stochastic roll response and evaluate the dynamic stability of the vessel. The study with respect to probabilistic methods for dynamic stability evaluation and stochastic analysis of the roll response in this work will hopefully provide useful references for the second generation of intact stability criteria which are under development as well as for stochastic dynamic analysis of nonlinear systems.

1.2 Stochastic Analysis and Reliability Evaluation

1.2.1 Dead ship condition in random beam seas

The dead ship condition is assumed to be the most classic stability failure mode and studies of ship rolling in beam waves were derived from Froude's time. Since then, a variety of methods, both analytical and numerical, have been derived to study the nonlinear roll motion in regular waves. These techniques are referred to as deterministic methods and conclusions about these methods have been given in Falzarano (1990), Jiang et al. (1996) and Roberts and Vasta (2000), etc. Even though the nonlinear phenomenon associated with excessive roll motion is considered more or less by these methods, the randomness of the wave excitation and the roll response in the nonlinear roll motion problem can not be incorporated.

In order to analyze the stochastic response of roll motion in random beam seas, the rolling behavior of the vessel is generally assumed to be decoupled from other motions and described by a single-degree-of-freedom (SDOF) model in which the nonlinearities associated with the damping and restoring terms as well as the randomness of the wave excitation are all incorporated (Roberts and Vasta, 2000). And also, various probabilistic strategies have been proposed. Among these strategies, the methodology based on the Markov diffusion theory is attractive because the probabilistic property of the roll motion is governed by the Fokker-Planck (FP) equation.

However, the Markov model is only valid for a system which is driven by white noise or filtered white noise. Fortunately, the random roll excitation moment in the SDOF model is a stationary Gaussian process with appropriate spectral density which can be modeled as filtered white noise by introducing the shaping filter technique.

Subsequently, the original SDOF model, also a second order differential equation, is coupled with the filter model and then extended to a Markov dynamic system. For such a coupled system, a host of useful response statistics can be obtained by solving the corresponding FP equation.

Coupling of the SDOF model and the filter model leads to another challenge. Analytical solutions of the FP equations are only available for some linear systems and a very limited class of nonlinear systems. Direct numerical methods aiming to solve the low-dimensional FP equations, such as the finite element method (Spencer Jr and Bergman, 1993) and the finite difference method (Wojtkiewicz et al., 1999), are hardly feasible for the nonlinear extended system with high-dimensional FP equations. In this regard, the so-called "curse of dimension" comes into play which means that difficulties arise due to the processing capacity as well as the storage needed for the computation increases dramatically with the dimension of the FP equation. Therefore several alternative techniques are developed to provide approximate solutions to the FP equations. These approaches include the stochastic averaging method (Dostal et al., 2012; Kougioumtzoglou and Spanos, 2014; Roberts, 1986), the moment closure technique (Francescutto and Naito, 2004; Su, 2012; Su and Falzarano, 2011), the local statistical linearization method (Dostal and Kreuzer, 2011), etc.

The path integration (PI) method is an efficient approximation for solving the FP equation and providing the stationary or non-stationary response probability density function (PDF) of the dynamic system. The method is based on the Markov property of the dynamic system and the evolution of the response PDF is computed in short time steps via a step-by-step solution technique. Specifically, based on the Chapman-Kolmogorov equation, the response PDF at a given time instant can be obtained when the response PDF at an earlier close time as well as the conditional PDF are already known. Prior to the research work in current dissertation, only low-dimensional PI procedures have been applied to the area of nonlinear ship rolling in random beam seas (Chai et al., 2013; Falzarano et al., 2012; Lin and Yim, 1995; Pirrotta and Santoro, 2011). In these studies, the external wave excitation was simplified as Gaussian white noise and then two-dimensional (2D) PI techniques were applied to estimate the stochastic roll response. However, as shown in Section 5.3, unsatisfactory results have been found in the Gaussian white noise approximation and it is inappropriate to be used for simulating the nonlinear roll motion in random seas. In this work, a second-order linear filter is applied to approximate the random excitation moment in the SDOF model and then a four-dimensional (4D) PI procedure is developed to address the challenge of determining the response of a vessel in random beam seas. The feasibility of the linear filter (sharping filter) technique as well as the rationality and high efficiency of the PI approach will be demonstrated in the following work.

As for the dynamic stability evaluation, ship capsizing caused by large amplitude roll motion is a rare event that also exhibits complex nonlinear features. Accordingly, the traditional approaches to address this challenging task are generally based on time

domain simulations (Ayyub et al., 2006). Other methods based on different assumptions have been carried out for studying ship capsizing, which include the Melnikov method (Jiang et al., 1996; Liu et al., 2016; Su and Falzarano, 2013), the split-time method (Belenky et al., 2010; Belenky et al., 2012) and the first-passage method (Dostal et al., 2012; Roberts, 1986; Su and Falzarano, 2013), etc.

For evaluation of the partial stability failure, conventional reliability theory can be applied if the partial stability failure event is associated with a Poisson distributed crossing event. In this work, the reliability associated with high-level response is considered. For one thing, the response statistics obtained by the 4D PI method, especially in the high-level response region, can directly be applied in the relevant reliability evaluation procedure. Also, prediction of the extreme roll responses and the associated risk assessment of ship stability in random seas are crucial for reliability based design and operation in practice. Furthermore, the roll response is narrow-banded due to the light roll damping and the performance of the Poisson estimate for the reliability evaluation will be discussed in this work.

1.2.2 Parametric roll in random longitudinal seas

For ships sailing in longitudinal waves, even though there is no direct excitation for the roll motion, large oscillation of the roll restoring moment within certain regions of wave encounter frequencies combined with insufficient roll damping could induce parametric roll, which is another failure mode discussed in this dissertation. The onset of parametric roll in regular waves can be predicted by applying the Mathieu instability criteria with the simplification that the roll motion is described by a SDOF model (Francescutto et al., 2004; Shin et al., 2004). For the actual seaway, the regular wave condition is hardly encountered and investigation of the parametric roll in irregular waves is therefore more realistic and more appropriate.

Similar to the dead ship condition in random beam seas, for the parametric roll in random longitudinal waves, the variation of the restoring moment as well as the subsequent roll response are stochastic. Therefore, appropriate numerical model and probabilistic approach are required in order to evaluate the dynamic stability of vessel which is suffering from the parametric roll.

In order to study the parametric roll behavior in random seas and estimate the risk of an associated large or extreme roll response, several powerful codes have been proposed (e Silva and Soares, 2013; France et al., 2003; Shin et al., 2004). In these procedures, the restoring moment is calculated at every time step by using the instantaneous wetted surface and therefore, these procedures are time consuming and difficult to apply during the early design stage. The computation time is depend on the number of DOFs as well as on the method for approximation of the restoring moment. On the other hand, the effect of time dependent restoring term, which is the main cause of parametric roll, should be correctly modeled. Several approximation procedures have

been proposed to describe the restoring term in a simplistic way, such as the Volterra series approach (Hua et al., 1999; Moideen et al., 2014), fluctuation of the metacentric height (GM) term by linear transfer functions (Song et al., 2013), the Grim effective wave method and other methods mentioned in Vidic-Perunovic (2011).

Grim (1961) introduced the effective wave model with the main idea that the instantaneous irregular wave surface can be replaced by an effective (or equivalent) regular wave with the wave length equal to the ship length and its crest or trough always positioned amidships. The equivalent wave is assumed to be fixed with respect to the vessel, but its amplitude is a random process. The concept of Grim effective wave model has been applied by several authors to study the parametric roll behavior of vessels with conventional hull forms (Bulian, 2006; Chang, 2008; Kröger, 1986). In this work, the Grim effective wave model is applied to approximate the time-varying roll restoring moment of the vessel sailing in random longitudinal waves. In such approach, heave and pitch motions are assumed to be quasi-static and the roll motion is approximated as a SDOF model with the restoring term fitted by a nonlinear expression with regard to the effective wave amplitude process and the roll angle.

Furthermore, for such a SDOF model, the random effective wave amplitude process serves as the driving term of the dynamic system and the shaping filter technique is applied in order to model the effective wave amplitude process. In this work, a fourth order linear filter is applied to approximate the driving process in the SDOF model and then the dynamic system is extended into a six-dimensional (6D) Markov system. For this coupled system, even though the probabilistic properties are governed by the FP equation, the PI procedure which works well for the 4D dynamic system, does suffer from a curse of the dimensionality and the PI technique is hardly applicable for solving the 6D FP equation.

Nonetheless, the Monte Carlo simulation (MCS) does not critically suffer from the curse of the dimensionality problem since the statistics of the response are obtained directly from the realizations. Basically, the MCS is the simplest and most versatile way to determine the response statistics of dynamic, although this simplicity is paid for by the random sampling uncertainty in the approach. For marine structures, the mean upcrossing rate for high-level responses and the associated probabilities of exceedance are of central importance in evaluation of the response statistics. However, the computation burden for the conventional MCS may be prohibitive for estimation of the high-level responses and the associated low levels of probability. In this work, a computationally efficient MCS (Naess and Gaidai, 2008; Naess and Moan, 2012), which is based on the regularity behavior of the upcrossing rate in the tail region, is applied in order to circumvent the above obstacle. In the efficient MCS approach, an extrapolation procedure is applied for prediction of the upcrossing rate in the far tail (which is nearly impossible to determine by means of the conventional MCS) on the basis of estimations obtained at more moderate levels. By taking advantage of the time-saving extrapolation technique, the efficient MCS method does give a reasonable

estimation of the extreme response with a dramatic reduction of the computation time.

1.3 Scope and Objectives of the Thesis

The main goal of this thesis is to study the nonlinear behavior of the roll motion in random waves, analyze the stochastic roll response and predict the extreme responses. To realize these objectives, the following sub-objectives have been achieved:

- To develop a 4D Markov system for describing the roll behavior in random beam seas and to develop a 4D PI procedure used to solve the high-dimensional FP equation, evaluate the stochastic response of the roll motion in random beam seas. The PI method is verified by the MCS results (paper 1).
- To verify the feasibility of the 4D extended system used for studying the stochastic roll response. Specifically, the random wave excitation is modeled by a second-order linear filter and a fourth-order linear filter, respectively (paper 2). The response statistics obtained from the 4D system are compared with those calculated by 6D MCS. The random wave excitation term is also approximated by an equivalent Gaussian white noise (paper 3) in order to study the rationality and accuracy of the corresponding 2D dynamic system used for studying the stochastic response of the roll motion in random beam seas.
- To investigate the influence of ship parameters, such as the roll damping coefficients and roll restoring coefficients on the stochastic roll response (paper 1). The effect of different nonlinear damping models on the stochastic roll response is also investigated (paper 4).
- To study the rolling behavior of the vessel under the action of beam wind and waves and investigate the influence of the steady heeling angle on the stochastic roll response (paper 4).
- To evaluate the exceedance probabilities for high level responses by applying the Poisson estimate and investigate its performance (paper 1).
- Predict the long-term extreme response in combination with the metocean information (additional paper 1).
- To predict the extreme roll response in random head seas by applying the linear (shaping) filter technique and an efficient MCS technique (paper 5).

This thesis is written in the form of a collection of 5 journal papers. Figure 1.1 shows how the scope of the papers is interconnected in this thesis. The 5 journal papers are included in Appendix A and summarized as follows:

Paper 1: This paper presents a four-dimensional (4D) path integration (PI) approach to study the stochastic roll response and reliability of a vessel in random beam seas. The theoretical principle and numerical implementation of the current state-of-the-art 4D PI method are presented. The numerical robustness and accuracy of the 4D PI method are

evaluated by comparing with the results obtained from the MCS method. The influence of the restoring terms and the damping terms on the stochastic roll response are investigated. Furthermore, based on the well-known Poisson estimate and the response statistics yielded by the 4D PI technique, evaluation of the reliability associated with high-level response is performed. The performance of the Poisson estimate is evaluated by the versatile MCS technique.

Paper 2: In this paper, a second order linear filter and a fourth order linear filter are applied in order model the random wave excitation. In this regard, a 4D dynamic system and a six-dimensional (6D) dynamic systems are established to evaluate the statistics of high-level roll responses when subjected to random wave excitation. For the 4D system, the response statistics can be obtained by the 4D PI method, while the response statistics for the 6D system are evaluated by the MCS technique. It is proved that, the 4D dynamic system can serve as an effective alternative to the 6D dynamic system in terms of determining the important response statistics, such as the upcrossing rates and exceedance probabilities for the specific high levels. Moreover, the feasibility of this simplification has been verified by various cases corresponding to different sea states.

Paper 3: In this paper, the random wave excitation is approximated by an equivalent Gaussian white noise and a two-dimensional (2D) PI technique is applied in order to obtain the response statistics of the dynamic system driven by this Gaussian white noise. The rationality and accuracy of applying the equivalent Gaussian white noise to simulate nonlinear ship rolling in random beam seas is studied.

Paper 4: In this paper, the 4D PI method is applied in order to study the effects of different damping models (i.e. the linear-plus-quadratic damping (LPQD) model and the linear-plus-cubic damping (LPCD) model) and the steady heeling angle on the response statistics of the roll motion in random beam seas. It has been found that the dynamic system with the LPCD model provides a less conservative estimate of the stochastic roll response. Furthermore, the existence of the steady heeling angle has a significant influence on the stochastic roll response and leads to a deterioration of the ship stability in random waves.

Paper 5: The main accomplishment of this paper is to study the parametric roll behavior in random head seas as well as to estimate the associated large or extreme roll response by means of probabilistic approaches. Specifically, the Grim effective wave model is applied in order to approximate the variation of the restoring moment in random head seas. The linear filter technique and an efficient MCS method, which is based on the combination of a standard MCS approach and an extrapolation technique, are applied in order to estimate the extreme roll response. It has been found that the efficient MCS technique gives a satisfactory estimation of the extreme response with a dramatic reduction of computation time.

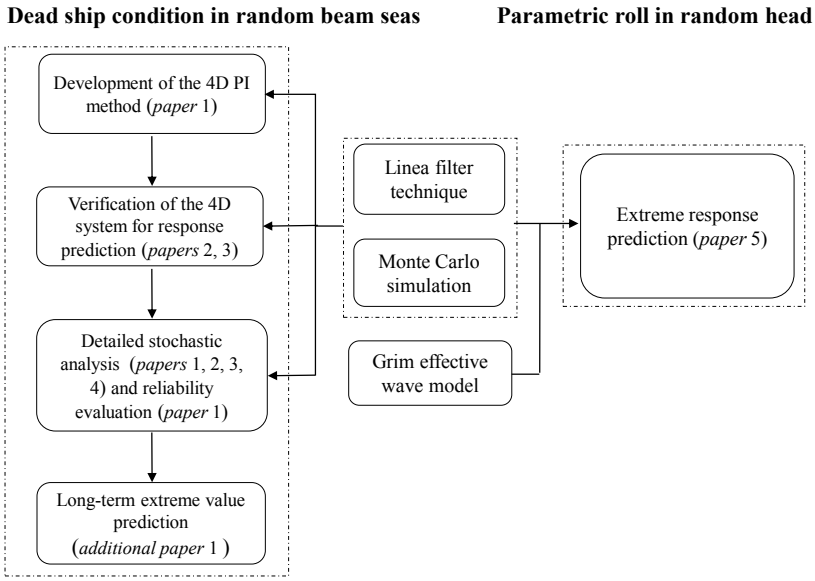

Figure 1.1: Scope of thesis and interconnection between the papers

1.4 Thesis Outline

The summary part of this thesis consists of the following chapters:

Chapter 1 includes the background, motivation and objectives of this thesis.

Chapter 2 introduces the ship motion in time domain as a six-degree-of-freedom (6DOF) model. The single-degree-of-freedom (SDOF) model used to describe the roll motion in random beam seas is presented and a SDOF model based on the Grim effective wave approximation is applied in order to describe the rolling behavior of the vessel sailing in random head seas.

Chapter 3 presents the basic stochastic processes, i.e. the Markov process, the white noise process and the Weiner process. The principle of the linear filter technique and the derivation of Forkker-Planck equation are included.

Chapter 4 addresses the methodologies used to calculate the response statistics of the roll motion in random seas. The principle and numerical implementation of the path integration method (PI), the standard Monte Carlo simulation method used to calculate mean upcrossing rate and the efficient MCS technique for extreme value prediction are introduced.

Chapter 5 summarizes the numerical results, relevant analysis and discussions are presented in this chapter.

Chapter 6 summarizes the work in the thesis and recommendations for the future work.

2 Ship Dynamics and Roll Motion in Waves

This chapter starts with the equation of linear ship motion in regular waves and then a six-degree-of-freedom (6DOF) system is built up to describe the ship motion in time-domain. In Section 2.2, a single-degree-of-freedom (SDOF) model is introduced in order to describe the rolling behavior of the vessel for the dead ship condition. For the cases of ship rolling in random head seas, the Grim effective wave model is introduced and the principle for this approximation is describe in Section 2.3.

2.1 Ship Motion in Time-domain

In the context of linear wave theory, the ship motion in regular waves (with frequency ω) is written as (Faltinsen, 1993):

$$\sum_{j=1}^{6}\left[(M_{kj}+A_{kj}(\omega))\cdot\ddot{\eta}_j(t)+B_{kj}(\omega)\cdot\dot{\eta}_j(t)+C_{kj}\eta_j(t)\right]=F_{exc,\mathrm{k}}(t),\ k=1,2,\cdots,6 \qquad (2.1)$$

where η_j represent the displacements of the vessel, M_{kj} are the components of the generalized mass matrix for the intact ship. $A_{kj}(\omega)$ and $B_{kj}(\omega)$ are hydrodynamic coefficients of added mass and damping term, respectively. C_{kj} denote the components of the matrix for restoring coefficients. $F_{exc,k}$ represent the wave excitation load, i.e. the sum of the Froude-Krylov force (moment) and the diffraction force (moment).

However, the added mass and damping term in equation (2.1) is frequency-dependent and this equation is valid only for steady state sinusoidal motions, limitations will be encountered when studying the linear transient behavior or nonlinear problems. Therefore, equation (2.1) should be modified to describe the cases where the time-dependence is more general.

The impulse response function method (Cummins, 1962) can be applied to determine the radiation force $F_{rad,k}$, which can be transformed as:

$$F_{rad,k}(t)=\sum_{j=1}^{6}\left\{-A_{kj}(\infty)\ddot{\eta}_j(t)-B_{kj}(\infty)\dot{\eta}_j(t)+\int_0^t K_{kj}(t-\tau)\dot{\eta}_j(\tau)d\tau\right\},\ k=1,2,\cdots,6 \qquad (2.2)$$

where $A_{kj}(\infty)$ and $B_{kj}(\infty)$ are the infinite added mass and the frequency-independent damping, respectively. $K_{kj}(t)$ is the retardation function, which can be given as (Ogilvie, 1964):

$$K_{kj}(t) = \frac{2}{\pi}\int_0^\infty (B_{kj}(\omega) - B_{kj}(\infty))\cos(\omega t)d\omega$$
$$= -\frac{2}{\pi}\int_0^\infty \omega(A_{kj}(\omega) - A_{kj}(\infty))\sin(\omega t)d\omega \tag{2.3}$$

Finally, the ship motion in time-domain is written as:

$$\sum_{j=1}^{6}\left[(M_{kj} + A_{kj}(\infty))\cdot\ddot{\eta}_j(t) + B_{kj}(\infty)\cdot\dot{\eta}_j(t) + \int_0^t K_{kj}(t-\tau)\dot{\eta}_j(\tau)d\tau + C_{kj}\eta_j(t)\right]$$
$$= F_{exc,k}(t),\ k = 1,2,\cdots,6 \tag{2.4}$$

2.2 Roll Motion in Random Beam Seas

The ship motion in waves is represented by a six-degree-of-freedom (6DOF) system (2.4), but the roll motion for dead ship condition is the most critical mode since large amplitude roll motion can lead to damage or even capsizing of the vessel. In order to understand the nonlinear behavior of the roll motion under random external excitation, the rolling behavior is assumed to be decoupled from other motions and described by the following single-degree-of-freedom (SDOF) model (Jiang et al., 2000; Ogilvie, 1964):

$$(I_{44} + A_{44}(\infty))\ddot{\theta}(t) + B_{44}(\infty)\dot{\theta}(t) + \int_0^t K_{44}(t-\tau)\dot{\theta}(\tau)d\tau + C_{44}\theta(t) = M(t) \tag{2.5}$$

where $\theta(t)$ and $\dot{\theta}(t)$ are the roll angle and the roll velocity, respectively. I_{44} is the moment of inertia in roll, $K_{44}(t)$ and C_{44} are the retardation function and restoring coefficient for the roll motion, respectively. $M(t)$ represents the roll excitation moment due to external waves.

For the dead ship condition in random beam seas, the assumption of the above decoupling is reasonable for qualitative studies (Roberts and Vasta, 2000). However, the SDOF model (2.5) is based on the linear wave theory with linear retardation function and linear restoring moment, which are valid for the small amplitude (i.e. linear) roll motion. For large amplitude roll motion in random beam seas, the nonlinearities associated with the damping and restoring terms as well as the randomness of the wave excitation term should be considered in the SDOF model.

For nonlinear roll motion, the roll damping normally has three kind of components: the wave damping (linear) due to radiation; the damping caused by vortex shedding and flow separation as well as the viscous friction damping. In general, these terms are coupled with each other and the quantitative evaluation of roll damping is difficult. Nevertheless, the empirical linear-plus-quadratic damping (LPQD) model, which has

been verified by numerous studies of experimental data, is selected to describe the damping term. This damping model is given as (Himeno, 1981):

$$M_D = B_{44}\dot{\theta}(t) + B_{44q}\dot{\theta}(t)\left|\dot{\theta}(t)\right| \tag{2.6}$$

where M_D is the roll damping (moment), B_{44} and B_{44q} are the linear and quadratic damping coefficients, respectively. In addition to the LPQD model, the linear-plus-cubic damping (LPCD) model, given as equation (2.7), is infinitely differentiable and mathematically preferable to the LPQD model.

$$M_D = \hat{B}_{44}\dot{\theta}(t) + B_{44c}\dot{\theta}^3(t) \tag{2.7}$$

in which $\hat{B}_{44}$ and B_{44c} are the linear and cubic damping coefficients for the LPCD model.

As mentioned above, the dependence of the restoring moment on the roll angle $\theta(t)$, has a nonlinear character for large amplitude roll motion. The restoring term is given by the following equation:

$$M_R = \Delta GZ(\theta(t)) \tag{2.8}$$

in which M_R is the restoring moment and Δ is the displacement of the vessel. The restoring arm GZ, which can be obtained from standard hydrostatic software, is usually given by nonlinear odd function of the roll angle, e.g.

$$GZ(\theta) = C_1\theta - C_3\theta^3 \tag{2.9}$$

where C_1 and C_3 are the linear and nonlinear roll restoring coefficients which are associated with the restoring arm.

The restoring arm in equation (2.9) is calculated in calm water. Theoretically speaking, for the rolling vessel, when the water is not calm, its surface experience a wave defamation and taking this effect into consideration could be a more accurate way to calculate the restoring moment. However, for the roll motion in beam seas as well as for the qualitative study, it is reasonable to treat the restoring arm the same as that in calm water (Belenky and Sevastianov, 2007). But when the ship is sailing in longitudinal waves, the change in the restoring moment is quite significant and this will be discussed in Section 2.3.

As for the random roll excitation moment, $M(t)$, it can be calculated by linear hydrodynamics and the roll excitation moment spectrum, $S_{MM}(\omega)$ is related to the wave energy spectrum, $S_{\zeta\zeta}(\omega)$, by the following relationship (Hsieh et al., 1994):

$$S_{MM}(\omega) = |F_{roll}(\omega)|^2 S_{\zeta\zeta}(\omega) \tag{2.10}$$

in which $|F_{roll}(\omega)|$ represents the wave excitation moment amplitude per unit wave

amplitude at frequency ω. Moreover, the sea state is assumed to be stationary during a short-term period. Therefore, the wave elevation and the roll excitation moment can be assumed to be stationary Gaussian processes.

Due to the presence of the convolution integral in equation (2.5), time-domain simulations of the roll response may be computationally demanding and it also introduces additional difficulties for applying the stochastic dynamic methods (Su, 2012). For simplicity, the frequency-dependent added mass and damping in equation (2.5) can be replaced by constant coefficients (Taghipour et al., 2008). Considering the nonlinear damping moment in equation (2.6) (or equation (2.7)) and nonlinear restoring moment described in equations (2.8) and (2.9), the SDOF model used to describe the roll motion in random beam seas is given as:

$$(I_{44} + A_{44}(\tilde{\omega}))\ddot{\theta}(t) + B_{44}(\tilde{\omega})\dot{\theta}(t) + B_{44q}\dot{\theta}(t)\left|\dot{\theta}(t)\right| + \Delta(C_1\theta(t) - C_3\theta^3(t)) = M(t) \qquad (2.11)$$

The added mass and linear damping coefficients, $A_{44}(\tilde{\omega})$ and $B_{44}(\tilde{\omega})$ are evaluated at some representative fixed frequency $\tilde{\omega}$ and considered as constants. That is, for narrow-banded wave excitation, values are evaluated at the peak excitation frequency, while for wide-banded excitation, values at the natural frequency of the roll motion, ω_0, are recommended. In addition, the linear damping coefficient $B_{44}(\tilde{\omega})$ can be regarded as B_{44l} in equation (2.6).

Dividing equation (2.11) by (I_{44} + A_{44}), the final form of the differential equation is obtained as:

$$\ddot{\theta}(t) + b_{44}\dot{\theta}(t) + b_{44q}\dot{\theta}(t)\,|\,\dot{\theta}(t)\,| + c_1\theta(t) - c_3\theta^3(t) = m(t) \qquad (2.12)$$

where

$$b_{44} = B_{44}(\tilde{\omega})/(I_{44} + A_{44}(\tilde{\omega})) \qquad (2.13)$$

$$b_{44q} = B_{44q}/(I_{44} + A_{44}(\tilde{\omega})) \qquad (2.14)$$

$$c_i = \Delta C_i/(I_{44} + A_{44}(\tilde{\omega}))\ \ i = 1,3 \qquad (2.15)$$

$$m(t) = M(t)/(I_{44} + A_{44}(\tilde{\omega})) \qquad (2.16)$$

are relative roll parameters. The natural frequency of the roll motion, ω_0, is determined as:

$$\omega_0 = \sqrt{\Delta C_1/(I_{44} + A_{44}(\tilde{\omega}))} = \sqrt{c_1} \qquad (2.17)$$

The spectrum of the relative roll excitation moment, $S_{mm}(\omega)$, can be expressed as:

$$S_{mm}(\omega) = \left|F_{roll}(\omega)\right|^2 S_{\zeta\zeta}(\omega) \Big/ (I_{44} + A_{44}(\tilde{\omega}))^2 \tag{2.18}$$

Finally, the SDOF model (2.12) can be transformed into the following state-space equation which is written as:

$$\begin{cases} dx_1 = x_2 dt \\ dx_2 = (-b_{44}x_2 - b_{44q}x_2 \mid x_2 \mid -c_1 x_1 + c_3 x_1^3 + x_3)dt \end{cases} \tag{2.19}$$

where $x_1 = \theta(t)$, $x_2 = \dot{\theta}(t)$ and $x_3 = m(t)$.

2.3 Roll Motion in Random Head Seas

For the cases of ship rolling in longitudinal (head or following) waves, large amplitude roll motion could be possible even through there is no direct excitation for the roll motion. This phenomenon is referred to as parametric roll and it is caused by sufficiently large oscillation of the roll restoring moment occurring within certain frequencies of wave encounter (approximately twice the natural roll frequency). Generally, parametric roll is coupled with heave and pitch motions, the following model given by Lewis (1988) can be considered for studying the rolling behavior:

$$(m + A_{33})\ddot{\eta}_3(t) + B_{33}\dot{\eta}_3(t) + C_{33}\eta_3(t) = F_3(t) \tag{2.20}$$

$$(I_{44} + A_{44})\ddot{\eta}_4(t) + B_{44}\dot{\eta}_4(t) + B_{44q}\dot{\eta}_4(t)\left|\dot{\eta}_4(t)\right| + \Delta GZ(\eta_3(t), \eta_4(t), \eta_5(t)) = M_4(t) \tag{2.21}$$

$$(I_{55} + A_{55})\ddot{\eta}_5(t) + B_{55}\dot{\eta}_5(t) + C_{55}\eta_5(t) = M_5(t) \tag{2.22}$$

in this coupled system, the restoring arm $GZ(\eta_3, \eta_4, \eta_5)$ is a nonlinear function of heave (η_3), roll (η_4 or θ) and pitch (η_5) motions. The analysis of the coupled motions can only be done by numerical computations and some approximations should be introduced in order to study the parametric roll in random waves.

When the ship is rolling in unidirectional head seas and assume that a quasi-static behavior in relation to the heave and pitch motions, the roll dynamics for the ship in irregular longitudinal long-crested waves can be represented by the following SDOF model (Bulian, 2006; Roberts, 1982; Roberts and Vasta, 2000):

$$(I_{44} + A_{44})\ddot{\theta}(t) + \hat{B}_{44}\dot{\theta}(t) + B_{44c}\dot{\theta}^3(t) + \Delta GZ(\theta(t), A_x(\xi(x,t))) = M(t) \tag{2.23}$$

where $\Delta GZ(\theta(t), A_x(\xi(x,t)))$ is the restoring moment in random longitudinal waves, $A_x(\xi(x,t))$ represents the effect of wave elevation process $\xi(x,t)$ along the vessel

(coordinate x) at time t, and $M(t)$ denotes a roll excitation moment.

The roll excitation moment $M(t)$ is small if the ship travels in about the same direction as the incident waves. It acts as an additive disturbance for the dynamic system and can be approximated by application of a linear strip method (Dostal and Kreuzer, 2014). For pure head (or following) seas, its influence can be neglected.

Regarding the most important time-varying restoring moment, it is expressed in terms of the displacement Δ and restoring arm $GZ(\theta(t), A_x(\xi(x,t)))$ of the vessel. The restoring arm is an instantaneous quantity which is difficult to estimate due to its nonlinear relationship with the instantaneous irregular wave surface $\xi(x,t)$. The restoring moment can be obtained by integration of the external pressure over the instantaneous wetted surface. However, such direct integration requires a significant computation effort and the much simpler Grim effective wave concept is applied herein in order to approximate the complicated restoring term. The derivation and principle of the effective wave method for approximation of the restoring term are given below, while more details on the relevant theoretical background are given by Grim (1961).

Assume that a right-hand ship fixed coordinate system $oxyz$ is placed at amidships with the positive z axis oriented vertically upwards. For a ship sailing with constant speed V in random head seas, the encounter frequency in the ship fixed frame is then given as:

$$\omega_e = \omega - \kappa(\omega) V \cos\chi \tag{2.24}$$

where χ is the heading angle (for head seas χ=180°), $\kappa(\omega)$ is the wave number with $\kappa(\omega) = \omega^2/g$ for the deep water case. For head sea condition, the wave spectrum with respect to the encounter frequency is formulated as:

$$S_{\xi\xi}(\omega_e) = \frac{S_{\xi\xi}(\omega)}{1-(2\omega/g)\cdot V\cos\chi} = \frac{S_{\xi\xi}(\omega)}{1+(2\omega/g)\cdot V} \tag{2.25}$$

In general, the irregular long-crested wave surface can be described by the following linear superposition scheme with deterministic spectral amplitudes if the corresponding wave spectrum is given.

$$\xi(x,t) = \sum_{n=1}^{\infty} \cos(\omega_{e,n} t - \kappa_n x + \varepsilon_n)\sqrt{2S_{\zeta\zeta}(\omega_n)\Delta\omega} \tag{2.26}$$

where ω_n is the discretized wave frequency and $\omega_{e,n}$ is the corresponding encounter frequency, κ_n and ε_n are the corresponding wave number and random phase angle. Moreover, ε_n is a random variable and uniformly distributed over $(0, 2\pi)$ and $\Delta\omega$ is a constant difference between successive frequencies.

The main idea of the effective wave model is that the irregular wave surface $\xi(x, t)$ can be approximated by an equivalent (or effective) regular wave $\xi_{eff}(x, t)$. It is assumed that

the largest fluctuation of the restoring term occurs when the regular longitudinal wave have a length close to the ship length, L. Although this is not always true, it is a reasonable approximation for qualitative study. Therefore, an equivalent regular wave with a wave length which is equal to the length of the vessel represents the most serious case:

$$\begin{aligned}\xi_{eff}(x,t) &= \xi_c(t)\cos(\frac{2\pi}{L}x) + \xi_s(t)\sin(\frac{2\pi}{L}x) \\ &= \bar{\xi}_{eff}(t)\cos(\frac{2\pi}{L}x + \varphi(t)), -\frac{L}{2} < x < \frac{L}{2}.\end{aligned} \tag{2.27}$$

where L is the length of the effective wave (which is also equal to the ship length), $\bar{\xi}_{eff}$ is the effective wave amplitude process. $\xi_c(t)$ and $\xi_s(t)$ are random amplitude processes and $\varphi(t)$ is the random phase.

The equivalence between the irregular wave surface (2.26) and the effective regular wave (2.27) can then be implemented by minimizing the following square error function:

$$\delta^2(\xi_c, \xi_s) = \int_{-L/2}^{L/2} (\xi(x,t) - \xi_{eff}(x,t))^2 dx \tag{2.28}$$

By introducing the basic property that $\frac{\partial \delta^2(\xi_c - \xi_s)}{\partial \xi_c} = \frac{\partial \delta^2(\xi_c - \xi_s)}{\partial \xi_s} = 0$, the Gaussian random processes $\xi_c(t)$ and $\xi_s(t)$ can be determined and given as:

$$\begin{aligned}\xi_c(t) &= \sum_{n=1}^{\infty} \mathrm{f}_c(\kappa_n)\cos(\omega_{e,n}t + \varepsilon_n)\sqrt{2S_{\zeta\zeta}(\omega_n)\Delta\omega} \\ \xi_s(t) &= \sum_{n=1}^{\infty} \mathrm{f}_s(\kappa_n)\cos(\omega_{e,n}t + \varepsilon_n)\sqrt{2S_{\zeta\zeta}(\omega_n)\Delta\omega}\end{aligned} \tag{2.29}$$

in which the transfer functions $\mathrm{f}_c(\kappa_n)$ and $\mathrm{f}_s(\kappa_n)$ are

$$\begin{aligned}\mathrm{f}_c(\kappa_n) &= \frac{2R\sin R}{\pi^2 - R^2} \\ \mathrm{f}_s(\kappa_n) &= \frac{2\pi\sin R}{\pi^2 - R^2}\end{aligned} \tag{2.30}$$

where $R=(L/2)\,\kappa_n$ and κ_n is the wave number associated with the n-th wave component with physical frequency ω_n.

If we set the random phase $\varphi(t)=0$ (i.e., the random amplitude $\xi_s(t)=0$ and $\bar{\xi}_{eff}=\xi_c(t)$), equation (2.27) is the original Grim effective wave model which is widely used for ships with conventional hull forms. Otherwise, it is the improved model described in Bulian (2008) and Jensen (2007), which can provide good results in terms of restoring variations, also for unconventional vessels. As for the former model, the crest or trough

of the equivalent regular wave is always situated amidships, the wave is assumed to be a standing wave (unmovable) with random amplitude $\xi_c(t)$. The latter model relates to a traveling wave and gives a much better approximation of the irregular wave surface. In this work, the simpler former model is applied since it works well for conventional ships and Figure 2.1 shows an example of this model, which includes the irregular wave surface $\xi(x, t)$ and the corresponding equivalent (effective) wave approximation $\xi_{eff}(x, t)$.

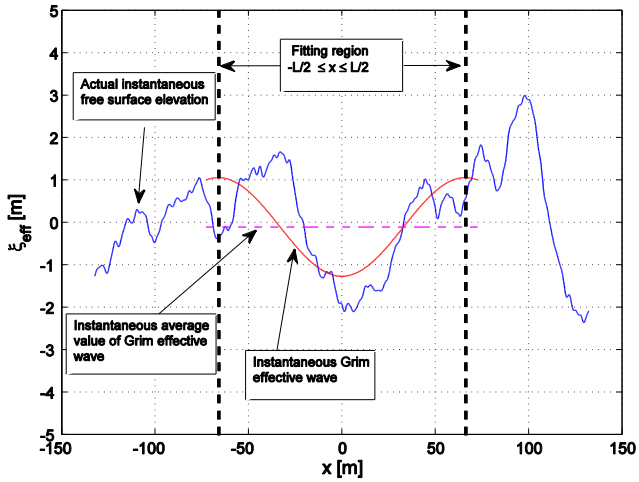

Figure 2.1: Example of effective wave model with the actual irregular surface $\xi(x,t)$ and the corresponding equivalent (effective) wave approximation $\xi_{eff}(x,t)$

In the following, the random amplitude process $\xi_c(t)$ is referred to as the effective wave amplitude process and the spectrum of effective wave amplitude process, also known as the effective wave spectrum, $S_{\xi_c}(\omega)$ can be obtained as:

$$S_{\xi_c}(\omega) = S_{\bar{\xi}_{eff}}(\omega) = \mathrm{f}_c^2(\kappa(\omega)) \cdot S_{\zeta\zeta}(\omega) = \frac{4R^2 \sin^2(R)}{(\pi^2 - R^2)^2} \cdot S_{\zeta\zeta}(\omega) \tag{2.31}$$

and the corresponding encounter spectrum for the effective wave amplitude process for the head seas conditions is given as:

$$S_{\xi_c}(\omega_e) = \frac{\mathrm{f}_c^2(\kappa(\omega)) \cdot S_{\zeta\zeta}(\omega)}{1 + (2\omega/g) \cdot V} \tag{2.32}$$

With the simplifications from the effective wave model, the restoring arm can be rewritten as follows:

$$\begin{aligned} GZ(\theta(t), A_x(\xi(x,t))) &\approx GZ(\theta(t), A_x(\xi_{eff}(x,t))) = GZ(\theta(t), \xi_c(t)) \\ &= GZ_0(\theta(t)) + \delta GZ(\theta(t), \xi_c(t)) \\ &= \sum\nolimits_{m=1,3,5\cdots}^{N_\theta} C_{0m}\theta^m + \delta GZ(\theta(t), \xi_c(t)) \end{aligned} \tag{2.33}$$

where GZ_0 is the restoring arm in calm water, C_{0m}(m=1, 3, 5…) is the related roll restoring coefficient for the nonlinear odd function GZ_0 and δGZ is the variation of the restoring arm in waves. The restoring term $GZ(\theta(t), \xi_c(t))$ is a binary function with respect to the effective wave amplitude process $\xi_c(t)$ and the roll angle $\theta(t)$. By means of a standard hydrostatic software, this function is computed by applying the equivalent regular waves of the same length as the ship length but with different wave amplitudes amidships. Specifically, for an equivalent regular wave with a given value of the wave amplitude being located at amidships, the corresponding restoring arm for different heeling angles and for this wave amplitude can be calculated hydrostatically. In addition, the wave amplitude ξ_c >0 means a wave crest case and ξ_c <0 represents an equivalent wave with wave trough positioned amidships. Subsequently, the restoring arms for different values of the wave amplitude can be obtained and the restoring arm in equation (2.33) can be expressed by a set of couples of heeling angles and effective wave amplitudes.

A nonlinear expression is applied in this work in order to fit the GZ surface.

$$GZ(\theta(t), \xi_c(t)) = \sum\nolimits_{m=1,3,5\cdots}^{N_\theta} (C_{0m} + \sum\nolimits_{l=1}^{N_\xi} C_{wml}\xi_c^l(t)) \cdot \theta^m(t) \tag{2.34}$$

By combing the SDOF model (2.23) with the approximate restoring term (2.34), the complete expression can be obtained. Dividing it by (I_{44}+A_{44}), the final form of the differential equation is given as:

$$\ddot{\theta}(t) + b_{44}\dot{\theta}(t) + b_{44c}\dot{\theta}^3(t) + \sum\nolimits_{m=1,3,5\cdots}^{N_\theta} (c_{0m} + \sum\nolimits_{l=1}^{N_\xi} c_{wml}\xi_c^l(t)) \cdot \theta^m(t) = 0 \tag{2.35}$$

and the natural roll frequency can be determined as:

$$\omega_0 = \sqrt{\Delta C_{01}/(I_{44} + A_{44})} = \sqrt{c_{01}} \tag{2.36}$$

where $b_{44} = \hat{B}_{44}/(I_{44} + A_{44})$ and $b_{44c} = B_{44c}/(I_{44} + A_{44})$. The coefficients C_{0m} and C_{wml} (m=1,3,5…; l=1,2,3…) can be obtained from a least square fitting of $GZ(\theta(t),\xi_c(t))$ and correspondingly c_{0m}=ΔC_{0m}/(I_{44}+A_{44}), (m=1,3,5…) and c_{wml} = ΔC_{wml}/(I_{44}+A_{44}).

The state-space function of the SDOF model (2.35) is written as:

$$\begin{cases} dx_1 = x_2 dt \\ dx_2 = (-b_{44}x_2 - b_{44q}x_2 \mid x_2 \mid - \sum\nolimits_{m=1,3,5\cdots}^{N_\theta} (c_{0m} + \sum\nolimits_{l=1}^{N_\xi} c_{wlm}x_3^l)) \cdot x_1^m) dt \end{cases} \tag{2.37}$$

where x_1= $\theta(t)$, x_2= $\dot{\theta}(t)$ and x_3=$\xi_c(t)$ denotes the driving process for the dynamic system.

3 Stochastic Theory

This chapter describes the basic stochastic processes and the linear filter technique used to generate filtered white noise. The stochastic differential equations (SDE) used to describe the roll motion in random waves are developed by coupling the roll motion equation with the linear filter equation. The Fokker-Planck equation is derived to study the probabilistic evolution of the stochastic systems.

3.1 Stochastic Process

A *stochastic process* is a family of random variables describing the development in time or space of a stochastic phenomenon. In this Section, the concepts of Markov process, white noise process and Wiener process are introduced in order to build the stochastic dynamic systems for describing the roll motion in random seas.

3.1.1 Markov process

A stochastic process $X(t)$ is said to be a Markov process if it satisfies the following conditional probability:

$$F(x_n,t_n\,|x_{n-1},t_{n-1};x_{n-2},t_{n-2};\ldots;x_1,t_1)=F(x_n,t_n\,|x_{n-1},t_{n-1}) \tag{3.1}$$

where F denotes the conditional cumulative distribution function (CDF), x_n represent the state value at time t_n and $t_1< t_2 <\ldots<t_{n-1} < t_n$.

If $X(t)$ is a time-continuous process, the relationship in equation (3.1) is equivalent to

$$p(x_n,t_n\,|x_{n-1},t_{n-1};x_{n-2},t_{n-2};\ldots;x_1,t_1)=p(x_n,t_n\,|x_{n-1},t_{n-1}) \tag{3.2}$$

where p represents the conditional probability density function (PDF).

From equations (3.1) and (3.2), it is shown that the conditional probability of the random process at time t_n depends only on the immediate past value at time t_{n-1} and it is independent of the history of the process earlier than t_{n-1}. A Markov process with continuous state, such as the process described by equation (3.2), is called as a diffusion process, and a Markov process with discrete states is referred to as the Markov chain.

By applying equation (3.2), the joint density function can be written as:

$$p(x_n,t_n;x_{n-1},t_{n-1};\ldots;x_1,t_1)=p(x_1,t_1)\prod_{i=2}^{n}p(x_i,t_i\,|x_{i-1},t_{i-1}),i\geq 2 \tag{3.3}$$

in which, the conditional PDF, $p(x_i, t_i|x_{i-1}, t_{i-1})$ is referred to as the transition probability density (TPD). The process is called homogeneous Markov process, if the TPD is only depend on the time interval $\Delta t= t_i - t_{i-1}$, and independent of time instants t_i and t_{i-1}, i.e.

$$p(x_i,t_i\,|x_{i-1},t_{i-1})=p(\Delta t;x_i,x_{i-1}) \tag{3.4}$$

3.1.2 White noise process

The Markov model is only valid for the system excited by white noise or filtered white noise. In this thesis, the white noise process always represents Gaussian white noise. A stationary stochastic process $X(t)$ is called as the Gaussian white noise if this process is governed by a (double-sided) spectrum with a constant spectral density:

$$S(\omega)=\frac{\sigma^2}{2\pi} \tag{3.5}$$

where the constant $\sigma > 0$ is the noise level and $X(t)$ is a standard Gaussian white noise when $\sigma =1.0$ and denoted as $N(t)$. The constant spectral density implies that the energy of the process is uniformly distributed over the whole frequency region.

The autocorrelation function of the white noise process is given as:

$$R(\tau)=\int_{-\infty}^{+\infty}S(\omega)\exp(i\omega\tau)d\omega=\sigma^2\delta(\tau) \tag{3.6}$$

where $\delta(\cdot)$ is the Dirac delta function and $R(\tau)=0$ for all $\tau\neq 0$ which means independence for the values of the stochastic process at two distinct time instants, i.e., $N(s)$ is independent of $N(t)$ if $t \neq s$.

3.1.3 Wiener process

A stochastic process $W(t)$ is said to be a Wiener process (or Brownian motion), if the following properties are satisfied:

- $W(t)$ is a continuous process with independent increments.
- The distribution of increment $W(t+dt)$-$W(t)$ is Gaussian.
- $W(0)=0$.
- The increment $dW(t)=W(t+dt)$-$W(t)$ and $\mathrm{E}\{W(t+dt)\text{-}W(t)\} = 0$, $\mathrm{E}\{dW(t)dW(s)\}= 0$ for $t \neq s$ and $\mathrm{E}\{dW(t)^2\}= dt$.

in which, dt represents the time increment and $\mathrm{E}\{\cdot\}$ denotes the expectation. Since the Wiener process has independent increments, it is a Markov process. In addition, from

conditions 2 and 4, it is found that the increment of the Wiener process satisfies the following condition:

$$dW(t) = N(t)dt \tag{3.7}$$

i.e. formally, a Gaussian white noise is the derivate of a Wiener process.

The Wiener process will be applied in the linear filter technique used to generate filtered white noise and then the dynamic systems (2. 19) and (2. 37) will be extended to Markov systems.

3.2 Stochastic Differential Equation (SDE)

3.2.1 Linear filter technique

For the dynamic systems (2.19) and (2.37), the driving processes $m(t)$ and $\xi_c(t)$ are assumed to be stationary Gaussian processes and governed by specific spectra $S_{mm}(\omega)$ and $S_{\xi_c}(\omega)$, respectively. Since the Markov model is valid for the system driven by white noise or filtered white noise, the linear filter technique, also known as the shaping filter technique, is applied in order to generate filtered white noise which complies with the required spectrum.

Spanos (1983) was the pioneer in introducing the filter algorithms to approximate the wave elevation and wave kinematics. Due to its simplicity and practicality, the filter techniques were widely used to model the wave loads and evaluate the response of stochastic dynamic systems in the field of ocean engineering (Francescutto and Naito, 2004; Su, 2012; Thampi and Niedzwecki, 1992). In general, the linear filter technique is applicable only for stationary stochastic process, therefore the driving process $m(t)$ and $\xi_c(t)$ can be adequately approximated by a suitable filter.

Dostal et al. (2012) proposed a second-order linear filter and a fourth-order linear filter to model the narrow-banded target spectrum. In this thesis, these two linear filters are used to approximate the random driving process in the dynamic systems (2.19) and (2.37). The second-order linear filter is given as:

$$\begin{cases} dx_3 = (x_4 - \beta x_3)dt + \gamma dW \\ dx_4 = -\alpha x_3 dt \end{cases} \tag{3.8}$$

where x_3 and x_4 are the state variables in the filter equation with x_3 representing the filter output, i.e. the driving process. $dW(t)=W(t+dt)-W(t)$ is the increment of a Wiener process with $\mathrm{E}\{dW(t)\}=0$, $\mathrm{E}\{dW(t)dW(s)\} = 0$ for $t \neq s$ and $\mathrm{E}\{dW(t)^2\}= dt$. Furthermore α, β, γ are the parameters of the second-order linear filter. The spectrum generated by the differential equation (3.8) is given as:

$$S_{2nd}(\omega)=\frac{1}{2\pi}\frac{\gamma^2\omega^2}{(\alpha-\omega^2)^2+(\beta\omega)^2} \tag{3.9}$$

The fourth-order linear filter, which represents a more accurate approximation, is given by the following differential equation:

$$\begin{cases} dx_5=(x_6-\lambda_1 x_5)dt \\ dx_6=(x_7-\lambda_2 x_5)dt+\gamma_1 dW \\ dx_7=(x_8-\lambda_3 x_5)dt \\ dx_8=-\lambda_4 x_5 dt \end{cases} \tag{3.10}$$

where x_5, x_6 , x_7 and x_8 are variables introduced for the state-space representation and x_5 represents the filter output. The spectrum generated by equation (3.10) will have the following form.

$$S_{4th}(\omega)=\frac{1}{2\pi}\frac{\gamma_1^2\omega^4}{[(\beta_1-\omega^2)^2+(\alpha_1\omega)^2][(\beta_2-\omega^2)^2+(\alpha_2\omega)^2]} \tag{3.11}$$

in which, α_1, α_2, β_1, β_2 and γ_1 are the parameters in the fourth-order linear filter and the parameters λ_1, λ_2, λ_3, and λ_4 in equation (11) can be determined by the following relationship: $\lambda_1=\alpha_1+\alpha_2$, $\lambda_2=\beta_1+\beta_2+\alpha_1\alpha_2$, $\lambda_3=\alpha_1\beta_2+\alpha_2\beta_1$, $\lambda_4=\beta_1\beta_2$.

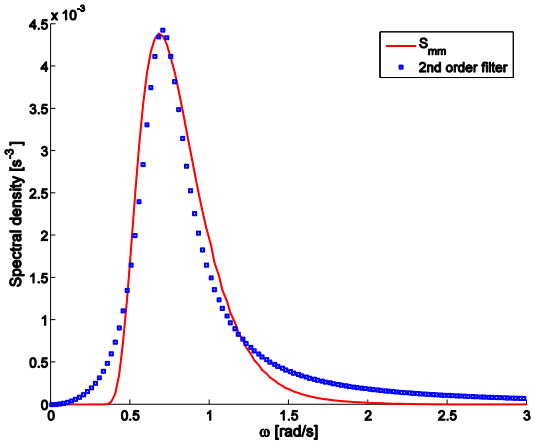

Figure 3.1: Target spectrum and the corresponding second-order filtered spectrum

The parameters α, β, γ in the second-order filter and α_1, α_2, β_1, β_2, γ_1 in the fourth-order filter are determined by a least-square algorithm which is utilized for fitting of the target spectrum. The bandwidth and the peak frequency of the filtered spectra can be adjusted by changing the values of these parameters. It is worth emphasizing that the filtered spectra (3.9) and (3.10) are double-sided, while the wave spectrum and the wave excitation spectrum are physically single-sided. This difference must be considered in the practical simulation. Figures 3.1 and 3.2 shows two examples of the filtered spectra

generated by equation (3.9) and equation (3.11), respectively.

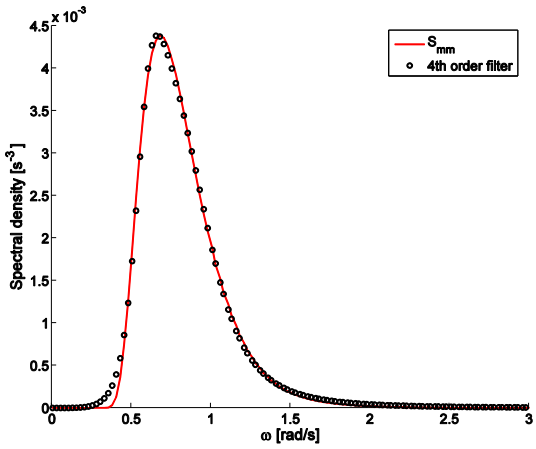

Figure 3.2: Target spectrum and the corresponding fourth-order filtered spectrum

3.2.2 Coupled dynamic systems

In this part, the dynamic system (2.19) is taken as the example for presenting the extension of the dynamic system. By combing the SDOF model (2.19) with the linear filters (3.8) and (3.10), the dynamic system will be extended into the following four-dimensional (4D) system described as

$$\begin{cases} dx_1 = x_2 dt \\ dx_2 = (-b_{44}x_2 - b_{44q}x_2 \mid x_2 \mid -c_1 x_1 + c_3 x_1^3 + x_3)dt \\ dx_3 = (x_4 - \beta x_3)dt + \gamma dW \\ dx_4 = -\alpha x_3 dt \end{cases} \tag{3.12}$$

and the the six-dimensional (6D) system is written as:

$$\begin{cases} dx_1 = x_2 dt \\ dx_2 = (-b_{44}x_2 - b_{44q}x_2 \mid x_2 \mid -c_1 x_1 + c_3 x_1^3 + x_5)dt \\ dx_5 = (x_6 - \lambda_1 x_5)dt \\ dx_6 = (x_7 - \lambda_2 x_5)dt + \gamma_1 dW \\ dx_7 = (x_8 - \lambda_3 x_5)dt \\ dx_8 = -\lambda_4 x_5 dt \end{cases} \tag{3.13}$$

The coupled dynamic systems (3.12) and (3.13) can be regarded as Markov systems and then expressed as the following Ito stochastic differential equation (SDE):

$$d\mathbf{x} = \mathbf{a}(\mathbf{x}, t)dt + \mathbf{b}(t)d\mathbf{W}(t) \tag{3.14}$$

where $\mathbf{x}(t)$ is a state-space vector process (e.g. $\mathbf{x}(t) = (x_1(t), x_2(t), x_3(t), x_4(t))^{\mathrm{T}}$ for the 4D

dynamic system), the vector $\mathbf{a}(\mathbf{x}, t)$ represents the drift term and $\mathbf{b}(t)d\mathbf{W}(t)$ is the diffusive term and $d\mathbf{W}(t) = \mathbf{W}(t+dt)-\mathbf{W}(t)$ represents a vector of increments of independent standard Wiener processes.

3.2.3 Solution to the SDE

The solution of a SDE is ambiguous, and basically, the strong solution and the weak solution concepts are used to define the solution from a mathematical view. Taking the Markov process $\mathbf{x}(t)$ in equation (3.14) as an example, the first definition reflects the interpretation that the process $\mathbf{x}(t)$ is determined by the governing equation and the exogenous input of the initial condition $\mathbf{x}_0$ at time t_0 in combination with the path of the Wiener process $\mathbf{W}(t)$ which is given in advance.

The other way of solving the SDE is to find the (conditional) response probability density function, $p(\mathbf{x}, t| \mathbf{x}_0, t_0)$, for the process $\mathbf{x}(t)$ if only the functions of $\mathbf{a}(\mathbf{x}, t)$ and $\mathbf{b}(t)$ are given. From a modelling point of view, the weak solution concept is more natural, since it does not specify the Wiener process $\mathbf{W}(t)$ beforehand. More specifically, the first interpretation can be considered as a deterministic interpretation (i.e. it deals with a generic single realization of the stochastic process), on the other hand, the second interpretation is based on the probabilistic properties of the process (i.e. the whole ensemble domain is considered).

For the dynamic systems studied in this thesis, the weak solution concept is applied. The response PDF, $p(\mathbf{x}, t| \mathbf{x}_0, t_0)$ will converge by increasing the time t to a stationary PDF, which is independent on the initial condition $\mathbf{x}_0$. Therefore, the response PDF can be written as $p(\mathbf{x}, t)$ and the influence from initial conditions can be neglected.

3.3 Fokker-Planck Equation

It is well known that Fokker-Planck equations describe the evolution of stochastic systems and the probabilistic properties of the Markov process $\mathbf{x}(t)$ is governed by the corresponding Fokker-Planck equation. In this Section, the Fokker-Planck equation for the process $\mathbf{x}(t)$ is derived and then the response probability density function of the dynamic system can be obtained by solving the Fokker-Planck equation.

The PDF of the process $\mathbf{x}$ at time t, $p(\mathbf{x},t)$, can be obtained by the basic equation, i.e. the well-known Chapman-Kolmogorov equation:

$$p(\mathbf{x},t) = \int p(\mathbf{x},t \mid \mathbf{x}',t')p(\mathbf{x}',t')d\mathbf{x}' \tag{3.15}$$

where $\mathbf{x}'$ and $p(\mathbf{x}', t')$ represent the process and PDF at a previous time t'.

For the time interval $\Delta t = t - t'$, the characteristic function for the random increment $\mathbf{x}$-$\mathbf{x}'$ is introduced:

$$M(u;\mathbf{x}') = E\left[\exp(iu(\mathbf{x}-\mathbf{x}'))\right] = \int \exp(iu(\mathbf{x}-\mathbf{x}'))\cdot p(\mathbf{x},t\,|\,\mathbf{x}',t')\,d\mathbf{x} \tag{3.16}$$

with the inverse function given as:

$$p(\mathbf{x},t\,|\,\mathbf{x}',t') = \frac{1}{2\pi}\int \exp(-iu(\mathbf{x}-\mathbf{x}'))\cdot M(u;\mathbf{x}')du \tag{3.17}$$

Substituting equation (3.17) into equation (3.15), the following expression can be obtained:

$$p(\mathbf{x},t) = \frac{1}{2\pi}\int\int \exp(-iu(\mathbf{x}-\mathbf{x}'))\cdot M(u;\mathbf{x}')\cdot p(\mathbf{x}',t')du d\mathbf{x}' \tag{3.18}$$

According to the property of the characteristic function $M(u;\,\mathbf{x}')$, it can be expressed as:

$$\begin{aligned} M(u;\mathbf{x}') &= 1 + \sum_{j=1}^{\infty}\frac{(iu)^j}{j!}\mu_j(\mathbf{x}') \\ \mu_j(\mathbf{x}') &= E\left[(\mathbf{x}-\mathbf{x}')^j\right] \end{aligned} \tag{3.19}$$

where μ_j represents the j-th moment of the increment $\mathbf{x}$-$\mathbf{x}'$. Therefore, equation (3.18) is transformed as:

$$p(\mathbf{x},t) = \sum_{j=0}^{\infty}\frac{1}{j!}\frac{1}{2\pi}\int\int \exp(-iu(\mathbf{x}-\mathbf{x}'))\cdot(iu)^j\,du\,\mu_j(\mathbf{x}')p(\mathbf{x}',t')d\mathbf{x}' \tag{3.20}$$

Because

$$\begin{aligned} \frac{1}{2\pi}\int \exp(-iu(\mathbf{x}-\mathbf{x}'))(iu)^j\,du &= (-\frac{\partial}{\partial\mathbf{x}})^j\,\frac{1}{2\pi}\int \exp(-iu(\mathbf{x}-\mathbf{x}'))du \\ &= (-\frac{\partial}{\partial\mathbf{x}})^j\,\delta(\mathbf{x}-\mathbf{x}') \end{aligned} \tag{3.21}$$

Since $\int \delta(\mathbf{x}-\mathbf{x}')\mu_j(\mathbf{x}')d\mathbf{x}' = \mu_j(\mathbf{x})$and we can find that

$$p(\mathbf{x},t) = p(\mathbf{x}',t') + \sum_{j=0}^{\infty}\frac{1}{j!}(-\frac{\partial}{\partial\mathbf{x}})^j\left[\mu_j(\mathbf{x})p(\mathbf{x},t)\right] \tag{3.22}$$

Divding equation (3.22) by Δt and passing to the limit $\Delta t \to 0$, the following expression can be obtained:

$$\frac{\partial p(\mathbf{x},t)}{\partial t} = \sum_{j=0}^{\infty}\frac{1}{j!}(-\frac{\partial}{\partial\mathbf{x}})^j\left[K_j(\mathbf{x})p(\mathbf{x},t)\right] \tag{3.23}$$

in which

$$K_j(\mathbf{x}) = \lim_{\Delta t \to 0} \frac{\mu_j(\mathbf{x})}{\Delta t}, \; j = 1, 2, \ldots. \tag{3.24}$$

where $K_j(\mathbf{x})$ represents the intensity coefficient and equation (3.24) is called the Kramers-Moyal expansion (Risken, 1989).

Assume that the Markov process $\mathbf{x}(t)$ is continuous and the Kramers-Moyal expansion stops with the higher-order intensity K_3, K_4… equals to zero, the distribution $p(\mathbf{x}, t)$ of the diffusion process $\mathbf{x}(t)$ follows the Fokker-Planck equation which is written as:

$$\frac{\partial p(\mathbf{x},t)}{\partial t} = -\frac{\partial}{\partial \mathbf{x}}\left[K_1(\mathbf{x})p(\mathbf{x},t)\right] + \frac{1}{2}\frac{\partial^2}{\partial \mathbf{x}^2}\left[K_2(\mathbf{x})p(\mathbf{x},t)\right] \tag{3.25}$$

Given the initial distribution $p(\mathbf{x}, t_0| \mathbf{x}_0, t_0)$, it can be shown that the resulting probability density is just the TPD, $p(\mathbf{x}, t| \mathbf{x}_0, t_0)$. Therefore, the transition probability can be found as the solution of the equation:

$$\frac{\partial p(\mathbf{x},t|\mathbf{x}_0,t_0)}{\partial t} = -\frac{\partial}{\partial \mathbf{x}}\left[K_1(\mathbf{x})p(\mathbf{x},t|\mathbf{x}_0,t_0)\right] + \frac{1}{2}\frac{\partial^2}{\partial \mathbf{x}^2}\left[K_2(\mathbf{x})p(\mathbf{x},t|\mathbf{x}_0,t_0)\right] \tag{3.26}$$

Furthermore, there is a close connection between the Fokker-Planck equation and the SDE equation, for one-dimensional case, the Fokker-Planck equation is given as:

$$\begin{aligned}\frac{\partial p(x,t|x_0,t_0)}{\partial t} &= -\frac{\partial}{\partial x}\left[K_1(x)p(x,t|x_0,t_0)\right] + \frac{1}{2}\frac{\partial^2}{\partial x^2}\left[K_2(x)p(x,t|x_0,t_0)\right] \\ &= -\frac{\partial}{\partial x}\left[a(x,t)p(x,t|x_0,t_0)\right] + \frac{1}{2}\frac{\partial^2}{\partial x^2}\left[b^2(t)p(x,t|x_0,t_0)\right]\end{aligned} \tag{3.27}$$

in which $a(x, t)$ represents the drift coefficient and $b^2(t)$ is the diffusion coefficient for the one-dimensional SDE, $dx = a(x, t)dt + b(t)d\mathrm{W}(t)$.

For n-dimensional SDE (3.14), $n > 1$, the Fokker-Planck equation is written as:

$$\begin{aligned}\frac{\partial p(\mathbf{x},t|\mathbf{x}_0,t_0)}{\partial t} &= -\frac{\partial}{\partial \mathbf{x}}\left[K_1(\mathbf{x})p(\mathbf{x},t|\mathbf{x}_0,t_0)\right] + \frac{1}{2}\frac{\partial^2}{\partial \mathbf{x}^2}\left[K_2(\mathbf{x})p(\mathbf{x},t|\mathbf{x}_0,t_0)\right] \\ &= \sum_{i=1}^{n} -\frac{\partial}{\partial x_i}\left[\mathbf{a}(\mathbf{x},t)p(\mathbf{x},t|\mathbf{x}_0,t_0)\right] \\ &\quad + \frac{1}{2}\sum_{i=1}^{n}\sum_{j=1}^{n}\frac{\partial^2}{\partial x_i \partial x_j}\left[(\mathbf{b}(t)\cdot\mathbf{b}^T(t))_{ij}\, p(\mathbf{x},t|\mathbf{x}_0,t_0)\right]\end{aligned} \tag{3.28}$$

Based on the derivation above, the Fokker-Planck equations for the one-dimensional and multidimensional SDE (14) are obtained. Furthermore, the Fokker-Planck equation can also be derived by other ways mentioned in Ochi (1990) and the methodologies for solving the Fokker-Planck equation will be described in Chapter 4.

4 Methodology

In this chapter, two categories of methodology are introduced in order to calculate and evaluate the response statistics of the roll motion in random seas. The first is the Markov-based 4D path integration method used for calculating the stochastic roll response for a vessel in random beam seas, and the principle as well as the numerical implementation for this state-of-the-art technique are presented in Sections 4.1 and 4.2, respectively. The straightforward Monte Carlo simulation, i.e. the second methodology which is based on the numerical calculation of the differential equation and direct counting work is introduced to verify the results calculated by the efficient 4D PI method. Furthermore, an efficient extrapolation scheme is introduced to the MCS technique and the enhanced (efficient) MCS method is able to provide reasonable and accurate estimation of the extreme response with a dramatic reduction of computation time.

4.1 Path Integration Method

The path integration (PI) method based on the Markov property of the dynamic system, is an efficient approximation for solving the FP equation. The main advantage of the Markov dynamic system and the PI method is that a host of useful and accurate response statistics can be obtained within one calculation. Wehner and Wolfer (1983) were the first to apply the numerical PI method to solve nonlinear FP equations and then various PI procedures, e.g. Naess and Moe (2000), Pirrotta and Santoro (2011), Lin and Yim (1995), Wang (2014), etc., have been developed and applied to address certain problems in the area of engineering. In the field of ocean engineering, Naess and Johnsen (1993) developed a three-dimensional (3D) PI procedure to estimate the response statistics of moored offshore structures. This topic as well as the 3D PI approach have were extended in Karlsen's (2006) work in order to calculate the response statistics of nonlinear, compliant offshore structures. In this dissertation, the PI algorithm is extended into four-dimensional (4D) in order to study the stochastic roll response in random beam seas. The main principle as well as the numerical implementation of the PI method will be introduced and described in Sections 4.1 and 4.2, respectively.

4.1.1 Time discretization of the SDE

In order to apply the numerical PI method, the SDE should be discretized with respect to time t. In this Section, the 4D dynamic system (3.12) is selected as the example case. The corresponding continuous SDE, i.e. equation (3.14), can be discretized as:

$$\mathbf{x} = \mathbf{x}' + \tilde{\mathbf{a}}(\mathbf{x}', t')\Delta t + \tilde{\mathbf{b}}(t')\Delta \mathbf{W}(t') \tag{4.1}$$

in which $\mathbf{x} = \mathbf{x}(t)$, $\mathbf{x}' = \mathbf{x}(t')$ and $\Delta t = t - t'$ is the finite positive time increment. $\tilde{\mathbf{a}}(\mathbf{x}', t')$ and $\tilde{\mathbf{b}}(t')$ are the transition functions of the discretization equation for the deterministic and stochastic parts, respectively. The time sequence $\{\mathbf{x}(t_0 + k \cdot \Delta t)\}_{k=0}^{\infty}$ is a Markov chain with initial time t_0 and it can approximate the time-continuous Markov process $\mathbf{x}$ described in the SDE (3.14) when the time decrement Δt is sufficient small. Since $\mathbf{W}(t)$ is a Wiener process, the independent increment $\Delta \mathbf{W}(t') = \mathbf{W}(t) - \mathbf{W}(t')$ is a Gaussian variable for every t'.

There are several ways to choose the transition functions in equation (4.1), the simplest discretization scheme is the Euler-Maruyama approximation, which is expressed as.

$$\mathbf{x} = \mathbf{x}' + \mathbf{a}(\mathbf{x}', t')\Delta t + \mathbf{b}(t')\Delta \mathbf{W}(t') \tag{4.2}$$

However, if we consider only the deterministic part of equation (4.2), the Euler-Maruyama approximation reduces to the Euler approximation: $\mathbf{x} = \mathbf{x}' + \mathbf{a}(\mathbf{x}', t')\Delta t$ with the accuracy only to the order of $O(\Delta t^2)$. Experiments have shown that, for Markov systems, the accuracy associated with approximating the deterministic terms is the most important (Mo, 2008). Therefore, a fourth-order Runge-Kutta scheme with the accuracy to the order of $O(\Delta t^5)$ should be implemented in order to improve the accuracy of the discretization process in following the time evolution of the deterministic part of equation (3.14). Then equation (4.2) can be replace by the following fourth-order Runge-Kutta-Maruyama (RKM) approximation:

$$\mathbf{x} = \mathbf{x}' + \mathbf{r}(\mathbf{x}', t', \Delta t) + \mathbf{b}(t')\Delta \mathbf{W}(t') \tag{4.3}$$

where the vector $\mathbf{r}(\mathbf{x}', t', \Delta t)$ is the explicit fourth-order Runge-Kutta (RK4) approximation. Generally, the RK4 scheme is given as:

$$\begin{aligned}
&\mathbf{x} = \mathbf{x}' + \mathbf{r}(\mathbf{x}', t', \Delta t) \\
&\mathbf{k}_1 = \mathbf{a}(\mathbf{x}', t'), \\
&\mathbf{k}_2 = \mathbf{a}(\mathbf{x}' + \tfrac{\Delta t}{2}\mathbf{k}_1, t' + \tfrac{\Delta t}{2}), \\
&\mathbf{k}_3 = \mathbf{a}(\mathbf{x}' + \tfrac{\Delta t}{2}\mathbf{k}_2, t' + \tfrac{\Delta t}{2}), \\
&\mathbf{k}_4 = \mathbf{a}(\mathbf{x}' + \Delta t\mathbf{k}_3, t' + \Delta t), \\
&\mathbf{r}(\mathbf{x}', t', \Delta t) = \tfrac{1}{6}(\mathbf{k}_1 + 2\mathbf{k}_2 + 2\mathbf{k}_3 + \mathbf{k}_4).
\end{aligned} \tag{4.4}$$

4.1.2 Principle of the PI method

Unlike the direct numerical techniques, such as the finite element method and the finite difference method, aiming to calculate the response statistics by solving the FP equation directly, the PI method captures the probabilistic evolution of the process $\mathbf{x}(t)$ by taking

advantage of the Markov property described in Section 3.1. In principle, the PI method is an approximation method and the evolution of the response statistics is obtained by a step-by-step solution technique based on short time steps.

If an initial PDF, $p(\mathbf{x}(t_0), t_0)$ is given, the distribution at time $t_1 = t_0 + \Delta t$ can be obtained by the Chapman-Kolmogorov equation:

$$p(\mathbf{x}^{(1)}, t_1) = \int_{R^4} p(\mathbf{x}^{(1)}, t_1 \mid \mathbf{x}^{(0)}, t_0) p(\mathbf{x}^{(0)}, t_0) d\mathbf{x}^{(0)} \tag{4.5}$$

where $\mathbf{x}^{(0)} = \mathbf{x}(t_0)$, $\mathbf{x}^{(1)} = \mathbf{x}(t_1)$.

Similarly, for the distribution at time $t_2 = t_1 + \Delta t$, it is given as:

$$p(\mathbf{x}^{(2)}, t_2) = \int_{R^4} p(\mathbf{x}^{(2)}, t_2 \mid \mathbf{x}^{(1)}, t_1) p(\mathbf{x}^{(1)}, t_1) d\mathbf{x}^{(1)} \tag{4.6}$$

and inserting equation (4.6) into equation (4.5), it leads to:

$$p(\mathbf{x}^{(2)}, t_2) = \int_{R^4} \int_{R^4} p(\mathbf{x}^{(2)}, t_2 \mid \mathbf{x}^{(1)}, t_1) p(\mathbf{x}^{(1)}, t_1 \mid \mathbf{x}^{(0)}, t_0) p(\mathbf{x}^{(0)}, t_0) d\mathbf{x}^{(0)} d\mathbf{x}^{(1)} \tag{4.7}$$

Therefore, the time evolution of the PDF of $\mathbf{x}(t)$ can be determined by the iterative algorithm (4.8) when the initial PDF is given,

$$p(\mathbf{x}, t) = \int_{R^4} \cdots \int_{R^4} \prod_{k=1}^{n} p(\mathbf{x}^{(k)}, t_k \mid \mathbf{x}^{(k-1)}, t_{k-1}) \cdot p(\mathbf{x}^{(0)}, t_0) d\mathbf{x}^{(0)} \ldots d\mathbf{x}^{(k-1)} \tag{4.8}$$

where $\mathbf{x} = \mathbf{x}^{(k)}$, $t = t_k = t_0 + (k\text{-}1)\Delta t$ and $d\mathbf{x} = \prod_{i=1}^{4} x_i$ for the 4D case.

For the one time-step TPD, also known as the short-time conditional PDF, $p(\mathbf{x}^{(k)}, t_k \mid \mathbf{x}^{(k-1)}, t_{k-1})$ is only dependent on the time increment Δt, i.e. the stochastic process $\mathbf{x}(t)$ for the dynamic system (3.14) is a homogeneous Markov process. The one time-step TPD, $p(\mathbf{x}, t \mid \mathbf{x}', t')$, is also governed by the Fokker-Planck equation, which is given as:

$$\begin{aligned} \frac{\partial p(\mathbf{x}, t \mid \mathbf{x}', t')}{\partial t} &= \sum_{i=1}^{4} -\frac{\partial}{\partial x_i} a_i(\mathbf{x}, t) p(\mathbf{x}, t \mid \mathbf{x}', t') \\ &\quad + \frac{1}{2} \sum_{i=1}^{4} \sum_{j=1}^{4} \frac{\partial^2}{\partial x_i \partial x_j} (\mathbf{b}(t) \cdot \mathbf{b}^T(t))_{ij} p(\mathbf{x}, t \mid \mathbf{x}', t') \end{aligned} \tag{4.9}$$

The one time-step TPD can be approximated by the following degenerate Gaussian distribution with the accuracy to the order of $O(\Delta t^2)$ (Risken, 1989):

$$\begin{aligned} p(\mathbf{x}, t \mid \mathbf{x}', t') &= \delta(x_1 - x_1' - r_1(\mathbf{x}', t', \Delta t)) \cdot \delta(x_2 - x_2' - r_2(\mathbf{x}', t', \Delta t)) \\ &\quad \cdot \tilde{p}(x_3, t \mid x_3', t') \cdot \delta(x_4 - x_4' - r_4(\mathbf{x}', t', \Delta t)) \end{aligned} \tag{4.10}$$

and

$$\tilde{p}(x_3,t \mid x_3',t')=\frac{1}{\sqrt{2\pi\gamma^2\Delta t}}\cdot\exp\left\{-\frac{(x_3-x_3'-r_3(\mathbf{x}',t',\Delta t))^2}{2\gamma^2\Delta t}\right\} \tag{4.11}$$

in which $\mathbf{r}_i(\mathbf{x}', t')\,\Delta t$, i=1,2,3,4 are Runge-Kutta increments for the state space variables.

For the one time-step integration (3.15) with the one time-step TPD given by equations (4.9) and (4.10), it can be expressed as:

$$\begin{aligned} p(\mathbf{x},t) &= \int_{R^4} p(\mathbf{x},t \mid \mathbf{x}',t')p(\mathbf{x}',t')d\mathbf{x}' \\ &= \int_{R^4} \delta(x_1-x_1'-r_1(\mathbf{x}',t',\Delta t))\cdot\delta(x_2-x_2'-r_2(\mathbf{x}',t',\Delta t)) \\ &\quad \cdot\delta(x_4-x_4'-r_4(\mathbf{x}',t',\Delta t))\cdot\tilde{p}(x_3,t \mid x_3',t')p(\mathbf{x}',t')d\mathbf{x}' \end{aligned} \tag{4.12}$$

Due to the property of the delta function, δ(·), equation (4.12) will reduce to the following one-dimensional integral:

$$p(\mathbf{x},t)=\int_{R^1}\tilde{c}\cdot\tilde{p}(x_3,t \mid x_3',t')p(\mathbf{x}',t')dx_3' \tag{4.13}$$

where $\tilde{c}$ is a constant due to the integration of delta function and the PDF (4.13) follows the normalization function:

$$\int_{R^4} p(\mathbf{x},t)d\mathbf{x}=1 \tag{4.14}$$

However, numerical calculation for equation (4.13) is difficult since the range of integration is difficult or even impossible to find. Therefore, a substitution $g(\mathbf{x}')=\mathbf{x}'+\mathbf{r}_i(\mathbf{x}',t')\Delta t$ is introduced in order to simplify the integral and then the one-dimensional integral will be transformed as (Karlsen, 2006):

$$p(\mathbf{x},t)=\int_{R^1}\left|J_{g^{-1}}\right|\cdot\tilde{p}(x_3,t \mid \bar{x}_3,t')p(g^{-1}(x_1,x_2,\bar{x}_3,x_4),t')d\bar{x}_3 \tag{4.15}$$

where $g^{-1}(x_1,x_2,\bar{x}_3,x_4)$ is the unique vector $\mathbf{x}'=(x_1',x_2',x_3',x_4')$ and $\left|J_{g^{-1}}\right|$ is a Jacobi determinant. $J_{g^{-1}}$ is defined as:

$$J_{g^{-1}}=\begin{bmatrix} \frac{\partial g_1^{-1}}{\partial x_1} & \frac{\partial g_1^{-1}}{\partial x_2} & \frac{\partial g_1^{-1}}{\partial x_3} & \frac{\partial g_1^{-1}}{\partial x_4} \\ \frac{\partial g_2^{-1}}{\partial x_1} & \frac{\partial g_2^{-1}}{\partial x_2} & \frac{\partial g_2^{-1}}{\partial x_3} & \frac{\partial g_2^{-1}}{\partial x_4} \\ \frac{\partial g_3^{-1}}{\partial x_1} & \frac{\partial g_3^{-1}}{\partial x_2} & \frac{\partial g_3^{-1}}{\partial x_3} & \frac{\partial g_3^{-1}}{\partial x_4} \\ \frac{\partial g_3^{-1}}{\partial x_1} & \frac{\partial g_4^{-1}}{\partial x_2} & \frac{\partial g_4^{-1}}{\partial x_3} & \frac{\partial g_4^{-1}}{\partial x_4} \end{bmatrix} \tag{4.16}$$

and $\tilde{p}(x_3,t \mid \bar{x}_3,t')$ is given as

$$\tilde{p}(x_3,t\,|\,\bar{x}_3,t') = \frac{1}{\sqrt{2\pi\gamma^2\Delta t}}\cdot\exp\left\{-\frac{(x_3-\bar{x}_3)^2}{2\gamma^2\Delta t}\right\} \tag{4.17}$$

Equation (4.8) describes the mathematical principle of the PI approach and equations (4.13)-(4.17) provide the basic methods for the numerical integration. Moreover, assume that the dynamic system is stationary, which will be mentioned in Section 4.4, the stationary distribution $f(\mathbf{x})$ for the random process $\mathbf{x}$ will be given as:

$$f(\mathbf{x}) = \lim_{t\to\infty} p(\mathbf{x},t) = \lim_{k\to\infty} p(\mathbf{x}^{(k)},t_k) \tag{4.18}$$

4.2 Numerical Implementation

In this Section, the numerical implementation of the 4D PI method, including the computation grid, interpolation methods and the integration techniques will be introduced.

4.2.1 Computation domain and grid

Basically, the numerical methods aiming to find the probabilistic distribution of the SDE are based on some discretization with respect to time and space, i.e. cell-to-cell mapping. For such cell mapping methods, a reasonable computation domain and the corresponding computation grid have to be determined at first (Pirrotta and Santoro, 2011). The computation domain is selected to be symmetrical in all dimensions and the size of the computation region in each dimension is identified by running a MCS with a low number of samples. For each dimension, the computation region is selected as:

$$-c_i\sigma_i \le x_i \le c_i\sigma_i,\ i=1,2,3,4 \tag{4.19}$$

in which σ_i is the standard deviation for i-th dimension estimated by the above simple MCS and the parameter c_i is a factor used to adjust the size of computation region.

Then, dividing the computation region (4.19) in a number of n_i -1 intervals uniformly. n_i denotes the grid number (or grid points) for each dimension and the computation cost as well as the storage needed for computation depend heavily on the dimensionality of the system and the grid number in each dimension.

For the numerical PI technique, the initial distribution $p(\mathbf{x}^{(0)}, t_0)$ used for the iterative algorithm (4.8) should be selected based on the computation region and grid in each dimension. It is chosen as a 4D Gaussian PDF with zero mean and variances evaluated by the above straightforward MCS.

$$p(\mathbf{x}^{(0)},t_0)=\prod_{i=1}^{4}\frac{1}{\sqrt{2\pi\sigma_i^2}}\exp(-\frac{x_{ij}^2}{2\sigma_i^2}),\ i=1,2,3,4;\ j=1,2,\ldots n_i \tag{4.20}$$

and the value of j-th grid point in i-th dimension, x_{ij} is given as:

$$\begin{aligned} x_{ij} &= -c_i\sigma_i+(j-1)dx_i \\ dx_i &= \frac{2c_i\sigma_i}{(n_i-1)} \end{aligned} \tag{4.21}$$

Since the simple MCS ensures the initial 4D Gaussian PDF include all the information corresponding to the selected parameters in the dynamic system (3.12) (Yurchenko et al., 2013), the initial distribution expressed by equations (4.20) and (4.21) could significantly improve the computational efficiency, even though the final stationary distribution $f(\mathbf{x})$ is independent of the initial distribution $p(\mathbf{x}^{(0)}, t_0)$.

4.2.2 Back-stepping scheme

For the numerical integration of equation (4.15), the substitution $g(\mathbf{x}')=\mathbf{x}'+\mathbf{r}_i(\mathbf{x}',t')\Delta t$ makes another challenge since we have to find $\mathbf{x}'$ and calculate $p(g^{-1}(x_1,x_2,\bar{x}_3,x_4),\ t)$. However, the value of the distribution p is known only at the grid points, but $\mathbf{x}' = g^{-1}(x_1,x_2,\bar{x}_3,x_4)$ is generally not in the grid, for which we store function values for the distribution p. A possible way is to use the values we already have for the distribution p at the former time t' at the grid points to interpolate the values at $\mathbf{x}'$, i.e. $g^{-1}(x_1,x_2,\bar{x}_3,x_4)$. In order to find $\mathbf{x}'$ at the former time-step, a back-stepping fourth-order Runge-Kutta scheme is introduced

$$\begin{aligned} &\mathbf{x}'=\bar{\mathbf{x}}-\mathbf{r}(\bar{\mathbf{x}},t,\Delta t)\\ &\mathbf{k}_1=\mathbf{a}(\bar{\mathbf{x}},t),\\ &\mathbf{k}_2=\mathbf{a}(\bar{\mathbf{x}}-\tfrac{\Delta t}{2}\mathbf{k}_1,t-\tfrac{\Delta t}{2}),\\ &\mathbf{k}_3=\mathbf{a}(\bar{\mathbf{x}}-\tfrac{\Delta t}{2}\mathbf{k}_2,t-\tfrac{\Delta t}{2}),\\ &\mathbf{k}_4=\mathbf{a}(\bar{\mathbf{x}}-\Delta t\mathbf{k}_3,t-\Delta t),\\ &\mathbf{r}(\mathbf{x},t,\Delta t)=\tfrac{1}{6}(\mathbf{k}_1+2\mathbf{k}_2+2\mathbf{k}_3+\mathbf{k}_4). \end{aligned} \tag{4.22}$$

in which $\bar{\mathbf{x}}=(x_1,x_2,\bar{x}_3,x_4)$.

Since the back-stepping procedure (4.22) is accurate to the order of $O(\Delta t^5)$, it can provide satisfactory values of $\mathbf{x}'$ at time t', i.e., the corresponding backward-mapped points at time t' for the grid points at time t.

4.2.3 Interpolation methods

In the current work, B-splines are applied in order to find the distribution p at the backward-mapped points, i.e. $\mathbf{x}' = g^{-1}(\bar{\mathbf{x}})$ and some basic B-spline interpolation schemes on a generalized grid are herein introduced.

The knots of the B-splines are assumed to be at the grid points, i.e. the knot sequence has constant increments due to the uniform grid described in equation (4.21). In one dimension, for the knot sequence of $y_1 < y_2 < \ldots < y_l < \ldots < y_m$, when the values of the function $h(x)$ at the knot points are given, the interpolation can be performed as follows:

$$\sum_{k=1}^{K} \Gamma_k B_{k,j}(y_l) = h(y_l) \tag{4.23}$$

in which m denotes the number of knot points (or the number of grid points). Γ_k, $k = 1, 2, \ldots, K$ are spline coefficients or control points, $B_{k,j}$ is the basis function and j represents the order of the B-spline.

The linear system (4.23) can be written in a matrix form,

$$\mathbf{S\Gamma} = \mathbf{v} \tag{4.24}$$

or

$$\begin{bmatrix} B_{1,j}(y_1) & B_{2,j}(y_1) & \cdots & B_{K,j}(y_1) \\ B_{1,j}(y_2) & B_{2,j}(y_2) & \cdots & B_{K,j}(y_2) \\ \vdots & & & \vdots \\ B_{1,j}(y_m) & B_{2,j}(y_m) & \cdots & B_{K,j}(y_m) \end{bmatrix} \begin{bmatrix} \Gamma_1 \\ \Gamma_2 \\ \vdots \\ \Gamma_K \end{bmatrix} = \begin{bmatrix} h(y_1) \\ h(y_2) \\ \vdots \\ h(y_m) \end{bmatrix} \tag{4.25}$$

where the vector $\mathbf{v}$ contains the values of the function $h(y)$ at the knot points $y_1, y_2 \ldots y_m$, the vector $\mathbf{\Gamma}$ contains the spline coefficients and the matrix $\mathbf{S}$ is called collocation matrix defined by $\mathbf{S}_{lk} = B_{k,j}(y_l)$.

The spline coefficients can be obtained by solving equation (4.24) and then the interpolating approximate function is given as:

$$\tilde{h}(y) = \sum_{k=1}^{K} \Gamma_k B_{k,j}(y) \tag{4.26}$$

and the function values for the variable y which is not at the knot points (or grid points) can be approximated by this expression.

When the knots of the B-splines are assumed to be at the grid points, it leads to cardinal splines, where all the basis functions $B_{k,j}$ have the same shape and are just translated along the axis. A basis function can be expressed analytically in some reference domain, and then scaled and translated to give the complete basis of the cardinal splines (Mo,

2008). Cubic B-spline is the most widely used in spline interpolation, it is composed of four pieces which are given as follows in the reference domain $[0,1]$:

$$\begin{aligned} p_1 &= \tfrac{1}{6}y^3 \\ p_2 &= -\tfrac{1}{2}y^3 + \tfrac{1}{2}y^2 + \tfrac{1}{2}y + \tfrac{1}{6} \\ p_3 &= \tfrac{1}{2}y^3 - y^2 + \tfrac{2}{3} \\ p_4 &= -\tfrac{1}{6}y^3 + \tfrac{1}{2}y^2 - \tfrac{1}{2}y + \tfrac{1}{6}, y \in [0,1] \end{aligned} \tag{4.27}$$

Similarly, the parabolic B-spline with uniform knot points is constituted by three pieces in the reference domain $[-\tfrac{1}{2}, \tfrac{1}{2}]$, which are given as:

$$\begin{aligned} p_1 &= \tfrac{1}{2}y^2 + \tfrac{1}{2}y + \tfrac{1}{8} \\ p_2 &= -y^2 + \tfrac{3}{4} \\ p_3 &= \tfrac{1}{2}y^2 - \tfrac{1}{2}y + \tfrac{1}{8}, y \in [-\tfrac{1}{2}, \tfrac{1}{2}] \end{aligned} \tag{4.28}$$

For the linear uniform B-spline, it has two pieces in the reference domain $[0,1]$, i.e

$$\begin{aligned} p_1 &= y \\ p_2 &= 1 - y,\ y \in [0,1] \end{aligned} \tag{4.29}$$

It has been shown that the interpolation by using the linear B-spline is unable to provide good estimate for the PI calculation even if the grid resolution is extremely high (Skaug, 2000). Cubic B-spline interpolation and parabolic B-spline interpolation works well in the PI calculations for a number of systems. Considering a cubic B-spline interpolation and that the function *h* in equation (4.23) is assumed to be zero outside the interpolated interval, the spline coefficients of equation (4.25) can be obtained by the following equation:

$$\mathbf{A\Gamma} = \mathbf{v} \tag{4.30}$$

where the matrix A is given as (Mo, 2008):

$$\mathbf{A} = \frac{1}{6}\begin{bmatrix} 4 & 1 & 0 & \cdots & 0 & 0 \\ 1 & 4 & 1 & \cdots & 0 & 0 \\ 0 & 1 & 4 & & 0 & 0 \\ & & & \ddots & & \\ 0 & 0 & 0 & \cdots & 4 & 1 \\ 0 & 0 & 0 & \cdots & 1 & 4 \end{bmatrix} \tag{4.31}$$

Since the matrix **A** is simple and strictly diagonal-dominant, the LU factorization can be applied in order to solve the equation (4.30) quickly. Similarly, for the parabolic B-spline, the corresponding matrix **A** has the following shape which is given as:

$$\mathbf{A} = \frac{1}{8}\begin{bmatrix} 6 & 1 & 0 & \cdots & 0 & 0 \\ 1 & 6 & 1 & \cdots & 0 & 0 \\ 0 & 1 & 6 & & 0 & 0 \\ & & & \ddots & & \\ 0 & 0 & 0 & \cdots & 6 & 1 \\ 0 & 0 & 0 & \cdots & 1 & 6 \end{bmatrix} \tag{4.32}$$

For multidimensional system, e.g. the 4D dynamic system (3.12), the interpolation should be based on the spline surface and the extension of splines from one dimension to multi-dimension has been described in De Boor et al. (1978).

4.2.4 Numerical integration

For the numerical integration of equation (4.15), it is build up by the product of the PDF, $p(g^{-1}(x_1, x_2, \bar{x}_3, x_4), t)$, which can be obtained by numerical interpolation and the Gaussian distribution, $\tilde{p}(x_3, t \mid \bar{x}_3, t')$, given in equation (4.17). It is known that, the most probability mass of the latter Gaussian distribution is centered on its mean value. Therefore, an integration region $[x_3 - r, x_3 + r]$ is chosen and r is a certain range beyond which the product value of the above two PDFs is assumed to be very small. In this work, the range r is selected to be 6 times the size of the standard deviation $\sqrt{\Delta t \cdot \gamma}$ (Karlsen, 2006).

Subsequently, for a given integration region $[x_3 - r, x_3 + r\ ]$, the Simpson's rule (4.33) is applied in order to calculate the integration (4.15)

$$p(\mathbf{x}, t) = \int_{R^1} F(\bar{x}_3) d\bar{x}_3 = \frac{\Delta \bar{x}_3}{3} \sum_{i=0}^{N} \mu F(\bar{x}_{3,i}) \tag{4.33}$$

in which

$$F(\bar{x}_3) = \left| J_{g^{-1}} \right| \cdot \tilde{p}(x_3, t \mid \bar{x}_3, t') p(g^{-1}(\mathbf{x}), t') \tag{4.34}$$

where the parameter μ in the Simpson's rule is given as:

$$\mu = \begin{cases} 1, & i = 0, N \\ 4, & mod(i, 2) = 1 \\ 2, & mod(i, 2) = 0 \end{cases} \tag{4.35}$$

and the step length $\Delta \bar{x}_3 = 2r/N$, $\bar{x}_{3,i} = x_3 - r + i \cdot \Delta \bar{x}_3$.

The numerical implementation of the PI method have been described above and the main steps for the numerical implementation is concluded and given in Figure 4.1 and

relevant explanation have been given in paper 1.

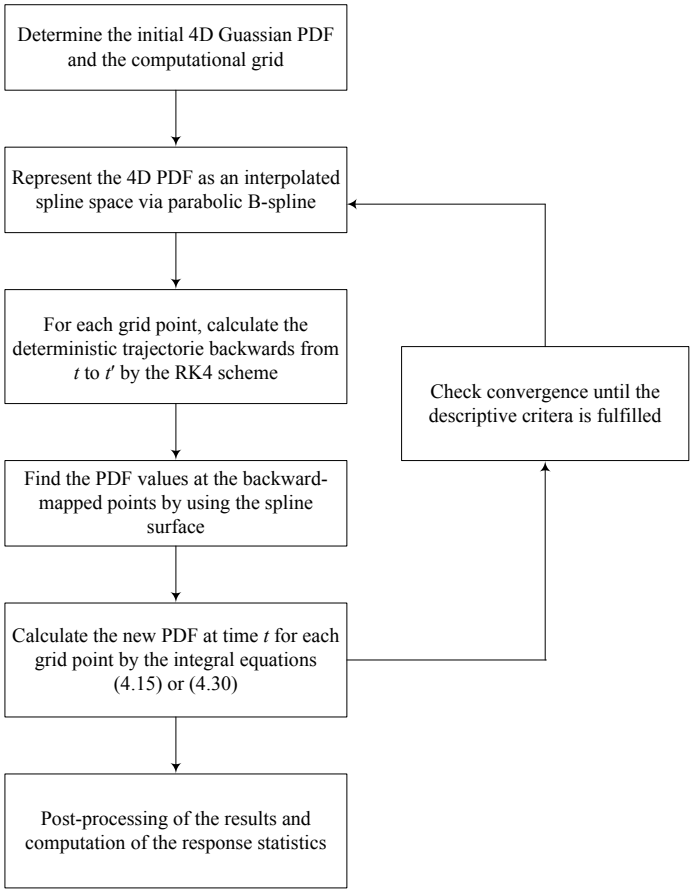

Figure 4.1: Flowchart of the numerical implementation of the 4D PI method

4.3 Mean Upcrossing Rate and Monte Carlo Simulation

The mean upcrossing rate is a key parameter for estimation of the large and extreme response statistics as well as for evaluation of the associated reliability of marine structures (Naess and Moan, 2012). The calculation of the mean upcrossing rate of the roll angle process is usually based on the Rice formulation (4.36) and the joint PDF of the roll angle process and the roll velocity process, which can be obtained directly by the 4D PI technique. The mean upcrossing rate $v^+(\zeta)$ is given as:

$$\begin{aligned} v^+(\zeta) &= \lim_{t\to\infty} v^+(\zeta;t) \\ v^+(\zeta;t) &= \int_0^\infty \dot{\theta} f_{\theta\dot{\theta}}(\zeta,\dot{\theta};t)d\dot{\theta} \end{aligned} \tag{4.36}$$

where $v^+(\zeta; t)$ denotes the expected number of upcrossing for the ζ-level per unit time at time instant t by the roll angle process $\theta(t)$.

As mentioned in Section 4.2, the joint PDF of the random process $\mathbf{x}(t)$ can be obtained by the 4D PI technique. By integrating through the entire range of the third and fourth dimensions, the joint PDF of the roll angle process and the roll velocity process at time instant t, $f_{\theta\dot{\theta}}(\theta,\dot{\theta};t)$ is determined. Due to the softening characteristic of the stiffness term, ship capsizing would be possible, but when the mean time to capsize is long enough, the dynamic system can be regarded as being highly reliable and the corresponding roll response reaches stationary conditions in an approximate sense (Roberts and Vasta, 2000). Therefore, the joint PDF can be represented by as a stationary joint PDF at a suitable reference point in time.

Furthermore, the standard Monte Carlo simulation technique can also be applied to obtain the empirical values of the upcrossing rates. For the coupled dynamic systems, obtained by combing the SDOF model for the roll motion and the filter models, the fourth-order RKM method is applied in order to solve the corresponding SDE and then time series of the roll response are obtained.

In practice, large amplitude roll motion or even ship capsizing may occur if the roll angle process exceeds the positive or negative angle of vanishing stability and then that particular realization is terminated since the subsequent roll angle process will exceed $\pi/2$ or - $\pi/2$ rapidly. A large number of realizations are required for the purpose of estimating the response statistics, especially for the high-level responses. The appropriate sample mean value of the upcrossing rate is given as:

$$\hat{v}^+(\zeta) = \frac{\sum_{i=1}^{k} n_i^+(\zeta; T_i)}{\sum_{i=1}^{k} T_i} \tag{4.37}$$

where $n_i^+(\xi; T_i)$ denotes the counted number of upcrossing of the level ζ during the time interval (0, T_i) for simulated time history No. i. Moreover, the practical simulation time T_i is not fixed for each realization, it is equal to the predetermined simulation time T if no capsizing occurs. Otherwise, it is the value of the termination time t_i for each case where capsizing occurs.

Moreover, the number of simulations, i.e. k, is selected according to the values of the upcrossing rates in the tail region and the length of the predetermined simulation time T. Usually, low upcrossing rates and short time periods T correspond to a large simulation number k. A fair approximation of the 95% confidence interval, $CI_{0.95}$, for the value of the empirical upcrossing rate can be expressed as:

$$CI_{0.95}(\zeta)=\left(\hat{\nu}^{+}(\zeta)-1.96\frac{\hat{s}(\zeta)}{\sqrt{k}},\hat{\nu}^{+}(\zeta)+1.96\frac{\hat{s}(\zeta)}{\sqrt{k}}\right) \tag{4.38}$$

where the empirical standard deviation is given as:

$$\hat{s}(\zeta)^2=\frac{1}{k-1}\sum_{i=1}^{k}\left(\frac{n_i^{+}(\zeta;T_i)}{T_i}-\hat{\nu}^{+}(\zeta)\right)^2 \tag{4.39}$$

4.4 Efficient Monte Carlo Simulation

The conventional (or standard) MCS method is not very efficient for estimating the mean upcrossing rate with respect to the far tail region. The numerical calculation and the counting procedure in order to get $n_i^{+}(\xi;T_i)$ in equation (4.37) require significant effort in connection with Monte Carlo simulation. Furthermore, the computation cost of the standard Monte Carlo simulation for calculating the response statistics with probability level lower than 10^{-7} is nearly formidable. In this Section, an efficient extrapolation scheme is introduced in order to provide a reasonable and accurate estimation of the extreme response with a dramatic reduction of the computation time.

The efficient extrapolation approach for the purpose of extreme response prediction derives from the idea that for the marine structures being considered, the mean upcrossing rate as a function of level ζ is in general highly regular in a specific way in the tail region. In fact, for a large class of stochastic process, the mean upcrossing rate tail (e.g. $\zeta \geq \zeta_0$) behaves similarly to $\exp\{-a(\zeta-b)^c\}$, where $a > 0$, $b \leq \zeta_0$, and $c > 0$ are suitable constants. Therefore, as discussed in detail in Naess and Gaidai (2008), it may be assumed that the mean upcrossing rate is approximated as:

$$\nu^{+}(\zeta)\approx q(\zeta)\exp\{-a(\zeta-b)^c\},\ \zeta\geq\zeta_0 \tag{4.40}$$

where the function $q(\zeta)$ is slowly varying compared with the exponential function $\exp\{-a(\zeta-b)^c\}$ in the tail region and the function $q(\zeta)$ can be replaced by a single constant q for large values of ζ. Equation (4.40) can be written as:

$$\ln\left|\ln((\nu^{+}(\zeta)/q))\right|\approx c\ln(\zeta-b)+\ln a,\ \zeta\geq\zeta_0 \tag{4.41}$$

in which, it is expected that an almost perfectly linear tail behavior will be obtained by plotting $\ln|\ln((\nu^{+}(\zeta)/q))|$ versus $\ln(\zeta-b)$.

In this Section, an optimized fitting scheme is introduced in order to find the optimal values of parameters a, b, c, q and these parameters can be determined by minimizing the following mean square error function:

$$F(q,a,b,c)=\sum_{j=1}^{N}\rho_j\left|\ln\hat{\nu}^{+}(\zeta_j)-\ln q+a(\zeta_j-b)^c\right|^2 \tag{4.42}$$

where $\hat{\nu}^{+}(\zeta_j)$, j =1, …, N denote a set of empirical mean upcrossing rates at different levels. ρ_j denotes a weight factor that puts more emphasis on the more reliable data points.

The choice of weight factors is arbitrary to some extent. In this work, the weight factor ρ_j = (ln$CI^{+}(\zeta j)$-ln$CI^{-}(\zeta j)$)$^{-2}$ is used in combination with a Levenberg-Marquardt least squares optimization method (Gill et al., 1981), where CI^{+} and CI^{-} are the bounds of the confidence interval determined by equation (4.38). Moreover, the Levenberg-Marquardt method can be transformed into a more simplified and transparent two-parameter optimization method. This is realized by considering the values of b and c in equation (4.42) are kept fixed and the optimization problem then reduces to a standard weighted linear regression problem. That is, with both b and c fixed, the optimal values of a and ln$q$ are found by using closed form weighted linear regression formulas in terms of ρ_j, and x_j=$(\zeta_j$-$b)^c$. The optimal values of a and q are given by the relations:

$$a^{*}(b,c)=-\frac{\sum_{j=1}^{N}\rho_j(x_j-\bar{x})(y_j-\bar{y})}{\sum_{j=1}^{N}\rho_j(x_j-\bar{x})^2} \tag{4.43}$$

and

$$\ln q^{*}(b,c)=\bar{y}+a^{*}(b,c)\bar{x} \tag{4.44}$$

where $\bar{x}=\sum_{j=1}^{N}\rho_j x_j\Big/\sum_{j=1}^{N}\rho_j$ and $\bar{y}=\sum_{l=1}^{N}\rho_j y_j\Big/\sum_{l=1}^{N}\rho_j$.

In order to calculate the final optimal set of parameters, the Levenberg-Marquardt method can now be applied to the function $\tilde{F}=F(q^{*}(b,c),a^{*}(b,c),b,c)$ to find the optimal values of b^{*} and c^{*}, and then the corresponding a^{*} and q^{*} can be calculated from equations (4.43) and (4.44). For estimation of a confidence interval for a predicted value of the upcrosing rate function provided by the optimal curve, the empirical confidence band is reanchored to the optimal curve. The weight factors ρ_j and the Levenberg-Marquardt scheme mentioned above can also be applied to determine the optimal parameters for the confidence interval. The range of the fitted curves that stay within the reanchored confidence band will determine an optimized confidence interval of the predicted value.

As a result of the efficient extrapolation, which is based on the assumption of regularity of mean upcrossing rate in the tail region, the empirical estimation of the upcrossing rate with respect to the far tail region can be achieved with sufficient accuracy for most practical prediction purposes with much less computational efforts than using the standard MCS method directly.

The efficient MCS method can be viewed as an important alternative of the PI method in order to evaluate the extreme response of the dynamic systems whose dimensions are greater than four. For the beam seas conditions, the SDOF model (2.11) is applied to describe the roll motion with the assumption that the influence of the other DOFs on the roll response can be neglected. When the assumption is invalid for some cases, the 4D system (3.12) should be extended since more motion modes will be included and the PI method would be inapplicable due to curse of dimensionality problem. For these cases, the efficient MCS method could be possible to provide reliable estimation of the upcrossing rate in the tail region within acceptable computation cost.

Furthermore, it should be noted that the efficient MCS method is based on the assumption that the response is a stationary process. It might not work very well for purely experiment results due to the discontinuous physical effects (Andersen and Jensen, 2014) since the assumptions for the stationary response as well as for the regularity of the mean upcrossing rate in the tail region will be less invalid. Moreover, for some commercial ships (such as the container carrier), a number of other damages will occur at large angles and the ship could probably start to fail before it reaches to the angle of vanishing stability. For such cases, the above assumptions could also not be guaranteed.

5 Numerical Results and Analysis

In this chapter, the 4D PI approach is introduced to study the stochastic response of the nonlinear roll motion in random beam seas. In Section 5.1, the robustness of the 4D PI method is verified by comparing with the MCS method and the Gaussian distribution. The 4D dynamic system is proved to be an appropriate model used to study the stochastic roll response by relevant studies in Section 5.2 and 5.3. The influence of ship parameters and wind excitation on the stochastic roll response are investigated in Sections 5.4 and 5.5, respectively. The reliability evaluation associated with high response levels is studied and discussed in Section 5.6. Subsequently, in Section 5.7 the PI method is combined with metocean application in order to study the long-term extreme response. Furthermore, for the case of stochastic roll motion in random head seas, the linear filter technique and the efficient MCS method are introduced in order to predict the extreme response and relevant description is given in Section 5.8.

5.1 Stochastic roll response in random beam seas

In this Section, the stochastic response of the roll motion in random beam seas is studied. An ocean surveillance ship is selected as the ship model, the GZ curve for this model and the relevant parameters for the vessel are given in *paper* 1.

The random stationary sea state is specified by the modified Pierson-Moskowitz spectrum, which is widely used for the fully developed sea states. The wave spectrum is given as:

$$S_{\xi\xi}(\omega)=\frac{5.058g^2H_s^2}{T_p^4\omega^5}\exp(-1.25\frac{\omega_p^4}{\omega^4}) \tag{5.1}$$

in which H_s denotes the significant wave height, ω_p is the peak frequency at which the wave spectrum $S_{\xi\xi}(\omega)$ has its maximum value and T_p is the corresponding peak period.

The sea state with H_s=4.0 m and T_p=11.0 s is selected for the subsequent study. The selected wave spectrum and the roll excitation moment per unit wave amplitude $|F_{roll}(\omega)|$ are presented in *paper* 1 (Figure 4). Subsequently, the roll excitation moment spectrum $S_{MM}(\omega)$ and the relative roll excitation moment spectrum $S_{mm}(\omega)$ can be obtained by equations (2.10) and (2.18), respectively.

After determining the target spectrum $S_{mm}(\omega)$, which is shown in Figure 5.1, the parameters α, β, γ in the second-order linear filter (3.8) should be determined in order to establish the 4D dynamic system (3.12). In this regard, the least-square scheme is

available as a part of the curve fitting algorithms in MATLAB and the fitting result is shown in Figure 5.1. It can be readily seen that the filtered spectrum is reasonable in terms of bandwidth, peak frequency and peak value.

In particular, for the roll motion cases, the transfer function between the roll excitation moment and the roll response in the SDOF model (2.12) is narrow banded and peaked near the natural roll frequency ω_0 due to the light roll damping. Therefore, in Figure 5.1, for the selected ship model, the obvious discrepancies between the spectrum generated by the second-order linear filter and the target spectrum $S_{mm}(\omega)$ in the low-frequency and high-frequency regions would not impact the subsequent roll response to a significant extent. However, a sight discrepancy between the above two spectra in the critical frequency region near ω_0 can be observed. The fitting accuracy in the critical region is crucial for evaluating the roll response since the latter is sensitive to the variation of the external excitation in this frequency region. Therefore, a constant, c, should be introduced as a correction factor for the filtered spectrum in order to decrease the discrepancy in the critical region. Then, the filtered spectrum (3.9) is changed into:

$$S_{2nd}(\omega) = \frac{1}{2\pi} \frac{(c \cdot \gamma)^2 \omega^2}{(\alpha - \omega^2)^2 + (\beta\omega)^2} \tag{5.2}$$

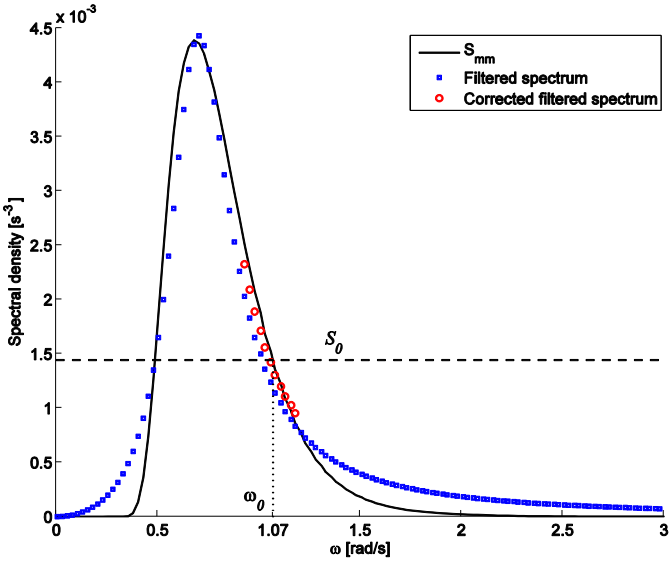

Figure 5.1: Relative roll excitation moment spectrum $S_{mm}(\omega)$, the corresponding filtered spectrum $S_{2nd}(\omega)$ and the corrected filtered spectrum (part) for the sea state with H_s=4.0 m and T_p=11.0 s, and spectrum of the equivalent Gaussian white noise, S_0

In this work, for the selected sea state and ship model, the correction factor c is taken to be 1.07 by considering the mean difference between the two spectral densities in the critical region. In addition, the corrected (or modified) spectrum in the critical region is

also presented in Figure 5.1. The 4D dynamic system (3.12) is established after the work of spectrum fitting, then the joint probability density function (PDF) of the roll angle process and the roll velocity process can be obtained directly by the 4D PI method. The joint PDF for the selected sea state calculated by the 4D PI method is presented in Figure 5.2.

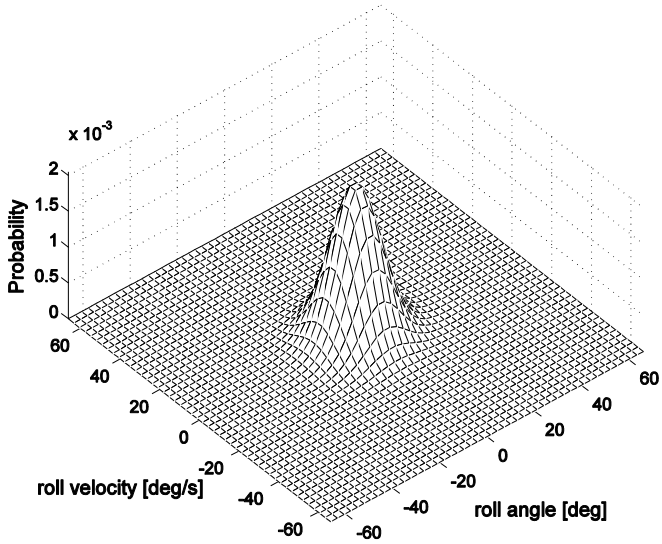

Figure 5.2: Joint PDF of the roll response obtained by the 4D PI method for the sea state with H_s=4.0 m and T_p=11.0 s.

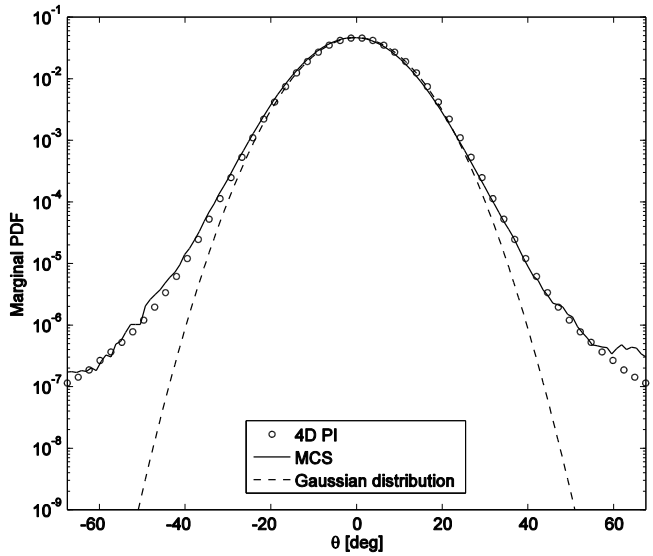

Figure 5.3: Marginal PDF of the roll angle process for the sea state with H_s=4.0 m and T_p=11.0 s.

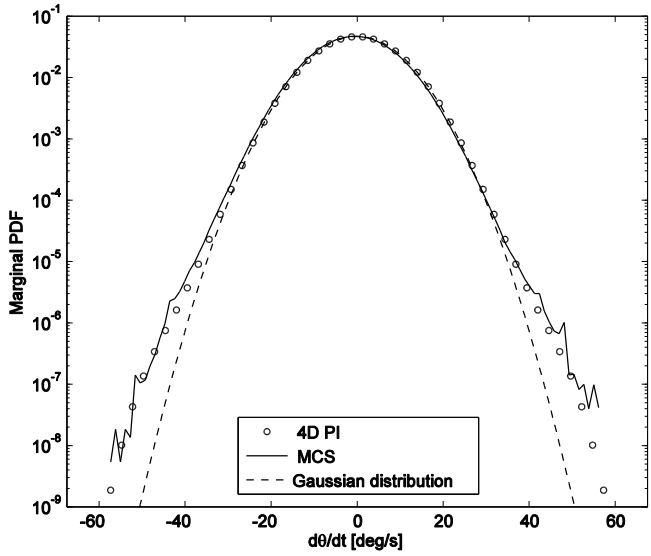

Figure 5.4: Marginal PDF of the roll velocity process for the sea state with H_s=4.0 m and T_p=11.0 s.

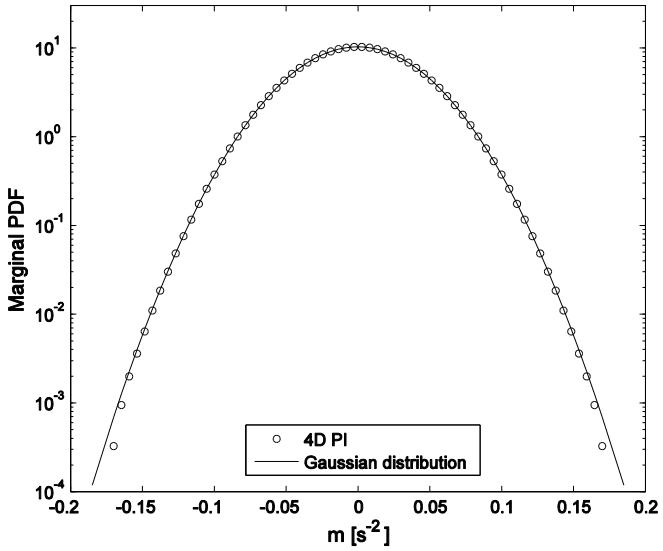

Figure 5.5: Marginal PDF of relative wave excitation process for the sea state with H_s=4.0 m and T_p=11.0 s.

The marginal PDF of the roll angle process and the marginal PDF of the roll velocity process obtained by the 4D PI method and the corresponding empirical estimations evaluated by Monte Carlo simulation are plotted in Figures 5.3 and 5.4, respectively. In addition, the marginal PDF of the relative roll excitation process $m(t)$, i.e., x_3 in the dynamic system equation (3.12), obtained by the 4D PI method is shown in Figure 5.5.

The Gaussian distributions of the marginal PDFs in Figures 5.3-5.5 are obtained by using the variances evaluated by the straightforward Monte Carlo simulation. Actually, they are the marginal PDFs of the 4D Gaussian PDF, $p(\mathbf{x}^{(0)}, t_0)$ in equation (4.20), which serves as the initial PDF in the 4D PI procedure. It is shown that the Gaussian distributions in Figures 5.3 and 5.4 give reasonable approximations of the statistics for the small amplitude motions. However, for the high-level responses, the distributions of the roll angle process and the roll velocity process are very different from the normal distribution, which underestimates the corresponding low probability levels. Moreover, it is shown in Figures 5.3 and 5.4 that the comparisons of the marginal PDFs obtained by the 4D PI method and Monte Carlo simulation demonstrate the high-level accuracy of the 4D PI method. As for the marginal PDF of the relative roll excitation process $m(t)$ in Figure 5.5, which is a stationary Gaussian process, the result obtained by the 4D PI method is found to be in good agreement with the Gaussian distribution. Since the marginal PDF of $m(t)$ determined by the 4D PI method is based on an iterative scheme (shown in Fig 4.1), the excellent agreement with the original Gaussian distribution, i.e. the distribution before the iterative procedure, provides another proof for the robustness and reliability of the 4D PI method.

The upcrossing rate calculated by the 4D PI method and the Rice formula (4.36) for the selected sea state and the corresponding empirical estimation of the upcrossing rate as well as the 95% confidence interval obtained by the 4D MCS method are shown in Figure 5.6. For Monte Carlo simulation, long-time domain simulations are required to obtain upcrossing rate for high response levels. It can be readily seen that the 4D PI technique yields quite accurate and reliable result, even in the high roll response region.

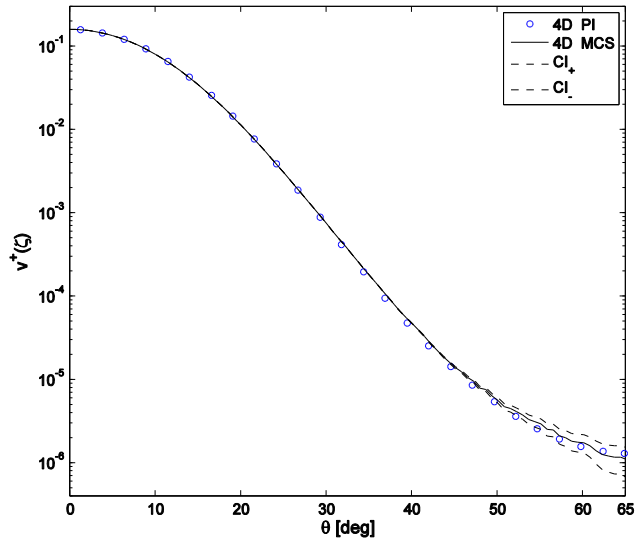

Figure 5.6: Upcrossing rate obtained by the 4D PI method and the empirical mean upcrossing rate evaluated by the 4D Monte Carlo simulation for the sea state with H_s=4.0 m and T_p=11.0 s.

5.2 Fourth-order Linear Filter

Basically, the fourth-order linear filter (3.10) provides a better approximation of the target spectrum than the second-order linear filter (3.8), but the subsequent coupled dynamic system could be more complicated to tackle. However, the PI method does suffer from a curse of the dimensionality problem, and the associated computation of the PI technique applied for the 6D coupled nonlinear system (3.13) is unaffordable at present.

On the other hand, it can be noted that the MCS method does not suffer critically from the curse of the dimensionality problem since the statistics of the response are obtained directly from the realizations. Even though the MCS method enables the empirical estimation of the response statistics to be determined, it is only a brute force alternative on the basis of straightforward counting. It cannot provide information at the same level of details as the PI method. Particularly, when the MCS method is applied to estimate the statistics of large roll response with low probability levels, the associated computation cost as well as the efficiency would be sacrificed in practice.

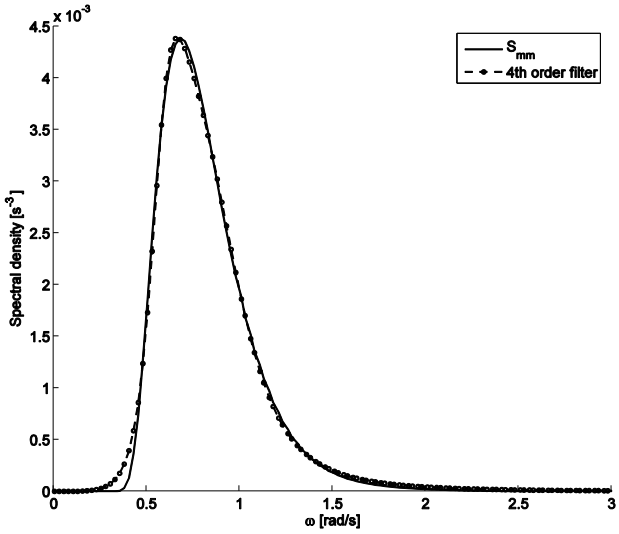

Figure 5.7: Relative roll excitation moment spectrum $S_{mm}(\omega)$ and the fourth-order filtered spectrum for the sea state with H_s=4.0 m and T_p=11.0 s.

In this Section, the feasibility of simplifying the 6D system by the 4D system in terms of determining the statistics of high-level roll response will be discussed. For the selected sea state with H_s=4.0 m and T_p=11.0 s, the relative wave excitation moment spectrum and the spectrum generated by the fourth-order linear filter (3.10) are plotted in Figure 5.7. In addition, the parameters $\alpha_1, \alpha_2, \beta_1, \beta_2, \gamma_1$ in the fourth-order linear filter can also be determined by minimizing the square errors between the filtered spectrum

and the target spectrum $S_{mm}(\omega)$. It is seen in Figure 5.7 that the fourth-order linear filter provides excellent approximation to the target spectrum.

Figure 5.8 presents the upcrossing rate obtained by the 4D PI method and the corresponding empirical estimation of the upcrossing rate as well as the 95% confidence interval evaluated by the 6D MCS method. Comparing the upcrossing rate calculated by the 4D PI method with the pertinent 6D MCS results demonstrate a satisfactory level of agreement, even in the large response region.

In addition, Figure 5.9 shows the spectra of the roll responses generated by the 4D dynamic system and the 6D dynamic system. Specifically, the random seeds for generating random driving processes in the above two systems are kept the same for the selected sea state. The corresponding RKM algorithms are applied to solve the SDEs and generate the samples of roll response. Obviously, in Figure 5.9, the response spectra are narrow banded and peaked near the natural roll frequency due to the light roll damping. Even though there are slight discrepancies in some local regions, the agreement of these two spectra is acceptable on the whole. The satisfactory results in Figures 5.8 and 5.9 illustrate that the statistics of the roll responses generated by the two different systems exhibit satisfactory agreement.

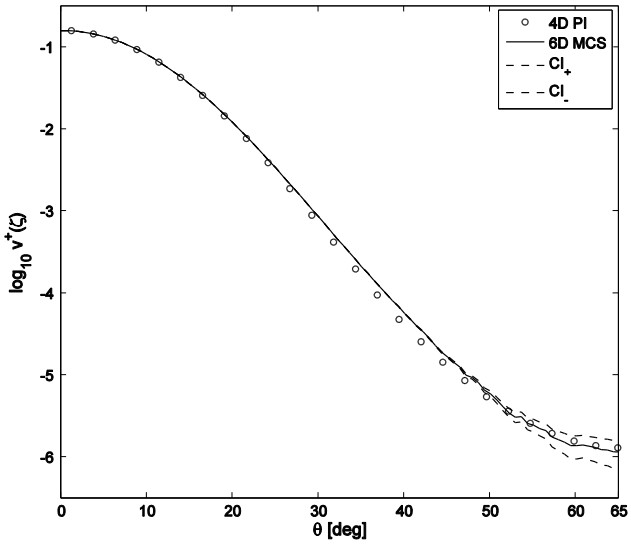

Figure 5.8: Upcrossing rate obtained by the 4D PI method and the empirical mean upcrossing rate evaluated by the 6D Monte Carlo simulation for the sea state with H_s=4.0 m and T_p=11.0 s.

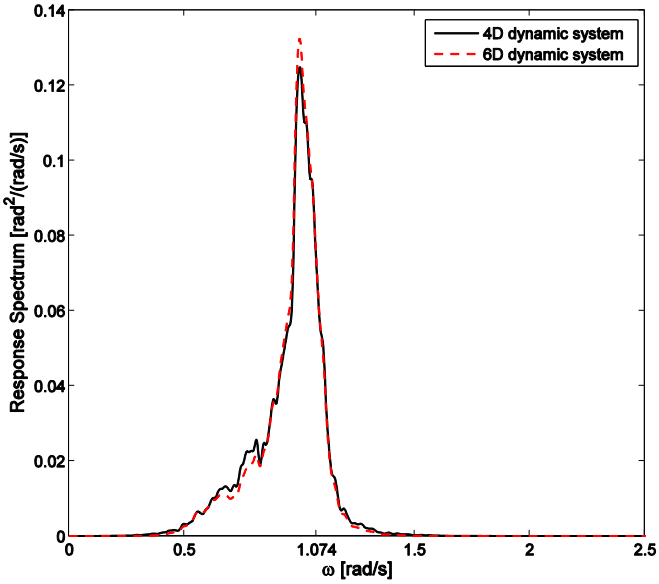

Figure 5.9: Roll response spectra of the ship model for the 4D dynamic system and the 6D dynamic system for the sea state with H_s=4.0 m and T_p=11.0 s.

The good agreements of the response statistics obtained by the 4D PI method and the MCS method (either 4D or 6D) in Sections 5.1 and 5.2 demonstrate the conclusion that the 4D PI method is capable of providing reliable estimation of the response statistics, even for high level responses with low probability levels. The 4D PI method has its advantage since it obtains different sets of response statistics within one calculation, whereas for the MCS method, a large amount of repeated calculations and counting procedures have to be conducted for each set of response statistics. Moreover, the computation cost of the MCS for the probability level lower than 10^{-7} is nearly formidable. And also, it is observed in Figures 5.3-5.4, for the high-level response, the statistics obtained by the MCS method are suffering from uncertainties.

Furthermore, as shown in Figures 5.8-5.9 and also more cases corresponding to different sea states presented in *paper* 2, the satisfactory agreements of the response statistics generated by the 4D dynamic system and the 6D dynamic system demonstrate that with the assistance of the correction factor, c, the 4D coupled system can serve as an effective alternative to the corresponding 6D extended system. In conclusion, the 4D dynamic system and the 4D PI method enables an appropriate theoretical model as well as an efficient numerical technique, respectively, to be applied for the study of stochastic roll response.

5.3 Equivalent Gaussian White Noise

In this Section, the random wave excitation is approximated by an equivalent Gaussian

white noise and the rationality and accuracy of applying the equivalent Gaussian white noise to simulate nonlinear ship rolling in random seas is studied.

As mentioned in Sections 5.1 and 5.2 that the roll response spectrum is narrow-banded and peaked near the natural roll frequency ω_0 due to the light roll damping. Theoretically speaking, Gaussian white noise may be serve as a simplification of the relative wave excitation spectrum $S_{mm}(\omega)$ if its spectral density equals to the value of $S_{mm}(\omega)$ at the frequency ω_0. Assume that the value of $S_{mm}(\omega)$ at the frequency ω_0 is S_0 and the corresponding Gaussian white noise is referred to as the equivalent Gaussian white noise. The spectrum of the equivalent Gaussian white noise is shown in Fig. 5.1 and the noise level σ can then be determined as:

$$\sigma^2 = 2\pi S_0 \tag{5.3}$$

The differential equation of the dynamic system (2.12) can then be simplified as:

$$\ddot{\theta}(t) + b_{44}\dot{\theta}(t) + b_{44q}\dot{\theta}(t)\,|\,\dot{\theta}(t)\,| + c_1\theta(t) - c_3\theta^3(t) = \sigma N(t) \tag{5.4}$$

Where $N(t)$ is a standard Gaussian white noise process and the corresponding two-dimensional (2D) state-space equation is given as:

$$\begin{cases} dx_1 = x_2 dt \\ dx_2 = (-b_{44}x_2 - b_{44q}x_2\,|x_2| - c_1x_1 + c_3x_1^3)dt + \sigma dW \end{cases} \tag{5.5}$$

Basically, low-dimensional cases, such as the dynamic system (5.5) are much easier to be tackled by the PI technique than the high-dimensional extended systems. For the 2D dynamic system (5.5), the time evolution of the PDF of the vector $(x_1(t), x_2(t))^{\mathrm{T}}$ is also determined by a time discrete approximation and an iterative algorithm similar to equations (4.3) and (4.8), respectively. The one time-step TPD described in equations (4.10) and (4.11) is simplified as:

$$p(\mathbf{x}, t\,|\,\mathbf{x}', t') = \delta(x_1 - x_1' - r_1(\mathbf{x}', t', \Delta t)) \cdot \tilde{p}(x_2, t\,|\,x_2', t') \tag{5.6}$$

and

$$\tilde{p}(x_2, t\,|\,x_2', t') = \frac{1}{\sqrt{2\pi\gamma^2\Delta t}} \cdot \exp\left\{-\frac{(x_2 - x_2' - r_2(\mathbf{x}', t', \Delta t))^2}{2\gamma^2\Delta t}\right\} \tag{5.7}$$

The initial PDF for the 2D PI approach is selected as a 2D Gaussian PDF by Monte Carlo simulation and the subsequent numerical implementation procedure for the 2D dynamic system is similar to the procedure in Fig. 4.1.

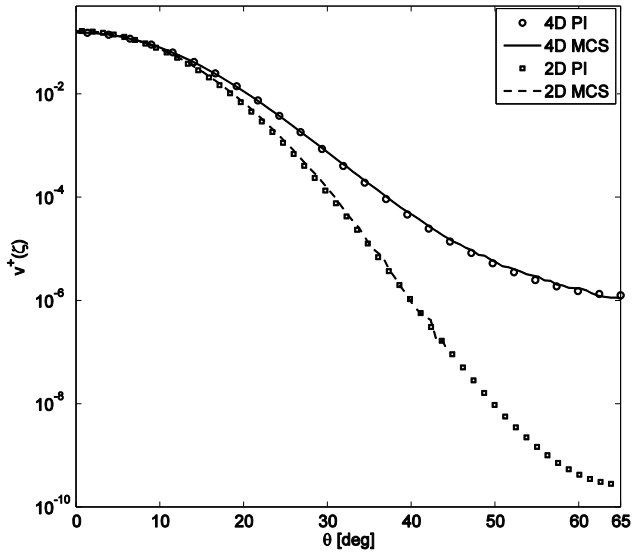

Figure 5.10: Upcrossing rates of the roll responses excited by filtered white noise (denoted as 4D PI and 4D MCS) and equivalent Gaussian white noise (denoted as 2D PI and 2D MCS) for the sea state with H_s=4.0 m and T_p=11.0 s.

Figure 5.10 provides relevant information about the roll responses for the 4D dynamic system and 2D dynamic system. In Figure 5.10, the mean upcrossing rates for these two systems are calculated by the 4D PI method and 2D PI method, respectively. MCS is applied in order to provide related empirical estimations of the upcrossing rates, which are also shown in Figure 5.10. The difference between the response statistics driven by filtered white noise and the equivalent Gaussian white noise is obvious. The equivalent Gaussian white noise results in weaker response than the filtered white noise and the 2D dynamic system (5.5) underestimates the response statistics for the selected ship model and sea sate.

This difference can also be observed in Figure 5.11, which provides the roll response spectra for the 4D dynamic system and 2D dynamic system, respectively. The response spectra of these two systems are obtained by means of Monte Carlo simulation and it is clearly seen that the roll response excited by the filtered white noise is much stronger than the response driven by the equivalent Gaussian white noise. Comparison of the response spectra illustrate that the discrepancy between the filtered spectrum generated by the second order linear filter and the spectrum of the equivalent Gaussian white noise in the critical frequency region the natural roll frequency ω_0, which is shown in Figure 5.1, would result in obvious differences of the roll responses. Moreover, in *paper* 3, another example given by a RoRo ferry model subjected to random wave excitation corroboration the above differences.

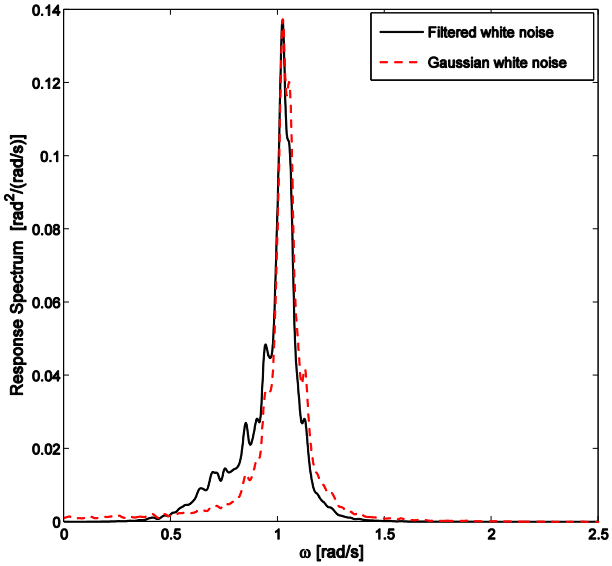

Figure 5.11: Roll response spectra of the ship model excited by filtered white noise and equivalent Gaussian white noise for the sea state with H_s=4.0 m and T_p=11.0 s.

Based on the observations in this Sections 5.2 and 5.3, we can find that the excitation spectrum near the natural roll frequency is essential for estimating the response statistics. The second order linear filter, with the assistance of the correction factor, c, provides a satisfactory approximation of the target spectrum $S_{mm}(\omega)$ in the critical region and thus the 4D dynamic system is recommended to be applied for studying the response statistics of the roll motion in random beam seas. In contrast, due to the unsatisfactory accuracy of the response statistics given by the 2D dynamic system, the equivalent Gaussian white noise cannot be recommended to approximate the random wave excitation as well as to study the nonlinear ship rolling in random seas.

5.4 Influence of Ship Parameters

The effects of the ship parameters, i.e. the restoring terms and the damping terms on the upcrossing rate are studied in this Section. Firstly, the influences of the restoring coefficients on the upcrossing rate, especially in the high response region are concerned. To highlight the effects of the linear and nonlinear restoring coefficients individually, the parameters as well as the parameters for the second-order linear filter for the selected sea state are assumed to be constant in the numerical simulations, except for the particular ship parameter whose effect is going to be studied. The original value of the relative linear roll restoring coefficient c_1 is 1.153 s^{-2}. We select 2% of the original value as the increment and decrement and then the range of c_1 value is determined as: 1.129, 1.153, 1.176 and 1.199 s^{-2}. Similarly, with the variation of 0.05 s^{-2} (5.46% of the

original c_3 value), the values of the relative nonlinear roll restoring coefficients for the subsequent study are: 0.815, 0.865, 0.915 and 0.965 s^{-2}.

For different c_1 and c_3 values, the upcrossing rates obtained by the 4D PI technique as well as the empirical estimation of the upcrossing rates obtained by the 4D Monte Carlo simulation (MCS) are plotted in Figs 5.12 and 5.13, respectively. It is seen that the roll response increases for decreasing c_1 values and for increasing c_3 values. This result is in accordance with common sense since large c_1 values and small c_3 values imply a large angle of vanishing stability and a large area under the GZ curve which correspond to enhanced intact stability against reliability failures.

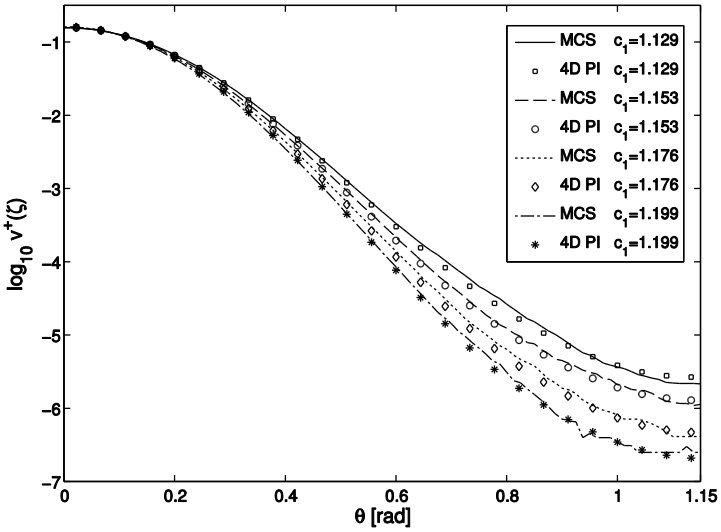

Figure 5.12: Influence of the relative linear roll restoring coefficient c_1 on the upcrossing rate.

In Figure 5.13, it is observed that the nonlinear restoring term c_3 significantly influences the response statistics in the high roll response region, which means the nonlinear restoring term plays a crucial role in this region. However, the variation of the nonlinear restoring term has no significant influence on the response statistics of small amplitude roll motions. For the effects of the linear restoring term c_1, it is seen in Figure 5.12 that the variation of c_1 result in a wider range of influence on the roll response that that of the c_3 values presented in Figure 5.13, e.g. one can observe that the variation of c_1 influences the stochastic roll response already from the low response region. In reality, the variation of the response statistics in the low roll response region (which is mainly caused by different c_1 values in the current Section) would influence the response statistics in the high roll response region to some extent, but it is the nonlinear restoring coefficient c_3 in all parameter sets in Figure 5.13 that plays a dominant role in this region. In practice, when a vessel is sailing in random seas, especially in longitudinal waves, the roll restoring curve (or the GZ curve) varies with time. Thus, the variation

of roll response induced by time-dependent c_1 values and c_3 values should be considered in dynamic stability analyses.

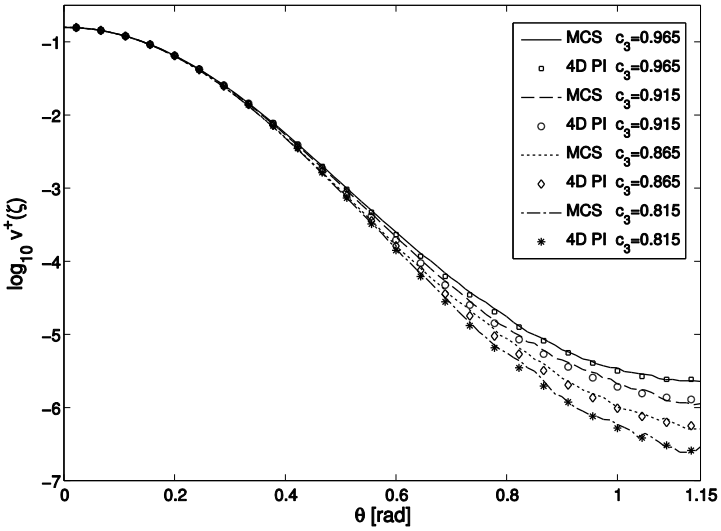

Figure 5.13: Influence of the relative nonlinear roll restoring coefficient c_3 on the upcrossing rate.

As mentioned in Section 2.2, the quantitative evaluation of the roll damping is difficult due to the coupling effects of different sources of the damping moment. In this part, the commonly applied empirical LPQD model (2.6) is applied in order to describe the damping model. Subsequently, the linear damping and nonlinear damping terms are modified individually to study their influence with the values of the filter parameters for the selected sea state and the restoring coefficients are kept constant. The values of the relative linear damping coefficient b_{44} is varied linearly from 0.085 to 0.100 s^{-1}. The variation of the relative nonlinear damping coefficients b_{44q} is 20% of the original value, 0.0519. Accordingly, the upcrossing rates obtained by the 4D PI method and empirical estimation of the upcrossing rates obtained by the 4D Monte Carlo simulation for different values of b_{44} and b_{44q} are shown in Figures 5.14 and 5.15, respectively.

The tendency observed in Figures 5.14 and 5.15 verify that the common knowledge that the presence of roll damping decreases the roll response and the vessels with small damping coefficients are much more prone to encounter stability failures than the vessels with large roll damping. Moreover, in Figure 5.15, the variation of b_{44q} mainly affects the response statistics in the high roll response region, while its influence on the stochastic response of small amplitude roll motions is limited. For the low roll response region, the variation of the linear damping term, i.e. b_{44}, would impact the distribution of the response statistics. As an extension of current study, different damping models, i.e. the LPQD model and the equivalent LPCD model have been proposed in *paper* 4 in order to investigate the influence of different damping models on the stochastic roll

response (especially on the high level response).

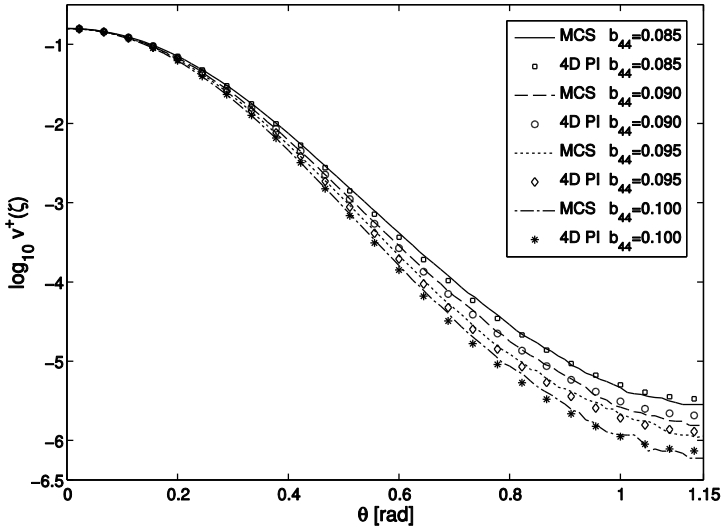

Figure 5.14: Influence of the relative linear damping coefficient b_{44} on the upcrossing rate.

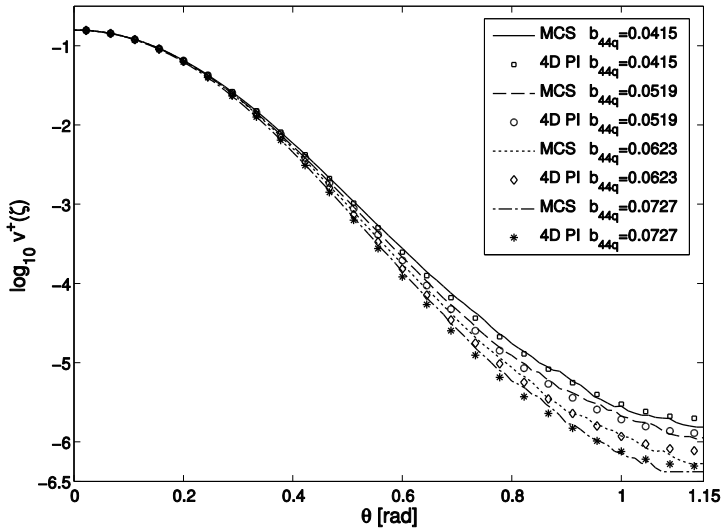

Figure 5.15: Influence of the relative nonlinear damping coefficient b_{44q} on the upcrossing rate.

Based on the observations in Figures 5.12-15 and the results above, we can draw the conclusion that the relative linear roll restoring coefficient c_1 and the relative linear damping coefficient b_{44}, mainly influence the response statistics in the low roll response region. On the contrary, for the high response region, the respective nonlinear terms, i.e. the relative nonlinear roll restoring coefficient c_3 and the relative linear damping

coefficient b_{44q}, have more significant and direct effects. Furthermore, the high-level agreements for the two classes of upcrossing rate, which are shown in Figures 5.12-5.15, verify the capacity of the 4D PI technique in providing accurate and reliable response statistics of the roll motion for different sets of ship parameters.

5.5 Roll Response under Wind and Irregular Beam Waves

The action of wind has been considered in the weather criterion of the current code for intact stability (IMO, 2008). In this Section, we aim to study the stochastic response of the roll motion under the action of wind and (beam) wave excitation. Considering the beam wind action, the roll motion described by equation (2.11) will be modified as:

$$\begin{aligned}(I_{44}+A_{44}(\tilde{\omega}))\ddot{\theta}(t)+B_{44}(\tilde{\omega})\dot{\theta}(t)+B_{44q}\dot{\theta}(t)\left|\dot{\theta}(t)\right| \\ +\Delta(C_1\theta(t)-C_3\theta^3(t))=M(t)+M_{wind}(t)\end{aligned} \tag{5.8}$$

in which $M_{wind}(t)$ denotes the excitation moment caused by wind action and it can be calculated by the following formula:

$$M_{wind}(t)=\frac{1}{2}\rho_{air}C_wA_wl_W(U_m+U(t))^2 \tag{5.9}$$

where ρ_{air} is the mass density of air and C_W denotes a wind pressure coefficient. U_m is the mean wind speed and $U(t)$ is the fluctuating wind speed. A_W represents the lateral windage and l_W is the wind moment arm. Generally, $(U(t)/U_m) << 1$ and the wind excitation moment (12) can be expressed as:

$$\begin{aligned}M_{wind}(t)&=\bar{M}_{wind}+M_f(t)\\&=\frac{1}{2}\rho_{air}C_wA_wl_WU_m^2+\rho_{air}C_wA_wl_WU_mU(t)\end{aligned} \tag{5.10}$$

in which $\bar{M}_{wind}$ and $M_f(t)$ denote the mean wind moment and fluctuating wind moment, respectively. The mean wind action results in a steady heeling angle θ_s and their relationship can be expressed as:

$$\bar{M}_{wind}=\Delta GZ(\theta_s)=\Delta(C_1\theta_s-C_3\theta_s^3) \tag{5.11}$$

As for the fluctuating wind moment, its spectral density is related to the wind spectrum $S_U(\omega)$, by the following relationship (Naess and Moan, 2012):

$$S_{M_f}(\omega)=(\rho_{air}C_wA_wl_WU_m)^2\cdot\chi(\omega)\cdot S_U(\omega) \tag{5.12}$$

where $\chi(\omega)$ is the aerodynamic admittance function, which can be determined as:

$$\chi(\omega)=\frac{1}{1+(\frac{\omega\sqrt{A_w}}{\pi U_m})^{4/3}} \tag{5.13}$$

and the wind spectrum, which governs the fluctuating wind speed, is given by the Davenport spectrum:

$$S_U(\omega) = 4K\frac{U_m^2}{\omega}\frac{X_D^2}{(1+X_D^2)^{4/3}} \tag{5.14}$$

where K=0.003 and the dimensionless variable X_D is given by the equation (Bulian and Francescutto, 2004):

$$X_D = 600\frac{\omega}{\pi U_m} \tag{5.15}$$

Dividing equation (5.8) by (I_{44} + A_{44}), the final format of the differential equation is given as:

$$\begin{aligned}&\ddot{\theta}(t) + b_{44}\dot{\theta}(t) + b_{44q}\dot{\theta}(t)\left|\dot{\theta}(t)\right| + c_1\theta(t) - c_3\theta^3(t)\\ &\qquad = (m(t) + m_f(t)) + \bar{m}_{wind}(t) = m_{sum}(t) + \bar{m}_{wind}\end{aligned} \tag{5.16}$$

In which $m(t)$, $m_f(t)$ and $\bar{m}_{wind}$ are relative moments. The total relative random external excitation is denoted as $m_{sum}(t)$, which is assumed to be the sum of the relative wave excitation $m(t)$ and the relative fluctuating wind moment $m_f(t)$. Correspondingly, the spectrum of $m_{sum}(t)$ is assumed to be given as the sum of the spectrum of the relative wave excitation moment and the spectrum of the relative fluctuating wind moment:

$$S_{sum}(\omega) = (S_{MM}(\omega) + S_{M_f}(\omega))\Big/(I_{44} + A_{44})^2 = S_{mm}(\omega) + S_{m_f}(\omega) \tag{5.16}$$

Finally, the SDOF model, i.e. equation (5.16) is transformed into the following state-space equation:

$$\begin{cases} dx_1 = x_2 dt \\ dx_2 = (-b_{44}x_2 - b_{44q}x_2\left|x_2\right| - c_1x_1 + c_3x_1^3 + x_3 + \bar{m}_{wind})dt \end{cases} \tag{5.17}$$

where x_1= $\theta(t)$, x_2=$\dot{\theta}(t)$and x_3=$m_{sum}(t)$.

The sea state with H_s=4.0 m and T_p=11.0 s is selected to determine the spectrum of relative wave excitation moment and the mean wind speed U_m is selected as 26 m/s according to the weather criterion of the IMO intact stability code and the wind pressure coefficient C_w=0.95 (Andersen, 2013). The spectrum of the relative wave excitation moment $S_{mm}(\omega)$ for the selected sea state, the spectrum of the relative fluctuating wind moment spectrum $S_{mf}(\omega)$ for selected U_m and the corresponding spectrum of the total relative random external excitation, $S_{sum}(\omega)$ are shown in Figure 5.16. The value of $S_{sum}(\omega)$ in the critical region near the natural frequency ω_0 dominates subsequent roll response. It can be seen that in Figure 5.16 that $S_{mf}(\omega)$ is peaked in the low-frequency region and its value in the critical region is negligible when compared with the values of $S_{mm}(\omega)$ and $S_{sum}(\omega)$. Therefore, the influence of the fluctuating wind moment on the stochastic roll response can be neglected in the simulation stage for the current ship

model.

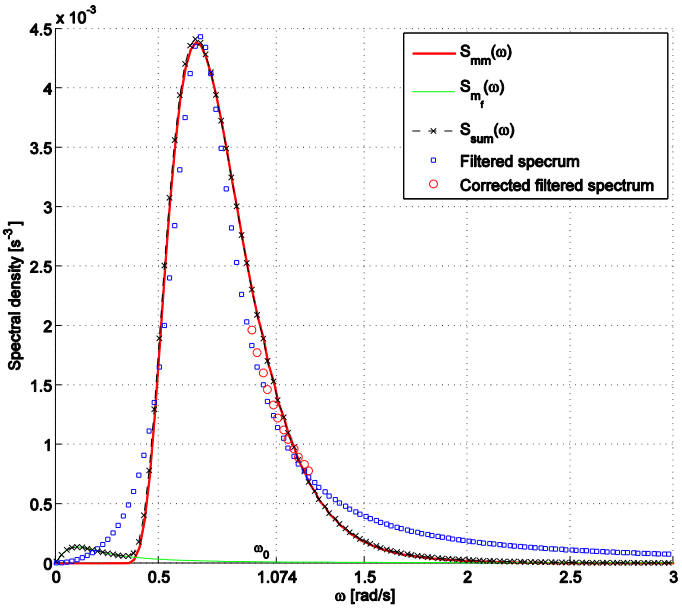

Figure 5.16: Relative wave excitation moment spectrum $S_{mm}(\omega)$ for the sea state with H_s=4.0 m and T_p=11.0 s, relative fluctuating wind spectrum $S_{mf}(\omega)$ for U_m=26 m/s and the spectrum for the total relative random external excitation $S_{sum}(\omega)$, filtered spectrum and the corrected filtered spectrum (part).

However, the effect of the mean wind action, which results in a heeling angle θ_s, on the response cannot be neglected. Relevant study with respect to the influence of steady heeling angle θ_s is given in *paper* 4. The dynamic system (5.17) can be extended to a 4D system and then the response statistics can be obtained by the 4D PI method. For the vessel without mean wind action, the PDFs of the roll response obtained by the 4D PI method is presented in Figures 5.2-5.4 and it is seen that the distribution of the roll response is symmetric. The symmetry is reasonable since the distribution of the random excitation (or the filtered white noise process) as well as the vessel properties are symmetric with respect origin. For the vessel with 5 degrees steady heeling angle, it is seen in Figure 5.17 that the distribution of the roll angle process is approximately symmetry with respect to the steady heeling angle θ_s. However, when the marginal PDF of the roll angle process is plotted with a logarithmic scale along the vertical axis, shown in Figure 5.18, the symmetry is not valid in the high level response region, for which the nonlinear effects associated with the damping and restoring terms have a significant influence on the distribution of the roll response.

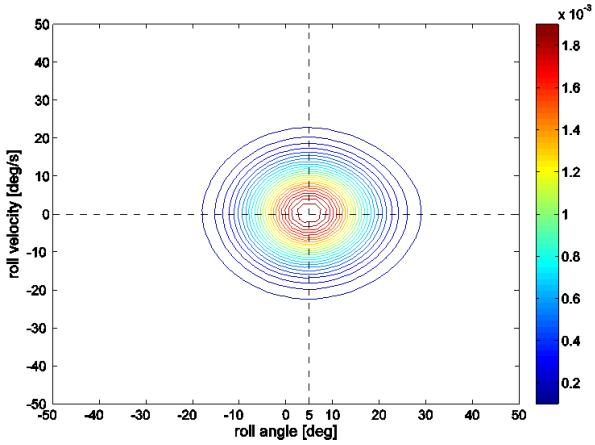

Figure 5.17: Contour lines of the joint PDF of the roll response for the vessel with 5 degrees steady heeling angle for the sea state with H_s=4.0 m and T_p=11.0 s.

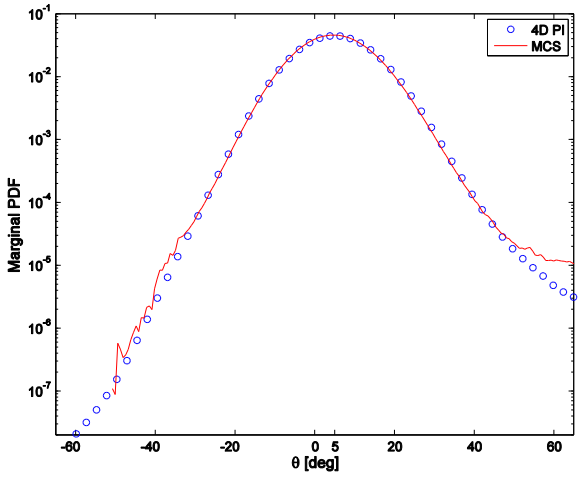

Figure 5.18: Logarithmical scaled marginal PDF of the roll angle process for the vessel with 5 degrees steady heeling angle for the sea state with H_s=4.0 m and T_p=11.0 s

The influence of the steady heeling angle on the upcrossing rate is presented in Figure 5.19. It can be seen that the existence of the steady heeling angle leads to an increases of the upcrossing rate. This implies that the mean wind action would induce the roll angle process cross high levels more frequently than the condition without steady heeling angle. More importantly, earlier deterministic nonlinear dynamics work conducted in Thompson (1997) and Spyrou et al. (2002) noted that even a small bias (i.e. steady heeling) has a disproportionate diminishing effect on a ship's safety margin. The stochastic analysis in this Section and the results presented in Figure 5.19 confirm and extend this statement for irregular sea conditions.

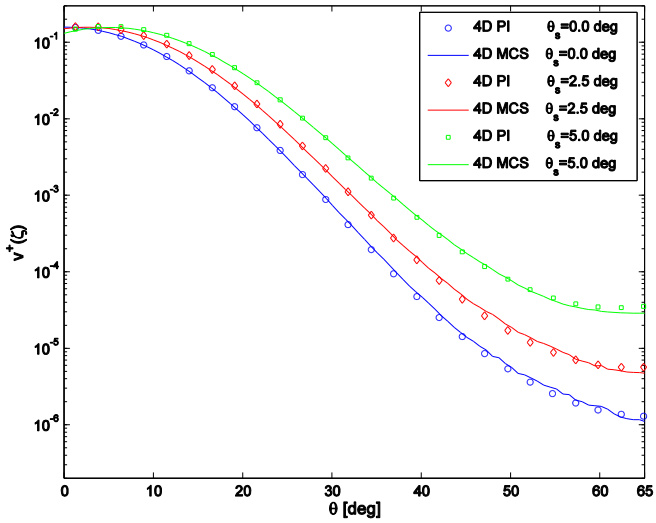

Figure 5.19: Upcrossing rates for the vessel with different steady heeling angles for the sea state with H_s=4.0 m and T_p=11.0 s.

5.6 Reliability Evaluation

In addition to the evaluation of stochastic roll response in the above Sections, estimation of the inherent reliability is also a closely connected research topic. In this Section, the reliability evaluation associated with high-level roll response is considered. For one thing, the response statistics obtained by the 4D PI method, especially in the high-level response region, can directly be applied in the reliability evaluation procedure. Also, prediction of the extreme roll response and the associated risk assessment of ship stability in random seas are crucial for reliability based design and operation in practice.

Roll angles near or beyond the maximum of the GZ curve can be regarded as high response levels. If the assumption of statistically independent upcrossings is valid for a certain level in this region, the corresponding crossing events are Poisson distributed. Under the Poisson assumption, the reliability evaluation is usually phrased in terms of the probability that the roll angle process $\theta(t)$ exceeds the specific level ζ at least once during a time interval of length T. Therefore, the exceedance probability for a duration of exposure time T can be expressed by a widely used approach which is given as follows (Jensen, 2012; Naess and Moan, 2012):

$$P_\zeta(T) = 1 - \exp(-\int_0^T v^+(\zeta;t)dt) \approx 1 - \exp(-v^+(\zeta)\cdot T) \tag{5.18}$$

where $v^+(\zeta)$ represents the mean upcrossing for the level ζ at a suitable reference point in time, which can be determined directly by the 4D PI method and the Rice formula.

Moreover, for high response levels, let $\Theta(T)=\max\{\theta(t): 0 \le t \le T\}$ denote the largest (or extreme) value of the roll angle process $\theta(t)$ over the time interval of length T. The cumulative distribution function (CDF) of $\Theta(T)$ under the Poisson assumption is approximately given in terms of the mean upcrossing rate by the following relationship for a stationary short-term sea state:

$$\text{Prob}(\Theta \le \zeta) = \exp(-\nu^{+}(\zeta) \cdot T) \tag{5.19}$$

Furthermore, the empirical estimation of the exceedance probability obtained by Monte Carlo simulation is given as:

$$P_{MC}(\Theta \le \zeta) = 1 - F_{MC}(\zeta, T) \tag{5.20}$$

where $F_{\text{MC}}(\zeta,T)$ is the empirical CDF of the extreme value $\Theta(T)$ over the time interval T, which can be evaluated in terms of simulated maximum roll angles ranked in ascending order.

The exceedance probability for the high-level response converges towards a normal distribution for a large number of realizations, N_t. Therefore, the 95% confidence interval of the exceedance probability during the exposure time T, $\Delta P(\zeta, T)$ can be evaluated by the following equation:

$$\Delta P(\zeta, T) = 1.96 \cdot \frac{2}{\sqrt{N_t}} \sqrt{P_{MC}(\zeta, T) \cdot (1 - P_{MC}(\zeta, T))} \tag{5.21}$$

Finally, the range of error tolerance of the empirical exceedance probability is:

$$\left[P_{MC}(\zeta, T) - \tfrac{1}{2}\Delta P(\zeta, T),\ P_{MC}(\zeta, T) + \tfrac{1}{2}\Delta P(\zeta, T)\right] \tag{5.22}$$

The reliability evaluation associated with high response levels for the selected sea states listed in *paper* 1 (Table 2) is conducted. The exceedance probabilities of high level response obtained by formula (5.18) for different sea states are presented in Figures 5.20, 5.21 and 5.22, respectively. The Poisson-assumption estimates based on the upcrossing rates obtained by the 4D PI method are denoted by ‘‘4D PI’’ in these Figures. The corresponding empirical exceedance probabilities as well as the 95% confidence intervals evaluated by MCS are also plotted in order to verify the Poisson estimation. Moreover, the short-term sea states are considered and the exposure time T for each sea stae is selected to be 3 hours.

Even though the proposed method based on the Poisson assumption usually leads to reliable predictions, it is seen in Figures 5.19-5.21 that its good performance for reliability evaluation associated with high level roll response would gradually decline as the roll response becomes serious. For the roll motion with light roll damping, the roll response is generally narrow-banded and the response maxima will have a tendency to occur in clumps when the external excitation strengthens or the exposure period T

increases. Under such circumstances, the assumption about independent upcrossings will tend to be less valid, which will influence the performance of the Poisson estimate. On the other hand, the Poisson estimate can take advantage of the reliable response statistics obtained by the 4D PI method. Its simplicity and accuracy, as presented in Figures 5.20-5.22, is attractive for practical applications, except for vessels with extremely light roll damping or under serious external excitation. For these cases, the highly reliable system assumption as well as the stationary approximation of the roll response mentioned in Section 4.3 would not be valid.

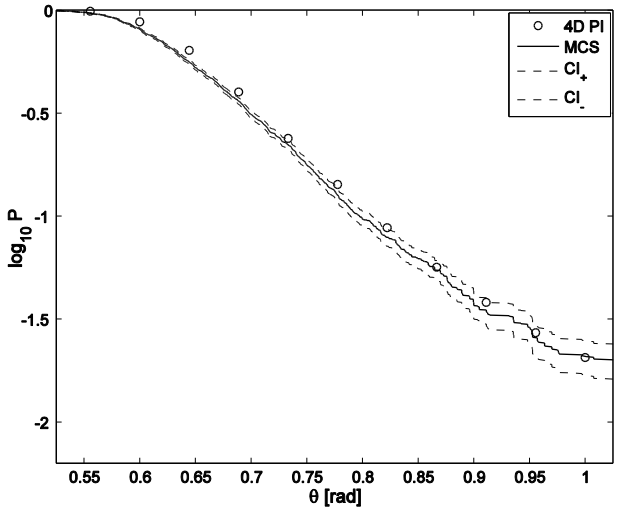

Figure 5.20: Exceedance probability of the roll angle process for the sea state with H_s=4.0m, T_p=11.0s, number of realizations N_t=5000, exposure time T=3h.

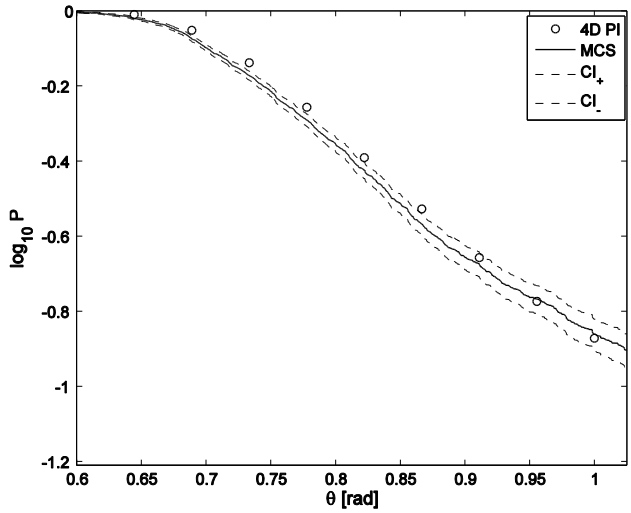

Figure 5.21: Exceedance probability of the roll angle process for the sea state with H_s=5.0m, T_p=12.0s, number of realizations N_t=2500, exposure time T=3h.

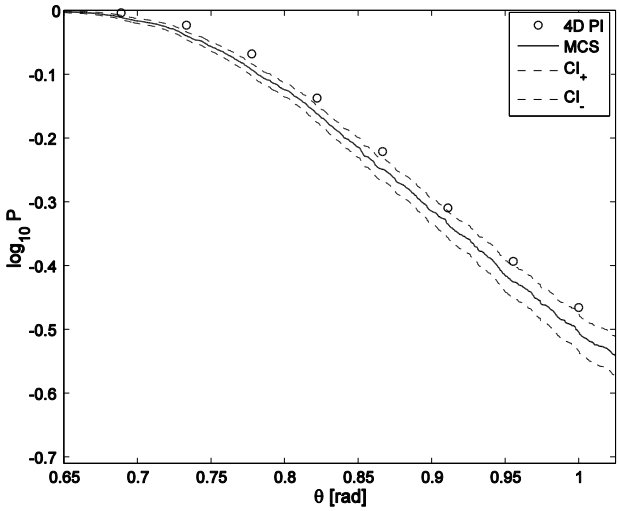

Figure 5.22: Exceedance probability of the roll angle process for the sea state with H_s=6.0m, T_p=13.0s, number of realizations N_t=2000, exposure time T=3h.

5.7 Long-term Response Evaluation

The short-term extreme response is evaluated by considering the vessel which is exposed to a particular sea state with a certain significant wave height and peak wave period. While, the long-term response analysis, which accounts for the occurrence rate and severity of the seaway, is a more general and more appropriate approach to evaluate the extreme roll response (Sagrilo et al., 2011). In this Section, the long-term extreme response of a vessel rolling in random beam seas is addressed.

For the long-term analysis, which considers the contribution from each short-term sea state, it is evaluated by a formulation proposed by Naess (1984) and given as:

$$F_{\tilde{\Theta}(T)}(\zeta) = \exp(-\bar{\nu}^{+}(\zeta)\cdot T) \tag{5.23}$$

where $F_{\tilde{\Theta}(T)}(\zeta)$ represents the CDF of the global extreme value which accounts for the contributions from all short-term sea states. $\bar{\nu}^{+}(\zeta)$ denotes the long-term mean upcrossing rate, which is given as:

$$\bar{\nu}^{+}(\zeta) = \int_{h_s}\int_{t_p} \nu^{+}(\zeta\,|h_s,t_p) f_{H_sT_p}(h_s,t_p)\,dh_s dt_p \tag{5.24}$$

in which $f_{H_sT_p}(h_s,t_p)$ is the joint PDF of H_s and T_p and $\nu^{+}(\zeta\,|h_s,\,t_p)$ denotes the mean upcrossing rate for the short-term contribution specified by the significant wave height H_s=h_s and the peak period T_p= t_p.

Generally, the number of occurrences of each sea state for a given sea area is recorded and described by a wave frequency table or wave scatter diagram that represents a discrete (empirical) joint distribution of H_s and T_p (Moan et al., 2005). However, the observations of some sea states, especially the extreme sea states are under the influence of uncertainty. It is necessary to fit and smooth the observed data by introducing a joint PDF model. In this work, the joint distribution of H_s and T_p is fitted by a conditional modelling approach (Haver, 2002), it consists of a marginal distribution of H_s and a conditional distribution of T_p given H_s:

$$f_{H_s T_p}(h_s, t_p) = f_{H_s}(h_s) f_{T_p|H_s}(t_p \,|\, h_s) \tag{5.25}$$

The marginal distribution of H_s is described by a two-parameter Weibull distribution:

$$f_{H_s}(h_s) = \frac{\beta_{Hs}}{\alpha_{Hs}} \left(\frac{h_s}{\alpha_{Hs}} \right)^{\beta_{Hs}-1} \exp\left\{ -\left(\frac{h_s}{\alpha_{Hs}} \right)^{\beta_{Hs}} \right\} \tag{5.26}$$

where α_{Hs}, β_{Hs} are scale and shape parameters for the Weibull distribution, respectively.

For the conditional distribution of T_p given H_s, it is modelled by a lognormal distribution:

$$f_{T_p|H_s}(t_p \,|\, h_s) = \frac{1}{\sqrt{2\pi}\sigma_{\ln T} t_p} \exp\left\{ -\frac{(\ln(t_p) - \mu_{\ln T})^2}{2\sigma_{\ln T}^2} \right\} \tag{5.27}$$

where the mean value μ_{lnT} and standard deviation σ_{lnT} of ln(Tp) are assumed to be dependent on the significant wave height h_s by the following relationship.

$$\begin{aligned} \mu_{\ln T} &= a_1 + a_2 h_s^{a_3} \\ \sigma_{\ln T}^2 &= b_1 + b_2 \exp(b_3 h_s) \end{aligned} \tag{5.28}$$

In this work, the environmental conditions are derived from historical data (2006-2014) available for the NDBC (National Data Buoy Center) buoy No. 42058, located at 14°55'23" N and 74°55'4" W, as shown in Figure B1 (given in Appendix B). The probabilities of occurrence for each sea state are summarized in Table B1 based on the 9 years data. On the basis of equations (5.25)-(5.28), the joint PDF of H_s and T_p for the selected location can be obtained. The joint PDF is presented in Figure 5.23 and the fitted occurrence rate for each sea state is given in Table B2.

Theoretically, in order to get the average long-term upcrossing rates (5.24) for the high-level responses, all the sea states in Tables B1 and B2 with nonzero occurrence rates should be considered. However, it is pointed in Sections 5.2 and 5.3 that the stochastic roll response, especially the high level response, is sensitive to the value of $S_{mm}(\omega)$ in the critical frequency region near the natural roll frequency ω_0. In addition, it is also observed in equations (2.18) and (5.1) that both of the significant wave height H_s and the peak period T_p have direct influences on $S_{mm}(\omega)$. The former parameter enhance the

value of $S_{mm}(\omega)$ in the critical region by intensifying the wave energy spectrum, while the influence of the latter parameter can be viewed as resonance. According to the short-term response statistics, the upcrossing rates for the sea states with 2.5 m $\leq H_s \leq$ 4.5 m and 7.5 s $\leq T_p \leq$ 10.5 s dominates the subsequent long-term upcrossing rate. While, the contributions from the other sea states in Tables B1 and B2 can be neglected due to the negligible product values of the short-term upcrossing rate and the occurrence rate of the sea state.

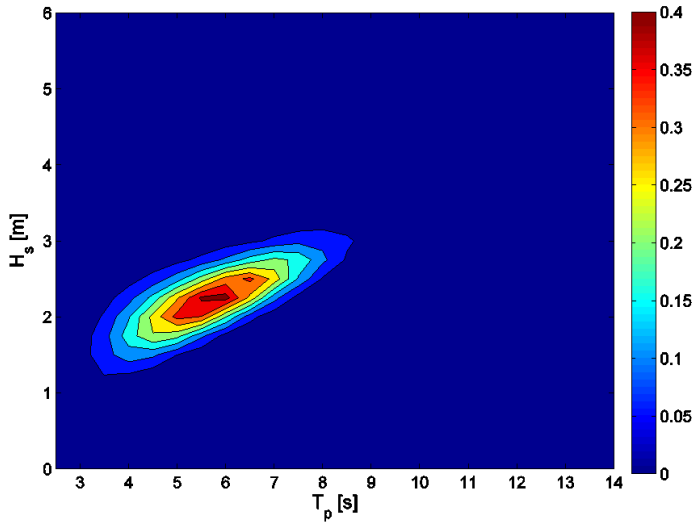

Figure 5.23: Fitter joint PDF of H_s and T_p at the site of the NDBC buoy, No. 42058 based on 9 years (2006-2014) of data.

On the basis of the short-term upcrossing rates for the sea states in the dominate region with 2.5 m $\leq H_s \leq$ 4.5 m and 7.5 s $\leq T_p \leq$ 10.5 s, the long-term analysis is executed. The long-term upcrossing rates in the high-level response region based on the empirical distribution of sea states (Table B1) and the fitted distribution of sea states (Table B1) are obtained and shown in Figure 5.24. The contribution of each sea state to the long-term upcrossing rate at the level of 64 degrees (i.e. the angle of vanishing stability) are given in Table 5.1.

It is observed in Fig. 5.24 that the value of the long-term upcrossing rate based on the fitted distribution of sea states is approximately 15% less than the value based on the empirical distribution, even though some extreme sea states with nonzero occurrence rates, such as H_s = 4.5 m, T_p =9.5 s and H_s = 4.5 m, T_p =10.5 s can be obtained in Tab B2. As for the contribution of each sea state to the long-term upcrossing rate, it depends on the value of the short-term upcrossing rate as well as on the occurance rate of the sea state. In the meantime, as it can be seen in Table 5.1, the sea states with T_p =8.5 s contribute the most to the final long-term upcrossing rate but the fitted model described by equations (5.25)-(5.28) provides a little smaller estimation of the distribution for the

condition with T_p=8.5 s when compared with the corresponding empirical value. The slight discrepancy results in the difference of the long-term upcrossing rates given in Figure 5.24. Theoretically, the long-term upcrossing rate based on the fitted distribution would be a better choice since the joint PDF model reduces inherent uncertainty of the observed data and it also considers the contributions of some extreme sea states which have not been observed in the wave scatter diagram.

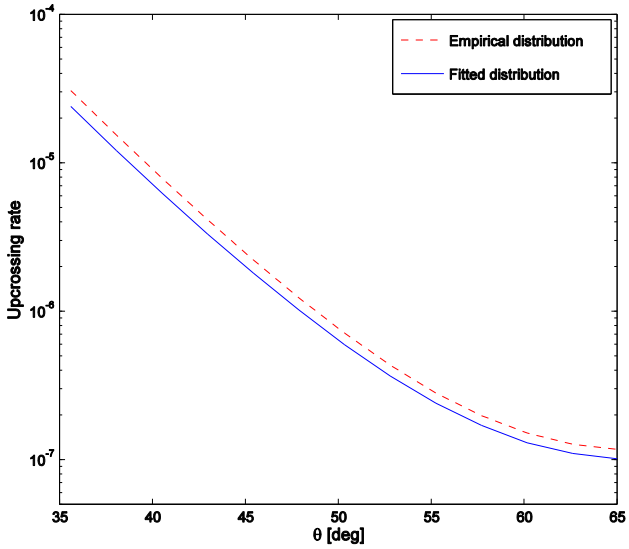

Figure 5.24: Long-term upcrossing rates based on the empirical distribution of sea states and the fitted distribution of sea states

Table 5.1 Contributions to the long-term upcrossing rate at the level of 64 degrees from the important sea states (given as percentages), based on the fitted distribution summarized in Table B2

H_s (m) \ T_p (s)	7.5	8.5	9.5	10.5
2.5	4.07	0.87	0.01	0.00
3.0	3.92	22.58	0.13	0.00
3.5	0.51	50.88	3.95	0.01
4.0	0.00	3.62	7.38	0.09
4.5	0.00	0.00	1.72	0.25

Furthermore, for the selected site, since only the sea states in the dominant region with 2.5 m $\leq H_s \leq$ 4.5 m and 7.5 s $\leq T_p \leq$ 10.5 s are accounted for calculating the long-term extreme response, the 4D PI method is feasible for long-term analysis within acceptable computation cost and accuracy.

5.8 Extreme Roll Response in Random Head Seas

This Section presents an efficient MCS technique and the linear filter approach in order to predict the extreme response of a vessel rolling in random head seas. In this work, a RoRo ship from Bulian (2006) is considered for the numerical simulation in the subsequent study. The main parameters of the vessel is given in *paper* 5 (Table 1). The concept of Grim effective wave model is applied herein in order to approximate the variation of the restoring moment in random waves. Based on the Grim effective wave approximation (2.33), the differential equation (2.35) is determined to describe the roll motion in random longitudinal seas.

The random stationary sea state is described by the modified Pierson-Moskowitz spectrum (5.1). The peak frequency of the sea spectrum is selected to be the value which corresponds to a wave length equals to the Grim's reference length (i.e. $\omega_p = \sqrt{2\pi g/L}$ =0.683 rad/s) and the significant wave height H_s is chosen to be 4.0 m for the subsequent study. The selected wave energy spectrum is presented in Figure 5.25. Assume that the ship is moving with a speed of V =2.5 m/s and the encounter spectrum for the effective wave amplitude process, i.e., the effective wave spectrum $S_{\xi_e}(\omega_e)$ (which is determined by equation (2.32)) is also shown in Figure 5.25.

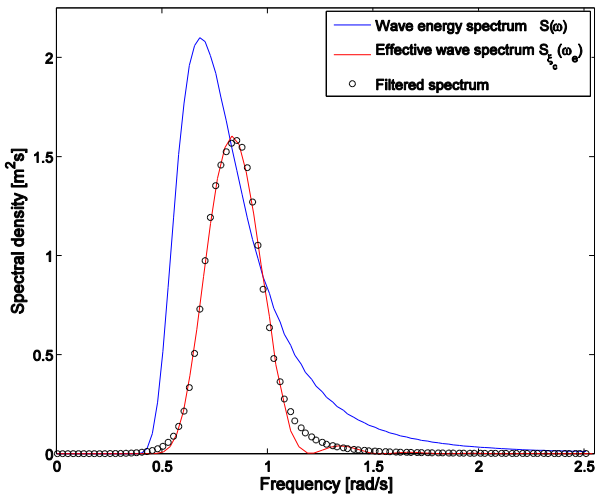

Figure 5.25: Wave energy spectrum for the sea state with H_s=4.0 m, T_p=9.2 s, encounter spectrum for the effective wave amplitude process $\xi_e(t)$ with vessel speed V=2.5 m/s in head seas and the filtered spectrum generated by the linear filter (3.11)

After determining the target spectrum, i.e. $S_{\xi_e}(\omega_e)$, the parameters α_1, α_2, β_1, β_2, γ_1 in the fourth-order linear filter (3.11) are obtained by minimizing the square error between the filtered spectrum and the desired spectrum. The fitting result for the linear filter is shown in Figure 5.25 and it can be readily seen that the spectrum obtained from the fourth order filter represents a good fitting. The SDOF model (2.35) is extended into a 6D dynamic system given in *paper* 5 (equation (18)). In addition, it was shown in Vidic-

Perunovic and Jensen (2009) and Bulian (2006) that the model based on the Grim effective wave model could tend to overestimate the roll response, therefore a correction factor k_c is introduced in order to reduce the parametric excitation by correcting the effective wave spectrum as:

$$S_{\xi_c,k_c}(\omega) = k_c^2 \cdot S_{\xi_c}(\omega) \tag{5.29}$$

accordingly, the effective wave amplitude process is corrected as:

$$\xi_{c,k_c}(t) = k_c \cdot \xi_c(t) \tag{5.29}$$

For the selected vessel, the correction factor k_c is taken to be 0.7 by comparison with the experimental data (Bulian, 2006). Roll responses can be obtained by solving the 6D SDE. It is seen from the examples of roll responses shown in *paper* 5 (Figure 9) that parametric roll occurs for the selected sea state and vessel model. Empirical estimation of the mean upcrossing rate can be obtained by generating multiple realizations.

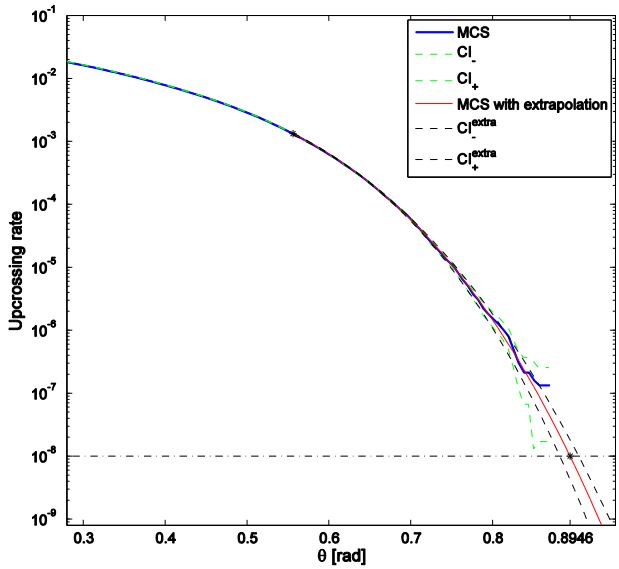

Figure 5.26: Empirical upcrossing rate obtained by the direct MCS with 95% confidence interval based on the 10000 hours of response time histories and the efficient MCS for the empirical upcrossing rate and confidence interval with the starting point ζ_0 =0.556, q= 0.0106, a= 23.253, b= 0.019, c= 3.887.

The following efforts have been devoted to demonstrate the advantage of the efficient MCS for giving accurate estimation of the extreme roll response with a dramatic reduction of computation time. Firstly, a standard MCS with 10000 hours of response time histories is executed and the empirical upcrossing rate as well as the 95% confidence interval are plotted in Figure 5.26. In the numerical simulation, 3334 realizations are generated for estimating the empirical mean upcrossing rate. Each

realization has a duration of 11,300 s with the first 500 s being removed to eliminate the transient effect of the roll response. The upcrossing rate in the far tail region as well as the corresponding confidence interval estimated by the efficient MCS are also presented in Figure 5.26. For a target crossing rate level of 10^{-8}, which requires formidable efforts for the conventional MCS technique, the roll response obtained by the proposed 10000 hours simulation and the efficient MCS based on the extrapolation procedure is predicted to be 0.8946 rad and the confidence interval is estimated to be (0.8821 0.9051).

Secondly, a standard MCS with only 100 hours of response time histories is executed. Figure 5.27 shows the corresponding empirical upcrossing rate and confidence interval. The 100 hours of simulated response time histories are constituted by 200 realizations. Each realization lasts 2300 s and the results of the first 500 s are neglected as the former case with 10000 hours of simulation. The expected roll response for the crossing rate level of 10^{-8} for this case is obtained as 0.9343 rad and the confidence interval is estimated to be (0.8757 0.9828).

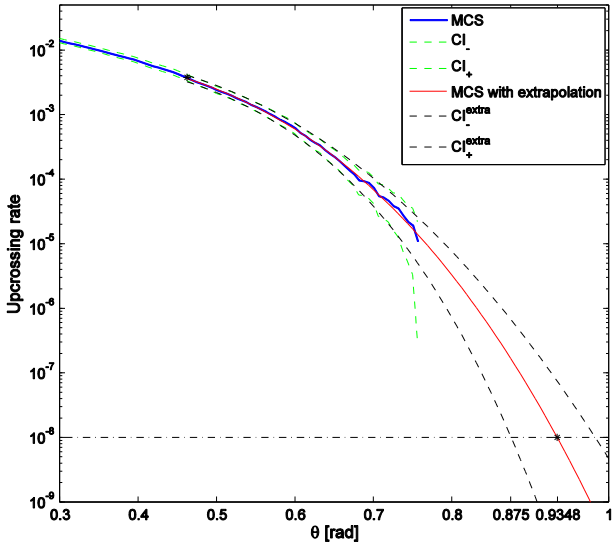

Figure 5.27: Empirical upcrossing rate obtained by the direct MCS with 95% confidence interval based on the 100 hours of response time histories and the efficient MCS for the empirical upcrossing rate and confidence interval with the starting point ζ_0 =0.4625, q= 0.011, a= 27.515, b= 0.0075, c= 3.167.

It can be seen from Figures 5.26-5.27 that the confidence interval becomes narrower when the ensemble simulation time increase. Generally, more realizations and longer simulation time provide more accurate distributions. Nonetheless, it seems that for the selected case, the good agreement of the predicted responses presented in Figures 5.26 and 5.27 demonstrates that 100 hours simulation is available to provide good estimates of the extreme response and that the reduction of simulation time is feasible and

reasonable. More importantly, for the time domain simulation, the computational cost and accuracy for a short-term sea state could be crucial for the subsequent long-term statistics prediction.

Furthermore, based on the Grim effective model, the phenomenon of parametric roll in random seas as well as the effect of vessel speed on the stochastic roll response are studied and relevant results are reported in paper 5.

6 Conclusions and Recommendations

6.1 Conclusions

The main conclusions of this thesis are described as follows.

- The theory of Markov processes was used in modelling the roll motion in random beam seas as a state space formulation. The 4D PI approach based on the Markov property of the dynamic system was found to give satisfactory estimation for different sets of ship parameters as well as for various external excitations. Comparisons with the results from MCS and Gaussian distribution demonstrated the robustness and reliability of the 4D PI method.
- The distributions of the roll response in random beam seas are very different from the Gaussian distribution. For the high-level responses, the Gaussian distribution will underestimate the stochastic roll response. It was found that the nonlinear effects associated with the restoring terms and the damping terms have a significant influence on the response statistics in the large roll response region. While, the linear damping and restoring terms mainly influence the response statistics in the low-response region.
- The satisfactory agreements of the response statistics generated by the 4D dynamic system (3.12) and (3.13) for the same external excitation demonstrate that with the assistance of the correction factor, the 4D coupled system can serve as an effective alternative to the corresponding 6D extended system. The 4D dynamic system is an appropriate model used to study the stochastic roll response. In contrast, due to the unsatisfactory accuracy of the response statistics given by the 2D dynamic system driven by the equivalent Gaussian white noise, the latter cannot be recommended to approximate the random wave excitation as well as to study the stochastic roll motion in random seas.
- The spectrum of the fluctuating wind moment is peaked in the low-frequency region, for the selected ship model, its influence on the stochastic roll response can be neglected since its value in the critical frequency region near the natural roll frequency is negligible. However, the effect of mean wind action, which results in a steady heeling angle, is important and cannot be neglected. The existence of the steady heeling angle leads to an increase of the upcrossing rate which implies that biased ship is much easier to encounter stability failures in random beam seas than the ship without steady heeling angles.
- The Poisson estimate can take advantage of the reliable response statistics obtained by the 4D PI method. Its simplicity and high efficiency is attractive for the reliability evaluation of roll motion in random waves. But for the roll motion with light roll damping, the roll response is generally narrow-banded and the

response maxima will have a tendency to occur in clumps when the external excitation strength or the exposure time period T increases. Under such circumstances, the assumption about independent upcrossing will tend to be less valid, which will influence the accuracy and performance of the Poisson estimate. Based on the observations in Figure 5.20-5.22 and discussions above, we can draw a conclusion that the Poisson estimation is available for reliability evaluation except for the vessels with extremely light roll damping or under serious external excitation.

- The long-term analysis was executed for predicting the extreme response. According to the products of the short-term upcrossing rates for specific sea states and the occurrence rate of the above sea states, it was found that for the selected site, the upcrossing rates for limited sea states (e.g. 2.5 m $\leq H_s \leq$ 4.5 m and 7.5 s $\leq T_p \leq$ 10.5 s in Section 5.7) dominate and determine the subsequent long-term upcrossing rate. Since only limited sea states are considered, the 4D PI method is feasible for long-term analysis within acceptable computation cost and accuracy.
- On the basis of the Grim effective wave model, the mathematical model of roll motion was established in order to describe the rolling behavior in random longitudinal seas. The linear filter technique and an efficient MCS method (based on the combination of a standard MCS approach and an extrapolation technique) were applied in order to approximate the effective wave amplitude process and estimate the extreme roll response. It has been found that the efficient MCS technique gives a satisfactory estimation of the extreme roll response with a dramatic reduction of computation time. Moreover, for practical applications, the linear filter technique and the extrapolated MCS method can be applied for long-term stochastic applications due to satisfactory accuracy and efficiency.

6.2 Recommendations for Future Work

The following topics are well suited for future work.

- The stochastic averaging method is widely used to tackle the high-dimensional Markov systems since it can lead to a dimension reduction. The FP equation can be solved if the dimension of averaged system is small enough. In this thesis, the 4D PI method is applied to solve the 4D FP equation without any techniques used for dimension reductions. Therefore, it is recommended to compare the response statistics calculated by the PI method with those obtained by the stochastic averaging method. The accuracy of the stochastic averaging method used for evaluating the response statistics of nonlinear high-dimensional systems will be studied.
- The SDOF model (2.11) is very important for qualitative studies and understanding the nonlinear behavior under stochastic excitation. However,

multi-degree-of-freedom model is recommended for actual ship design since this model can provide more accurate and realistic estimations for the ship responses. The PI method is not available due to the "curse of dimension" problem, but the efficient MCS approach proposed in *paper* 5 could be a possible way to predict the extreme responses within acceptable computation cost. Moreover, the Grim effective wave model is just an approximation used for modeling the variation of restoring moment in random longitudinal waves. This model is used for qualitative studies as well as for early stage ship design. But for detailed ship design, multi-degree-of-freedom model is recommended and the efficient MCS method can be applied to predict the extreme roll response.

- In Section 5.5, for the selected vessel model, the influence of the fluctuating wind moment on the stochastic roll response can be neglected because the spectrum of the fluctuating wind moment is peaked in the low-frequency region, which is far away from the critical frequency region near the natural roll frequency. But for the vessels with very large natural roll periods (e.g. 30 s), the effect of fluctuating wind action could be a possible critical problem and relevant studies are recommended.
- The external wave excitation moment in equation (2.11) is determined by the linear hydrodynamic theory and limitations will be observed for modelling the severe roll motion. Improving the hydrodynamic modelling and approximate the forces as stochastic processes could be one of the goals in the future.
- It was mentioned in Section 5.6 that the Poisson estimate could be invalid for vessels with extremely light roll damping or under serious external excitation. The average conditional exceedance rate method has been proved be to a reliable method for predicting the extreme response of narrow-banded processes (Naess et al., 2010). This method is recommended for the above cases for which the Poisson estimate is unavailable.

References

Andersen, I.M.V., 2013. Wind loads on post-panamax container ship. Ocean Engineering 58, 115-134.

Andersen, I.M.V., Jensen, J.J., 2014. Measurements in a container ship of wave-induced hull girder stresses in excess of design values. Marine Structures 37, 54-85.

Ayyub, B.M., Kaminskiy, M., Alman, P.R., Engle, A., Campbell, B.L., Thomas III, W.L., 2006. Assessing the probability of the dynamic capsizing of vessels. Journal of ship research 50 (4), 289-310.

Belenky, V., Bassler, C., Dipper, M., Campbell, B., Weems, K., Spyrou, K., 2010. Direct Assessment Methods for Nonlinear Ship Response in Severe Seas, Proc. of ITTC Workshop on Seakeeping, Seoul, Korea.

Belenky, V., de Kat, J.O., Umeda, N., 2008. Toward performance-based criteria for intact stability. Marine Technology 45 (2), 101-120.

Belenky, V., Weems, K.M., Bassler, C.C., Dipper, M.J., Campbell, B.L., Spyrou, K.J., 2012. Approaches to rare events in stochastic dynamics of ships. Probabilistic Engineering Mechanics 28, 30-38.

Belenky, V.L., Sevastianov, N.B., 2007. Stability and safety of ships: risk of capsizing. The Society of Naval Architects and Marine Engineers (SNAME), New York.

Bulian, G., 2006. Development of analytical nonlinear models for parametric roll and hydrostatic restoring variations in regular and irregular waves. University of Trieste, PhD Thesis.

Bulian, G., 2008. On an improved Grim effective wave. Ocean Engineering 35 (17), 1811-1825.

Bulian, G., Francescutto, A., 2004. A simplified modular approach for the prediction of the roll motion due to the combined action of wind and waves. Proceedings of the Institution of Mechanical Engineers, Part M: Journal of Engineering for the Maritime Environment 218 (3), 189-212.

Chai, W., Fan, J., Zhu, R., Huang, X., Miao, G., 2013. Calculation of Ship Rolling Capsizing Probability by Path Integral Solution. Journal of Shanghai Jiaotong University 2, 028.

Chang, B., 2008. On the parametric rolling of ships using a numerical simulation method. Ocean Engineering 35 (5), 447-457.

Cummins, W., 1962. The impulse response function and ship motions. DTIC Document.

De Boor, C., De Boor, C., De Boor, C., De Boor, C., 1978. A practical guide to splines. Springer-Verlag New York.

Dostal, L., Kreuzer, E., 2011. Probabilistic approach to large amplitude ship rolling in random seas. Proceedings of the Institution of Mechanical Engineers, Part C: Journal of Mechanical Engineering Science 225 (10), 2464-2476.

Dostal, L., Kreuzer, E., 2014. Assessment of Extreme Rolling of Ships in Random Seas, ASME 2014 33rd International Conference on Ocean, Offshore and Arctic Engineering. American Society of Mechanical Engineers.

Dostal, L., Kreuzer, E., Namachchivaya, N.S., 2012. Non-standard stochastic averaging of large-amplitude ship rolling in random seas. Proceedings of the Royal Society A: Mathematical, Physical and Engineering Science, 4146-4173.

e Silva, S.R., Soares, C.G., 2013. Prediction of parametric rolling in waves with a time domain non-linear strip theory model. Ocean Engineering 72, 453-469.

Ellermann, K., 2009. The motion of floating systems: nonlinear dynamics in periodic and random waves. Journal of Offshore Mechanics and Arctic Engineering 131 (4), 041104.

Faltinsen, O., 1993. Sea loads on ships and offshore structures. Cambridge university press.

Falzarano, J., Su, Z., Jamnongpipatkul, A., 2012. Application of Stochastic Dynamical System to Nonlinear Ship Rolling Problems, Proceedings of the 11th International Conference on the Stability of Ships and Ocean Vehicles, Atehns, Greece.

Falzarano, J.M., 1990. Predicting complicated dynamics leading to vessel capsizing.

France, W.N., Levadou, M., Treakle, T.W., Paulling, J.R., Michel, R.K., Moore, C., 2003. An investigation of head-sea parametric rolling and its influence on container lashing systems. Marine Technology 40 (1), 1-19.

Francescutto, A., Bulian, G., Lugni, C., 2004. Nonlinear and stochastic aspects of parametric rolling modeling. Marine Technology 41 (2), 74-81.

Francescutto, A., Naito, S., 2004. Large amplitude rolling in a realistic sea. International shipbuilding progress 51 (2), 221-235.

Gill, P.E., Murray, W., Wright, M.H., 1981. Practical optimization. Academic Press: London.

Grim, O., 1961. Beitrag zu dem Problem der Sicherheit des Schiffes im Seegang. Schiffbau-Versuchsanstalt.

Haver, S., 2002. On the prediction of extreme wave crest heights, 7th Int. Workshop on Wave Hindcasting and Forecasting, Banff, Canada. Citeseer.

Himeno, Y., 1981. Prediction of Ship Roll Damping. A State of the Art. DTIC Document.

Hsieh, S.-R., Troesch, A.W., Shaw, S.W., 1994. A nonlinear probabilistic method for predicting vessel capsizing in random beam seas, Proceedings of the Royal Society of London A: Mathematical, Physical and Engineering Sciences. The Royal Society, pp. 195-211.

Hua, J., Wang, W.-H., Chang, J.-R., 1999. A representation of GM-variation in waves by the Volterra system. Journal of marine science and technology 7 (2), 94-100.

IMO, 2008. International Code on Intact Stability. London, International Maritime Organization.

ITTC, 2014. Stability in Waves Committee – Final report and recommendations to the 27th ITTC., Proceedings of the 27th International Towing Tank Conference, Copenhagen.

Jensen, J.J., 2007. Efficient estimation of extreme non-linear roll motions using the first-order reliability method (FORM). Journal of marine science and technology 12 (4), 191-202.

Jensen, J.J., 2012. Probability of parametric roll in random seaways, Parametric Resonance in Dynamical Systems. Springer, pp. 91-105.

Jiang, C., Troesch, A., Shaw, S., 2000. Capsize criteria for ship models with memory-dependent hydrodynamics and random excitation. Philosophical Transactions of the Royal Society of London A: Mathematical, Physical and Engineering Sciences 358 (1771), 1761-1791.

Jiang, C., Troesch, A.W., Shaw, S.W., 1996. Highly nonlinear rolling motion of biased ships in random beam seas. Journal of ship research 40 (2), 125-135.

Karlsen, H.C., 2006. Statistics of wave induced nonlinear loads and responses. Norwegian University of Science and Technology, PhD Thesis, 2006:180.

Kougioumtzoglou, I.A., Spanos, P.D., 2014. Stochastic response analysis of the softening Duffing oscillator and ship capsizing probability determination via a numerical path integral approach. Probabilistic Engineering Mechanics 35, 67-74.

Kröger, H., 1986. Rollsimulation von schiffen im seegang. Schiffstechnik 33, 187-216.

Lewis, E.V., 1988. Principles of Naval Architecture: Motions in waves and controllability. Society of Naval Architects &.

Lin, H., Yim, S.C., 1995. Chaotic roll motion and capsize of ships under periodic excitation with random noise. Applied Ocean Research 17 (3), 185-204.

Liu, Y., Han, F., Lu, Y., 2016. Stability and capsizing analysis of nonlinear ship rolling in wind and

stochastic beam seas. Applied Ocean Research 57, 52-63.

MAIB, U., 2014. MAIB Annual Report 2014. Maritime Accident Investigation Branch, Government of UK.

Mo, E., 2008. Nonlinear stochastic dynamics and chaos by numerical path integration. Norwegian University of Science and Technology, PhD Thesis, 2008:18.

Moan, T., Gao, Z., Ayala-Uraga, E., 2005. Uncertainty of wave-induced response of marine structures due to long-term variation of extratropical wave conditions. Marine Structures 18 (4), 359-382.

Moideen, H., Somayajula, A., Falzarano, J.M., 2014. Application of volterra series analysis for parametric rolling in irregular seas. Journal of ship research 58 (2), 97-105.

Naess, A., 1984. Technical note: On the long-term statistics of extremes. Applied Ocean Research 6 (4), 227-228.

Naess, A., Gaidai, O., 2008. Monte Carlo methods for estimating the extreme response of dynamical systems. Journal of Engineering Mechanics 134 (8), 628-636.

Naess, A., Gaidai, O., Batsevych, O., 2010. Prediction of extreme response statistics of narrow-band random vibrations. Journal of Engineering Mechanics 136 (3), 290-298.

Naess, A., Johnsen, J., 1993. Response statistics of nonlinear, compliant offshore structures by the path integral solution method. Probabilistic Engineering Mechanics 8 (2), 91-106.

Naess, A., Moan, T., 2012. Stochastic dynamics of marine structures. Cambridge University Press.

Naess, A., Moe, V., 2000. Efficient path integration methods for nonlinear dynamic systems. Probabilistic Engineering Mechanics 15 (2), 221-231.

Ochi, M.K., 1990. Applied probability and stochastic processes: In Engineering and Physical Sciences. Wiley-Interscience.

Ogilvie, T.F., 1964. Recent progress toward the understanding and prediction of ship motions, 5th Symposium on naval hydrodynamics. Bergen, Norway, p. 2.5.

Pirrotta, A., Santoro, R., 2011. Probabilistic response of nonlinear systems under combined normal and Poisson white noise via path integral method. Probabilistic Engineering Mechanics 26 (1), 26-32.

Risken, H., 1989. Fokker-Planck Equation. Springer.

Roberts, J., 1982. Effect of parametric-excitation on ship rolling motion in random waves. Journal of ship research 26 (4), 246-253.

Roberts, J., 1986. Response of an oscillator with non-linear damping and a softening spring to non-white random excitation. Probabilistic Engineering Mechanics 1 (1), 40-48.

Roberts, J., Vasta, M., 2000. Markov modelling and stochastic identification for nonlinear ship rolling in random waves. Philosophical Transactions of the Royal Society of London. Series A: Mathematical, Physical and Engineering Sciences 358 (1771), 1917-1941.

Sagrilo, L., Næss, A., Doria, A., 2011. On the long-term response of marine structures. Applied Ocean Research 33 (3), 208-214.

Shin, Y., Belenky, V., Paulling, J., Weems, K., Lin, W., 2004. Criteria for parametric roll of large containerships in longitudinal seas. Discussion. Transactions-Society of Naval Architects and Marine Engineers 112, 14-47.

Skaug, C., 2000. Random vibration and the path integral method. Norwegian University of Science and Technology, PhD Thesis.

SLF, I., 2011. 53/WP. 4, Report of the Working Group (Part 1). London.

Song, K.-H., Kim, Y., Park, D.-M., 2013. Quantitative and qualitative analyses of parametric roll for ship design and operational guidance. Proceedings of the Institution of Mechanical Engineers, Part M: Journal of Engineering for the Maritime Environment 227 (2), 177-189.

Spanos, P., 1983. ARMA algorithms for ocean wave modeling. Journal of Energy Resources Technology 105 (3), 300-309.

Spencer Jr, B., Bergman, L., 1993. On the numerical solution of the Fokker-Planck equation for nonlinear stochastic systems. Nonlinear Dynamics 4 (4), 357-372.

Spyrou, K., Cotton, B., Gurd, B., 2002. Analytical expressions of capsize boundary for a ship with roll bias in beam waves. Journal of ship research 46 (3), 167-174.

Su, Z., 2012. Nonlinear response and stability analysis of vessel rolling motion in random waves using stochastic dynamical systems. Texas A&M University.

Su, Z., Falzarano, J.M., 2011. Gaussian and non-Gaussian cumulant neglect application to large amplitude rolling in random waves. International shipbuilding progress 58 (2), 97-113.

Su, Z., Falzarano, J.M., 2013. Markov and Melnikov based methods for vessel capsizing criteria. Ocean Engineering 64, 146-152.

Taghipour, R., Perez, T., Moan, T., 2008. Hybrid frequency–time domain models for dynamic response analysis of marine structures. Ocean Engineering 35 (7), 685-705.

Thampi, S.K., Niedzwecki, J.M., 1992. Filter approach to ocean structure response prediction. Applied Ocean Research 14 (4), 259-271.

Thompson, J., 1997. Designing against capsize in beam seas: recent advances and new insights. Applied Mechanics Reviews 50 (5), 307-325.

Vidic-Perunovic, J., 2011. Influence of the GZ calculation method on parametric roll prediction. Ocean Engineering 38 (2), 295-303.

Vidic-Perunovic, J., Jensen, J.J., 2009. Parametric roll due to hull instantaneous volumetric changes and speed variations. Ocean Engineering 36 (12), 891-899.

Wang, Y., 2014. A path integration algorithm for stochastic structural dynamic systems. Applied Mathematics and Computation 228, 423-431.

Wehner, M.F., Wolfer, W., 1983. Numerical evaluation of path-integral solutions to Fokker-Planck equations. Physical Review A 27 (5), 2663.

Wojtkiewicz, S.F., Johnson, E.A., Bergman, L.A., Grigoriu, M., Spencer Jr, B.F., 1999. Response of stochastic dynamical systems driven by additive Gaussian and Poisson white noise: Solution of a forward generalized Kolmogorov equation by a spectral finite difference method. Computer methods in applied mechanics and engineering 168 (1), 73-89.

Yurchenko, D., Naess, A., Alevras, P., 2013. Pendulum's rotational motion governed by a stochastic Mathieu equation. Probabilistic Engineering Mechanics 31, 12-18.

Appendix A

A.1 Paper 1

Stochastic dynamic analysis and reliability of a vessel rolling in random beam seas

Wei Chai, Arvid Naess and Bernt J. Leira

Published in Journal of Ship Research, (2015), Vol. 59. (2), pp. 113-131

Is not included due to copyright

A.2 Paper 2

Filter models for prediction of stochastic ship roll response

Wei Chai, Arvid Naess and Bernt J. Leira

Published in Probabilistic Engineering Mechanics (2015), Vol. 41, pp. 104-114.

Probabilistic Engineering Mechanics 41 (2015) 104–114

Contents lists available at ScienceDirect

Probabilistic Engineering Mechanics

journal homepage: www.elsevier.com/locate/probengmech

Filter models for prediction of stochastic ship roll response

Wei Chai [a,*], Arvid Naess [b,c], Bernt J. Leira [a]

[a] Department of Marine Technology, Norwegian University of Science and Technology, Trondheim, Norway
[b] Centre for Ships and Ocean Structures, Norwegian University of Science and Technology, Trondheim, Norway
[c] Department of Mathematical Sciences, Norwegian University of Science and Technology, Trondheim, Norway

ARTICLE INFO

Article history:
Received 12 November 2014
Received in revised form
25 May 2015
Accepted 2 June 2015
Available online 27 June 2015

Keywords:
Filter approaches
Path integration method
Nonlinear ship rolling
Stochastic response
Monte Carlo simulation

ABSTRACT

In this paper, the shaping filter technique is introduced to study the stochastic roll response of a vessel in random beam seas. Specifically, the roll motion is described as a single-degree-of-freedom (SDOF) model in which the stationary random wave excitation term is approximated as the output of a shaping filter, i.e. a filtered white noise process. Therefore, the original SDOF model can be extended into a four-dimensional (4D) and a six-dimensional (6D) dynamic system, respectively, when this second-order nonlinear differential equation couples with the second-order linear filter and the fourth-order linear filter used to model the random wave excitation. Basically, the fourth-order linear filter provides a better approximation, but the subsequent dynamic system would be more complicated to tackle. In this regard, the 4D coupled system can be viewed as a Markov system whose probability properties are governed by the Fokker–Planck (FP) equation. Furthermore, the 4D path integration (PI) method, an efficient approximate technique based on the Markov property of the dynamic system, is applied to solve the 4D FP equation and then the response statistics are derived. In contrast, the statistics of the roll response in the 6D extended system are evaluated directly by a 6D Monte Carlo simulation. The advantages of the 4D PI method as well as the feasibility of simplifying the 6D system by the 4D system in terms of determining the statistics of high-level roll response are demonstrated through various cases corresponding to different sea states. Furthermore, the influence of external excitations on the statistics of high roll response levels is also illustrated by these cases.

1. Introduction

Large amplitude roll motion in realistic seas is a serious threat to ship stability because it can lead to damage or even capsizing of the vessel. However, assessing the response statistics of large amplitude roll motion excited by random wave excitations is a challenging task. In this situation, the dynamic behaviors of the roll motion, especially the high-level roll responses, are influenced significantly by various effects which are nonlinear in nature or inherently random. Principally, elaborate theoretical models as well as appropriate mathematical techniques are essential to analyze this kind of problem [1].

For the cases of beam seas, the roll motion can be treated as decoupled from other motion modes and governed by a single-degree-of-freedom (SDOF) model in which the nonlinear effects associated with damping and restoring terms as well as the random wave excitation term are all incorporated [2]. The methodology based on the theory of Markov diffusion processes to evaluate the stochastic roll response is attractive since the probability distribution of the roll response is governed by the Fokker–Planck (FP) equation. However, the theory of Markov processes is only valid for the dynamic systems excited by Gaussian white noise. On the other hand, for the SDOF model of roll motion, the external excitation is generally non-white.

Nevertheless, the random wave excitation term is a stationary process with appropriate spectral density and it can be modeled as filtered white noise or colored white noise via the shaping filter technique. Spanos [3–5] was the pioneer in introducing the filter algorithms to approximate the wave elevation and wave kinematics. Subsequently, the filter approaches were widely used to model the wave loads and evaluate the responses of the nonlinear systems in the field of ocean engineering (e.g. [6–11]). In this paper, two different filter models, a second-order linear filter and a fourth-order linear filter, are used to approximate the random wave excitation process. Correspondingly, a four-dimensional (4D) and a six-dimensional (6D) extended dynamic system are created when the original SDOF model, a second-order nonlinear differential equation, is coupled with the filters used to generate filtered white noise. In this regard, the coupled dynamic systems can be viewed as excited by Gaussian white noise processes.

* Corresponding author.
E-mail address: chai.wei@ntnu.no (W. Chai).

http://dx.doi.org/10.1016/j.probengmech.2015.06.002
0266-8920/

However, analytical solutions of the FP equation are known only for some linear systems and a very restricted class of nonlinear systems. Direct numerical methods aiming to solve the low-dimensional FP equations, such as the finite-element method [12] and the finite difference method [13] are hardly feasible for the nonlinear extended dynamic systems with high-dimensional FP equations. In these cases, the so-called "curse of dimension" comes into play which means that difficulties arise due to the processing capacity as well as the storage needed for the computation increases dramatically with the dimension of the FP equations. Therefore, several alternative techniques are developed to provide approximate solutions to the FP equations, such as the stochastic averaging method [2], the local statistical linearization method [9], the Gaussian closure method [7,10], etc.

The path integration (PI) method is an efficient approximation to find the stationary and non-stationary response probability density functions (PDF) of the Markov dynamic systems. This method is based on the Markov property of the dynamic system and the evolution of the response PDF is computed in short time steps via a step-by-step solution technique. Specifically, according to the Chapman–Kolmogorov equation, the response PDF at a given time instant can be obtained when the response PDF at an earlier close time instant as well as the conditional PDF with a Gaussian form are already known. The main advantage of the PI method and the Markov dynamic system is that a host of accurate and useful response statistics can be obtained within one calculation. Wehner and Wolfer [14] were the first to apply the numerical PI method to solve nonlinear FP equations and then various PI procedures were developed and applied to address certain problems in the area of engineering, e.g., [15–20] etc. In the field of marine engineering, Naess and Johnsen [21] developed a three-dimensional (3D) PI procedure to estimate the response statistics of moored offshore structures and this research topic as well as the PI technique were extended in Karlsen's research work [22]. In their work, the PI method has been shown to be capable of providing satisfactory estimation of the stochastic response, even in the tail region for low probability levels. Recently, this algorithm was successfully extended to 4D for studying the stochastic roll response of a ship in random beam seas [23,24].

Unfortunately, the PI method does suffer from a curse of dimensionality problem. Currently, some 4D problems can be analyzed by the PI method at an acceptable computational cost. However, the associated computation for the 6D coupled nonlinear system is unaffordable at present. On the other hand, it may be noted that the Monte Carlo simulation method does not suffer critically from the curse of dimensionality problem since the statistics of the response are obtained directly from the realizations. Basically, the Monte Carlo simulation is the simplest and most versatile way to determine the response statistics of the dynamic systems. For the cases of ship rolling, the nonlinear damping and restoring moments as well as the time-dependent wave excitation term can be directly dealt with. Even though Monte Carlo simulation enables the empirical estimation of response statistics for the 6D augmented system to be determined, this work, on the basis of straightforward counting, is only a brute force alternative and has its drawback at the same time. It cannot provide information at the same level of detail as the PI method [25]. Particularly, when the Monte Carlo method is applied to estimate the statistics of large roll response with low probability levels or evaluate different kinds of response statistics in one step, the associated computational cost as well as the efficiency would be sacrificed in practice.

In this paper, the upcrossing rate for high-level roll responses and the probabilities of exceedance are of central importance in evaluation of the response statistics. The feasibility of replacing the 6D extended system by the 4D coupled system in terms of determining the above two aspects will be discussed. The main scheme of the proposed work is shown in Fig. 1. Specifically, for different sea states, the response statistics calculated by the 4D PI method will be compared with that evaluated by the pertinent 6D Monte Carlo simulation. If the simplicity is practicable, the 4D dynamic system and the efficient 4D PI method, with its advantage in providing different kinds of response statistics within one calculation, can be applied to address the challenge of determining the stochastic roll response subjected to random wave excitation. The numerical approaches as well as the results and conclusions obtained in this work hopefully can provide useful references for ship stability research and stochastic dynamic analysis of nonlinear systems.

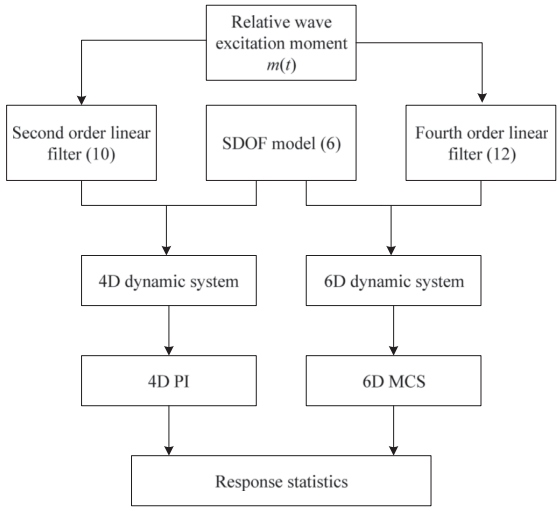

Fig. 1. Main scheme of the work.

2. Mathematical model of roll motion

By neglecting coupling, the rolling behavior of the vessel in random beam seas can be represented by the following SDOF equation:

$$I\ddot{\theta}(t) + B(\dot{\theta}(t)) + C(\theta(t)) = M(t) \tag{1}$$

where $\theta(t)$ and $\dot{\theta}(t)$ are the roll angle and the roll velocity, respectively. I is the virtual or total moment of inertia in roll, B is the damping moment term, C is the restoring moment term and $M(t)$ represents the random wave excitation moment.

The virtual moment of inertia I, generally consists of two parts: the moment of inertia in roll I_{44} and the added mass moment term A_{44}, i.e.

$$I = I_{44} + A_{44} \tag{2}$$

The roll damping normally has three kinds of components: the wave damping due to radiation at the free surface; the damping caused by vortex shedding and flow separation as well as the viscous friction damping. In general, these terms are coupled with each other, hence the quantitative evaluation of the roll damping is difficult. Nevertheless, the linear-plus-quadratic damping (LPQD) model, which has been verified by numerous studies of experimental data, is a good expression used in the SDOF Eq. (1). This model is given as

$$B(\dot{\theta}(t)) = B_{44}\dot{\theta}(t) + B_{44q}\dot{\theta}(t)|\dot{\theta}(t)| \tag{3}$$

where B_{44} and B_{44q} are linear and quadratic damping coefficients, respectively.

The restoring moment term is usually given by a nonlinear odd function of the roll angle, i.e.

$$C(\theta(t)) = \Delta(C_1\theta(t) - C_3\theta^3(t)) \tag{4}$$

in which, Δ is the displacement of the vessel, C_1 and C_3 are the linear and the nonlinear roll restoring coefficients of the restoring arm, respectively. It should be noted that the roll motion has a softening characteristic since the nonlinear stiffness term is negative. For the softening cases, ship capsizing would happen when the roll angle exceeds the angle of vanishing stability beyond which the restoring force becomes negative [19].

The random wave excitation moment $M(t)$ can be described by the wave excitation moment spectrum, $S_{MM}(\omega)$. The latter is related to the wave energy spectrum, $S_{\zeta\zeta}(\omega)$, by the following relationship [10,26]:

$$S_{MM}(\omega) = |F_{roll}(\omega)|^2 S_{\zeta\zeta}(\omega) \tag{5}$$

where $|F_{roll}(\omega)|$ represents the roll moment amplitude per unit wave height at frequency ω. It is the transfer function between the wave energy spectrum and the wave excitation moment spectrum and it depends on ship geometry and frequency ω. Generally, for beam seas, long waves with low frequencies are effective for roll motion, but the excitation due to short waves with high frequencies is almost negligible [27]. Moreover, the wave elevation and the wave excitation moment are assumed to be stationary Gaussian processes.

Dividing Eq. (1) by $(I_{44}+A_{44})$, the final form of the differential equation is given as

$$\ddot{\theta}(t) + b_{44}\dot{\theta}(t) + b_{44q}\theta(t)|\dot{\theta}(t)| + c_1\theta(t) - c_3\theta^3(t) = m(t) \tag{6}$$

where b_{44}, b_{44q}, c_1, c_3 are relative roll parameters [24]. In this case, the spectrum of the relative wave excitation moment, $S_{mm}(\omega)$, can be expressed as

$$S_{mm}(\omega) = |F_{roll}(\omega)|^2 S_{\zeta\zeta}(\omega)/(I_{44} + A_{44})^2 \tag{7}$$

Moreover, the natural frequency of the roll motion, ω_0, is determined as

$$\omega_0 = \sqrt{\Delta C_1/(I_{44} + A_{44})} = \sqrt{c_1} \tag{8}$$

Finally, the SDOF model (6) can be transformed into the state-space equation written as

$$\begin{cases} dx_1 = x_2 dt \\ dx_2 = (-b_{44}x_2 - b_{44q}x_2|x_2| - c_1x_1 + c_3x_1^3 + x_3)dt \end{cases} \tag{9}$$

where $x_1=\theta(t)$, $x_2=\dot{\theta}(t)$, *and* $x_3=m(t)$.

3. Shaping filter technique

General filtering techniques are available only for the stationary stochastic processes [6]. Thus, the relative wave excitation moment $m(t)$ can be approximated quite satisfactory by a suitable shaping filter. The linear filtering theory is widely used in the engineering community due to its simplicity and practicality. Dostal et al. [9] proposed a second-order linear filter and a fourth-order linear filter to model the narrow-banded target spectrum and these two filters are also available for the desired spectrum, $S_{mm}(\omega)$.

In this case, the relative wave excitation moment, $S_{mm}(\omega)$ can be approximated by the following second-order linear filter:

$$\begin{cases} dx_3 = (x_4 - \beta x_3)dt + \gamma dW \\ dx_4 = -\alpha x_3 dt \end{cases} \tag{10}$$

where x_3 and x_4 are the state variables in the filter equation with x_3 representing the filter output $m(t)$. $d\mathbf{W}(t)=\mathbf{W}(t+dt)-\mathbf{W}(t)$ is the increment of a Wiener process with $E\{d\mathbf{W}(t)\}=0$ and $E\{d\mathbf{W}(t)\,d\mathbf{W}(t+dt)\}=\delta(dt)$, $\delta(\cdot)$ represents the Dirac delta function. Furthermore α, β, γ are the parameters of the second-order linear filter. The spectrum generated by the differential equation (10) is given as

$$S_{2nd}(\omega) = \frac{1}{2\pi}\frac{\gamma^2\omega^2}{(\alpha - \omega^2)^2 + (\beta\omega)^2} \tag{11}$$

The fourth-order linear filter that represents a more accurate approximation is given by the following differential equation:

$$\begin{cases} dx_5 = (x_6 - \lambda_1 x_5)dt \\ dx_6 = (x_7 - \lambda_2 x_5)dt + \gamma_1 dW \\ dx_7 = (x_8 - \lambda_3 x_5)dt \\ dx_8 = -\lambda_4 x_5 dt \end{cases} \tag{12}$$

where x_5, x_6 ,x_7 and x_8 are variables introduced for the state-space representation and x_5 represents the filter output $m(t)$. The spectrum generated by Eq. (12) will have the following form:

$$S_{4th}(\omega) = \frac{1}{2\pi}\frac{\gamma_1^2\omega^4}{[(\beta_1 - \omega^2)^2 + (\alpha_1\omega)^2][(\beta_2 - \omega^2)^2 + (\alpha_2\omega)^2]} \tag{13}$$

where the parameters α_1, α_2, β_1, β_2 and γ_1 are the parameters in the fourth-order linear filter and the parameters λ_1, λ_2, λ_3, and λ_4 in Eq. (12) can be determined by the following relationship: $\lambda_1=\alpha_1+\alpha_2$, $\lambda_2=\beta_1+\beta_2+\alpha_1\alpha_2$, $\lambda_3=\alpha_1\beta_2+\alpha_2\beta_1$, $\lambda_4=\beta_1\beta_2$.

The parameters α, β, γ in the second-order filter and α_1, α_2, β_1, β_2, γ_1 in the fourth-order filter are determined by a least-square algorithm which is utilized for fitting of the target spectrum, $S_{mm}(\omega)$. The bandwidth and the peak frequency of the filtered spectra can be adjusted by changing the values of these parameters. It is worth emphasizing that the filtered spectra (11) and (13) are double-sided, while the wave spectrum and the wave excitation spectrum are physically single-sided. This difference must be considered in the practical simulation.

By combining the governing equation of the roll motion (9) with the second-order filter (10), the extended dynamic system is formed. Therefore, the roll motion in random beam seas can be described by the following 4D state-space equation:

$$\begin{cases} dx_1 = x_2 dt \\ dx_2 = (-b_{44}x_2 - b_{44q}x_2|x_2| - c_1x_1 + c_3x_1^3 + x_3)dt \\ dx_3 = (x_4 - \beta x_3)dt + \gamma dW \\ dx_4 = -\alpha x_3 dt \end{cases} \tag{14}$$

The 6D state-space equation for modeling the stochastic roll motion can be established in the similar way, i.e., by integrating the SDOF model (9) and the fourth-order filter (12).

4. Path integration method

Eq. (14) represents a Markov dynamic system driven by Gaussian white noise [28]. It can be expressed as an *Itô* stochastic differential equation (SDE):

$$d\mathbf{x} = \mathbf{a}(\mathbf{x}, t)dt + \mathbf{b}(t)d\mathbf{W}(t) \tag{15}$$

where $\mathbf{x}(t)=(x_1(t),\ldots,x_4(t))^{\mathrm{T}}$ is a four-dimensional state space vector process, the vector $\mathbf{a}(\mathbf{x},t)$ denotes the drift term and $\mathbf{b}(t)d\mathbf{W}(t)$ is the diffusive term. The vector $d\mathbf{W}(t)=\mathbf{W}(t+dt)-\mathbf{W}(t)$ represents independent increments of a standard Wiener process.

The solution $\mathbf{x}(t)$ to Eq. (15) is a Markov process and its transition probability density (TPD), also known as the conditional PDF, $p(\mathbf{x},t \mid \mathbf{x}',t')$ satisfies the FP equation which is casted in the following form:

$$\frac{\partial}{\partial t}p(\mathbf{x},t|\mathbf{x}',t') = -\sum_{i=1}^{4}\frac{\partial}{\partial x_i}a_i(\mathbf{x},t)p(\mathbf{x},t|\mathbf{x}',t') + \frac{1}{2}\sum_{i=1}^{4}\sum_{j=1}^{4}\frac{\partial^2}{\partial x_i\partial x_j}(\mathbf{b}(t)\cdot\mathbf{b}^T(t))_{ij}p(\mathbf{x},t|\mathbf{x}',t') \tag{16}$$

Unlike direct numerical techniques, such as the finite-element method and the finite difference method, aiming to solve the FP Eq. (16) and obtain the TPD directly, the PI method captures the probabilistic evolution of the process $\mathbf{x}(t)$ by taking advantage of the Markov property. In principle, the PI method is an approximation approach and the PDF of the process $\mathbf{x}(t)$ can be determined by the following basic equation, i.e., the well-known Chapman–Kolmogorov equation:

$$p(\mathbf{x},t) = \int_{R^4} p(\mathbf{x},t|\mathbf{x}',t')p(\mathbf{x}',t')d\mathbf{x}' \tag{17}$$

where

$d\mathbf{x}' = \prod_{i=1}^{4} dx'_i$.

Specifically, the value of the PDF at time t, $p(\mathbf{x},t)$, can be calculated by Eq. (17) with the value of previous PDF at time t' as well as the value of conditional PDF, $p(\mathbf{x},t \mid \mathbf{x}',t')$. For a numerical solution of the SDE (15), a time discrete approximation should be introduced. Naess and Moe [15] proposed a fourth-order Runge–Kutta–Maruyama (RKM) discretization approximation:

$$\mathbf{x}(t) = \mathbf{x}(t`) + \mathbf{r}(\mathbf{x}(t`),t`)\Delta t + \mathbf{b}(t`)\Delta\mathbf{W}(t`) \tag{18}$$

where the vector $\mathbf{r}(\mathbf{x}(t`),t`)$ is the explicit fourth-order Runge–Kutta approximation or Runge–Kutta increment. Since $\mathbf{W}(t)$ is a Wiener process, the independent increment $\Delta\mathbf{W}(t')=\mathbf{W}(t)-\mathbf{W}(t')$ is a Gaussian variable for every t'.

If we consider only the deterministic part of Eq. (15), the approximation (18) reduces to the fourth-order Runge–Kutta approximation $\mathbf{x}(t)=\mathbf{x}(t')+\mathbf{r}(\mathbf{x}(t'),t')\Delta t$. Experiments have shown that, for the Markov systems, the accuracy associated with approximating the deterministic terms is the most important [16]. In this regard, the accuracy of the fourth-order RKM approximation is satisfactory since the fourth-order Runge–Kutta approximation follows the time evolution of the deterministic part of Eq. (15) with an accuracy to the order of $O(\Delta t^5)$.

The time sequence $\{\mathbf{x}(i\cdot\Delta t)\}_{i=0}^{\infty}$ is a Markov chain and it can approximate the time-continuous Markov process solution of the SDE (15) when the time increment $\Delta t=t-t'$ is sufficiently small. Moreover, the conditional PDF of the process $\mathbf{x}(t)$, $p(\mathbf{x},t \mid \mathbf{x}',t')$, follows a (degenerate) Gaussian distribution and it can be written as (see also [21])

$$p(\mathbf{x},t|\mathbf{x}`,t`) = \delta(x_1 - x`_1 - r_1(\mathbf{x}`,\Delta t))\cdot\delta(x_2 - x`_2 - r_2(\mathbf{x}`,\Delta t)) \cdot\tilde{p}(x_3,t|x`_3,t`)\cdot\delta(x_4 - x`_4 - r_4(\mathbf{x}`,\Delta t)) \tag{19}$$

where $\tilde{p}(x_3,t|x'_3,t')$ is given by the relation

$$\tilde{p}(x_3,t|x`_3,t`) = \frac{1}{\sqrt{2\pi\gamma^2\Delta t}}\cdot\exp\left\{-\frac{(x_3 - x`_3 - r_3(\mathbf{x}`,\Delta t))^2}{2\gamma^2\Delta t}\right\} \tag{20}$$

in which $r_i(\mathbf{x}',\Delta t)$, $i=1,2,3,4$, are the Runge–Kutta increments for the state space variables.

Since the expression for the conditional PDF is known, the time evolution of the PDF of $\mathbf{x}(t)$ can be determined by the iterative algorithm (21) if an initial PDF $p(\mathbf{x}^{(0)},t_0)$ is given

$$p(\mathbf{x},t) = \int_{R^4}\cdots\int_{R^4}\prod_{i=1}^{n}p(\mathbf{x}^{(i)},t_i|\mathbf{x}^{(i-1)},t_{i-1}) \cdot p(\mathbf{x}^{(0)},t_0)d\mathbf{x}^{(0)}\ldots d\mathbf{x}^{(n-1)} \tag{21}$$

where $\mathbf{x}=\mathbf{x}^{(n)}$, $t=t_n=t_0+n\cdot\Delta t$.

Eq. (21) describes the mathematical principle of the PI approach. In this work, the initial PDF $p(\mathbf{x}^{(0)},t_0)$ is chosen as a quaternary Gaussian PDF in four dimensions with zero mean and variances evaluated by a simple Monte Carlo simulation [16]. The straightforward Monte Carlo simulation ensures that the initial quaternary Gaussian PDF includes all the information corresponding to the selected parameters of the dynamic system, and it also provides a rational computational domain for the subsequent simulation [18]. As for the numerical implementation of the iterative algorithm (21), it represents the PDF at the previous time t' as an interpolating spline surface via Parabolic B-spline and then it evaluates the PDF at time t by several specific steps. The numerical iterative algorithm and the associated specific computational steps have been systematically described by Iourtchenko et al. [29] and Yurchenko et al. [30]. Furthermore, the capability of the PI method in producing accurate and reliable solutions for the stochastic dynamic systems has been demonstrated by numerous examples [15,16].

5. Numerical results

In this section, the performance of the proposed 4D PI method for roll response prediction and the feasibility of simplifying the 6D dynamic system by means of the 4D dynamic system in terms of evaluating the important statistics of the roll response will be presented.

5.1. Stochastic roll response in random seas

An ocean surveillance ship in Ref. [10] is considered for the numerical simulation in order to study the stochastic roll response. The main parameters of the vessel are stated in Table 1, and Fig. 2 presents the GZ curve of the real ship.

In this work, the random stationary sea state is specified by the modified Pierson–Moskowitz (P–M) spectrum, which is widely used for the fully developed sea states. The wave spectrum is given as

$$S_{\xi\xi}(\omega) = \frac{5.058g^2H_s^2}{T_p^4\omega^5}\exp(-1.25\frac{\omega_p^4}{\omega^4}) \tag{22}$$

where H_s denotes the significant wave height, ω_p is the peak frequency at which the wave spectrum $S_{\xi\xi}(\omega)$ has its maximum, and T_p is the corresponding peak period.

The sea state with $H_s=4.0$ m, $T_p=11.0$ s is selected for the

Table 1
List of ship parameters.

Parameters	Dimensional value
$I_{44}+A_{44}$	5.540×10^7 kg m^2
Δ	2.017×10^7 N
b_{44}	0.095 s^{-1}
b_{44q}	0.0519
c_1	1.153 s^{-2}
c_3	0.915 s^{-2}
ω_0	1.074 rad/s

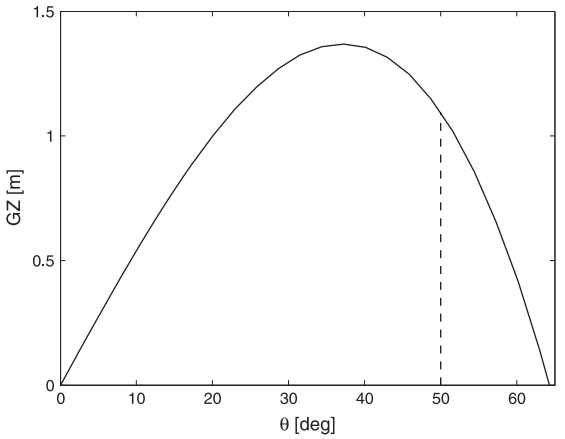

Fig. 2. GZ curve for the selected vessel.

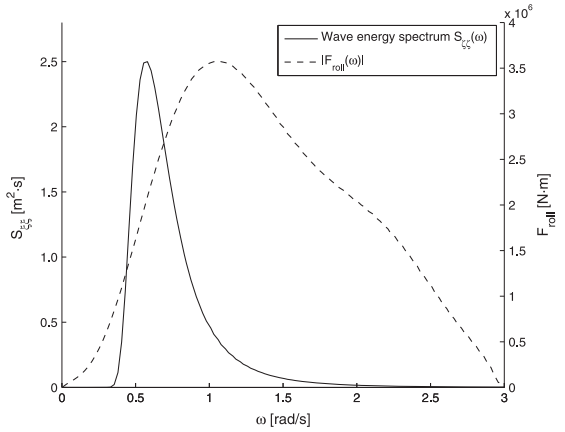

Fig. 3. Wave energy spectrum $S_{\zeta\zeta}(\omega)$ and roll excitation moment per unit wave height, $|F_{roll}(\omega)|$ [10].

subsequent study. Fig. 3 presents the selected wave energy spectrum, $S_{\zeta\zeta}(\omega)$ and roll excitation moment per unit wave height, $|F_{roll}(\omega)|$. Then the wave excitation moment spectrum, S_{MM} and the relative wave excitation moment spectrum S_{mm} for the selected sea state are determined by Eqs. (5) and (7), respectively.

After determining the target spectrum S_{mm}, the parameters α, β, γ in the second-order filter (10) and the parameters α_1, α_2, β_1, β_2, γ_1 in the fourth-order filter (12) are obtained by minimizing the square errors between the filtered spectrum and the desired spectrum. In this regard, the least square algorithm is available in the curve fitting applications of MATLAB. The fitting results for the two linear filters are shown in Figs. 4 and 5. It can be readily seen that both of the filtered spectra are satisfactory in terms of bandwidth, peak frequency and peak value, while the fourth-order linear filter in Fig. 5 represents a better fitting precision. Particularly, for the roll motion cases, the transfer function between the wave excitation term and the roll response in the SDOF model (1) is narrow-banded due to the light roll damping. Therefore, in Fig. 4, for the selected ship model, the obvious discrepancies between the spectrum generated by the second-order linear filter and the target spectrum in the low-frequency and the high-frequency regions would not impact the subsequent roll responses significantly. Whereas, the fitting accuracy near the natural roll

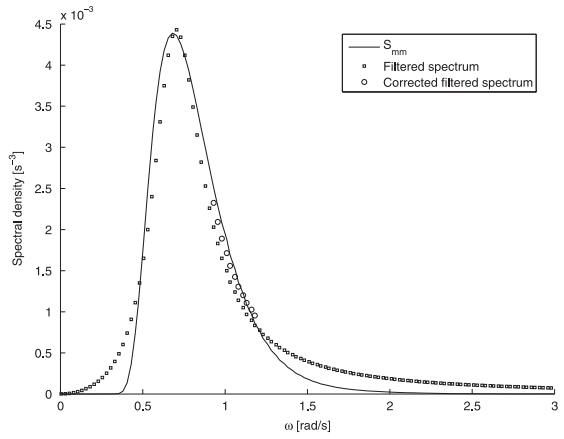

Fig. 4. Relative wave excitation moment spectrum and the second-order filtered spectrum, the corrected filtered spectrum (part) for the sea state with $H_s=4.0$ m, $T_p=11.0$ s.

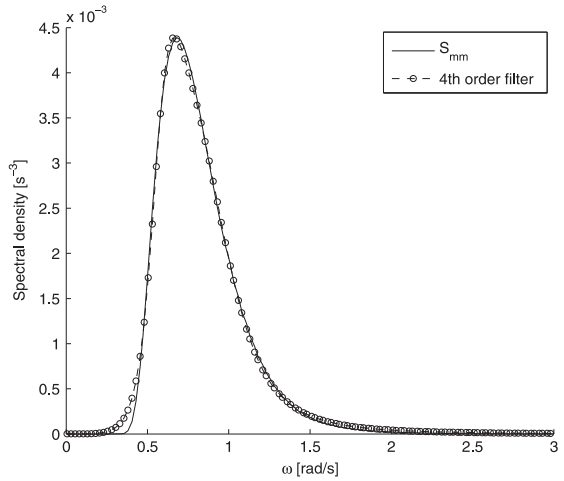

Fig. 5. Relative wave excitation moment spectrum and the fourth-order filtered spectrum for the sea state with $H_s=4.0$ m, $T_p=11.0$ s.

frequency, ω_0, is crucial for evaluating the roll response because the latter is sensitive to the variation of the external excitation in the critical frequency region near ω_0.

In Fig. 4, a slight discrepancy between the two spectra in the critical region can be observed. Thus, we introduce a constant, c, which serves as a correction factor for the second-order filter in order to decrease the discrepancy in this region. Then, the filtered spectrum (11) changes to the following expression:

$$S_{2nd}(\omega) = \frac{1}{2\pi}\frac{(c\cdot\gamma)^2\omega^2}{(\beta-\omega^2)^2+(\alpha\omega)^2} \tag{23}$$

In this work, for the selected sea state and vessel model, the correction factor c is taken to be 1.07 by considering the mean difference between the two spectral densities in the critical region. The corrected spectrum in the critical region is also presented in Fig. 4. In addition, for the same ship model, the value of the correction factor c would vary slightly for different sea states and the rationality of introducing the correction factor will be verified by the following study with the assistance of Monte Carlo simulation.

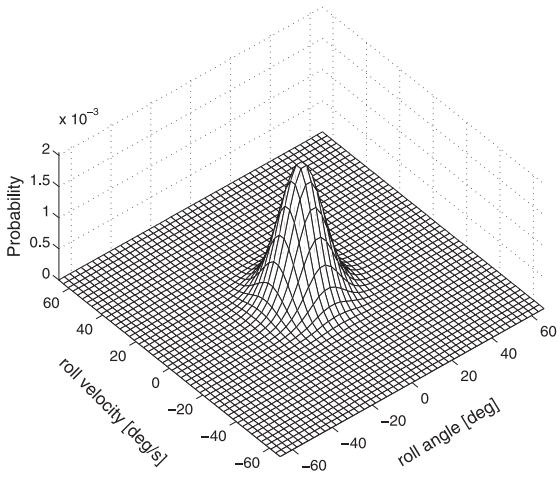

Fig. 6. Joint PDF of the roll response obtained by the 4D PI method for the sea state with $H_s=4.0$ m, $T_p=11.0$ s.

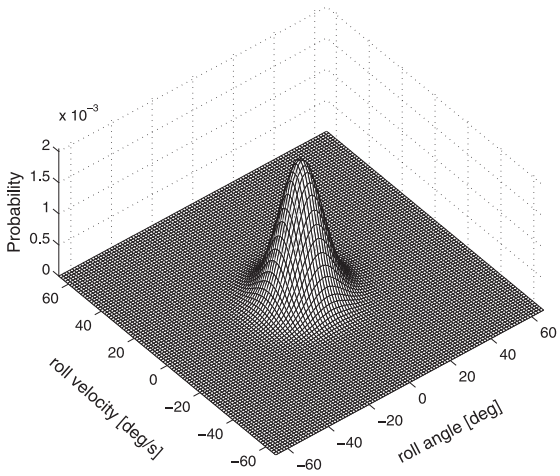

Fig. 7. Joint PDF of the roll response obtained by the 6D Monte Carlo simulation for the sea state with $H_s=4.0$ m, $T_p=11.0$ s.

As described in Section 3, the 4D dynamic system and 6D dynamic system are established after the work of spectrum fitting. For the 4D system, the joint probability density function (PDF) of the roll angle and the roll velocity can be obtained directly by the 4D PI method. The joint PDF of the roll response for the selected sea state calculated by the 4D PI method is presented in Fig. 6, while Fig. 7 displays the joint PDF evaluated by Monte Carlo simulation. The joint PDF of the roll response yielded by the 4D PI approach is found to be in good agreement with the results extracted from the 6D Monte Carlo simulation. It can be observed in Figs. 6 and 7 that the PDF of the roll response is symmetric. Further, the mean upcrossing rate of the roll response can be determined by the Rice formula (24), benefiting from the joint PDF of the roll response obtained by the 4D PI approach:

$$\nu^+(\zeta;\, t) = \int_0^\infty \dot{\theta} f_{\theta\dot{\theta}}(\zeta,\, \dot{\theta};\, t)\, d\dot{\theta} \tag{24}$$

where $\nu^+(\zeta;t)$ denotes the expected number of upcrossing for the ζ-level per unit time at time t by the roll angle process $\theta(t)$, $f_{\theta\dot{\theta}}(\theta,\, \dot{\theta};\, t)$ is the joint PDF of the roll angle and the roll velocity at time t.

For nonlinear ship rolling in random beam seas, due to the presence of negative nonlinear stiffness term in the SDOF model (6), ship capsizing may happen when the predetermined simulation time T is long enough or the intensity of the external excitation is strong enough. We should note that the response of the dynamic system with softening stiffness, e.g. the SDOF model (6) with negative nonlinear stiffness term, is not strictly stationary. Nevertheless, if the meantime to capsize is long enough, the dynamic system can be regarded as a highly reliable system and the corresponding roll response reaches stationarity in an approximate sense [2].

The advantage of the PI method is noticeable, i.e. sufficient response statistics can be obtained within one simulation. However, the main drawback of this technique is that the computation cost is unaffordable for the 6D nonlinear coupled system. Whereas, the Monte Carlo simulation for the 6D system is attractive due to its simplicity and versatility and the curse of dimension problem does not influence it so much. The numerical calculation and the counting procedure in order to obtain the response statistics require significant effort in connection with the Monte Carlo simulation. Since we focus on the two important aspects of response statistics, i.e., the upcrossing rate of high-level roll response and the probability of exceedance for the specific high levels, the Monte Carlo simulation can serve as an alternative way to evaluate the above two aspects for the 6D system.

For the 6D dynamic system, the fourth-order RKM method is applied to solve the corresponding SDE and then the time series of the roll response are obtained. In the numerical simulation, ship capsizing is assumed to occur if the roll angle process exceeds the positive or negative angle of vanishing stability and then the single realization is terminated because the subsequent roll angle process $\theta(t)$ will exceed $\pi/2$ or $-\pi/2$ rapidly. A large number of realizations are required for evaluating the response statistics, especially for the high-level responses with low probability levels and the appropriate sample mean value of the upcrossing rate can be obtained as

$$\hat{\nu}^+(\zeta) = \frac{\sum_{i=1}^k n_i^+(\zeta;\, T_i)}{\sum_{i=1}^k T_i} \tag{25}$$

where $n_i^+(\xi;\, T_i)$ denotes the counted number of upcrossing of the level ζ within a time duration of length T_i for simulated time history no. i. The practical simulation time T_i is not fixed for each simulation, it is equal to the predetermined simulation time T if no capsizing occurs. Otherwise, it is the value of the termination time t_i for each case where capsizing occurs [31].

Moreover, the number of realizations, k, e.g. $k=1000$–5000, is selected according to the values of the upcrossing rates in the tail region and the length of the predetermined simulation time T. Usually, low upcrossing rates and short time periods T correspond to a large simulation number k. A fair approximation of the 95% confidence interval, $\mathrm{CI}_{0.95}$, for the value of $\hat{\nu}^+(\zeta)$ can be expressed as (e.g. [32])

$$\mathrm{CI}_{0.95}(\zeta) = \left(\hat{\nu}^+(\zeta) - 1.96\frac{\hat{s}(\zeta)}{\sqrt{k}},\, \hat{\nu}^+(\zeta) + 1.96\frac{\hat{s}(\zeta)}{\sqrt{k}}\right) \tag{26}$$

where the empirical standard deviation $\hat{s}(\xi)$ is given as

$$\hat{s}(\zeta)^2 = \frac{1}{k-1}\sum_{i=1}^k \left(\frac{n_i^+(\zeta;\, T_i)}{T_i} - \hat{\nu}^+(\zeta)\right)^2 \tag{27}$$

For the selected sea state, the marginal PDF of the roll angle process calculated by the 4D PI approach and the empirical PDF

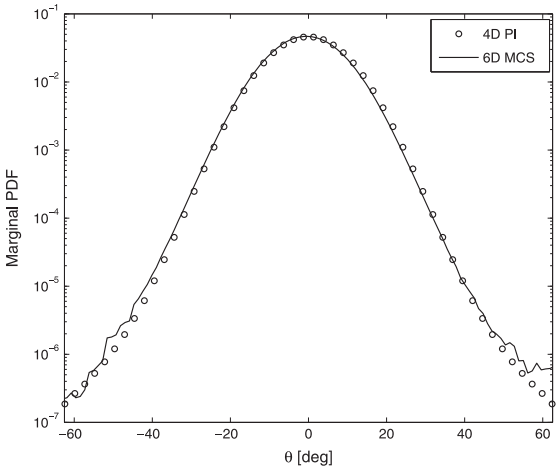

Fig. 8. Marginal PDF of the roll angle process $\theta(t)$ obtained by the 4D PI method and the 6D Monte Carlo simulation (MCS), for the sea state with $H_s=4.0$ m, $T_p=11.0$ s.

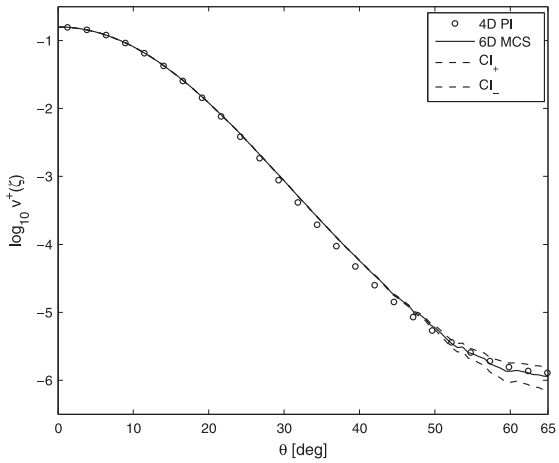

Fig. 9. Upcrossing rates obtained by the 4D PI method and the 6D Monte Carlo simulation (MCS), for the sea state with $H_s=4.0$ m, $T_p=11.0$ s.

evaluated by the 6D Monte Carlo simulation are plotted in Fig. 8. In Fig. 9, the mean upcrossing rate obtained by the 4D PI approach and the Rice formula (24) and the empirical estimation of the upcrossing rate $\hat{\nu}^+(\zeta)$ as well as the 95% confidence interval provided by the Monte Carlo simulation are plotted. Moreover, both of Figs. 8 and 9 are plotted with a logarithmic scale along the vertical axis. In the 6D Monte Carlo simulation, the simulation number k is selected to be 3000 and the predetermined simulation time T is 1.0×10^5 s (about 17,030 natural roll periods) for each simulation. Comparing the marginal PDF of the roll angle process and the upcrossing rate evaluated by the 4D PI method with the pertinent 6D Monte Carlo simulation results demonstrate a satisfactory level of agreement, even in the large roll response region.

Fig. 10 shows the spectra of roll responses generated by the 4D dynamic system and the 6D dynamic system. Specifically, the random seeds for generating white noise processes are kept the same in these two systems for the selected sea state. The white noise processes are filtered and the corresponding RKM algorithms are applied to solve the equations and generate the

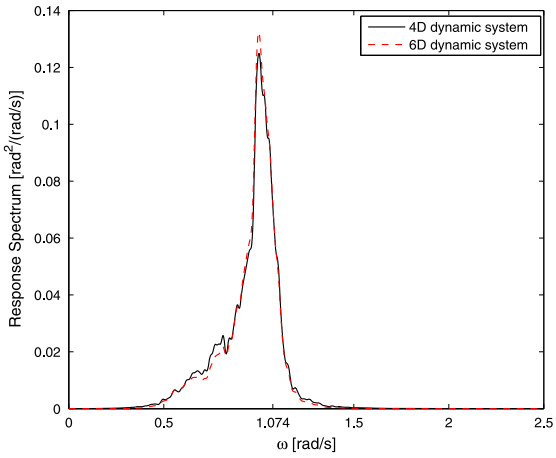

Fig.10. Roll response spectra for the 4D dynamic system and the 6D dynamic system for the sea state with $H_s=4.0$ m, $T_p=11.0$ s.

samples of the roll responses. In Fig. 10, the response spectra are narrow banded and peaked near the natural roll frequency due to the light roll damping. Even though there are slight discrepancies in some local regions, the agreement of these two spectra is acceptable on the whole. Moreover, the satisfactory result in Fig. 10 corroborates the fact observed in Figs. 6–9, i.e., that the statistics of the roll responses generated by the two different systems exhibit satisfactory agreements.

In conclusion, the acceptable agreements of the two sets of response statistics obtained by the different approaches, as shown in Figs. 6–9, verifies the capability of the 4D PI method in providing accurate and reliable results. The satisfactory results in these Figures in combination with the good agreement in Fig. 9 also illustrate the rationality of introducing the correction factor c into the second-order linear filter (11).

5.2. Influence of the wave excitations on the statistics of large roll response

In this part, the research effort is devoted to study the upcrossing rates for the large roll response angles as well as the exceedance probabilities for the specific high level for different sea states. As we can see in Eq. (22), for the selected modified P–M spectrum, the wave energy spectrum is determined by two parameters, i.e., the peak period T_p and the significant wave height H_s. Obviously, these two factors also influence the wave excitation spectrum, $S_{MM}(\omega)$ and the statistics of roll response. To highlight the effects of these two parameters individually, the coefficients of the ship model and the wave spectrum are assumed to be constant in the numerical simulations except the parameter whose effect is going to be studied.

Firstly, we investigate the effects of peak period by introducing four sea states with the value of significant wave height fixed to 4.0 m. The peak periods increase linearly from 10.0 to 11.5 s (with 5% increment). The spectra for these four sea states are shown in Fig. 11, while Fig. 12 displays the corresponding relative wave excitation spectra. It can be seen in Figs. 11 and 12 that when the peak frequency of the wave energy spectrum is close to the peak frequency of the transfer function $|F_{roll}(\omega)|$, the subsequent wave excitation spectrum has a large peak value as well as a large spectral area, which means that the close peak frequencies of the above two terms lead to intensive roll excitation energy. This phenomenon can be viewed as a kind of resonance effect.

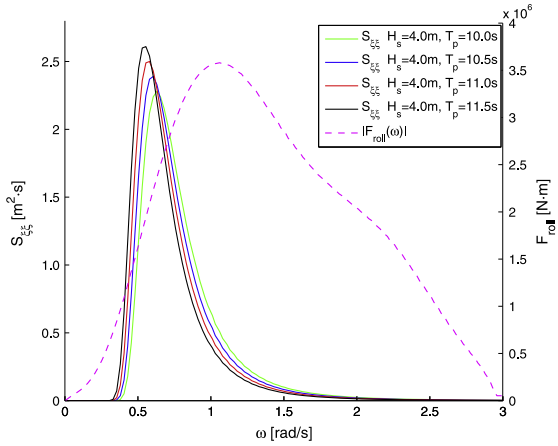

Fig.11. Wave energy spectra for the sea states with different peak periods and roll excitation moment per unit wave height.

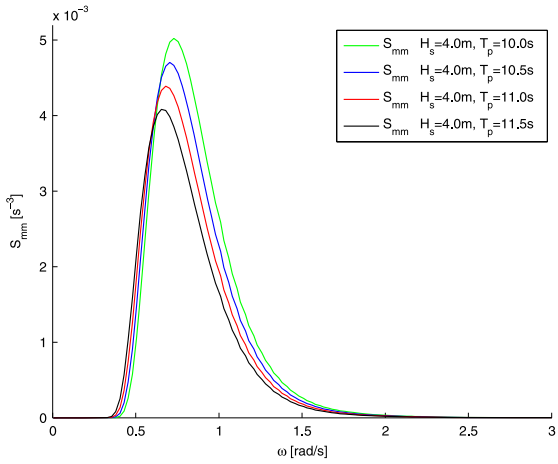

Fig.12. Relative wave excitation spectra for the sea states with different peak periods.

Table 2
Parameter values of the second-order filter (14) and the fourth-order filter (16) for the sea states with different peak periods.

Sea states		Second-order filter			Fourth-order filter				
H_s (m)	T_p (s)	α	β	γ	λ_1	λ_2	λ_3	λ_4	γ_1
4.00	10.0	0.561	0.370	0.0467	0.931	1.573	0.550	0.393	0.0390
4.00	10.5	0.527	0.371	0.0453	0.939	1.498	0.519	0.347	0.0379
4.00	11.0	0.495	0.366	0.0432	0.932	1.429	0.486	0.309	0.0362
4.00	11.5	0.457	0.366	0.0417	0.938	1.367	0.460	0.275	0.0350

Moreover, for the selected ship model, the resonance increases the value of S_{mm} in the critical frequency region near ω_0. The fitting results of the second-order filter and the fourth-order filter for these relative excitation spectra are shown in Table 2.

When the roll angle is near or beyond the maximum of the GZ curve, it can be regarded as a large roll response [33]. In addition, the International Maritime Organization (IMO) has specific requirements for the static stability in the large roll region. Referring to the 2008 Intact Stability (IS) code [34], we select θ=30–50° as

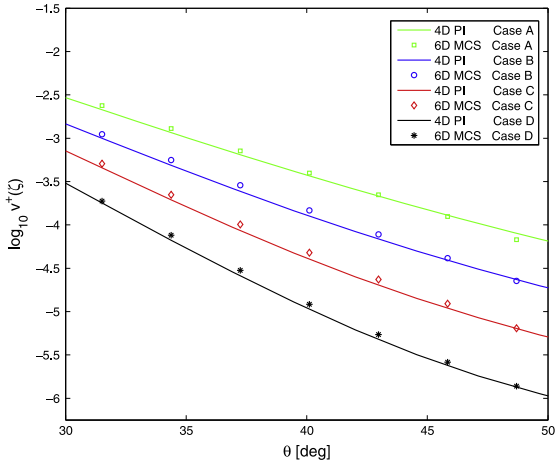

Fig.13. Upcrossing rates of high-level roll responses for the sea states with different peak periods determined by the 4D PI method and the 6D Monte Carlo simulation (MCS), Case A: H_s=4.0 m, T_p=10.0 s; Case B: H_s=4.0 m, T_p=10.5 s; Case C: H_s=4.0 m, T_p=11.0 s; Case D: H_s=4.0 m, T_p=11.5 s.

the large roll region for the subsequent study. Fig. 13 presents the upcrossing rates in this region for these sea states with different peak periods. The two sets of upcrossing rates are determined by the 4D PI method and the 6D Monte Carlo simulation, respectively. For each case, the correction factor c is introduced into the second-order filter and it can be seen that the resonance effect increases the intensity of external excitation and then leads to large roll response. Obviously, the upcrossing rates of the large roll response evaluated by the 4D PI approach experience a good agreement with the pertinent 6D Monte Carlo simulation data.

Generally, there are two types of intact stability failures: total intact stability failure and partial intact stability failure [35]. Ship capsizing is defined as the former category, while the latter can be associated with exceeding large or extreme roll angles, such as the flooding angle θ_f, which may lead to damage of the vessel. In this work, we set the value of flooding angle to 50°, as shown in Fig. 2. If the assumption of statistically independent upcrossing or exceedance is valid for this specific high level, the stability failure event can be evaluated by means of the Poisson estimate. Therefore, for the 4D system with highly reliable property, the probability that the process $\theta(t)$ exceeds the specific high level, θ_f during a time interval of length T can be approximated as

$$P_{PI}(\theta_f, T) = 1 - \exp\left(-\int_0^T \nu^+(\theta_f; t)dt\right) = 1 - \exp(-\nu^+(\theta_f)\cdot T) \tag{28}$$

where $\nu^+(\theta_f)$ represents the mean upcrossing rate of the level θ_f at a suitable reference point in time, which can be determined directly by the PI method and the Rice formula (24).

For the 6D dynamic system, the probability of exceeding the level θ_f during the predetermined simulation time T, $P_{MC}(\theta_f,T)$ can be evaluated by the 6D Monte Carlo simulation, i.e., running a sufficient number, N_t, of simulations with the same predetermined simulation T and then ranked the simulated maximum roll angles in ascending order [36]. The exceedance probability P_{MC} converges towards a normal distribution for a large number of realizations. Thus, the 95% confidence interval of the exceedance probability, ΔP, can be calculated by the following equation [37]:

$$\Delta P = 1.96\cdot\frac{2}{\sqrt{N_t}}\sqrt{P_{MC}(\theta_f, T)\cdot(1 - P_{MC}(\theta_f, T))} \tag{29}$$

Table 3
Comparison of exceedance probabilities for the level θ_f for sea states with different peak periods obtained by the 4D PI method and the 6D Monte Carlo method, $T=1$ h.

H_s (m)	T_p (s)	P_{PI}	P_{MC}	$CI_{0.95}$
4.00	10.0	0.2186	0.2040	(0.1928, 0.2152)
4.00	10.5	0.0690	0.0656	(0.0587, 0.0725)
4.00	11.0	0.0192	0.0225	(0.0184, 0.0266)
4.00	11.5	0.0041	0.0047	(0.0028, 0.0066)

Finally, the range of error tolerance of the exceedance probability can be given as follows:

$$P_{MC}(\theta_f, T) - \Delta P/2 \le P \le P_{MC}(\theta_f, T) + \Delta P/2 \tag{30}$$

In this work, for each sea state, we run 10 groups of numerical simulations to evaluate the probability of exceedance for the level θ_f. Each group includes a sufficient number, $N_t=5000$, of realizations as well as unique random seeds for generating the random wave excitations (i.e., the filtered white noise processes). Therefore, the exceedance probability evaluated by the 6D Monte Carlo simulation is the ensemble average of the 10 exceedance probabilities.

The time duration, T, for Eqs. (28) and (30) is selected to be 1 h. Subsequently, the results for the exceedance probabilities estimated by the two different methods are stated in Table 3 and the estimated 95% confidence intervals are also given in the Table. It is seen that the exceedance probabilities evaluated by the 4D PI method based on the Poisson assumption of the exceedance events agree with the empirical estimation of exceedance probabilities obtained via the 6D Monte Carlo simulation. The fact that resonance causes large roll response can also be observed in Table 3, i.e. the resonance leads to a large exceedance probability for the specific high level.

Secondly, the influences of the significant wave height H_s on the wave excitation spectra and the statistics of large roll response are considered. In this case, a similar analysis as previously stated is conducted by keeping the peak period of the wave energy spectra fixed to 11.0 s, while the values of the four significant wave heights vary linearly through 4.50–3.75 m. Accordingly, the subsequent relative wave excitation spectra are presented in Fig. 12 and the fitting results for the four relative wave excitation spectra are shown in Table 4. It is worth pointing out that the four spectra in Fig. 14 have the same peak frequency and the values of the parameters in the filters are almost unchanged for these sea states except the parameter γ in the second-order filter and γ_1 in the fourth-order filter which determine the peak values of the filtered spectra. However, as shown in Table 2, for the previous case, most of the parameters in the filters would change for the sea states with different peak periods.

In Fig. 15, the upcrossing rates of high roll response levels, for the sea states with different significant wave heights, obtained by the 4D PI method and the 6D Monte Carlo simulation are plotted. Further, for the selected sea states, the exceedance probabilities for the specific high level evaluated by these two approaches are presented in Table 5. The predetermined simulation time, the realization numbers as well as the other parameters for the 6D Monte Carlo simulation are kept the same as in the previous study. As shown in Eqs. (22) and (7), the spectral density of the wave energy spectrum and the spectral density of relative wave excitation spectrum are proportional to the square of the significant

Table 4
Parameter values of the second-order filter (14) and the fourth-order filter (16) for the sea states with different significant wave heights.

Sea states		Second-order filter			Fourth-order filter				
H_s (m)	T_p (s)	α	β	γ	λ_1	λ_2	λ_3	λ_4	γ_1
4.50	11.0	0.495	0.365	0.0486	0.931	1.428	0.485	0.309	0.0406
4.25	11.0	0.495	0.367	0.0458	0.934	1.428	0.486	0.309	0.0388
4.00	11.0	0.495	0.366	0.0432	0.932	1.429	0.486	0.309	0.0362
3.75	11.0	0.495	0.368	0.0405	0.932	1.429	0.486	0.309	0.0340

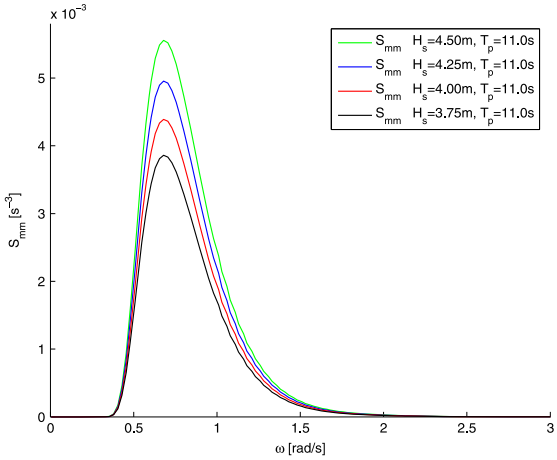

Fig.14. Relative wave excitation spectra for the sea states with different significant wave heights.

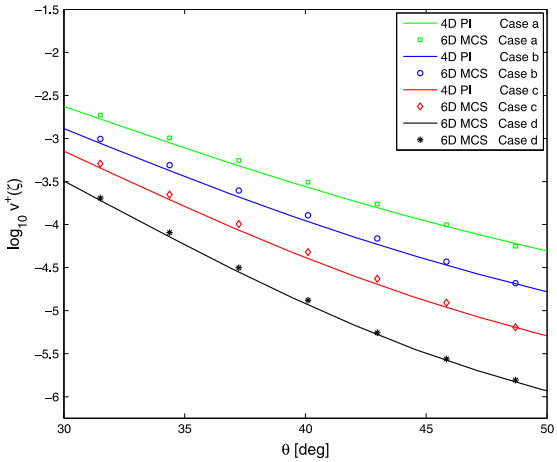

Fig.15. Upcrossing rate of the high-level roll responses for the sea states with different significant wave heights, determined by the 4D PI method and the 6D Monte Carlo simulation (MCS), Case a: $H_s=4.50$ m, $T_p=11.0$ s; Case b: $H_s=4.25$ m, $T_p=11.0$ s; Case c: $H_s=4.00$ m, $T_p=11.0$ s; Case d: $H_s=3.75$ m, $T_p=11.0$ s.

Table 5
Comparison of exceedance probabilities for the level θ_f for the sea states with different significant wave heights obtained by the 4D PI method and the 6D Monte Carlo method, $T=1$ h.

H_s (m)	T_p (s)	P_{PI}	P_{MC}	$CI_{0.95}$
4.50	11.0	0.1706	0.1729	(0.1624, 0.1834)
4.25	11.0	0.0610	0.0618	(0.0551, 0.0685)
4.00	11.0	0.0192	0.0225	(0.0184, 0.0266)
3.75	11.0	0.0045	0.0046	(0.0027, 0.0067)

wave height. Therefore, the increase in significant wave height results in large roll response which can be observed in Fig. 15 and Table 5. Moreover, the response statistics, i.e., the upcrossing rates for high roll response levels in Fig. 15 and the exceedance probabilities in Table 5, evaluated by the two different approaches demonstrate satisfactory agreements.

The effects of the peak period and significant wave height on the large roll response as well as on the exceedance probability for the specific high level, θ_f have been investigated. Both of the two parameters have significant influences on the wave excitation moments and the subsequent roll response, but they are based on different mechanisms. The former parameter enhances the roll response by means of resonance, while the latter serves to intensify the wave energy spectrum. It can also be observed that the large roll response is sensitive to the variation of the wave excitation. Moreover, the variations of the two parameters are linear, whereas the variations of the corresponding roll response are evidently nonlinear, which clearly illustrate the nonlinear characteristics of the dynamic systems.

More importantly, the good agreements of the two sets of statistics obtained by the 4D PI method and the 6D Monte Carlo simulation, which can be observed in Figs. 13 and 15; Tables 3 and 5 demonstrate the same conclusion as stated at the end of Section 5.1, i.e., that the 4D PI method is capable of providing reliable estimation of the response statistics, even for high level responses with low probability levels. Furthermore, the satisfactory agreements of the exceedance probabilities in Tables 3 and 5 illustrate the rationality of the assumption of statistically independent upcrossings and the Poisson estimate for the specific high level, θ_f. The 4D PI method obtains the two sets of statistics within one calculation, whereas, for the 6D Monte Carlo simulation, a large amount of repeated calculations and counting procedures have to be conducted for each set of response statistics. The computation time for the 4D PI method with 64^4 nodes (i.e., the grid number is 64 in each direction) applied to a given 4D system is around 5 h on a personal computer. As for the computational effort of the 6D Monte Carlo simulation for determining all kinds of response statistics, it depends on the probability levels in the tail region and would be around 0.5–2.0 times of that for the 4D PI method. Moreover, the computation cost of the Monte Carlo simulation for the probability level lower than 10^{-7} is formidable. In the meantime, for the high-level response, the statistics obtained by the Monte Carlo simulation are suffering from uncertainties.

On the basis of the calculations and results above, we can draw the conclusion that with the assistance of the correction parameter, c, the 4D extended system (14) can serve as an effective alternative to the corresponding 6D system in terms of determining the important statistics of roll response. In this regard, the 4D dynamic system and the 4D PI method enables an appropriate theoretical model as well as an efficient numerical technique, respectively, to be applied for the study of stochastic roll response.

6. Conclusions

In this paper, a second-order linear filter and a fourth-order linear filter have been introduced to model the random wave excitations associated in the roll motion. In this regard, a four-dimensional (4D) dynamic system and a six-dimensional (6D) dynamic system were established to evaluate the statistics of high-level roll responses when subjected to random wave excitations. Specifically, relying on the Markov properties of the 4D dynamic systems, the 4D PI method was introduced to solve the FP equation of the 4D system and then the response statistics, such as the upcrossing rates and the exceedance probabilities for the specific extreme roll angle were derived. For the 6D system, the response statistics were evaluated directly by 6D Monte Carlo simulations.

The main accomplishment of the present work is that the 4D dynamic system can serve as an efficient alternative to the 6D dynamic system in terms of determining the important response statistics. In this regard, a correction factor, c should be introduced in connection with the second-order filter. The idea is based on the property of light roll damping and it aims to improve the fitting accuracy of the second-order filter in the critical region near the natural roll frequency. Sea states with different peak periods and sea states with different significant wave heights were used as examples to demonstrate the versatility of the simplification. The influences of the peak period and significant wave height on the wave excitation spectrum and the subsequent roll response have also been investigated. The satisfactory agreement of the response statistics obtained by the 4D PI approach and 6D Monte Carlo simulation demonstrates the rationality and feasibility of the simplification.

Furthermore, the high accuracy of the roll response statistics provided by the 4D PI technique illustrates the great performance and high efficiency of the 4D PI method in calculating the statistics of the high roll response levels when subjected to random wave excitation.

Acknowledgments

The authors wish to thank Dr. Eirik Mo for guidance and assistance in connection with the high-dimensional path integration technique. The support from China Scholarship Council (CSC) (Grant no. 201306230077), affiliated with the Ministry of Education of the P.R. China, is greatly acknowledged.

References

[1] K. Ellermann, The motion of floating systems: nonlinear dynamics in periodic and random waves, J. Offshore Mech. Arct. Eng. 131 (2009) 041104.
[2] J. Roberts, M. Vasta, Markov modelling and stochastic identification for nonlinear ship rolling in random waves, Philos. Trans. R. Soc. Lond. Ser. A: Math. Phys. Eng. Sci. 358 (2000) 1917–1941.
[3] P.D. Spanos, ARMA algorithms for ocean wave modeling, J. Energy Resour. Technol. 105 (1983) 300–309.
[4] P. Spanos, Filter approaches to wave kinematics approximation, Appl. Ocean Res. 8 (1986) 2–7.
[5] P. Spanos, S. Bhattacharjee, Stochastic characterization of ocean depth and filter approximations for wave kinematics, Appl. Ocean Res. 16 (1994) 177–184.
[6] S.K. Thampi, J.M. Niedzwecki, Filter approach to ocean structure response prediction, Appl. Ocean Res. 14 (1992) 259–271.
[7] A. Francescutto, S. Naito, Large amplitude rolling in a realistic sea, Int. Shipbuild. Prog. 51 (2004) 221–235.
[8] L. Dostal, E. Kreuzer, N.S. Namachchivaya, Non-standard stochastic averaging of large-amplitude ship rolling in random seas, Proc. R. Soc. A: Math. Phys. Eng. Sci. 468 (2012) 4146–4173.
[9] L. Dostal, E. Kreuzer, Probabilistic approach to large amplitude ship rolling in random seas, Proc. Inst. Mech. Eng. Part C: J. Mech. Eng. Sci. 225 (2011) 2464–2476.
[10] Z. Su, Nonlinear Response and Stability Analysis of Vessel Rolling Motion in Random Waves Using Stochastic Dynamical Systems, Texas A&M University, 2012.
[11] P. Alevras, D. Yurchenko, Stochastic rotational response of a parametric pendulum coupled with an SDOF system, Probab. Eng. Mech. (2013).
[12] B. Spencer Jr., L. Bergman, On the numerical solution of the Fokker–Planck equation for nonlinear stochastic systems, Nonlinear Dyn. 4 (1993) 357–372.
[13] S.F. Wojtkiewicz, E.A. Johnson, L.A. Bergman, M. Grigoriu, B.F. Spencer Jr., Response of stochastic dynamical systems driven by additive Gaussian and Poisson white noise: solution of a forward generalized Kolmogorov equation by a spectral finite difference method, Comput. Methods Appl. Mech. Eng. 168 (1999) 73–89.
[14] M.F. Wehner, W. Wolfer, Numerical evaluation of path-integral solutions to Fokker–Planck equations, Phys. Rev. A 27 (1983) 2663.
[15] A. Naess, V. Moe, Efficient path integration methods for nonlinear dynamic systems, Probab. Eng. Mech. 15 (2000) 221–231.

[16] E. Mo, Nonlinear Stochastic Dynamics and Chaos by Numerical Path Integration (Ph.D. thesis), Norwegian University of Science and Technology, 2008.
[17] D. Iourtchenko, E. Mo, A. Naess, Reliability of strongly nonlinear single degree of freedom dynamic systems by the path integration method, J. Appl. Mech. 75 (2008) 061016.
[18] A. Pirrotta, R. Santoro, Probabilistic response of nonlinear systems under combined normal and Poisson white noise via path integral method, Probab. Eng. Mech. 26 (2011) 26–32.
[19] I.A. Kougioumtzoglou, P.D. Spanos, Stochastic response analysis of the softening Duffing oscillator and ship capsizing probability determination via a numerical path integral approach, Probab. Eng. Mech. 35 (2014) 67–74.
[20] I.A. Kougioumtzoglou, P.D. Spanos, Nonstationary stochastic response determination of nonlinear systems: a Wiener path integral formalism, J. Eng. Mech. 140 (2014).
[21] A. Naess, J. Johnsen, Response statistics of nonlinear, compliant offshore structures by the path integral solution method, Probab. Eng. Mech. 8 (1993) 91–106.
[22] H.C. Karlsen, Statistics of Wave Induced Nonlinear Loads and Responses (Ph.D. thesis), Norwegian University of Science and Technology, 2006.
[23] W. Chai, A. Naess, B.J. Leira, Stochastic dynamic analysis of nonlinear ship rolling in random beam seas, in: G. Deodatis, P.D. Spanos (Eds.), Proceedings of the 7th International Conference on Computational Stochastic Mechanics, Santorini, Greece, 2014.
[24] W. Chai, A. Naess, B.J. Leira, Stochastic dynamic analysis and reliability of a vessel rolling in random beam seas, J. Ship Res. 59 (2015) 113–131.
[25] M. Dimentberg, O. Gaidai, A. Naess, Random vibrations with strongly inelastic impacts: response PDF by the path integration method, Int. J. Non-Linear Mech. 44 (2009) 791–796.
[26] C. Jiang, A.W. Troesch, S.W. Shaw, Highly nonlinear rolling motion of biased ships in random beam seas, J. Ship Res. 40 (1996) 125–135.
[27] G. Bulian, A. Francescutto, A simplified modular approach for the prediction of the roll motion due to the combined action of wind and waves, Proc. Inst. Mech. Eng. Part M: J. Eng. Marit. Environ. 218 (2004) 189–212.
[28] A.H. Jazwinski, Stochastic Processes and Filtering Theory, Dover Publications, 2007.
[29] D.V. Iourtchenko, E. Mo, A. Naess, Response probability density functions of strongly non-linear systems by the path integration method, Int. J. Non-Linear Mech. 41 (2006) 693–705.
[30] D. Yurchenko, A. Naess, P. Alevras, Pendulum's rotational motion governed by a stochastic Mathieu equation, Probab. Eng. Mech. 31 (2013) 12–18.
[31] B.M. Ayyub, M. Kaminskiy, P.R. Alman, A. Engle, B.L. Campbell, W.L. Thomas III, Assessing the probability of the dynamic capsizing of vessels, J. Ship Res. 50 (2006) 289–310.
[32] A. Naess, O. Gaidai, P. Teigen, Extreme response prediction for nonlinear floating offshore structures by Monte Carlo simulation, Appl. Ocean Res. 29 (2007) 221–230.
[33] V. Belenky, C. Bassler, M. Dipper, B. Campbell, K. Weems, K. Spyrou, Direct assessment methods for nonlinear ship response in severe seas, in: Proceedings of the ITTC Workshop on Seakeeping, Seoul, Korea, 2010.
[34] ISLF 51, Revision of the Intact Stability Code, Report of the Working Group (Part 1), London, 2008.
[35] V. Belenky, J.O. de Kat, N. Umeda, Toward performance-based criteria for intact stability, Mar. Technol. 45 (2008) 101–120.
[36] K.A. McTaggart, Ship capsize risk in a seaway using fitted distributions to roll maxima, J. Offshore Mech. Arct. Eng. 122 (2000) 141–146.
[37] D. Paroka, N. Umeda, Capsizing probability prediction for a large passenger ship in irregular beam wind and waves: comparison of analytical and numerical methods, J. Ship Res. 50 (2006) 371–377.

A.3 Paper 3

Stochastic nonlinear ship rolling in random beam seas by the path integration method

Wei Chai, Arvid Naess and Bernt J. Leira

Published in Probabilistic Engineering Mechanics (2016), Vol. 44, pp. 43-52

Probabilistic Engineering Mechanics 44 (2016) 43–52

Contents lists available at ScienceDirect

Probabilistic Engineering Mechanics

journal homepage: www.elsevier.com/locate/probengmech

Stochastic nonlinear ship rolling in random beam seas by the path integration method

Wei Chai [a,*], Arvid Naess [b,c], Bernt J. Leira [a]

[a] Department of Marine Technology, Norwegian University of Science and Technology, Trondheim, Norway
[b] Department of Mathematical Sciences, Norwegian University of Science and Technology, Trondheim, Norway
[c] Centre for Ships and Ocean Structures, Norwegian University of Science and Technology, Trondheim, Norway

ARTICLE INFO

Article history:
Received 12 August 2015
Accepted 1 October 2015
Available online 21 October 2015

Keywords:
Path integration method
Nonlinear ship rolling
Stochastic response
Monte Carlo simulation

ABSTRACT

Nonlinear ship rolling in random seas is a serious threat to ship stability. In this work, the dynamic stability of the vessel in random seas is evaluated by means of probabilistic methods. Specifically, the Markov diffusion theory is applied in order to study the stochastic aspects of the roll motion driven by random wave loads. The roll motion is modeled as a single-degree-of-freedom (SDOF) model in which the nonlinear damping and restoring terms as well as the random wave excitation are all incorporated. The stationary wave excitation moment in the SDOF model is represented as a filtered white noise by employing a second order linear filter. Therefore, a four-dimensional (4D) Markov dynamic system is established by combing the SDOF model with the linear filter model. Because the probabilistic property of the 4D Markov system is governed by the Fokker–Planck (FP) equation, the response statistics of roll motion can be obtained by solving the FP equation via an efficient 4D path integration (PI) method, which is based on the Markov property of the coupled dynamic system. Furthermore, the random wave excitation is approximated by an equivalent Gaussian white noise, and a two-dimensional (2D) PI technique is applied in order to obtain the response statistics of the dynamic system driven by this Gaussian white noise. The rationality and accuracy of applying the equivalent Gaussian white noise to simulate nonlinear ship rolling in random seas is studied. Moreover, the accuracy of the response statistics computed by the 4D and 2D PI techniques is verified by means of the versatile Monte Carlo simulation technique.

1. Introduction

Ship sailing in random beam seas is considered as the worst condition with respect to navigation ability. Under such circumstance, roll resonance caused by wave excitation may lead to large amplitude roll motion or even capsizing. Nonlinear roll motion in random seas is one of the main reasons leading to stability failure. However, the current criteria of the International Maritime Organization (IMO) for evaluation of the intact stability are simply based on hydrostatic analysis [1]. There is no consideration with respect to the dynamic behaviors associated with the nonlinearities of roll damping and restoring terms as well as the randomness of wave excitation, which are important for stability assessment. With the awareness of the deficiencies of the current criteria for dynamic stability evaluation, the IMO is currently developing the next generation of intact stability criteria with a certain consideration of the physics associated with the dynamics of nonlinear roll motion and the randomness of wave excitation and roll response. For the direct assessment of ship dynamic stability in the framework of the next generation of intact stability criteria currently being developed, elaborate theoretical models as well as appropriate mathematical techniques are essential.

In this work, the dynamic stability in random seas is evaluated by means of a probabilistic approach, which means that the nonlinear stochastic roll response is in focus. Actually, prediction of the stochastic roll response is crucial for reliability based design and operation in practice, and also the response statistics are commonly used to characterize the dynamics of a random system. For the case of beam seas, the rolling ship is described as a single-degree-of-freedom (SDOF) system subjected to random external forcing and the nonlinearities associated with the damping and restoring terms are incorporated. However, for such nonlinear models, assessing the statistics of high-level response and the corresponding low probability levels is a difficult task, and limited progress has been made in the past decades [2].

The methodology based on time domain Monte Carlo simulation is the most commonly used technique for investigation of random systems as well as for evaluation of the stochastic

* Corresponding author.
E-mail address: chai.wei@ntnu.no (W. Chai).

http://dx.doi.org/10.1016/j.probengmech.2015.10.002
0266-8920/

responses. For example, the versatile Monte Carlo simulation technique can be applied to gain information about the spectral components and probability density functions of the response [3], to estimate the upcrossing rate and exceedance probabilities, etc. Moreover, for nonlinear ship rolling in random seas, Monte Carlo simulation is attractive in the sense that the nonlinear damping and restoring terms as well as the time-dependent random wave excitation can be directly dealt with. However, Monte Carlo simulation is only a brute force method and its accuracy and associated computational efficiency for prediction of the extreme responses would be a main drawback.

Besides the straightforward Monte Carlo simulation, Markov diffusion theory is attractive and popular for stochastic dynamic analysis of nonlinear systems since the probabilistic property of the dynamic system is governed by the Fokker–Planck equation. Because the Markov model is only valid for a system driven by Gaussian white noise or filtered white noise processes, a second-order linear filter is introduced in order to approximate the stationary wave excitation process [4]. Therefore, a four-dimensional (4D) augmented dynamic system is created by coupling the original SDOF model, a second-order nonlinear differential equation, with the linear filter employed to model the random wave excitation process as a filtered white noise process. The justification of applying the Markov diffusion theory for nonlinear dynamic systems subjected to random wave excitation has been mentioned in Naess and Johnsen [5]. For the extended Markov system, a host of useful response statistics can be obtained by solving the corresponding FP equation.

However, for the nonlinear coupled dynamic system associated with the high-dimensional FP equation, direct numerical solutions of the FP equation, e.g. by means of the finite-element method [6] and the finite difference method [7], are hardly feasible because of the so-called "curse of dimension" problem, i.e. difficulties arise due to the processing and storage needed for the computation. In addition the accuracy is hard to assess. As an alternative, the path integration (PI) method is applied in order to calculate the stochastic response of such extended dynamic systems. For the PI method, which is based on the Markov property of the dynamic system, no attempt is made to solve the FP equation directly and the evolution of the response probability density function (PDF) is calculated via a step-by-step solution technique invoking the total probability law. Specifically, the response PDF at a given time instant can be obtained when the response PDF at an earlier close time instant as well as the conditional PDF are already known. The PI method can provide high accuracy solutions to a range of problems, e.g. three dimensional (3D) PI procedures have been applied in Naess and Johnsen [5] and Karlsen [8] to estimate the response statistics of moored structures subjected to random wave loads. Iourtchenko et al. [9] studied the response PDFs of strongly non-linear SDOF systems excited by additive Gaussian excitation via a two dimensional (2D) PI technique, etc.

So far, only low-dimensional PI procedures have been applied to the area of nonlinear ship rolling. Lin and Yim [10] and Falzarano et al. [11] treated the wave excitation as regular waves perturbed by Gaussian white noise and evaluated the probabilisty distributions of roll response by 2D PI algorithms. Chai et al. [12] studied the roll response and the associated reliability property of a vessel excited by Gaussian white noise via a 2D PI procedure and first-passage theory. Kougioumtzoglou and Spanos [13] recently developed a one-dimensional (1D) path integral framework, which is based on the statistical linearization and stochastic averaging method, for determining the stochastic response and the first-passage PDFs of ships rolling under random loads. However, these researches include certain simplifications in modeling the random wave excitation. In this paper, the feasibility of simplifying the random wave excitation as an equivalent Gaussian white noise process for prediction of the stochastic roll response will be studied.

In the present paper, the random wave excitation will be modeled as a filtered white noise via a second-order linear filter and an equivalent Gaussian white noise. Then, the 4D PI and 2D PI methods will be applied in order to evaluate the stochastic roll responses of the corresponding dynamic system. The comparison of the statistics of roll response excited by the filtered white noise with that excited by the corresponding equivalent Gaussian white noise will demonstrate serious deficiencies in the application of the latter excitation to simulate nonlinear ship rolling in random seas.

2. Modeling aspects

2.1. Equation of rolling motion

For the uncoupled roll motion in random beam seas, the governing equation is given by the following SDOF model:

$$(I_{44} + A_{44})\ddot{\theta}(t) + B(\dot{\theta}(t)) + \Delta GZ(\theta(t)) = M(t) \tag{1}$$

where $\theta(t)$ and $\dot{\theta}(t)$ are the roll angle and the roll velocity, respectively. I_{44} is the moment of inertia, A_{44} represents the added mass coefficient. $B(\dot{\theta}(t))$ is the damping moment term and $\Delta GZ(\theta(t))$ is the restoring moment term. $M(t)$ denotes the random wave excitation moment.

The damping moment term, consisting of wave radiation, viscous and vortex shedding components, is difficult to quantitatify, because these components are coupled with each other. Nevertheless, there are two empirical damping models commonly used to describe the roll damping term [14].

The linear-plus-quadratic damping (LPQD) model has been verified by numerous studies of experimental data [15] and it is expressed as:

$$B(\dot{\theta}(t)) = B_{44l}\dot{\theta}(t) + B_{44q}\dot{\theta}(t)|\dot{\theta}(t)| \tag{2}$$

where B_{44l} and are B_{44q} linear and quadratic damping coefficients, respectively.

On the other hand, the LPQD model is only once continuously differentiable and mathematically inferior to the linear-plus-cubic damping (LPCD) model [16], which is infinitely differentiable and given by the following cubic polynomial:

$$B(\dot{\theta}(t)) = B_{44l}\dot{\theta}(t) + B_{44c}\dot{\theta}^3(t) \tag{3}$$

in which, B_{44c} is the cubic damping coefficient.

The restoring term is expressed in terms of the displacement Δ and the restoring arm GZ, which can be obtained from standard hydrostatic software. The restoring arm is usually given by a nonlinear odd function of the roll angle, i.e.

$$GZ(\theta) = C_1\theta - C_3\theta^3 \tag{4}$$

where C_1 and C_3 are the linear and nonlinear roll restoring coefficients of the restoring arm. It should be noted that the roll motion has a softening characteristic since the nonlinear restoring term is negative. For the softening cases, ship capsizing would occur when the roll angle exceeds the angle of vanishing stability beyond which the restoring moment becomes negative.

As for the wave excitation moment, it is a stationary Gaussian process which is described by the wave excitation moment spectrum, $S_{MM}(\omega)$. The latter is related to the wave energy spectrum, $S_{\xi\xi}(\omega)$, by the following relationship [17]:

$$S_{MM}(\omega) = |F_{roll}(\omega)|^2 S_{\xi\xi}(\omega) \tag{5}$$

where $|F_{roll}(\omega)|$ represents the roll moment amplitude per unit wave height at frequency ω. When the relevant information about $|F_{roll}(\omega)|$ (which can be obtained e.g. based on strip theory) is absent, the wave excitation moment can be approximated by the following equation ([18,19]):

$$M(t) = \Delta C_1 \alpha_0 \eta(t) \tag{6}$$

where α_0 is the effective wave slope coefficient, which can be estimated by using strip theory or by experiments, and $\eta(t)$ is the wave slope process. Moreover, the wave slope spectrum, $S_{\eta\eta}(\omega)$, is given as:

$$S_{\eta\eta}(\omega) = \frac{\omega^4}{g^2} S_{\xi\xi}(\omega) \tag{7}$$

Dividing Eq. (1) by $(I_{44}+A_{44})$, the final form of the differential equation is obtained as:

$$\ddot{\theta}(t) + b(\dot{\theta}(t)) + c_1\theta(t) - c_3\theta^3(t) = m(t) \tag{8}$$

where b_{44l}, b_{44q} and b_{44c} are relative damping coefficients, c_1 and c_3 are relative roll restoring coefficients [2], and the relative wave excitation moment, $m(t)$, which is approximated by Eq. (6), corresponds to the following spectrum:

$$S_{mm}(\omega) = S_{MM}(\omega)/(I_{44}+A_{44})^2 = \omega_0^4\alpha_0^2 S_{\eta\eta}(\omega) = \omega_0^4\alpha_0^2 \frac{\omega^4}{g^2} S_{\xi\xi}(\omega) \tag{9}$$

Moreover, the natural roll frequency, ω_0, is given as:

$$\omega_0 = \sqrt{\Delta C_1/(I_{44}+A_{44})} = \sqrt{c_1} \tag{10}$$

Finally, the SDOF model (8) can be transformed into the state-space equation written as:

$$\begin{cases} dx_1 = x_2 dt \\ dx_2 = (-b(x_2) - c_1 x_1 + c_3 x_1^3 + x_3)dt \end{cases} \tag{11}$$

where $x_1 = \theta(t)$, $x_2 = \dot{\theta}(t)$, $x_3 = m(t)$.

2.2. Shaping filter technique

The random wave excitation term in the SDOF model (8) is a stationary process given by an approximate spectral density and it can be modeled as a filtered white noise. Dostal and Kreuzer proposed a second-order linear filter to represent the target spectrum [20] and this filter is also available for the desired spectrum, $S_{mm}(\omega)$ in the present work. The filter is expressed by the following differential equation:

$$\begin{cases} dx_3 = (x_4 - \beta x_3)dt + \gamma \mathrm{dW} \\ dx_4 = -\alpha x_3 dt \end{cases} \tag{12}$$

where x_3 and x_4 are state variables in the filter equation with x_3 representing the filter output $m(t)$. $\mathrm{d}W(t) = W(t+dt) - W(t)$ is the increment of a Wiener process with $\mathrm{E}\{\mathrm{d}W(t)\} = 0$ and $E\{\mathrm{d}W(t)\mathrm{d}W(t+\mathrm{d}t)\} = \delta(\mathrm{d}t)$, where $\delta(\cdot)$ represents the Dirac function. The spectrum generated by the differential Eq. (12) is given as:

$$S_{Filter}(\omega) = \frac{1}{2\pi} \frac{\gamma^2\omega^2}{(\alpha - \omega^2)^2 + (\beta\omega)^2} \tag{13}$$

in which α, β, γ are the parameters of the linear filter and they are determined by means of a least-square algorithm which is applied in order to fit the desired spectrum, $S_{mm}(\omega)$. It is worth emphasizing that the filtered spectrum (13) is double-sided, while the wave energy spectrum and the roll excitation spectrum are physically single-sided. This difference must be considered in the practical simulation.

By combining the state-space Eq. (11) with Eq. (12), the extended dynamic system is formed. Therefore, the roll motion in random beam seas can be described by the following 4D state space equation:

$$\begin{cases} dx_1 = x_2 dt \\ dx_2 = (-b(x_2) - c_1 x_1 + c_3 x_1^3 + x_3)dt \\ dx_3 = (x_4 - \beta x_3)dt + \gamma \mathrm{dW} \\ dx_4 = -\alpha x_3 dt \end{cases} \tag{14}$$

Furthermore, the roll response spectrum, which has a peak near the natural roll frequency ω_0, is narrow-banded due to the light roll damping. Theoretically speaking, Gaussian white noise may be able to serve as a simplification of the relative wave excitation spectrum $S_{mm}(\omega)$ if its spectral density equals to the value of $S_{mm}(\omega)$ at the frequency ω_0. Assume that the value of $S_{mm}(\omega)$ at the frequency ω_0 is S_0 and the corresponding Gaussian white noise is referred to as the equivalent Gaussian white noise. The noise level, σ, of the equivalent Gaussian white noise can then be determined as:

$$\sigma^2 = 2\pi S_0 \tag{15}$$

The differential equation of the dynamic system (8) can then be simplified as:

$$\ddot{\theta}(t) + b(\dot{\theta}(t)) + c_1\theta(t) - c_3\theta^3(t) = \sigma N(t) \tag{16}$$

where $N(t)$ is a standard Gaussian white noise process and the corresponding 2D state-space equation is given as:

$$\begin{cases} dx_1 = x_2 dt \\ dx_2 = (-b(x_2) - c_1 x_1 + c_3 x_1^3)dt + \sigma \mathrm{dW} \end{cases} \tag{17}$$

3. Path integration method

Eqs. (14) and (17) represent two Markov dynamic systems driven by Gaussian white noise [21]. In this Section, the main efforts will be devoted to describing the mathematical principle of the 4D path integration (PI) method for the dynamic system (14). The 2D PI method for the dynamic system (17) will be briefly introduced.

The dynamic system (14) can be expressed by an *Itô* stochastic differential equation (SDE):

$$d\mathbf{x} = a(\mathbf{x}, t)dt + b(t)d\mathbf{W}(t) \tag{18}$$

in which $\mathbf{x}(t) = (x_1(t), \ldots, x_4(t))^{\mathrm{T}}$ is a 4D state space vector process, the vector $a(\mathbf{x},t)$ is the drift term and $b(t)d\mathbf{W}(t)$ represents the diffusive term. The vector $d\mathbf{W}(t) = \mathbf{W}(t+dt) - \mathbf{W}(t)$ denotes independent increments of a standard Wiener process.

The solution $\mathbf{x}(t)$ to Eq. (18) is a Markov process and its transition probability density (TPD), also known as the conditional PDF, $p(\mathbf{x},t \mid \mathbf{x}',t')$ satisfies the FP equation, which is of the following form:

$$\frac{\partial}{\partial t} p(\mathbf{x}, t|\mathbf{x}', t') = -\sum_{i=1}^{4} \frac{\partial}{\partial x_i} a_i(\mathbf{x}, t) p(\mathbf{x}, t|\mathbf{x}', t') + \frac{1}{2}\sum_{i=1}^{4}\sum_{j=1}^{4} \frac{\partial^2}{\partial x_i \partial x_j} (b(t)\cdot b^T(t))_{ij} p(\mathbf{x}, t|\mathbf{x}', t') \tag{19}$$

As mentioned in Section 1, for the PI method, no attempt is made to solve the FP Eq. (19) directly. The PI method is based on the Markov property of the dynamic system, and the PDF of $\mathbf{x}(t)$ is obtained by exploiting the following basic equation:

$$p(\mathbf{x}, t) = \int_{R^4} p(\mathbf{x}, t|\mathbf{x}', t')p(\mathbf{x}', t')d\mathbf{x}' \tag{20}$$

where $d\mathbf{x}' = \prod_{i=1}^{4} dx_i'$.

For a numerical solution of the SDE (18), the TPD, $p(\mathbf{x},t|\mathbf{x}',t')$ can always be given as an analytical, closed form expression if the time increment $\Delta t=t-t'$ is sufficiently small. Therefore, if an initial PDF, $p(\mathbf{x}^{(0)}, t_0)$ is given, the time evolution of the PDF of $\mathbf{x}(t)$ can be determined by the following iterative algorithm:

$$p(\mathbf{x}, t) = \int_{R^4}\cdots\int_{R^4}\prod_{i=1}^{n} p(\mathbf{x}^{(i)}, t_i|\mathbf{x}^{(i-1)}, t_{i-1}) \cdot p(\mathbf{x}^{(0)}, t_0)d\mathbf{x}^{(0)}\ldots d\mathbf{x}^{(n-1)} \tag{21}$$

where $\mathbf{x}=\mathbf{x}^{(n)}$, $t = t_n = t_0+n\cdot\Delta t$.

The mathematical principle of the PI method has been formulated in Eqs. (20) and (21). As for the specific numerical implementation of the PI method for the dynamic system (18), a time discrete approximation should be introduced. Based on the proper time increment $\Delta t=t-t'$, Naess and Moe [22] proposed a fourth-order Runge−Kutta-Maruyama (RKM) approximation:

$$\mathbf{x}(t) = \mathbf{x}(t') + r(\mathbf{x}(t'), t')\Delta t + b(t')\Delta\mathbf{W}(t') \tag{22}$$

where the vector $r(\mathbf{x}(t'), t')$ is the explicit fourth-order Runge–Kutta (RK4) approximation or Runge–Kutta increment. Because $\mathbf{W}(t)$ is a Wiener process, the independent increment $\Delta\mathbf{W}(t')=\mathbf{W}(t)-\mathbf{W}(t')$ is a Gaussian variable and the TPD, $p(\mathbf{x},t\mid\mathbf{x}',t')$ is a Gaussian PDF for every t'.

With the introduction of the time discrete approximation, the time sequence $\{\mathbf{x}(i\cdot\Delta t)\}_{i=0}^{\infty}$ is a Markov chain and it can approximate the time-continuous Markov solution of the SDE (18) when the time increment Δt is sufficiently small. If only the deterministic part of Eq. (18) is considered, the approximation (22) reduces to the RK4 approximation $\mathbf{x}(t)=\mathbf{x}(t')+r(\mathbf{x}(t'),t')\Delta t$. Experiments have shown that, for the Markov systems, the accuracy related to approximation of the deterministic terms is most important [23]. In this regard, the accuracy of the fourth-order RKM approximation is satisfactory since the fourth-order Runge–Kutta approximation represents the time evolution of the deterministic part of Eq. (22) with an accuracy to the order of $O(\Delta t^5)$.

The conditional PDF of the process $\mathbf{x}(t)$, $p(\mathbf{x},t\mid\mathbf{x}',t')$, follows a (degenerate) Gaussian distribution, which is written as:

$$p(\mathbf{x}, t|\mathbf{x}', t') = \delta(x_1 - x_1' - r_1(\mathbf{x}', \Delta t))\cdot\delta(x_2 - x_2' - r_2(\mathbf{x}', \Delta t)) \cdot\tilde{p}(x_3, t|x_3', t')\cdot\delta(x_4 - x_4' - r_4(\mathbf{x}', \Delta t)) \tag{23}$$

where $\tilde{p}(x_3, t|x'_3, t')$ is given by the relation:

$$\tilde{p}(x_3, t|x'_3, t') = \frac{1}{\sqrt{2\pi\gamma^2\Delta t}}\cdot\exp\left\{-\frac{(x_3 - x'_3 - r_3(\mathbf{x}', \Delta t))^2}{2\gamma^2\Delta t}\right\} \tag{24}$$

For the numerical implementation of the 4D PI approach, a reasonable computational domain and the corresponding computational grid have to be determined at first. In this work, the initial PDF, $p(\mathbf{x}^{(0)}, t_0)$, is chosen as a 4D Gaussian PDF with zero mean and variances in the four dimensions evaluated by a simple Monte Carlo simulation [23]. The straightforward Monte Carlo simulation ensures that the initial 4D Gaussian PDF includes all the information corresponding to the selected parameters of the dynamic system, and it also provides a rational computational domain and computational grid for the subsequent calculation [24]. Then, for the implementation of the iterative algorithm (21) for each grid point, the PDF at the previous time t' is represented as an interpolating spline surface via parabolic B-spline and the PDF at time t can be evaluated by several specific steps. The numerical iterative algorithm and the associated computational steps have been systematically described by Iourtchenk et al. [9] and Yurchenko et al. [25].

For the 2D dynamic system (17), the time evolution of the PDF of the vector $(x_1(t), x_2(t))^{\mathrm{T}}$ is also determined by an iterative algorithm and a time discrete approximation similar to Eqs. (21) and (22), respectively. The conditional PDF described in Eqs. (23) and (24) is simplified as:

$$p(\mathbf{x}, t|\mathbf{x}', t') = \delta(x_1 - x_1' - r_1(\mathbf{x}', \Delta t))\cdot\tilde{p}(x_2, t|x_2', t') \tag{25}$$

and

$$\tilde{p}(x_2, t|x'_2, t') = \frac{1}{\sqrt{2\pi\gamma^2\Delta t}}\cdot\exp\left\{-\frac{(x_2 - x'_2 - r_2(\mathbf{x}', \Delta t))^2}{2\gamma^2\Delta t}\right\} \tag{26}$$

Similarly, the initial PDF for the 2D PI approach is selected as a 2D Gaussian PDF by Monte Carlo simulation and the subsequent numerical implementation procedures for 2D systems have already been described in Naess et al. [26]. Furthermore, the ability of the PI method with respect to providing accurate and reliable solutions for stochastic dynamic systems has been demonstrate by numerous examples ([22,23]).

4. Mean upcrossing rate

The mean upcrossing rate is a key parameter for a detailed assessment of the large and extreme response statistics of marine structures subjected to stochastic load processes [27]. Calculation of the mean upcrossing rate is usually based on the Rice formula (27) if the joint PDF of the roll angle process and the roll velocity process is known. The latter can be obtained directly by the PI method, and then the upcrossing rate is given as:

$$\nu^+(\zeta; t) = \int_0^{\infty}\dot{\theta}f_{\theta\dot{\theta}}(\zeta, \dot{\theta}; t)d\dot{\theta} \tag{27}$$

where $\nu^+(\zeta;t)$ denotes the expected (or average) number of upcrossings for the ζ-level per unit time at time t by the roll angle process $\theta(t)$, $f_{\theta\dot{\theta}}(\theta, \dot{\theta}; t)$ is the joint PDF of the roll angle process and the roll velocity process at the time instant t.

Furthermore, the standard Monte Carlo simulation technique can serve as a validation for the mean upcrossing rate obtained by the numerical PI method and the Rice formula, even though extensive long simulations are required for estimation of the extreme response statistics. As mentioned in Section 2, due to the softening characteristic of the restoring term, ship capsizing would occur when the predetermined simulation time T is long enough or the intensity of the external excitation is strong enough. If the mean time to capsize is long enough, the dynamic system can be regarded as a highly reliable system and the corresponding roll response reaches stationarity in an approximate sense [15,28]. Therefore, the practical time-variant upcrossing rate $\nu^+(\zeta;t)$ can be approximated as a time-invariant parameter, i.e. the mean upcrossing rate, $\nu^+(\zeta)$ at a suitable reference point in time.

For the 4D dynamic system (14) and the 2D dynamic system (17), the fourth-order RKM method is applied to solve the SDEs and then the time series of the roll response are obtained. For a stationary sea state, the appropriate sample mean value of the upcrossing rate can be obtained from the time series of the roll response:

$$\hat{\nu}^+(\zeta) = \frac{\sum_{i=1}^{k} n_i^+(\zeta; T_i)}{\sum_{i=1}^{k} T_i} \tag{28}$$

where $n_i^+(\xi; T_i)$ denotes the counted number of upcrossings for the level ζ within a time duration of length T_i for simulated time history no. i. The conditions for the roll angle process $\theta(t)$ to

upcross the level ζ during the time interval $(t, t+\Delta t)$ is given as [27]:

$$\zeta - \dot{\theta}(t)\cdot\Delta t < \theta(t) \le \zeta \tag{29}$$

and

$$\dot{\theta}(t) > 0 \tag{30}$$

The practical simulation time T_i may not be fixed for each simulation, but it is equal to the predetermined simulation time T if no capsizing occurs. Otherwise, it is the value of termination time for each case where capsizing occurs. Moreover, the number of simulations, k, e.g. k=1000–5000, is selected according to the values of upcrossing rates in the tail region and the length of the predetermined simulation time T. Usually, low upcrossing rates and short time periods T correspond to a large simulation number k.

From a practical point of view, a good approximation of the exceedance probability and distribution of the extreme response can be given in terms of the mean upcrossing rate if the upcrossing event for the high response levels are statistically independent. Under this assumption, the crossing events for the high response levels are Poisson distributed, and the probability of exceedance for a specific high level, ζ is given as:

$$P_{exc}(\zeta; T) = 1 - \exp\left(-\int_0^T \nu^+(\zeta; t)dt\right) = 1 - exp(-\nu^+(\zeta)\cdot T) \tag{31}$$

Moreover, let $\Theta(T)=\max\{\theta(t): 0 \le t \le T\}$ denote the largest (or extreme) value of the roll angle process $\theta(t)$ over the time interval of length T. For a stationary short-term sea state (traditionally taken as 3–6 h), the cumulative distribution function (CDF) of $\Theta(t)$ under the Poisson assumption is approximately given as:

$$\text{Prob}(\Theta \le \zeta) = exp(-\nu^+(\zeta)\cdot T) \tag{32}$$

Eqs. (31) and (32) clearly indicate the crucial role of the mean upcrossing rate in determining the extreme value distribution. It is well known that the exact extreme value distribution is not completely determined by the upcrossing alone. Nevertheless, the Poisson estimate, which is expressed by the above two equations, is a good approximation and widely used in reliability engineering due to its simplicity and accuracy. However, for the dynamic systems with extremely light roll damping or under serious external excitation, the high reliability assumption of the system as well as the Poisson estimate for the high response levels would not be valid.

5. Numerical examples

In this section, two different ship models are selected in order to study the performance of the equivalent Gaussian white noise for estimating the response statistics of ship rolling in random beam seas. The feasibility and rationality of applying the equivalent Gaussian white noise to simulate nonlinear ship rolling in random seas will be illustrated by comparing with the response statistics for the case that the excitation is represented by filtered white noise.

5.1. Ship model 1

A RoRo ferry model used in Ref. [1] is selected as the first ship model and the main parameters of the example vessel are given in Table 1. The damping term for ship model 1 is given in terms of the LPCD model. Due to lack of relevant information about $|F_{roll}(\omega)|$, the wave excitation term $M(t)$ in the SDOF model (1) and the spectrum of relative excitation moment spectrum, $S_{mm}(\omega)$ are approximated by Eqs. (6) and (9), respectively. Moreover, the effective wave slope coefficient, α_0 is selected to be 0.705 according to a similar sample model in the relevant IMO report [29].

Table 1
Main parameters for the RORO ship.

Parameters	Dimensional value
$I_{44}+A_{44}$	2.2×10^9 kg m^2
Δ	1.68×10^8 N
b_{44}	0.095 s^{-1}
b_{44c}	0.959 s
c_1	0.265 s^{-2}
c_3	0.116 s^{-2}
ω_0	0.515 rad/s

In this work, the modified Pierson–Moskowitz (P–M) spectrum, widely used for fully developed sea states, is adopted in this analysis:

$$S_{\xi\xi}(\omega) = \frac{5.058g^2H_s^2}{T_p^4\omega^5}\exp\left(-1.25\frac{\omega_p^4}{\omega^4}\right) \tag{33}$$

where H_s denotes the significant wave height, ω_p is the peak frequency at which the wave spectrum $S_{\xi\xi}(\omega)$ has its maximum, and T_p is the corresponding peak period (or modal period). The specific sea state with H_s=8.0 m, T_p=15.5 s is selected for the subsequent study. The wave energy spectrum and the corresponding wave slope spectrum, $S_{\eta\eta}(\omega)$ (which is determined by Eq. (7)) are presented in Fig. 1.

It can be observed that the wave slope spectrum, $S_{\eta\eta}(\omega)$ is more broad-banded than the corresponding wave energy spectrum, $S_{\xi\xi}(\omega)$ and also the peak of the spectrum moves towards much higher frequencies. The related relative roll excitation moment spectrum, $S_{mm}(\omega)$, which has the same spectral shape as $S_{\eta\eta}(\omega)$, is plotted in Fig. 2. The second order linear filter usually exhibits good performance for the narrow-banded target spectrum, e.g. [20,30], but for the not narrow-banded spectrum, $S_{mm}(\omega)$, the overall fitting results would not be so good. Nevertheless, the roll response spectrum is narrow-banded and peaked near the natural roll frequency, ω_0, due to the light roll damping, and the excitation

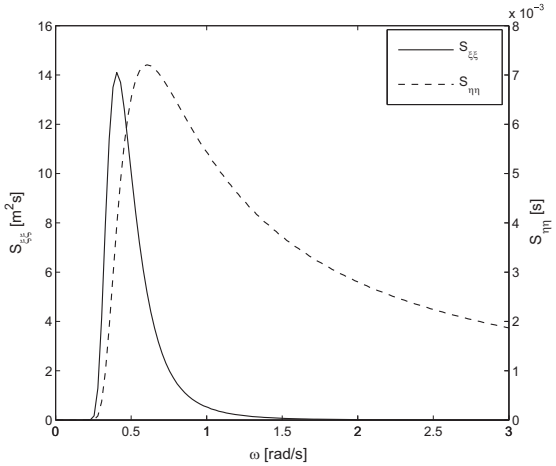

Fig. 1. Wave energy spectra for the sea state with H_s=8.0 m, T_p=15.5 s and the corresponding wave slope spectrum.

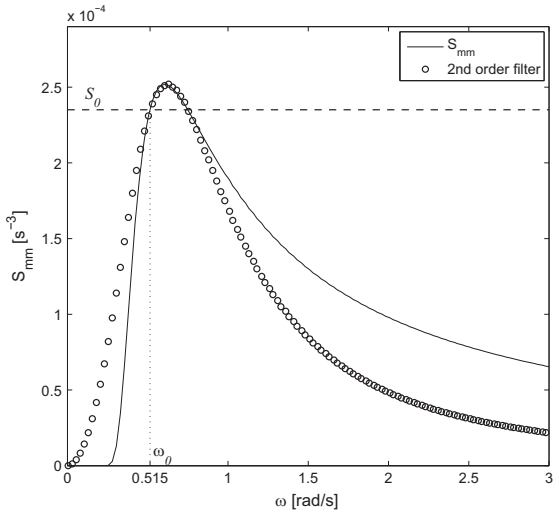

Fig. 2. Relative roll excitation moment spectrum, S_{mm}, for the sea state with $H_s=8.0$ m, $T_p=15.5$ s, the filtered spectrum versus the spectrum of equivalent Gaussian white noise, S_0.

spectrum near ω_0 is essential for estimating the response statistics.

Therefore, for the current ship model, the main concern regarding the result of the fitting is focused on the accuracy in the critical frequency region near ω_0. The parameters α, β, γ in the second-order filter (12) are determined by minimizing the mean square errors between the filtered spectrum and the target spectrum, S_{mm} in the critical frequency region. The result of fitting for the selected sea state is shown in Fig. 2 and the obvious differences between the two spectra in the low-frequency and high-frequency regions would not influence the subsequent roll response to a significant extent. Moreover, the spectrum of the equivalent Gaussian white noise with a constant spectral level, S_0, which is equal to the spectral density of $S_{mm}(\omega)$ at the frequency of ω_0 is also plotted in Fig. 2.

The 4D dynamic system (14) and 2D dynamic system (17) are established after the spectrum fitting has been performed. Monte Carlo simulation is applied to gain information about the roll response spectra excited by the filtered white noise as well as the equivalent Gaussian white noise, which are shown in Fig. 3. It can be clearly seen that both of the response spectra are narrow-banded and peaked near ω_0, i.e. at 0.515 rad/s. In the region with frequencies greater than ω_0, the discrepancies between the input excitation spectra, shown in Fig. 2, do not influence the subsequent response spectra to a significant extent. However, for the frequencies lower than ω_0, the intensity of the equivalent Gaussian white noise is higher than the corresponding filtered white noise, which results in a stronger roll response in the low frequency region. Therefore, for this case, the equivalent Gaussian white noise approximate overestimates the roll response to a certain extent.

Furthermore, the joint PDFs of the roll angle and the roll velocity for the 4D dynamic system and the 2D dynamic system can be obtained by the PI methods directly. The joint PDF of the roll response calculated by the 4D PI method for the selected sea state is presented in Fig. 4, and Fig. 5 displays the joint PDF of the roll response excited by equivalent Gaussian white noise via the 2D PI method. From Figs. 4 and 5 it is clearly seen that the PDFs of roll response are symmetric because the distributions of the external excitation (filtered white noise and equivalent Gaussian white

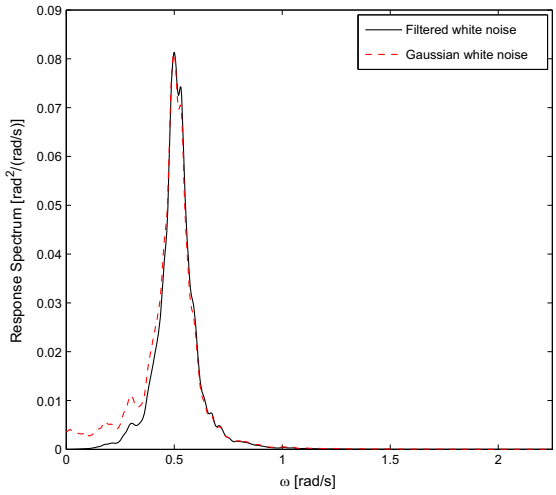

Fig. 3. Response spectra for ship model 1 excited by filtered white noise and equivalent Gaussian white noise.

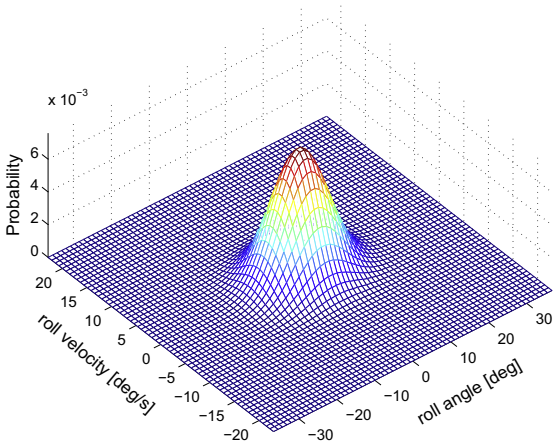

Fig. 4. Joint PDF of roll response excited by filtered white noise for ship model 1.

noise) as well as the vessel properties are symmetric with respect to the origin. Good agreement of the overall distributions is observed in Figs. 4 and 5, since these two Figures mainly present the probabilistic distributions in the low response region and not enough information with respect to the distributions of high-level responses are given.

In order to observe the statistics of high-level responses, the marginal PDFs of the roll angle process and the upcrossing rates for the two dynamic systems are plotted in logarithmical scale and presented in Figs. 6 and 7, respectively. The response statistics obtained by the PI techniques in these two Figures are denoted by "4D PI" and "2D PI" and the corresponding empirical estimation of the marginal PDFs and upcrossing rates are also included in Figs. 6 and 7. It is seen that the roll response excited by the equivalent Gaussian white noise can serve as a good approximation of the response excited by the corresponding filtered white noise in the small amplitude response region, e.g., roll angle less than 15°. However, the discrepancies between the response statistics, which are generated by different excitations, become

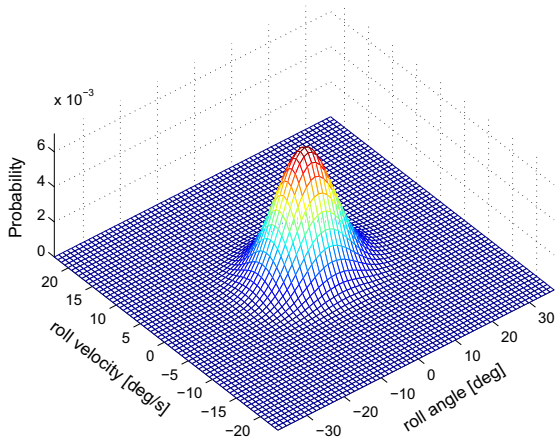

Fig. 5. Joint PDF of roll response excited by equivalent Gaussian white noise for ship model 1.

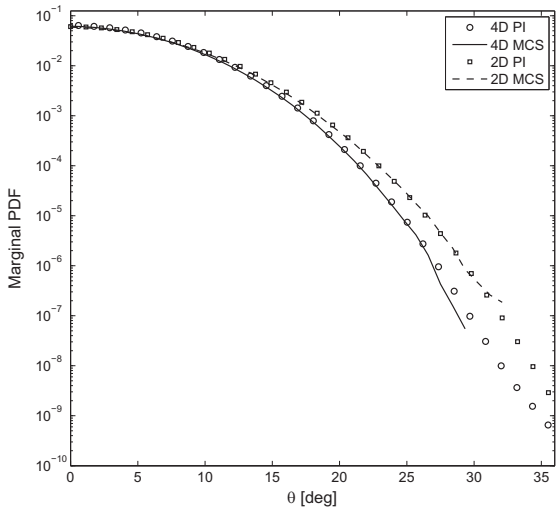

Fig. 6. Marginal PDFs of roll angle process for ship model 1 excited by filtered white noise (denoted as 4D PI and 4D MCS) and equivalent Gaussian white noise (denoted as 2D PI and 2D MCS).

evident as the response level increases. The differences are even more pronounced in the tail region, which illustrates that the equivalent Gaussian white noise impels more energy into the dynamic system than the corresponding filtered white noise. Therefore, the 2D dynamic system generates stronger response in the tail region and overestimates the extreme roll response.

5.2. Ship model 2

Next, an ocean surveillance ship described in Refs [2,31], is considered and denoted as ship model 2. The parameters of the ship model are listed in Table 2 and the damping term is expressed by a LPQD model. The modified P–M spectrum (33) with H_s=4.0 m, T_p=11.0 s is selected as the specific sea state for the subsequent study.

With the specific energy spectrum $S_{\xi\xi}(\omega)$ and the roll moment amplitude per unit wave height $|F_{roll}(\omega)|$ shown in Fig. 8, the roll

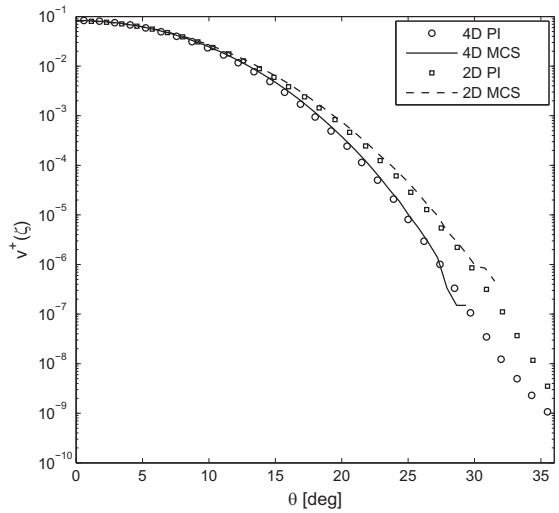

Fig. 7. Upcrossing rates for ship model 1 excited by filtered white noise (denoted as 4D PI and 4D MCS) and equivalent Gaussian white noise (denoted as 2D PI and 2D MCS).

Table 2
Main parameters for the ocean surveillance ship.

Parameters	Dimensional value
$I_{44}+A_{44}$	5.540×10^7 kg m^2
Δ	2.017×10^7 N
b_{44}	0.095 s^{-1}
b_{44q}	0.0519
c_1	1.153 s^{-2}
c_3	0.915 s^{-2}
ω_0	1.074 rad/s

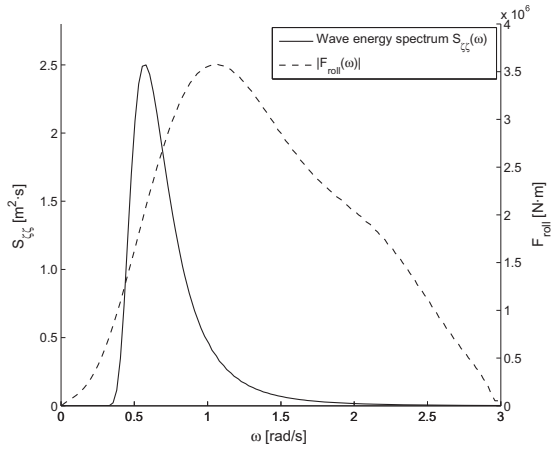

Fig. 8. Wave energy spectra for the sea state with H_s=4.0 m, T_p=11.0 s and roll excitation moment per unite wave height, $|F_{roll}(\omega)|$.

excitation moment spectrum for this case is determined by means of Eq. (5). Then the relative roll excitation moment spectrum $S_{mm}(\omega)$ is obtained and presented in Fig. 9. It can be observed that the bandwidth of the target spectrum $S_{mm}(\omega)$ determined by Eq. (5) with relevant information about $|F_{roll}(\omega)|$ given by strip theory is much lower than that of the desired spectrum $S_{mm}(\omega)$ in Fig. 2,

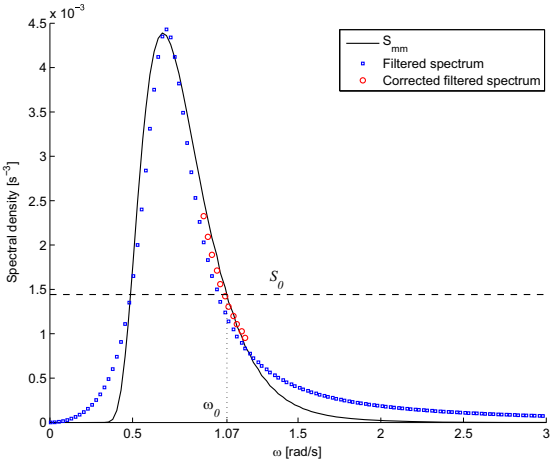

Fig. 9. Relative roll excitation moment spectrum, S_{mm}, the filtered spectrum, the corrected filtered spectrum for the sea state with H_s=4.0 m, T_p=11.0 s, and spectrum of equivalent Gaussian white noise, S_0.

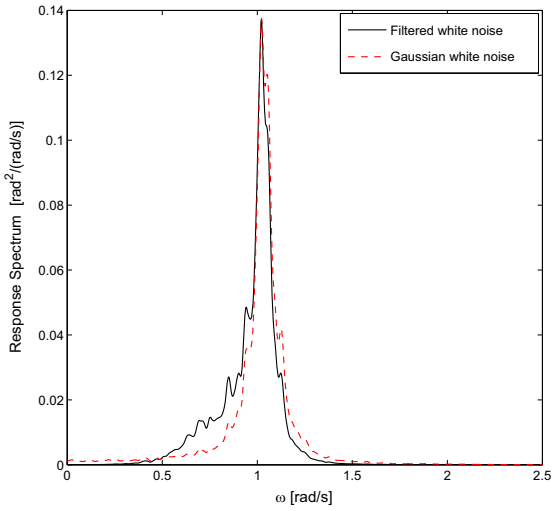

Fig. 10. Response spectra for ship model 2 excited by filtered white noise and equivalent Gaussian white noise.

which is approximated by Eq. (9). Therefore, the second order linear filter (12) is introduced to fit the target spectrum $S_{mm}(\omega)$ from an overall perspective.

The result of fitting is shown in Fig. 9 and it can be readily seen that the filtered spectrum is reasonable in terms of bandwidth, peak frequency and peak value. However, a slight discrepancy between the filtered spectrum and the target spectrum in the critical frequency region near ω_0 can be observed. Therefore, a correction factor, c should be introduced in order to decrease the discrepancies in the critical region. The filtered spectrum is then changed into:

$$S_{Filter}(\omega) = \frac{1}{2\pi} \frac{(c\cdot\gamma)^2\omega^2}{(\alpha - \omega^2)^2 + (\beta\omega)^2} \tag{34}$$

In this work, for ship model 2 and the selected sea state, the correction factor c is take to be 1.07 by considering the mean difference between the two spectral densities in the critical region. The corrected filtered spectrum in the critical region and the spectrum of the equivalent Gaussian white noise, S_0 are also presented in Fig. 9. The response spectra of the 4D dynamic system and the 2D dynamic system are then obtained by means of Monte Carlo simulation and the results are presented in Fig. 10. Comparison of the response spectra for different systems illustrate that the discrepancies between the filtered spectrum generated by the second order linear filter and the spectrum of the equivalent Gaussian white noise in the critical frequency region near ω_0 would result in obvious differences of the roll response for ship model 2. Moreover, it is clearly seen from Fig. 10 that the roll response excited by the filtered white noise is much stronger than the response driven by the equivalent Gaussian white noise.

This result can also be observed in Figs. 11 and 12, which provide information with respect to the joint PDFs of the roll response for the 4D dynamic system and 2D dynamic system, respectively. The joint PDFs are obtained by the 4D and 2D PI techniques and the stronger roll response in Fig. 11 appears in terms of a lower peak in the central region and a wider distribution of the joint PDF. Similar to ship model 1, the marginal PDFs of the roll angle process obtained by the PI techniques are plotted in Fig. 13 and the corresponding upcrossing rates are shown in Fig. 14. Monte Carlo simulation is applied in order to provide related empirical estimations of the marginal PDFs and the upcrossing rates, which are

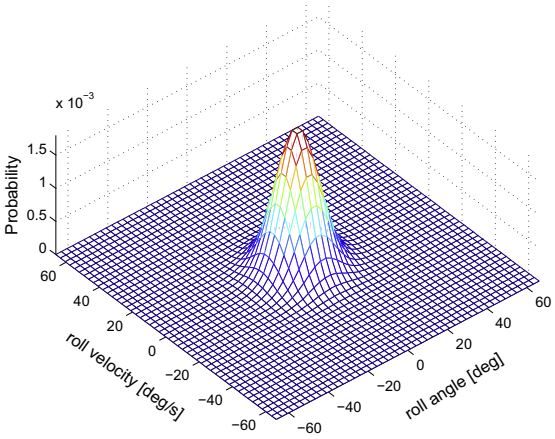

Fig. 11. Joint PDF of roll response for ship model 2 excited by filtered white noise.

also given in Figs. 13 and 14, respectively. The differences between the response statistics driven by filtered white noise and equivalent Gaussian white noise are even more distinct than the discrepancies observed in Figs. 6 and 7 for ship model 1. For this case, the equivalent Gaussian white noise results in weaker response than the filtered white noise and the 2D dynamic system (17) underestimates the response statistics.

Based on the study in this Section, some meaningful and valuable conclusions can be drawn. Firstly, it is observed in Figs. 6,7 and Figs. 13,14 that both the 4D PI technique and the 2D PI technique provide reliable and high-accuracy estimation of the response statistics, even in the tail regions with low probability levels. Moreover, in these figures, for the probability level of the response statistics lower than 10^{-7}, the computation cost for Monte Carlo simulation is formidable. However, the PI approach can provide nice results in the tail region within one calculation, which demonstrates the superiority of the PI method. Secondly, because the light roll damping of the SDOF model (8), the response

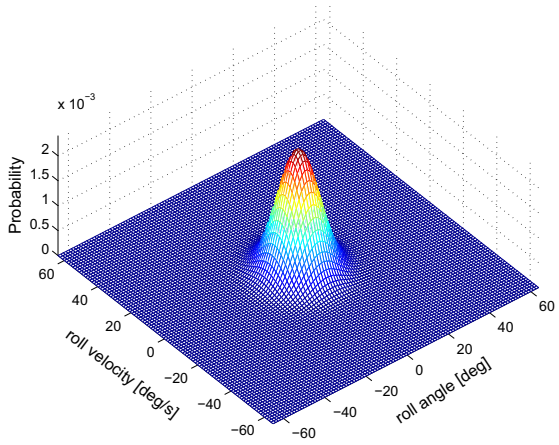

Fig. 12. Joint PDF of roll response for ship model 2 excited by equivalent Gaussian white noise.

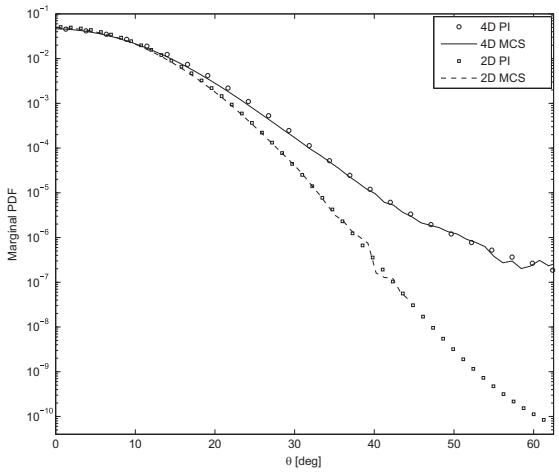

Fig. 13. Marginal PDFs of roll angle process for ship model 2 excited by filtered white noise (denoted as 4D PI and 4D MCS) and equivalent Gaussian white noise (denoted as 2D PI and 2D MCS).

spectrum is narrow-banded and the fitting results of the external excitation moment spectrum in the critical frequency region near ω_0 is crucial for prediction of the response statistics. The discrepancies between the filtered spectrum and the spectrum of the equivalent Gaussian white noise in the critical region would induce significant differences between the subsequent response statistics, especially in the tail regions. Finally, for ship model 1, the equivalent Gaussian white noise impel more energy into the dynamic system than the corresponding filtered white noise and then overestimate the response statistics. But for ship model 2, the roll response excited by filtered white noise is stronger than the response driven by the equivalent Gaussian white noise, which means that the latter underestimate the response statistics. Therefore, the equivalent Gaussian white noise is unable to provide accurate estimation of the response statistics and it is inappropriate to be used for simulation of the nonlinear ship rolling in random seas.

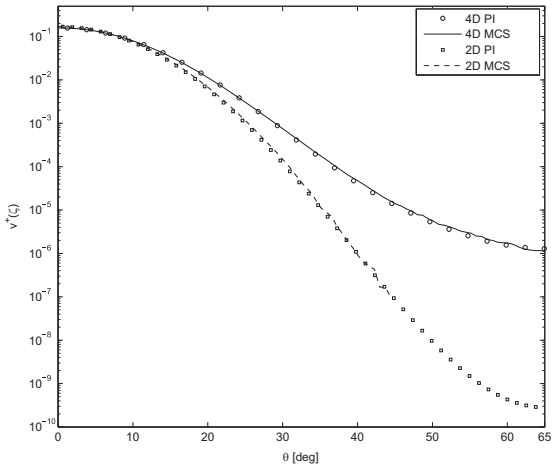

Fig. 14. Upcrossing rates for ship model 2 excited by filtered white noise (denoted as 4D PI and 4D MCS) and equivalent Gaussian white noise (denoted as 2D PI and 2D MCS).

6. Conclusions

In this paper, the stochastic theory and probabilistic approaches have been applied in studying the nonlinear ship rolling in random beam seas. The Markov diffusion theory served as the basic principle in this work and the shaping filter technique was employed to model the random wave excitation as well as to establish a Markov dynamic system with state space formulation for description of the stochastic roll motion. Based on the property of light roll damping and narrow-banded response spectrum, the excitation spectrum near the natural roll frequency is essential for estimating the response statistics and a second order linear filter was introduced to approximate the target wave excitation spectrum. In this regard, the 4D PI method based on the Markov property of the coupled dynamic system was applied to solve the FP equation, which governs the probabilistic property of the Markov system.

Moreover, the random wave excitation was also simplified as an equivalent Gaussian white noise and the corresponding response statistics were calculated by the 2D PI procedure. To verify the response statistics calculated by the 4D and 2D PI procedures, comparisons have been made with the results obtained by the straightforward Monte Carlo simulation technique. Excellent agreement was observed and the superiority of the PI method in providing high-accuracy results for the high level responses within one calculation was also presented in the comparisons.

Furthermore, based on the study of two different ship models, significant differences have been found between the response statistics excited by filtered white noise and that driven by the equivalent Gaussian white noise. Due to the unsatisfactory accuracy of the response statistics given by the 2D dynamic systems, the equivalent Gaussian white noise cannot be recommended in order to study nonlinear ship rolling in random seas.

Acknowledgments

Support from the China Scholarship Council (CSC) (Grant no. 201306230077), affiliated with the Ministry of Education of the PR China, is gratefully acknowledged. Grants from the Norwegian University Fund through UNIFOR in Oslo are also greatly acknowledged.

References

[1] L. Dostal, E. Kreuzer, N.S. Namachchivaya, Non-standard stochastic averaging of large-amplitude ship rolling in random seas, Proc. R. Soc. A: Math. Phys. Eng. Sci. 471 (2012) 4146–4173.

[2] W. Chai, A. Naess, B.J. Leira, Stochastic Dynamic Analysis and Reliability of a Vessel Rolling in Random Beam Seas, J. Ship Res. 59 (2015) 113–131.

[3] K. Ellermann, Nonlinear dynamics of offshore systems in random seas, in: IUTAM Symposium on Fluid-Structure Interaction in Ocean Engineering, Springer, 2008, pp. 45–56.

[4] W. Chai, A. Naess, B.J. Leira, Filter models for prediction of stochastic ship roll response, Probab. Eng. Mech. 41 (2015) 104–114.

[5] A. Naess, J. Johnsen, Response statistics of nonlinear, compliant offshore structures by the path integral solution method, Probab. Eng. Mech. 8 (1993) 91–106.

[6] B. Spencer Jr, L. Bergman, On the numerical solution of the Fokker-Planck equation for nonlinear stochastic systems, Nonlinear Dyn. 4 (1993) 357–372.

[7] S.F. Wojtkiewicz, E.A. Johnson, L.A. Bergman, M. Grigoriu, B.F. Spencer Jr, Response of stochastic dynamical systems driven by additive Gaussian and Poisson white noise: solution of a forward generalized Kolmogorov equation by a spectral finite difference method, Comput. Methods Appl. Mech. Eng. 168 (1999) 73–89.

[8] H.C. Karlsen, Statistics of Wave Induced Nonlinear Loads and Responses (Ph.D. thesis), Norwegian University of Science and Technology, Norway, 2006.

[9] D.V. Iourtchenko, E. Mo, A. Naess, Response probability density functions of strongly non-linear systems by the path integration method, Int. J. Non-Linear Mech. 41 (2006) 693–705.

[10] H. Lin, S.C. Yim, Chaotic roll motion and capsize of ships under periodic excitation with random noise, Appl. Ocean. Res. 17 (1995) 185–204.

[11] J. Falzarano, Z. Su, A. Jamnongpipatkul, Application of stochastic dynamical system to nonlinear ship rolling problems, in: Proceedings of the 11th International Conference on the Stability of Ships and Ocean Vehicles, Atehns, Greece, 2012.

[12] W. Chai, J. Fan, R. Zhu, X. Huang, G. Miao, Calculation of Ship Rolling Capsizing Probability by Path Integral Solution, J. Shanghai Jiaotong Univ. 2 (2013) 028.

[13] I.A. Kougioumtzoglou, P.D. Spanos, Stochastic response analysis of the softening Duffing oscillator and ship capsizing probability determination via a numerical path integral approach, Probab. Eng. Mech. 35 (2014) 67–74.

[14] G. Malara, P.D. Spanos, F. Arena, Maximum roll angle estimation of a ship in confused sea waves via a quasi-deterministic approach, Probab. Eng. Mech. 35 (2014) 75–81.

[15] J. Roberts, M. Vasta, Markov modelling and stochastic identification for nonlinear ship rolling in random waves, Philos. Trans. R. Soc. Lond. Ser. A: Math. Phys. Eng. Sci. 358 (2000) 1917–1941.

[16] M. Bikdash, B. Balachandran, A. Navfeh, Melnikov analysis for a ship with a general roll-damping model, Nonlinear Dyn. 6 (1994) 101–124.

[17] C. Jiang, A.W. Troesch, S.W. Shaw, Highly nonlinear rolling motion of biased ships in random beam seas, J. Ship Res. 40 (1996) 125–135.

[18] D. Paroka, N. Umeda, Capsizing probability prediction for a large passenger ship in irregular beam wind and waves: comparison of analytical and numerical methods, J. Ship Res. 50 (2006) 371–377.

[19] G. Bulian, A. Francescutto, A simplified modular approach for the prediction of the roll motion due to the combined action of wind and waves, Proc. Inst. Mech. Eng. Part. M: J. Eng. Marit. Environ. 218 (2004) 189–212.

[20] L. Dostal, E. Kreuzer, Probabilistic approach to large amplitude ship rolling in random seas, Proc. Inst. Mech. Eng. Part. C: J. Mech. Eng. Sci. 225 (2011) 2464–2476.

[21] A.H. Jazwinski, Stochastic Processes and Filtering Theory, Dover Publications, USA, 2007.

[22] A. Naess, V. Moe, Efficient path integration methods for nonlinear dynamic systems, Probab. Eng. Mech. 15 (2000) 221–231.

[23] E. Mo, Nonlinear stochastic dynamics and chaos by numerical path integration (Ph.D. thesis), Norwegian University of Science and Technology, Norway, 2008.

[24] A. Pirrotta, R. Santoro, Probabilistic response of nonlinear systems under combined normal and Poisson white noise via path integral method, Probab. Eng. Mech. 26 (2011) 26–32.

[25] D. Yurchenko, A. Naess, P. Alevras, Pendulum's rotational motion governed by a stochastic Mathieu equation, Probab. Eng. Mech. 31 (2013) 12–18.

[26] A. Naess, F. Kolnes, E. Mo, Stochastic spur gear dynamics by numerical path integration, J. Sound. Vib. 302 (2007) 936–950.

[27] A. Naess, T. Moan, Stochastic dynamics of marine structures, Cambridge University Press, United Kingdom, 2012.

[28] J. Roberts, Response of an oscillator with non-linear damping and a softening spring to non-white random excitation, Probab. Eng. Mech. 1 (1986) 40–48.

[29] I. SLF, 52/INF. 2, Information Collected by the Intercessional Correspondence Group on Intact Stability, Submitted by Japan, London, UK, 2009.

[30] A. Francescutto, S. Naito, Large amplitude rolling in a realistic sea, Int. Shipbuild. Prog. 51 (2004) 221–235.

[31] Z. Su, Nonlinear response and stability analysis of vessel rolling motion in random waves using stochastic dynamical systems, Texas A&M University, Texas, 2012.

A.4 Paper 4

Stochastic roll response for a vessel with nonlinear damping models and steady heeling angles in random beam seas

Wei Chai, Arvid Naess and Bernt J. Leira

Published in Ocean Engineering (2016), Vol. 120, pp. 202-211.

Ocean Engineering 120 (2016) 202–211

Contents lists available at ScienceDirect

Ocean Engineering

journal homepage: www.elsevier.com/locate/oceaneng

Stochastic roll response for a vessel with nonlinear damping models and steady heeling angles in random beam seas

Wei Chai [a,*], Arvid Naess [b,c], Bernt J. Leira [a]

[a] Department of Marine Technology, Norwegian University of Science and Technology, Trondheim, Norway
[b] Centre for Ships and Ocean Structures, Norwegian University of Science and Technology, Trondheim, Norway
[c] Department of Mathematical Sciences, Norwegian University of Science and Technology, Trondheim, Norway

ARTICLE INFO

Article history:
Received 15 October 2015
Received in revised form
28 April 2016
Accepted 8 May 2016
Available online 18 May 2016

Keywords:
Stochastic roll response
Path integration method
Nonlinear damping models
Initial heeling angle

ABSTRACT

Loss of ship stability is most frequently associated with extreme roll motion. For the case of random beam sea, a single-degree-of-freedom (SDOF) model is applied in the present study in order to represent the stochastic rolling behavior. The random wave excitation term in the SDOF model is approximated as a filtered white noise process by applying a second order linear filter. Accordingly, the original SDOF model is extended into a four-dimensional (4D) dynamic system. The coupled dynamic system can be viewed as a Markov system whose probabilistic properties are governed by the corresponding Fokker–Planck equation. Based on the convenient Markov property, a host of useful response statistics can be obtained by an efficient path integration (PI) method. Different nonlinear damping models, i.e. the linear-plus-quadratic damping (LPQD) model and the linear-plus-cubic damping (LPCD) model, and their effects on the stochastic roll response are investigated and the influence of the steady heeling angle on the response level associated with ship rolling in random seas is also studied. Furthermore, the accuracy of the response statistics computed by the PI technique is verified by means of the versatile Monte Carlo simulation (MCS) technique.

1. Introduction

Excessive rolling motion is considered to be a major cause of stability failure or even capsizing of ships exposed to ocean waves. For large amplitude roll motion, the nonlinear effects associated with the damping and restoring terms have a significant influence on the high-level roll response. Currently, the criteria of the International Maritime Organization (IMO) for evaluation of the intact stability are based on both hydrostatics and dynamics (IMO, 2008). In addition, due to the stochastic nature of the ocean environment and the corresponding wave excitation, the assessment of extreme rolling motion should inevitably be based on dynamic considerations and probabilistic approaches. With the awareness of the deficiencies of the current criteria for intact stability evaluation, the IMO is currently developing the next generation of such criteria with a certain consideration of the physics associated with the dynamics of nonlinear roll motion and the randomness of wave excitation and roll response (Francescutto, 2016). In this work, the dynamic stability is evaluated by means of a probabilistic approach, which may provide insight associated with the nonlinear roll dynamics in random beam seas. Hopefully, this may also serve as a contribution to the second generation IMO intact stability criteria which are currently being developed.

The problem of estimating the stochastic response of such nonlinear dynamic systems excited by random external loads has been a demanding challenge in the past decades. For this type of problem, elaborate theoretical model as well as appropriate mathematical techniques are essential (Ellermann, 2009). In the literature, the roll motion is generally assumed to be decoupled from the other motions and governed by a single-degree-of-freedom (SDOF) model in which the nonlinearities associated with the damping and restoring terms as well as the randomness of the wave excitation are all incorporated (Roberts and Vasta, 2000). Even though the SDOF model is not recommended for actual ship design, it is a very important model for qualitative studies and understanding of the nonlinear behavior under stochastic excitation. The methodology based on the Markov model has been a popular way to analysis the stochastic response of the nonlinear roll motion in random seas (Francescutto and Naito, 2004; Su and Falzarano, 2013; Chai et al., 2015b). Since the Markov model is only valid for a dynamic system driven by white noise or filtered white noise, a second order linear filter is introduced in order to approximate the random wave excitation as a filtered white noise process. Subsequently, the original SDOF model, also a second order differential equation, is extended into a four-dimensional

* Corresponding author.

http://dx.doi.org/10.1016/j.oceaneng.2016.05.019
0029-8018/

(4D) Markov dynamic system. For the coupled system, the probabilistic properties of the roll motion is governed by the Fokker–Planck (FP) equation.

The extended dynamic system usually corresponds to a high-dimensional FP equation, but analytical solutions to high-dimensional FP equations are only available for some linear systems and a very restricted class of nonlinear systems. As for numerical solutions, the path integration (PI) method has been proved to be an efficient approximation for solving the high-dimensional FP equations. This method is based on the Markov property of the dynamic system and the global solution, i.e., the evolution of the response statistics, is calculated by linking the explicitly known local solutions via a step-by-step solution technique (Mo, 2008). In addition to its efficiency, the high-dimensional PI method is able to provide reliable estimation of the response statistics, even for high response levels which are associated with low probabilities (Naess and Johnsen, 1993; Karlsen, 2006; Chai et al., 2015b).

As an alternative to the efficient PI method, Monte Carlo simulation (MCS) is another approach that can be applied in order to determine the response statistics of nonlinear systems subjected to random external or parametric forcing. The nonlinear and time-dependent terms in the dynamic system can then be easily dealt with. However, the MCS approach is only a brute force alternative and the associated computational efficiency will be sacrificed for estimation of extreme responses with low probability levels. In this work, the straightforward MCS method will serve as a verification tool to evaluate the response statistics obtained by the efficient PI method.

The nonlinearity of the roll damping moment has been recognized to be crucial for evaluating ship stability since Froude's time, however, the dynamic effects of the damping term have not been taken into consideration in the current intact stability criteria. Moreover, for traditional ship motion analysis and the associated reliability-based design, the damping and restoring terms are usually linearized for simplicity (Bulian and Francescutto, 2004). Generally, the damping moment has three kinds of components: the damping caused by radiation at the free surface and the damping caused by vortex shedding and flow separation as well as the viscous friction damping. Since these terms are coupled with each other, the quantitative evaluation of roll damping moment is difficult and empirical models are applied to describe the roll damping term. The linear-plus-quadratic damping (LPQD) model, which has been verified by numerous studies of experimental data, is widely used to describe the damping term in the SDOF model for the roll motion (Roberts and Vasta, 2000). On the other hand, the LPQD model is only once continuously differentiable, while another empirical damping model, the linear-plus-cubic damping (LPCD) model is infinitely differentiable and mathematically preferable to the LPQD model. In this work, the LPQD model is approximated by the LPCD model with the assistance of a numerical procedure proposed by Bikdash et al. (1994) and the effect of different damping models (i.e., the equivalent LPQD and LPCD models) on the stochastic roll response, especially on the high level response will be studied.

In practice, it has been observed that the stability properties of vessels with steady heeling (i.e. roll bias) are worse than those which correspond to upright conditions, i.e., vessels without such a steady heeling angle. However, current intact stability criteria only consider the influence of the heeling moment on the ship stability in a hydrostatic manner. Generally, heeling moments can be caused by wind load, by transverse displacements of masses or by lateral pull during towing work, etc. (Biran and Pulido, 2013). As for the most common mean wind action, the heeling moment is proportional to the square of the wind velocity and it also depends on the lateral projected area of the above-sea surface part of the hull. The performance of a "biased vessel" in random beam seas has been studied by stochastic linearization (Bulian and Francescutto, 2004) and the Melnikov criterion (Jiang et al., 2000, 1996), etc. Up to now, there seems to be no investigation with respect to the effect of a steady heeling moment on the distribution of random roll motion as well as on the stochastic roll response. By application of the efficient PI method, the above effects can be investigated directly since a host of useful response statistics can be obtained by solving the corresponding FP equation.

The present paper is organized as follows. Section 2 describes the SDOF model for the roll motion and the linear filter technique used to approximate the random wave excitation is also presented. The principle and numerical implementation of the efficient PI method are described in Section 3. Results from numerical simulations are presented in Section 4 where the response statistics obtained by the conventional MCS technique are also given. Furthermore, in this Section, the influence of different damping models and steady heeling angles on the stochastic roll response are also illustrated.

2. Physical modeling

2.1. Mathematical model of roll motion

By neglecting the coupling with other modes of motion, the rolling behavior of the vessel in random beam seas can be represented by the following SDOF model for qualitative study (Roberts and Vasta, 2000):

$$(I_{44} + A_{44})\phi(t) + B(\phi(t)) + \Delta(C_1\phi(t) - C_1\phi^3(t)) = M(t) \tag{1}$$

where $\phi(t)$ and $\dot{\phi}(t)$ are the roll angle and the roll velocity, respectively. I_{44} is the moment of inertia, A_{44} denotes the added mass coefficient. $B(\dot{\phi}(t))$ is the damping moment term and $\Delta(C_1\phi(t) - C_3\phi^3(t))$ is the restoring moment term. Δ is the displacement of the vessel, C_1 and C_3 are the linear and nonlinear roll restoring coefficients of the restoring arm, respectively. $M(t)$ represents the random wave excitation moment due to external waves.

It should be noted that the roll motion has a softening characteristic since the nonlinear stiffness term is negative. For the softening cases, ship capsizing would occur when the roll angle exceeds the angle of vanishing stability beyond which the restoring moment becomes negative.

The roll excitation moment is assumed to be a stationary Gaussian process and it can be characterized by the roll excitation moment spectrum, $S_{MM}(\omega)$. The latter is related to the wave energy spectrum, $S_{\xi\xi}(\omega)$, by the following relationship:

$$S_{MM}(\omega) = |F_{roll}(\omega)|^2 S_{\xi\xi}(\omega) \tag{2}$$

where $|F_{roll}(\omega)|$ represents the roll moment amplitude per unit wave height at frequency ω which can be obtained e.g. by application of strip theory. The wave elevation process is governed by the wave energy spectrum and it is also assumed to be a stationary Gaussian process during a short-term period.

The LPQD model is widely used to describe the damping moment term, and the empirical model is expressed as:

$$B(\dot{\phi}(t)) = B_{44l}\,\dot{\phi}(t) + B_{44q}\dot{\phi}(t)|\dot{\phi}(t)| \tag{3}$$

in which, B_{44l} and B_{44q} are the linear and quadratic damping coefficients for the LPQD model, respectively.

However, the LPQD is only once continuously differentiable and this is not very appealing for analytical treatment e.g. by application of the perturbation method, bifurcation analysis and so on. The LPCD model is infinitely differentiable and it is often applied in order to approximate the LPQD model by the following expression:

$$B(\dot{\phi}(t)) = \hat{B}_{44l}\,\dot{\phi}(t) + B_{44c}\dot{\phi}^3(t) \tag{4}$$

where $\hat{B}_{44l}(t)$ and B_{44c} are the linear and cubic damping coefficients for the LPCD model.

As for the equivalence of the above two damping models, Dalzell (1978) proposed a least-square algorithm over a given finite range of roll velocities and suggested an iterative procedure to determine this range. According to Dalzell's method, the coefficients in the above two models have the following relationship:

$$\hat{B}_{44l} \approx B_{44l} + \frac{5}{16}\dot{\phi}_c B_{44q} \tag{5}$$

and

$$B_{44c} \approx \frac{35}{48\dot{\phi}_c}B_{44q} \tag{6}$$

where $\dot{\phi}_c$ represents the range of roll velocity $\dot{\phi}$ over which the least-square algorithm is executed.

Dividing Eq. (1) by $(I_{44}+A_{44})$, the final form of the differential equation is given as:

$$\ddot{\phi}(t) + b_{44l}\dot{\phi}(t) + b_{44q}\dot{\phi}(t)|\dot{\phi}(t)| + c_1\phi(t) - c_1\phi^3(t) = m(t) \tag{7}$$

where b_{44}, b_{44q}, c_1 and c_3 are roll parameters and $m(t)$ is the corresponding wave excitation moment.

Moreover, large amplitude roll motion in beam seas is mainly caused by resonance effects. Due to the light roll damping, the value of $S_{mm}(\omega)$ near the natural roll frequency, ω_0 will be crucial for the subsequent roll response and the natural roll frequency is determined as:

$$\omega_0 = \sqrt{\Delta G_1/(I_{44} + A_{44})} = \sqrt{c_1} \tag{8}$$

Finally, the SDOF model (7) can be transformed into a second-order state-space equation, which is written as:

$$\begin{cases} dx_1 = x_2 dt \\ dx_2 = (-b_{44l}x_2 - b_{44q}x_2|x_2| - c_1x_1 + c_3x_1^3 + x_3)dt \end{cases} \tag{9}$$

where $x_1=\phi(t)$, $x_2=\dot{\phi}(t)$, $x_3=m(t)$.

2.2. Modeling the wave excitation moment

In the SDOF model (7), the wave excitation moment $m(t)$ is a stationary Gaussian process which is represented by an appropriate spectral density. Accordingly, the linear filter technique can be applied in order to provide the required approximation (Thampi and Niedzwecki, 1992). As mentioned above, the Markov theory is valid only for the system driven by white noise or filtered white noise and application of the linear filter guarantees the Markov property of the dynamic system. In this work, a second-order linear filter is introduced in order to approximate the target spectrum, $S_{mm}(\omega)$.

The second-order linear filter is given by the following differential equation (Dostal and Kreuzer, 2011):

$$\begin{cases} dx_3 = (x_4 - \beta x_3)dt + \gamma dW \\ dx_4 = -\alpha x_3 dt \end{cases} \tag{10}$$

in which x_3 and x_4 represent the state variables in the filter equation and the variable x_3 is the filter output, that is, the relative wave excitation process, $m(t)$. $dW(t)=W(t+dt)-W(t)$ represents an infinitesimal increment of a standard Wiener process with $E\{dW(t)\}=0$ and $E\{dW(t)dW(s)\}=0$ for $t\neq s$ and $E\{dW(t)^2\}=dt$. The spectrum generated by the second-order linear filter (10) is denoted as $S_{Filter}(\omega)$ and given as:

$$S_{Filter}(\omega) = \frac{1}{2\pi}\frac{\gamma^2\omega^2}{(\alpha-\omega^2)^2 + (\beta\omega)^2} \tag{11}$$

where α, β, γ are the parameters of the linear filter and they are determined by minimizing the least square error between the spectral density of the filtered spectrum $S_{Filter}(\omega)$ and the spectral density of the target spectrum, $S_{mm}(\omega)$. It is worth emphasizing that the filtered spectrum (11) is double-sided, while the wave energy spectrum $S_{\xi\xi}(\omega)$ and the corresponding relative roll excitation spectrum $S_{mm}(\omega)$ are physically single-sided. This difference needs to be reflected when performing the simulation itself.

Since the filtered white noise process x_3 is the output of the filter (10) and since it also represents "the driving process" of the SDOF model (10), an extended dynamic system can be formed by combing these two equations. Therefore, the roll motion in random beam seas can be described by the following 4D state space equation:

$$\begin{cases} dx_1 = x_2 dt \\ dx_2 = (-b_{44l}x_2 - b_{44q}x_2|x_2| - c_1x_1 + c_3x_1^3 + x_3)dt \\ dx_3 = (x_4 - \beta x_3)dt + \gamma \mathrm{d}W \\ dx_4 = -\alpha x_3 dt \end{cases} \tag{12}$$

It should be noted that the coupled dynamic system represented by the stochastic differential equation (SDE) (12) is a Markov diffusion process and the probabilistic property of this random process can be obtained by the PI technique, which will be presented in the next Section.

3. D PI method

The SDE (12) can be constructed as an *Itô* SDE which is given on the following form:

$$d\mathbf{x} = \mathbf{a}(\mathbf{x}, t)dt + \mathbf{b}(t)d\mathbf{W}(t) \tag{13}$$

where the state space vector $\mathbf{x}(t)=(x_1(t),\ldots, x_4(t))^{\mathrm{T}}$ is introduced, the vector $\mathbf{a}(\mathbf{x},t)$ is the drift term and $\mathbf{b}(t)d\mathbf{W}(t)$ represents the diffusive term. The vector $d\mathbf{W}(t)=\mathbf{W}(t+dt)-\mathbf{W}(t)$, where $\mathbf{W}(t)=(0, 0, W(t), 0)^{\mathrm{T}}$ and $\mathbf{b}(t)=(b_{ij}(t))$ denotes a 4×4 matrix. From the SDE (13) it can be obtained that $\mathbf{x}(t)$ is a Markov process and the Markov property will be applied for the purpose of formulating the PI procedure.

For the Markov process, its transition probability density, $p(\mathbf{x},t|\mathbf{x}',t')$, also known as the conditional probability density function (PDF) is governed by the FP equation, which is expressed as:

$$\frac{\partial}{\partial t}p(\mathbf{x}, t|\mathbf{x}', t') = -\sum_{i=1}^{4}\frac{\partial}{\partial x_i}a_i(\mathbf{x}, t)p(\mathbf{x}, t|\mathbf{x}', t') + \frac{1}{2}\sum_{i=1}^{4}\sum_{j=1}^{4}\frac{\partial^2}{\partial x_i \partial x_j}(b(t)\cdot b^T(t))_{ij}p(\mathbf{x}, t|\mathbf{x}', t') \tag{14}$$

where $\mathbf{x}'$ denotes the state space vector at time t' and $t'<t$.

For high dimensional dynamic systems, such as the 4D dynamic system (12), direct numerical methods for solution of the FP equation will hardly be feasible. Under such circumstance, the curse of dimensionality problem, i.e., difficulties which arise due to the processing capacity as well as the storage needed for the computation, will be magnified. The PI method, based on the Markov property of the dynamic system, is applied in order to give an efficient approximation for solving the high-dimensional FP equation. The principle and numerical implementation of the PI method are described below.

For numerical solution of the time continuous SDE in Eq. (13), discretization of the equation with respect to time t is essential. In

this regard, Naess and Moe (2000) proposed a fourth-order Runge-Kutta-Maruyama (RKM) approximation:

$$\mathbf{x}(t) = \mathbf{x}(t') + \mathbf{r}(\mathbf{x}(t'), t', \Delta t) + b(t')\Delta\mathbf{W}(t') \tag{15}$$

where $\Delta t = t - t'$ is the time increment and the vector $\mathbf{r}(\mathbf{x}(t'), t')$ denotes the explicit fourth-order Runge–Kutta (RK4) increment or RK4 approximation. Since $\mathbf{W}(t)$ is a Wiener process, for short time increment Δt, the independent increment $\Delta\mathbf{W}(t') = \mathbf{W}(t) - \mathbf{W}(t')$ is a Gaussian variable for every t' (a constant is considered to be a Gaussian variable with zero standard deviation).

With the introduction of the time discrete approximation, the time sequence $\{\mathbf{x}(i\cdot\Delta t)\}_{i=0}^{\infty}$ is a Markov chain and it can approximate the time-continuous Markov solution of the SDE (13) when the time increment Δt is sufficiently small. If the diffusion term $\mathbf{b}(t')\Delta\mathbf{W}(t')$ is removed from the RKM approximation (15), the dynamic system is purely deterministic and the time discretization scheme for the corresponding deterministic system is the RK4 scheme, which is given as: $\mathbf{x}(t) = \mathbf{x}(t') + r(\mathbf{x}(t'), t', \Delta t)$ with an accuracy to the order $O(\Delta t^5)$. Since the accuracy related to approximation of the deterministic system is most important in order to establish the corresponding Markov system (Mo, 2008), the accuracy of the RKM approximation (15) is satisfactory for an appropriate time increment Δt.

For a time increment $\Delta t = t - t'$, the transition probability density of Eq. (15), $p(\mathbf{x}, t|\mathbf{x}', t')$, is given as a (degenerate) Gaussian distribution, which is written as:

$$\begin{aligned} p(\mathbf{x}, t|\mathbf{x}', t') = {} & \delta(x_1 - x'_1 - r_1(\mathbf{x}', t', \Delta t)) \\ & \cdot\delta(x_2 - x'_2 - r_2(\mathbf{x}', t', \Delta t)) \cdot\tilde{p}(x_3, t|x'_3, t') \\ & \cdot\delta(x_4 - x'_4 - r_4(\mathbf{x}', t', \Delta t)) \end{aligned} \tag{16}$$

where $\tilde{p}(x_3, t|x'_3, t')$ is given by the relation:

$$\tilde{p}(x_3, t|x'_3, t') = \frac{1}{\sqrt{2\pi\gamma^2\Delta t}} \cdot \exp\left\{ -\frac{(x_3 - x'_3 - r_3(\mathbf{x}', t', \Delta t))^2}{2\gamma^2\Delta t} \right\} \tag{17}$$

in which $r_i(\mathbf{x}', t', \Delta t) = r_i(\mathbf{x}(t'), t', \Delta t)$, $i = 1,2,3,4$ are the Runge–Kutta increments for the state space variables.

For the PI method, the evolution of the response statistics, such as the PDF of the random process (also a Markov process) $\mathbf{x}$ at time t can be obtained by the following basic equation:

$$p(\mathbf{x}, t) = \int_{R^4} p(\mathbf{x}, t|\mathbf{x}', t')p(\mathbf{x}', t')d\mathbf{x}' \tag{18}$$

where $d\mathbf{x}' = \prod_{i=1}^{4} dx'_i$.

Since the expression for the TPD is obtained (i.e., the (Eqs. (16) and 17)), the PDF of $\mathbf{x}(t)$ can be obtained by the following iterative algorithm if an initial PDF (i.e. at time t_0) is given:

$$\begin{aligned} p(\mathbf{x}, t) = {} & \int_{R^4} \cdots \int_{R^4} \prod_{s=1}^{n} p(\mathbf{x}^{(s)}, t_s|\mathbf{x}^{(s-1)}, t_{s-1}) \\ & \cdot p(\mathbf{x}^{(0)}, t_0) d\mathbf{x}^{(0)} \ldots d\mathbf{x}^{(n-1)} \end{aligned} \tag{19}$$

where $\mathbf{x} = \mathbf{x}^{(n)} = \mathbf{x}(t_n)$, $t = t_n = t_0 + n\cdot\Delta t$, $\mathbf{x}^{(s)} = \mathbf{x}(t_s)$ and $t_s = t_0 + s\cdot\Delta t$.

Eq. (19) describes the mathematical principle of the PI method and it can be seen that the global evolution of the response statistics is obtained by linking local solutions via a step-by-step solution technique. As for the numerical implementation of the 4D PI approach, discretization should also be introduced with respect to the four state space variables. A reasonable computational domain and the corresponding computational grid have to be determined at first. In this work, the initial PDF, $p(\mathbf{x}^{(0)}, t_0)$, is chosen as a 4D Gaussian PDF with zero mean and variances in the four dimensions evaluated by a simple MCS (Mo, 2008). The straightforward MCS ensures that the initial 4D Gaussian PDF includes all the information corresponding to the parameters of the dynamic system, such as the roll parameters in Eq. (7) and the parameters of the linear filter in Eq. (11) and it also provides a rational computational domain and computational grid for the subsequent calculation.

For the numerical implementation of the iterative algorithm (19) for each grid point, the PDF at the previous time t', $p(\mathbf{x}', t')$ is represented as an interpolating spline surface via parabolic B-splines. The PDF at time t, $p(\mathbf{x}, t)$ can be evaluated by several specific steps. The numerical iterative algorithm and the associated computational steps have been systematically described by Yurchenko et al. (2013) and Chai et al. (2015b).

4. Numerical simulation results

4.1. Stochastic roll response and MCS

In this work, an ocean surveillance ship which is described in Su (2012) is selected to study the stochastic response of the roll motion in random beam seas. The main parameters of the selected vessel are presented in Table 1 and the roll restoring arm (i.e. the GZ curve) for the ship is presented in Fig. 1.

The random stationary sea state is represented by the modified Pierson-Moskowitz spectrum, which is widely used for fully developed sea states. The wave energy spectrum is given as:

$$S_{\xi\xi}(\omega) = \frac{5.058g^2H_s^2}{T_p^4\omega^5} \exp\left(-1.25\frac{\omega_p^4}{\omega^4} \right) \tag{20}$$

where $g = 9.81$ m s^{-2}, H_s denotes the significant wave height, ω_p represents the peak frequency at which the wave spectrum $S_{\xi\xi}(\omega)$ has its maximum value, and T_p is the corresponding peak period.

For the present analysis, three different sea states, i.e., different external excitations, are considered. The wave energy spectra for the different sea states and the roll excitation moment per unit wave height, $|F_{roll}(\omega)|$ are presented in Fig. 2.

As mentioned above, the parameters α, β, γ of the second-order linear filter (11) can be determined by the least square scheme which is available as part of the curve fitting algorithms in MATLAB. The parameters of the linear filter for the target spectrum $S_{mm}(\omega)$ which correspond to different sea states are given in Table 2 and the fitting result of the relative wave excitation spectrum for sea state 1 with $H_s = 4.0$ m and $T_p = 11.0$ s is shown in Fig. 3. It can be seen in Fig. 3 that the filtered spectrum is reasonable with regards to the bandwidth, peak frequency and peak value.

However, due to the light damping of the roll behavior, the fitting accuracy in the critical frequency region near the natural roll frequency ω_0 is essential for estimating the stochastic roll response. In order to decrease the discrepancy between the spectral density of the filtered spectrum $S_{Filter}(\omega)$ and the spectral density of the target spectrum, $S_{mm}(\omega)$ in the critical region, a correction factor, c, is introduced. The filtered spectrum (11) changes to the following expression:

Table 1
List of ship parameters.

Parameters	Dimensional value
$I_{44}+A_{44}$	5.540×10^7 kg m^2
Δ	2.017×10^7 N
b_{44}	0.095 s^{-1}
b_{44c}	0.0519 s
c_1	1.153 s^{-2}
c_3	0.915 s^{-2}
ω_0	1.074 rad/s

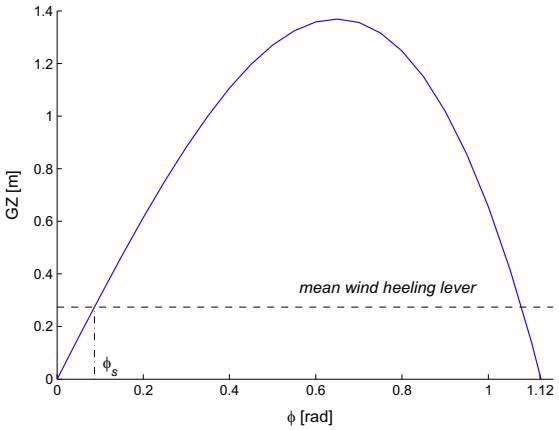

Fig. 1. GZ curve for the selected vessel.

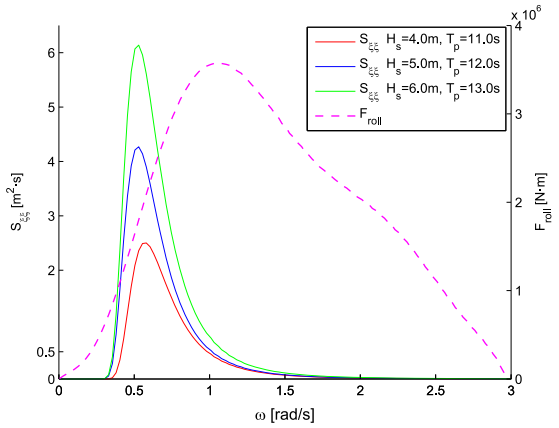

Fig. 2. Wave energy spectra for different sea states and the rolling excitation moment amplitude per unite wave height $|F_{roll}(\omega)|$.

Table 2
Parameters of the second-order linear filter which correspond to different sea states with target spectrum $S_{mm}(\omega)$ for the excitation moment.

Sea States	H_s (m)	T_p (s)	α	β	γ
Sea state 1	4.0	11.0	0.495	0.366	0.0432
Sea state 2	5.0	12.0	0.441	0.364	0.0498
Sea state 3	6.0	13.0	0.390	0.365	0.0555

$$S_{Filter}(\omega) = \frac{1}{2\pi} \frac{(c\cdot\gamma)^2\omega^2}{(\alpha - \omega^2)^2 + (\beta\omega)^2} \tag{21}$$

Correspondingly, the driving process x_3 in the dynamic system (12) will be the corrected value, i.e., $c \cdot x_3$. For the selected sea state and vessel model, the correction factor c is taken as 1.07 by considering the mean difference between the two spectral densities in the critical region. Moreover, for the same vessel model, the correction factor would vary slightly for different sea states. The corrected spectrum in the critical region is also shown in Fig. 5. The rationality of introducing the correction factor has been verified in Chai et al. (2015a) and the obvious discrepancies between the two spectral densities in the low-frequency and high-frequency regions, which are far away from the critical frequency region, would not influence the roll response to a significant extent.

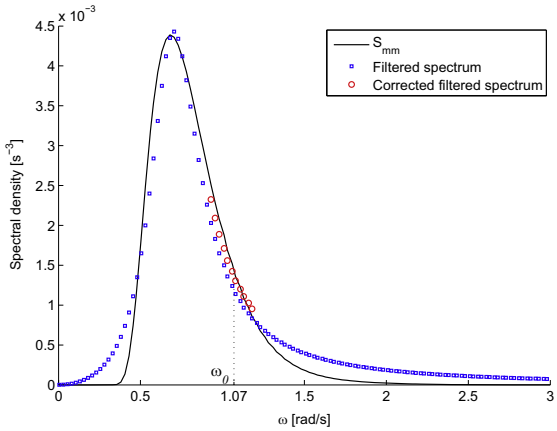

Fig. 3. Relative roll excitation moment spectrum $S_{mm}(\omega)$, the corresponding filtered spectrum and the corrected filtered spectrum (part) for sea state 1 with H_s=4.0 m and T_p=11.0 s.

Having performed the spectrum fitting, all the parameters in the 4D dynamic system (12) are determined. As mentioned in Section 3, the joint PDF of the random process $\mathbf{x}(t)$ can be obtained by the 4D PI technique. By integrating through the entire range of the third and fourth dimensions, the joint PDF of the roll angle process and the roll velocity process at time instant t, $f_{\phi\dot{\phi}}(\phi, \dot{\phi}; t)$ is determined. Due to the softening characteristic of the stiffness term, ship capsizing would be possible, but when the mean time to capsize is long enough, the dynamic system can be regarded as being highly reliable and the corresponding roll response reaches stationary conditions in an approximate sense (Roberts and Vasta, 2000). Therefore, the joint PDF $f_{\phi\dot{\phi}}(\phi, \dot{\phi}; t)$can be represented by $f_{\phi\dot{\phi}}(\phi, \dot{\phi}; t)$as a stationary joint PDF at a suitable reference point in time. The joint PDF of the roll response for the sea state with H_s =4.0 m and T_p=11.0 s is shown in Fig. 4, while Fig.5 presents the contour lines of the joint PDF.

For marine structures subjected to random wave excitation, the mean upcrossing rate is a key parameter for estimation of extreme

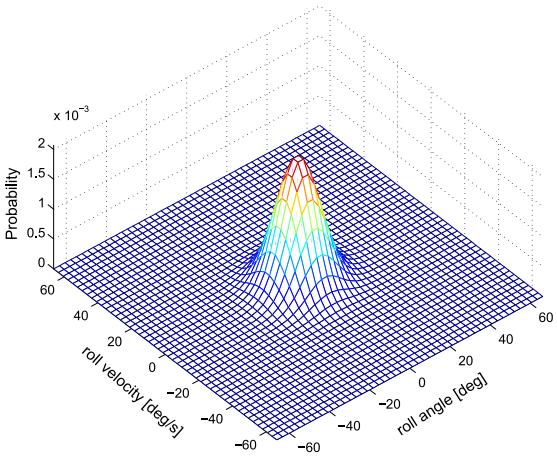

Fig. 4. Joint PDF of the roll response obtained by the 4D PI method for sea state 1 with H_s=4.0 m and T_p=11.0 s.

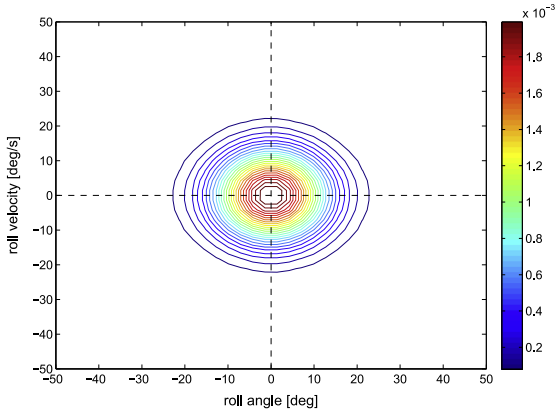

Fig. 5. Contour lines of the joint PDF of the roll response for the sea state with H_s =4.0 m and T_p=11.0 s.

response statistics (Naess et al., 2006). Calculation of the mean upcrossing rate for the roll angle process is usually based on the Rice formula (22) by application of the joint PDF of the roll angle process and the roll velocity process (which can be obtained by the 4D PI method). The Rice formula is given as:

$$\nu^+(\zeta;\, t) = \int_0^\infty \dot{\phi} f_{\phi\dot{\phi}}(\zeta,\, \dot{\phi};\, t) d\dot{\phi} \tag{22}$$

where $\nu^+(\zeta;\, t)$ denotes the expected number of upcrossing for the ζ-level per unit time at time t by the roll angle process $\phi(t)$.

The mean upcrossing rate is important for assessment of operation safety and also for reliability based design approaches. For high response levels, the reliability evaluation is usually based on the probability that the roll angle process $\phi(t)$ exceeds the specific level ζ at least once during a time interval of length T. If the assumption of statistical independence between the upcrossings is valid for that specific level, the corresponding exceedance probability can be expressed by the Poisson estimate:

$$P_\zeta(T) = 1 - \exp\left(- \int_0^T \nu^+(\zeta;\, t) dt \right) \approx 1 - \exp(- \nu^+(\zeta) \cdot T \Big) \tag{23}$$

where $\nu^+(\zeta)$ represents the mean upcrossing for the level ζ at a suitable reference point in time.

Furthermore, the standard MCS technique can serve as a validation of the mean upcrossing rate obtained by the 4D PI method and the Rice formula. It should be noted that this direct-counting method has its main drawback with respect to the computational efficiency and accuracy associated with estimation of the extreme response levels (which correspond to low values of the probability). However, this obstacle will not be encountered when applying the PI method based on the Markov assumption.

For the 4D dynamic system (12), the fourth-order RKM method is applied in order to solve the corresponding SDE and then time series of the roll response are obtained. In the numerical simulation, ship capsizing is assumed to occur if the roll angle process exceeds the positive or negative angle of vanishing stability and then that particular realization is terminated since the subsequent roll angle process will exceed $\pi/2$ or $-\pi/2$ rapidly. A large number of realizations are required for the purpose of estimating the response statistics, especially for the high-level responses. The appropriate empirical mean value of the upcrossing rate is based on MCS and given as:

$$\hat{\nu}^+(\zeta) = \frac{\sum_{i=1}^k n_i^+(\zeta;\, T_i)}{\sum_{i=1}^k T_i} \tag{24}$$

where $n_i^+(\xi;\, T_i)$ denotes the counted number of upcrossings of the level ζ during the time interval $(0,\, T_i)$ for simulated time history No. i. Moreover, the practical simulation time T_i is not fixed for each realization, it is equal to the predetermined simulation time T if no capsizing occurs. Otherwise, it is the value of the termination time t_i for each case where capsizing occurs.

The number of realizations, k, e.g. k=1000–5000, is selected according to the value of the upcrossing rate in the tail region and the length of the predetermined simulation time T. Generally, a low upcrossing rate and short time periods T correspond to a large number of simulations, i.e. k. A fair approximation of the 95% confidence interval (CI), $\mathrm{CI}_{0.95}$, for the empirical estimation of the mean upcrossing rate (24), is given by a normal distribution (Naess and Moan, 2012):

$$\mathrm{CI}_{0.95}(\zeta) = \left(\hat{\nu}^+(\zeta) - 1.96\frac{\hat{s}(\zeta)}{\sqrt{k}},\, \hat{\nu}^+(\zeta) + 1.96\frac{\hat{s}(\zeta)}{\sqrt{k}} \right) \tag{25}$$

where the empirical standard deviation $\hat{s}(\xi)$ is given as

$$\hat{s}(\zeta)^2 = \frac{1}{k-1} \sum_{i=1}^k \left(\frac{n_i^+(\zeta;\, T_i)}{T_i} - \hat{\nu}^+(\zeta) \right)^2 \tag{26}$$

For the selected sea state, the marginal PDF of the roll response obtained by the 4D PI method and the corresponding empirical estimation obtained the 4D MCS technique are shown in Fig. 6. Fig. 7 presents the mean upcrossing rate calculated by application of the 4D PI method and the Rice formula versus the empirical value of the upcrossing rate $\hat{\nu}^+(\zeta)$ as well as the 95% confidence interval provided by the 4D MCS method. For the MCS results in Figs. 6 and 7, the number of realizations, k, is selected to be 3000 and the predetermined simulation time T is 1.0×10^5 s for each of the realizations. It can be seen from Figs. 6 and 7 that the comparison of the marginal PDF and the upcrossing rate obtained by the 4D PI method and the standard MCS technique demonstrates satisfactory agreement. The 4D PI method can provide good results for the response statistics, even in the tail region with very low probability levels, but the response statistics obtained by the MCS

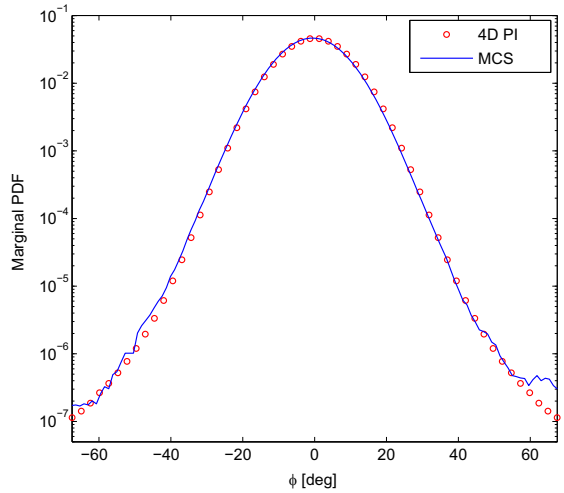

Fig. 6. Marginal PDF of the roll angle process obtained by the 4D PI method and the corresponding empirical estimation obtained by the 4D MCS method, for the sea state with H_s=4.0 m and T_p=11.0 s.

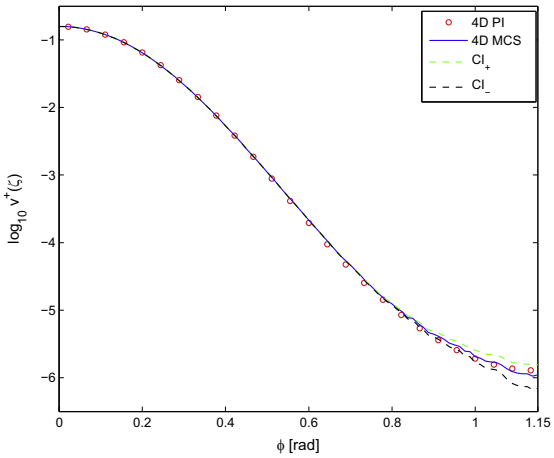

Fig. 7. Log plot of the mean upcrossing rate obtained by the 4D PI method and the corresponding empirical estimation obtained by the 4D MCS method, for the sea state with $H_s=4.0$ m and $T_p=11.0$ s.

method are suffering from uncertainties in this region.

4.2. Influence of different nonlinear damping models

In this work, we focus on the influence of two damping models which are equivalent in a least square sense (i.e., the LPQD and LPCD models) on the statistics of the roll motion, especially for high roll response levels. The equivalence of the above two damping models is determined by a least-square algorithm described by Eqs. (5) and (6). The equivalence of the LPQD and LPCD models is shown in Fig. 8 and it is illustrated that the two damping models have a good agreement in the least-square sense. Moreover, decay tests are performed for the dynamic system (12) by application of these two damping models and the results are presented in Fig. 9. The decay tests are started with the same initial condition, i.e., $\phi=15°$ and $\dot{\phi}=0.5°/s$. It can be seen that the free decay curves for the dynamic system with different damping models are almost the same.

Next, the performance of these two damping models is investigated with respect to the response statistics of roll motion when the ship is excited by a random wave process. Fig. 10

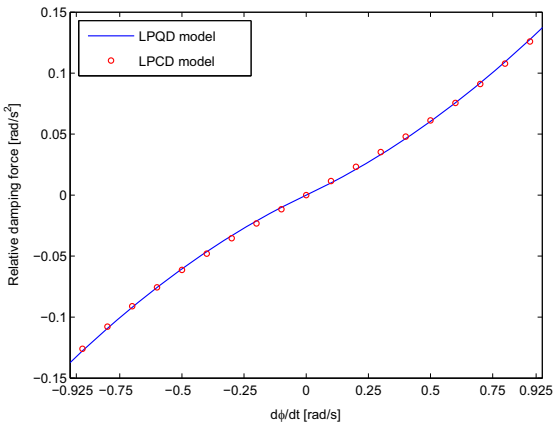

Fig. 8. Fitting results for the LPQD and LPCD models by applying the least square method (5) and (6).

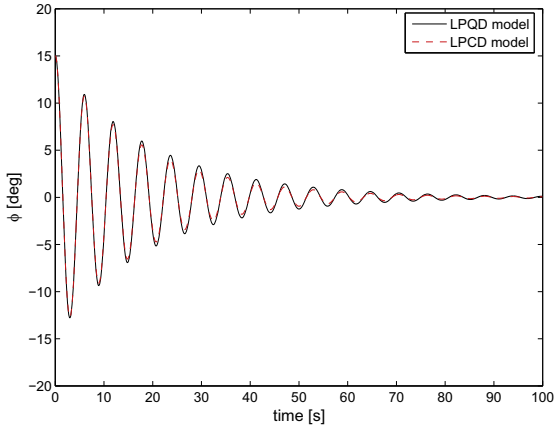

Fig. 9. Free decay responses for the dynamic system (13) with the LPQD and LPCD models, for initial conditions $\theta=15°$, $\dot{\theta}=0.5°/s$.

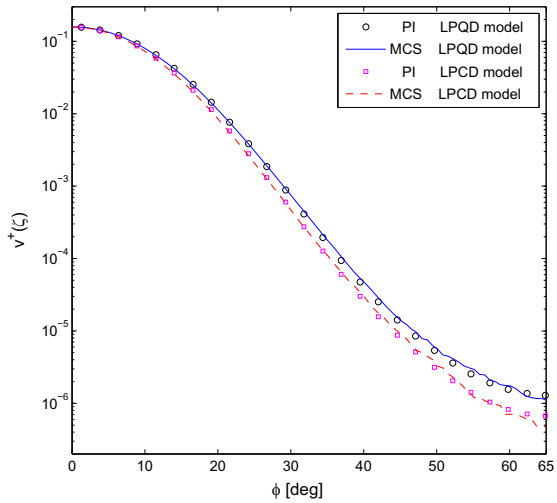

Fig. 10. Upcrossing rates for the dynamic system (13) with the LPQD and LPCD models for the sea state with $H_s=4.0$ m and $T_p=11.0$ s.

presents the upcrossing rates for the roll motion which is described by the dynamic system (13) with the LPQD and LPCD models for the case of sea state 1 in Table 2. The mean upcrossing rates are calculated by the 4D PI method and the corresponding empirical estimates are obtained by the 4D MCS technique. Similarly, for sea states 2 and 3 in Table 2, the upcrossing rates obtained by the above two approaches are shown in Figs. 11 and 12, respectively. It is illustrated by Figs. 10–12 that the 4D PI method is able to provide high-accuracy results for both of the damping models when compared with the corresponding empirical estimates. More importantly, it has been observed in the above three figures that the upcrossing rates for the roll motion (when subjected to the same sea state) which correspond to different damping models are quite different, even though these two damping models match well in a least–square sense as well as in the decay tests.

The discrepancies between the upcrossing rates, especially in the tail region, illustrate that the equivalent LPCD model determined by the proposed least-square algorithm leads to a less

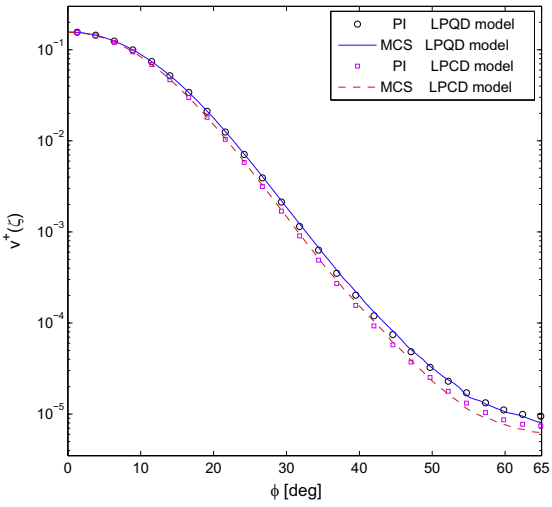

Fig. 11. Upcrossing rates for the dynamic system (13) with the LPQD and LPCD models for the sea state with $H_s=5.0$ m and $T_p=12.0$ s.

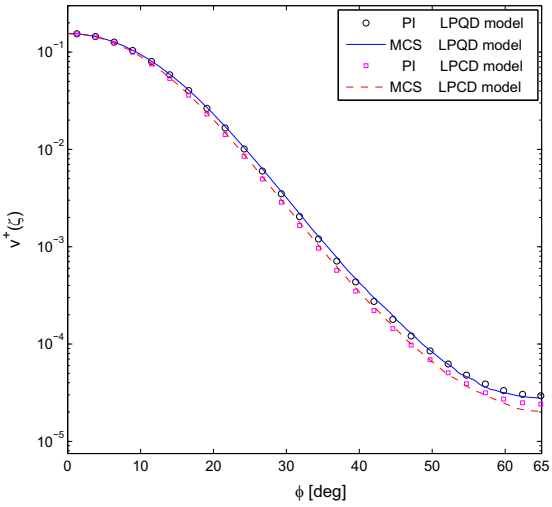

Fig. 12. Upcrossing rates for the dynamic system (13) with the LPQD and LPCD models for the sea state with $H_s=6.0$ m and $T_p=13.0$ s.

conservative estimate of the extreme response for the dynamic system. Therefore, the least-square algorithm cannot guarantee the accuracy of the stochastic response of the roll motion in random seas. The stochastic roll response in the tail region is sensitive to the value of roll damping moments as well as to the selection of roll damping models. Furthermore, the method of stochastic linearization is the most frequently used method for analyzing the stochastic responses of many nonlinear dynamic systems subjected to random excitation (Roberts and Spanos, 2003). The stochastic linearization method can provide reasonable estimates for the mean square response. However, when this technique is applied to linearize the nonlinear LPQD model (3), it can be anticipated that even more significant discrepancies will be observed with respect to the upcrossing rate in the tail region.

4.3. Influence of the steady heeling angle

The mean wind action $\bar{M}_{wind}$ results in a heeling angle ϕ_s of the vessel and the relationship between these quantities can be expressed as:

$$\bar{M}_{wind} = \Delta(G_1\phi_s - G_1\phi_s^3) \tag{27}$$

Then, the SDOF model (7) is changed into (Chai, 2016):

$$\ddot{\phi}(t) + b_{44l}\dot{\phi}(t) + b_{44q}\dot{\phi}(t)|\dot{\phi}(t)| + c_1\phi(t) - c_1\phi^3(t) = m(t) + \bar{m}_{wind} \tag{28}$$

where $\bar{m}_{wind}$ is the mean wind moment which will also be added into the dynamic system (12).

For the selected vessel model with a mean wind heeling action, the corresponding mean wind heeling lever and the heeling angle ϕ_s are presented in Fig. 1. It can be seen that the area under the GZ curve decreases with the existence of a wind heeling moment. That implies a reduced capacity with respect to ship stability failure. Currently, the intact stability criteria only apply the hydrostatic weather criterion in order to evaluate the stability of a vessel with a wind heeling arm. The present Section is on the other hand devoted to studying the effect of a wind heeling moment, i.e., the steady heeling angle, on the distribution of the roll motion in random seas as well as on the stochastic roll response.

For the vessel with 5° steady heeling angle under the sea state with $H_s=4.0$ m and $T_p=11.0$ s, the joint PDF of the roll response can be calculated by the 4D PI method. Fig. 13 displays the contour lines of the joint PDF of the roll response, and the marginal PDF of the roll angle process is presented in Fig. 14. It can be observed in Figs. 4–6 that the distribution of the roll response is symmetric when a steady heeling angle is not present. The symmetry is reasonable since the distribution of the random excitation (or the filtered white noise process) as well as the vessel properties are symmetric with respect to the origin. For the vessel with a 5° steady heeling angle, it is seen in Figs. 13–14 that the distribution of the roll angle process is approximately symmetric with respect to the steady heeling angle. However, when the marginal PDF of the roll angle process in Fig. 14 is plotted with a logarithmic scale along the vertical axis in Fig. 15, the symmetry is not valid in the high level response region, for which the nonlinear effects associated with the damping and restoring terms have a significant influence on the distribution of the roll response.

The influence of the steady heeling angle on the upcrossing rate is presented in Fig. 16 for the case that sea state 1 in Table 2 is selected for the analysis. It can be readily seen that the existence of

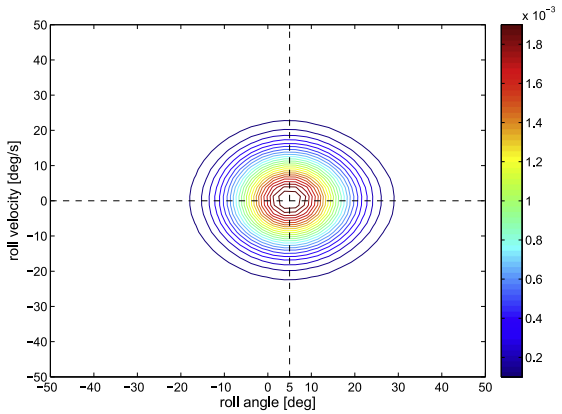

Fig. 13. Contour lines of the joint PDF of the roll response for the vessel with 5° steady heeling angle for the sea state with $H_s=4.0$ m and $T_p=11.0$ s.

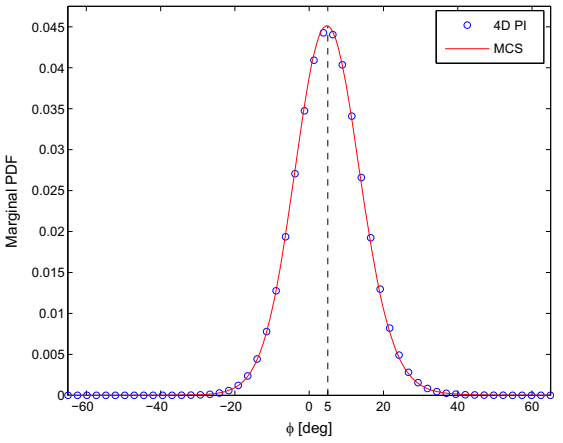

Fig. 14. Marginal PDF of the roll angle process for the vessel with 5° steady heeling angle for the sea state with $H_s=4.0$ m and $T_p=11.0$ s.

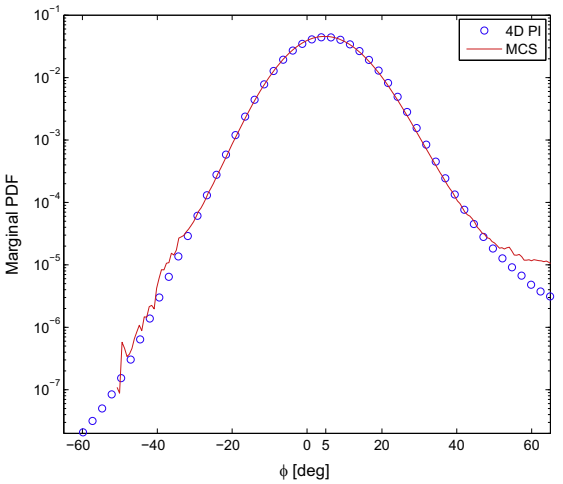

Fig. 15. Logarithmical scaled marginal PDF of the roll angle process for the vessel with 5° steady heeling angle for the sea state with $H_s=4.0$ m and $T_p=11.0$ s.

the steady heeling angle leads to an increases of the upcrossing rate. This implies that when a vessel has steady heeling angle, the roll response would cross high levels more frequently than for the condition without a steady heeling angle. According to the Poisson estimate (23), an increase of the upcrossing rate indicates that the existence of the initial heeling angle leads to a reduction of the capacity of the vessel with respect to stability failure. More importantly, earlier deterministic nonlinear dynamics work conducted in Thompson (1997) and Spyrou et al. (2002) noted that even a small bias (i.e. steady heeling) has a disproportionate diminishing effect on a ship's safety margin. The stochastic analysis in this work as well as the results presented in Fig. 16 confirm and extend this statement for irregular sea state conditions. Furthermore, in Figs. 15 and 16, the satisfactory agreement of the stochastic responses obtained by the 4D PI method and the 4D MCS approach demonstrate that the 4D PI procedure can provide reliable results for dynamic systems where a mean wind heeling action is present.

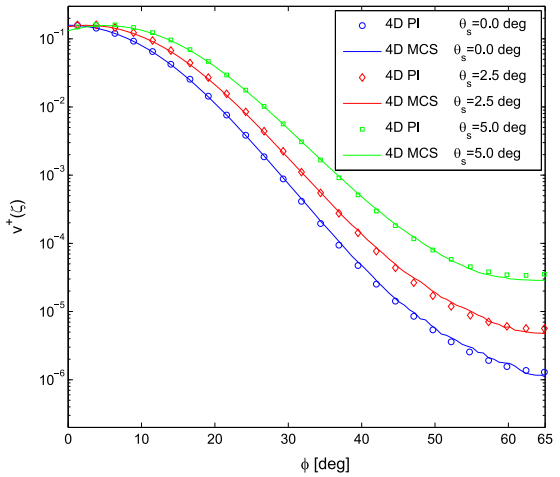

Fig. 16. Upcrossing rates for vessel with different steady heeling angles for the sea state with $H_s=4.0$ m and $T_p=11.0$ s.

5. Conclusions

In this article, an efficient 4D PI method, based on the Markov property of the dynamic system as well as the 4D MCS were applied in order to study the influence of nonlinear damping models and the steady heeling angle on the response statistics of the roll motion in random beam seas. The good agreement of the response statistics obtained by the proposed numerical procedure and the MCS results demonstrate that the 4D PI method can provide reliable and satisfactory calculations for such dynamic systems in the case of different damping models (i.e. the LPQD model and the LPCD model) as well as for SDOF models with a mean wind heeling action being present.

The LPCD model can serve as an equivalent damping model for the LPQD model by applying a least-square scheme. Even though this equivalence exhibits a good performance for the decay test, the dynamic system with the LPCD model provides a less conservative estimate of the stochastic roll response in random seas. The discrepancies of the upcrossing rates, especially in the high-level response region, should not be ignored when performing a dynamic analysis.

Furthermore, the existence of the steady heeling angle has a significant influence on the stochastic roll response and leads to a deterioration of the ship stability. The probabilistic distribution of the roll angle process for the vessel with a steady heeling angle is approximately symmetric with respect to the steady heeling angle. However, in the high-level response region, the response statistics are influenced by nonlinear effects associated with the damping and the restoring terms. This implies that the symmetry properties no longer apply.

Acknowledgments

The first author would like to thank the financial support from the China Scholarship Council (CSC) (Grant no. 201306230077), affiliated with the Ministry of Education of the P.R. China. Grants from the "Norwegian ship-owners' association fund" at Norwegian University of Science and Technology (NTNU) and the support from the Department of Marine Technology, NTNU are also gratefully acknowledged.

References

Bikdash, M., Balachandran, B., Navfeh, A., 1994. Melnikov analysis for a ship with a general roll-damping model. Nonlinear Dyn. 6 (1), 101–124.

Biran, A., Pulido, R.L., 2013. Ship Hydrostatics and Stability. Butterworth-Heinemann, Amsterdam, Netherland.

Bulian, G., Francescutto, A., 2004. A simplified modular approach for the prediction of the roll motion due to the combined action of wind and waves. Proc. Inst. Mech. Eng. M J. Eng. Marit. Environ. 218 (3), 189–212.

Chai, W., 2016. Reliability evaluation of the roll motion under the wind and irregular beam waves. J. Ocean Eng. Sci. 1 (2), 149–156.

Chai, W., Naess, A., Leira, B.J., 2015a. Filter models for prediction of stochastic ship roll response. Probab. Eng. Mech. 41, 104–114.

Chai, W., Naess, A., Leira, B.J., 2015b. Stochastic dynamic analysis and reliability of a vessel rolling in random beam seas. J. Ship Res. 59, 113–131.

Dalzell, J., 1978. A note on the form of ship roll damping. J. Ship Res. 22, 178–185.

Dostal, L., Kreuzer, E., 2011. Probabilistic approach to large amplitude ship rolling in random seas. Proc. Inst. Mech. Eng. C J. Mech. Eng. Sci. 225 (10), 2464–2476.

Ellermann, K., 2009. The motion of floating systems: nonlinear dynamics in periodic and random waves. J. Offshore Mech. Arct. Eng. 131 (4), 041104.

Francescutto, A., 2016. Intact stability criteria of ships–Past, present and future. Ocean Eng.

Francescutto, A., Naito, S., 2004. Large amplitude rolling in a realistic sea. Int. Shipbuild. Prog. 51 (2), 221–235.

IMO, 2008. International Code on Intact Stability. International Maritime Organization, London.

Jiang, C., Troesch, A., Shaw, S., 2000. Capsize criteria for ship models with memory-dependent hydrodynamics and random excitation. Philos. Trans. R. Soc. Lond. A Math. Phys. Eng. Sci. 358 (1771), 1761–1791.

Jiang, C., Troesch, A.W., Shaw, S.W., 1996. Highly nonlinear rolling motion of biased ships in random beam seas. J. Ship Res. 40 (2), 125–135.

Karlsen, H.C., 2006. Statistics of Wave Induced Nonlinear Loads and Responses (Ph. D Thesis). Norwegian University of Science and Technology, Trondheim, Norway.

Mo, E., 2008. Nonlinear Stochastic Dynamics and Chaos by Numerical Path Integration (Ph.D Thesis). Norwegian University of Science and Technology, Trondheim, Norway.

Naess, A., Johnsen, J., 1993. Response statistics of nonlinear, compliant offshore structures by the path integral solution method. Probab. Eng. Mech. 8 (2), 91–106.

Naess, A., Karlsen, H.C., Teigen, P., 2006. Numerical methods for calculating the crossing rate of high and extreme response levels of compliant offshore structures subjected to random waves. Appl. Ocean Res. 28 (1), 1–8.

Naess, A., Moan, T., 2012. Stochastic Dynamics of Marine Structures. Cambridge University Press, New York, USA.

Naess, A., Moe, V., 2000. Efficient path integration methods for nonlinear dynamic systems. Probab. Eng. Mech. 15 (2), 221–231.

Roberts, J., Vasta, M., 2000. Markov modelling and stochastic identification for nonlinear ship rolling in random waves. Philos. Trans. R. Soc. Lond. Ser. A Math. Phys. Eng. Sci. 358 (1771), 1917–1941.

Roberts, J.B., Spanos, P.D., 2003. Random vibration and statistical linearization. Courier Corporation.

Spyrou, K., Cotton, B., Gurd, B., 2002. Analytical expressions of capsize boundary for a ship with roll bias in beam waves. J. Ship Res. 46 (3), 167–174.

Su, Z., 2012. Nonlinear Response and Stability Analysis of Vessel Rolling Motion in Random Waves Using Stochastic Dynamical Systems. Texas A&M University, Houston, USA.

Su, Z., Falzarano, J.M., 2013. Markov and Melnikov based methods for vessel capsizing criteria. Ocean Eng. 64, 146–152.

Thampi, S.K., Niedzwecki, J.M., 1992. Filter approach to ocean structure response prediction. Appl. Ocean Res. 14 (4), 259–271.

Thompson, J., 1997. Designing against capsize in beam seas: recent advances and new insights. Appl. Mech. Rev. 50 (5), 307–325.

Yurchenko, D., Naess, A., Alevras, P., 2013. Pendulum's rotational motion governed by a stochastic Mathieu equation. Probab. Eng. Mech. 31, 12–18.

A.5 Paper 5

Monte Carlo simulation and Grim effecitve wave model for predicting the extreme response of a vessel rolling in random head seas

Wei Chai, Arvid Naess, Bernt J. Leira and Gabriele Bulian

Published in Ocean Engineering (2016), Vol. 123, pp. 191-203

Ocean Engineering 123 (2016) 191–203

Contents lists available at ScienceDirect

Ocean Engineering

journal homepage: www.elsevier.com/locate/oceaneng

Efficient Monte Carlo simulation and Grim effective wave model for predicting the extreme response of a vessel rolling in random head seas

Wei Chai [a,*], Arvid Naess [b,c], Bernt J. Leira [a], Gabriele Bulian [d]

[a] Department of Marine Technology, Norwegian University of Science and Technology, Trondheim, Norway
[b] Centre for Ships and Ocean Structures, Norwegian University of Science and Technology, Trondheim, Norway
[c] Department of Mathematical Sciences, Norwegian University of Science and Technology, Trondheim, Norway
[d] Department of Engineering and Architecture, University of Trieste, Trieste, Italy

ARTICLE INFO

Article history:
Received 10 November 2015
Received in revised form
12 July 2016
Accepted 13 July 2016

Keywords:
Parametric roll
The Grim effective wave
Linear filter approach
Extreme response prediction
Monte Carlo simulation

ABSTRACT

In this paper, a computationally efficient Monte Carlo simulation (MCS) approach is introduced in order to estimate the extreme response statistics of parametric rolling in random longitudinal seas. Basically, parametric roll is caused by sufficiently large oscillations of the roll restoring moment occurring within certain frequencies of wave encounter (approximately twice the natural roll frequency). The concept of the Grim effective wave is applied herein in order to approximate the variation of the restoring moment in random waves. A fourth order linear filter is introduced to model the random effective wave amplitude process, which is assumed to be the driving process for the variation of the restoring term as well as for the stochastic nonlinear system of the roll motion by application of the Grim effective wave approximation. For the stochastic dynamical system, the roll response is a random process and an extrapolation procedure is developed for estimating the extreme values of the response statistics by assuming regular behavior in the tail region of the mean upcrossing rate. The rationality of the linear filter model and the feasibility of an efficient MCS method based on extrapolation techniques for predicting the extreme roll response are illustrated. Furthermore, the phenomenon of parametric roll in random seas as well as the effect of vessel speed on the stochastic roll response are investigated.

1. Introduction

Parametric roll in longitudinal (head or following) waves is a phenomenon possibly leading to the occurrence of excessive roll motion, which may represent a serious threat to ship stability. Even though there is no direct excitation for the roll motion of a vessel sailing in pure head or following seas, large oscillation of the roll restoring moment within certain regions of wave encounter frequencies combined with insufficient roll damping, and thus limited dissipation capabilities, could induce parametric roll response (Paulling, 2011). The onset of parametric roll in regular waves can be predicted by applying the Mathieu instability criteria with the simplification that the roll motion is descried by a single degree-of-freedom (SDOF) model (Francescutto et al., 2004; Shin et al., 2004; Spyrou, 2000). For the SDOF model, when the wave encounter frequency is approximately twice the natural roll frequency with the corresponding wave length being of the order of the ship length, large amplitude roll motion can be observed if the wave height is large enough. This phenomenon is referred to as principal resonance or low cycle resonance. However, the regular wave condition is an ideal condition which is hardly encountered in an actual seaway and investigation of the parametric roll considering irregular waves is therefore more appropriate for a realistic and accurate evaluation of the ship safety at sea.

For the random wave scenario, the primary mechanism leading to the inception of parametric roll is also the variation of the restoring moment. It needs to be noted that the time-varying restoring term and the subsequent roll response are stochastic. Therefore, the dynamic stability of the vessel and the large or extreme response induced by the parametric roll have to be evaluated by means of probabilistic approaches. Furthermore, the nonlinearities associated with the damping and restoring terms should also be considered in the large amplitude roll motion (Chai et al., 2015b). For nonlinear stochastic dynamic systems, such as the parametric roll in random seas, elaborate theoretical model as well as appropriate mathematical techniques are essential (Ellermann, 2009).

In order to study the parametric roll behavior in random seas

* Corresponding author.
E-mail addresses: chai.wei@ntnu.no, chaiweihappy1988@gmail.com (W. Chai).

http://dx.doi.org/10.1016/j.oceaneng.2016.07.025
0029-8018/

and estimate the risk of an associated large or extreme roll response, several 6-DOF nonlinear simulation tools such as LAMP (Shin et al., 2004), FREDYN (France et al., 2003) and a nonlinear strip theory model proposed by e Silva and Soares (2013) etc. have been applied for the numerical simulation. Moreover, several other tools are mentioned by Peters et al. (2011) and relevant benchmark studies regarding parametric roll have been described by Spanos and Papanikolaou (2009). However, these powerful simulation codes, which calculate the restoring moment at every time step by using the instantaneous wetted surface, are time consuming and are difficult to be applied for predicting the extreme roll response with very low probability levels. Therefore, some simplifications are required in order to reduce the computation time which depends on the number of DOFs as well as on the method for approximation of the restoring term. On the other hand, the effect of time-varying restoring moment, the main cause of the parametric roll, should be correctly modeled. Generally, the restoring term is included in the nonlinear model for the roll degree of freedom in a simplistic way (Vidic-Perunovic and Jensen, 2009) and several approximation procedures have been proposed, such as the Volterra series approach (Hua et al., 1999; Moideen et al., 2014), fluctuation of the metacentric height (GM) term by linear transfer functions (Song et al., 2013), the Grim effective wave method and other methods mentioned in Vidic-Perunovic (2011), etc.

Grim (1961) introduced the effective wave concept with the main idea that the instantaneous irregular sea surface can be replaced by an equivalent (or effective) regular wave with the wave length equal to the ship length and its crest or trough always positioned amidships. The equivalent wave is assumed to be fixed with respect to the vessel, but its amplitude is a random process. Even though use of the effective wave concept is an approximation, its simplicity could be sufficiently accurate for engineering calculations (Umeda and Yamakoshi, 1992). The concept of the Grim effective wave has been applied by several authors to study the parametric roll behavior of vessels with conventional hull forms (Bulian, 2006; Chang, 2008; Kröger, 1986) and the verification work with respect to applying the Grim effective model for calculating the response of parametric rolling have already executed and reported by Bulian. To improve the accuracy of the original approach and in order to allow the use of the concept also for unconventional ships, the Grim effective wave has been extended into a traveling effective wave whose amplitude and phase are described by stochastic processes (Bulian, 2008). The same type of improved equivalent wave was also used previously, in a numerical framework by Jensen (2007).

In this paper, we approximate the time-varying roll restoring moment according to Bulian (2006) in order to simulate the stochastic roll response in the time domain. In such an approach, heave and pitch motions are assumed to be quasi-static and the roll motion is approximated as a SDOF model with the restoring term fitted by a nonlinear expression with regard to the effective wave amplitude process and the roll angle (Bulian, 2006). Furthermore, the stability boundaries of a vessel sailing in irregular waves can be approximately established by means of the stochastic linearization technique. However, the main interest of the present study is the large or extreme roll response near or beyond the stability boundaries, which is important for reliability based design and operation in practice.

The effective wave amplitude process, which serves as the driving term of the stochastic nonlinear system, is assumed to be Gaussian and governed by a specific spectrum. Traditionally, the linear superposition method with deterministic spectral amplitude or stochastic spectral amplitude is applied in order to generate the Gaussian process (Tucker et al., 1984). In this paper, we introduce a fourth order linear filter to approximate the effective wave amplitude process (Chai et al., 2015a). The linear filter technique uses a white noise process to generate a Gaussian random process which complies with the required spectrum and the advantages of the filter technique will be described in Section 3 in detail. By combing it with the filter model, the SDOF model of the roll motion can be extended into a high-dimensional Markov system since the extended dynamic system can be viewed as being driven by a white noise process. Therefore, the probabilistic properties of the Markov system is governed by the corresponding Fokker-Planck (FP) equation. However, numerical methods for the solution of FP equations do suffer from a curse of dimensionality and they are hardly applicable for obtaining the response statistics by solving the high-dimensional FP equation.

On the other hand, the Monte Carlo simulation (MCS) method does not critically suffer from dimensionality problems, since the response statistics are obtained directly from the realizations instead of by solving the FP equation. Basically, it is the simplest and most versatile way to determine the response statistics of stochastic dynamic system, although this simplicity is paid for by the random sampling uncertainty inherent in the approach. For ships and marine structures, the mean upcrossing rate for high-level roll responses and the associated probabilities of exceedance are of central importance in evaluation of the response statistics (Naess et al., 2007a). However, the computational burden of this straightforward method may be prohibitive for estimation of the high-level responses and the associated low levels of probability. In this paper, a computationally efficient MCS method is proposed in order to circumvent this obstacle. In the efficient MCS approach presented herein, an extrapolation procedure is applied for prediction of the upcrossing rate in the far tail (which is nearly impossible to determine by means of the conventional MCS) on the basis of the estimations obtained at more moderate levels and assuming further a regular behavior of the mean upcrossing rates in the tail regions (Naess and Gaidai, 2008). It has been shown that, with the advantage of the time-saving extrapolation technique, the efficient MCS method does give an accurate estimation of the extreme responses with a dramatic reduction of the computation time (Naess et al., 2007b).

The aim of the work reported in this paper is to predict the extreme response of parametric roll in random longitudinal seas by application of the filter technique and the efficient MCS method. The paper is organized as follows. In Section 2, a mathematical model based on the Grim effective wave approximation for the parametric roll in random longitudinal seas is presented. Section 3 describes a linear filter model for the random effective wave amplitude process which is governed by the effective wave spectrum based on the Grim effective wave approximation. In Section 4, the principle of the efficient MCS by utilization of an extrapolation procedure is presented and Section 5 illustrates the performances of the efficient MCS and the linear filter by numerical simulations. The feasibility of these two techniques for the purpose of predicting extreme response levels associated with parametric roll is also demonstrated in Section 5.

2. Mathematical model of ship motion

By assuming a quasi-static behavior in relation to the heave and pitch motions, the roll dynamics for the ship in irregular longitudinal long-crested waves can be represented by the following SDOF model (Bulian, 2006; Dostal et al., 2012):

$$(I_{44} + A_{44})\ddot{\theta}(t) + B(\dot{\theta}(t)) + \Delta GZ(\theta(t), A_x(\xi(x,t))) = M(t) \quad (1)$$

where $\theta(t)$ and $\dot{\theta}(t)$ are the roll angle and the roll velocity, respectively. I_{44} is the moment of inertia of the vessel, A_{44} represents

the added moment of inertia. $B(\dot{\theta}(t))$ is the damping moment term of the roll motion and $\Delta GZ(\theta(t), A_x(\xi(x,t)))$ is the restoring moment in random longitudinal waves. where $A_x(\xi(x, t))$ accounts for the effect of wave elevation process $\xi(x,t)$ along the vessel (coordinate x) at time t, and $M(t)$ denotes a roll excitation moment.

The damping moment normally has three kinds of components: the free surface radiated wave damping, the damping caused by vortex shedding and flow separation as well as the viscous friction damping. Furthermore, at forward speed, lift contributions to roll damping also arises. Generally, the quantitative evaluation of the roll damping is difficult because these terms are coupled with each other. Nevertheless, an empirical damping model can be applied in order to describe the roll damping moment. This model is expressed as:

$$B(\dot{\theta}(t)) = B_{44}\dot{\theta}(t) + B_{44q}\dot{\theta}(t)|\dot{\theta}(t)| + B_{44c}\dot{\theta}^3(t) \tag{2}$$

where B_{44} is the linear coefficient damping coefficient, B_{44q} and B_{44c} are quadratic and cubic damping coefficients, respectively.

The roll excitation moment $M(t)$ is small if the ship travels in about the same direction as the incident waves. It acts as an additive disturbance for the dynamic system and can be approximated by application of a linear strip method (Dostal and Kreuzer, 2014). For long-crest head seas, its influence can be neglected.

Regarding the most important time-varying restoring moment, it is expressed in terms of the displacement Δ and restoring arm $GZ(\theta(t), A_x(\xi(x,t)))$ of the vessel. The restoring arm is an instantaneous quantity which is difficult to estimate due to its nonlinear relationship with the instantaneous irregular wave surface $\xi(x,t)$. The restoring moment can be obtained by integration of the external pressure over the instantaneous wetted surface. However, such direct integration requires a significant computation effort and the much simpler Grim effective wave concept is applied herein in order to approximate the complicated restoring term. The derivation and principle of the effective wave method for approximation of the restoring term are given below, while more details on the relevant theoretical background are given by Grim (1961) and Bulian (2008).

For a ship sailing with constant speed V in random long-crest head seas, it is convenient to describe the sea state in a coordinate which is fixed to the ship. Assume that a right-hand ship fixed coordinate system ($oxyz$) is placed at amidships with the positive z axis oriented vertically upwards, while the positive x direction points to the bow. The encounter frequency in the ship fixed frame is then given as:

$$\omega_e = \omega - \kappa(\omega)V\ \cos\ \chi \tag{3}$$

where χ is the angle between the vessel heading and the direction of wave propagation (for head seas $\chi=180°$ and for following seas $\chi=0°$), $\kappa(\omega)$ is the wave number with $\kappa(\omega)=\omega^2/g$ for the deep water case. For head sea condition, the wave spectrum with respect to the encounter frequency is formulated as:

$$S(\omega_e) = \frac{S(\omega)}{1 - (2\omega/g)\cdot V\ \cos\ \chi} = \frac{S(\omega)}{1 + (2\omega/g)\cdot V} \tag{4}$$

where $S(\omega)$ is the wave spectrum, also known as the wave energy spectrum. In general, the irregular long-crested wave surface can be described by the following linear superposition scheme with deterministic spectral amplitudes if the corresponding wave spectrum is given.

$$\xi(x, t) = \sum_{n=1}^{\infty} \cos(\omega_{e,n}t - \kappa_n x + \epsilon_n)\sqrt{2S(\omega_n)\Delta\omega} \tag{5}$$

where $\xi(x,t)$ represents the random wave elevation process, which is evolving in space x (measured in the ship-fixed reference system) and time t. ω_n is the discretized wave frequency and $\omega_{e,n}$ is the corresponding encounter frequency, κ_n and ϵ_n are the corresponding wave number and random phase angle. Moreover, ϵ_n is a random variable and uniformly distributed over $[0,\ 2\pi)$ and $\Delta\omega$ is a constant difference between successive frequencies.

The main idea of the effective wave model is that the irregular wave surface $\xi(x,t)$ can be approximated by an equivalent (or effective) regular wave $\xi_{eff}(x,t)$. It is assumed that the largest fluctuation of the restoring term occurs when the regular longitudinal wave have a length close to the ship length. Although this is not always true, it is a reasonable approximation for the most common cases. Therefore, an equivalent regular wave with a wave length which is equal to the length of the vessel (as given below) represents the most serious case (Bulian, 2008; Dostal et al., 2012; Jensen, 2007):

$$\begin{aligned}\xi_{eff}(x, t) &= \xi_c(t)\cos\left(\frac{2\pi}{L}x\right) + \xi_s(t)\sin\left(\frac{2\pi}{L}x\right)\\ &= \bar{\xi}_{eff}(t)\cos\left(\frac{2\pi}{L}x + \varphi(t)\right), -\frac{L}{2} < x < \frac{L}{2}.\end{aligned} \tag{6}$$

where L is the length of the effective wave (which is also equal to the ship length), $\bar{\xi}_{eff}(t)$ is the effective wave amplitude process. $\xi_c(t)$ and $\xi_s(t)$ are random amplitude processes and $\phi(t)$ is the random phase. In Eq. (6), the average value of the equivalent wave has been neglected since it is irrelevant to roll motion if quasi-static heave and pitch motions are assumed.

The equivalence between the irregular wave surface (5) and the effective regular wave (6) can then be implemented by minimizing the following square error function:

$$\delta^2(\xi_c, \xi_s) = \int_{-L/2}^{L/2} (\xi(x, t) - \xi_{eff}(x, t))^2 dx \tag{7}$$

By introducing the basic property that $\frac{\partial\delta^2(\xi_c,\xi_s)}{\partial\xi_c} = \frac{\partial\delta^2(\xi_c,\xi_s)}{\partial\xi_s} = 0$, the Gaussian random processes $\xi_c(t)$ and $\xi_s(t)$ can be determined and given as:

$$\begin{aligned}\xi_c(t) &= \sum_{n=1}^{\infty} f_c(\kappa_n)\cos(\omega_{e,n}t + \epsilon_n)\sqrt{2S(\omega_n)\Delta\omega}\\ \xi_s(t) &= \sum_{n=1}^{\infty} f_s(\kappa_n)\cos(\omega_{e,n}t + \epsilon_n)\sqrt{2S(\omega_n)\Delta\omega}\end{aligned} \tag{8}$$

in which the transfer functions $f_c(\kappa_n)$ and $f_s(\kappa_n)$ are

$$\begin{aligned}f_c(\kappa_n) &= \frac{2R\ \sin\ R}{\pi^2 - R^2}\\ f_s(\kappa_n) &= \frac{2\pi\ \sin\ R}{\pi^2 - R^2}\end{aligned} \tag{9}$$

where $R=(L/2)\kappa_n$ and κ_n is the wave number associated with the n-th wave component with physical frequency ω_n.

If we set the random phase $\phi(t)=0$ (i.e., the random amplitude $\xi_s=0$ and $\bar{\xi}_{eff}(t) = \xi_c(t)$), Eq. (6) is the original Grim's effective wave model which is widely used for the ships with conventional hull forms. Otherwise, it is the improved model described in Bulian (2008) which can provide good results in terms of restoring variations, also for unconventional vessels. As for the former model, the crest or trough of the equivalent regular wave is always situated amidships, the wave is assumed to be a standing wave (unmovable) with random amplitude $\xi_c(t)$. The latter model relates to a traveling wave and gives a much better approximation of the irregular wave surface. In this paper, a RORO ship from Bulian (2006) is selected for the subsequent study and the simpler former model is applied since it works well for conventional ships. In the following, the random amplitude process $\xi_c(t)$ is referred to as the effective wave amplitude process $\bar{\xi}_{eff}(t)$ and the spectrum of effective wave amplitude process, also known as the effective wave spectrum (Bulian, 2006; Dostal et al., 2012; Grim, 1961), can be

obtained as:

$$S_{\xi_c}(\omega) = S_{\xi_{eff}}(\omega) = f_c^2(\kappa(\omega))\cdot S(\omega) = \frac{4R^2\sin^2(R)}{(\pi^2 - R^2)^2}\cdot S(\omega) \tag{10}$$

and the corresponding encounter spectrum for the effective wave amplitude process for the head seas conditions is given as:

$$S_{\xi_c}(\omega_e) = \frac{f_c^2(\kappa(\omega))\cdot S(\omega)}{1 + (2\omega/g)\cdot V} \tag{11}$$

With the simplifications from the effective wave model, the restoring arm can be rewritten as follows:

$$\begin{aligned} GZ(\theta(t), A_x(\xi(x,t))) &\approx GZ(\theta(t), A_x(\xi_{eff}(x,t))) \\ &= GZ(\theta(t), \xi_c(t)) \\ &= GZ_0(\theta(t)) + \delta GZ(\theta(t), \xi_c(t)) \\ &= \sum_{m=1,3,5\cdots}^{N_\theta} C_{0m}\theta^m + \delta GZ(\theta(t), \xi_c(t)) \end{aligned} \tag{12}$$

where GZ_0 is the restoring arm in still water which is usually given by a nonlinear odd function of the roll angle, $C_{0m}(m=1,3,5\ldots)$ is the related roll restoring coefficient and δGZ is the variation of the restoring arm in waves. The restoring term $GZ(\theta(t), \xi_c(t))$ is a binary function with respect to the effective wave amplitude process $\xi_c(t)$ and the roll angle (also referred to as heeling angle) $\theta(t)$. By means of a standard hydrostatic software, this function is computed by applying the equivalent regular waves of the same length as the ship length but with different wave amplitudes amidships. Specifically, for an equivalent regular wave with a given value of the wave amplitude being located at amidships, the corresponding restoring arm for different heeling angles and for this wave amplitude can be calculated hydrostatically. In addition, the wave amplitude $\xi_c > 0$ means a wave crest case and $\xi_c < 0$ represents an equivalent wave with wave trough positioned amidships. The restoring arms for different values of the wave amplitude can then be obtained and the restoring arm in Eq. (12) can be expressed by a set of couples of heeling angles and effective wave amplitudes. A nonlinear expression is applied in this work in order to fit the GZ surface.

$$GZ(\theta(t), \xi_c(t)) = \sum_{m=1,3,5\cdots}^{N_\theta}\left(C_{0m} + \sum_{l=1}^{N_\xi} C_{wml}\xi_c^l(t)\right)\cdot\theta^m(t) \tag{13}$$

By combining the SDOF model (1) with the damping model (2) and the approximate restoring term (13), the complete expression can be obtained. Diving it by $(I_{44}+A_{44})$, the final form of the differential equation is given as:

$$\begin{aligned} &\ddot{\theta}(t) + b_{44}\dot{\theta}(t) + b_{44q}\dot{\theta}(t)|\dot{\theta}(t)| + b_{44c}\theta^3(t) \\ &\quad + \sum_{m=1,3,5\cdots}^{N_\theta}\left(c_{0m} + \sum_{l=1}^{N_\xi} c_{wml}\xi_c^l(t)\right)\cdot\theta^m(t) = 0 \end{aligned} \tag{14}$$

and the natural roll frequency can be determined as:

$$\omega_0 = \sqrt{\Delta C_{01}/(I_{44}+A_{44})} = \sqrt{c_{01}} \tag{15}$$

where $b_{44}=B_{44}/(I_{44}+A_{44})$; $b_{44q}=B_{44q}/(I_{44}+A_{44})$; $b_{44c}=B_{44c}/(I_{44}+A_{44})$. The coefficients C_{0m} and C_{wml} $(m=1,3,5\ldots;\ l=1,2,3\ldots)$ can be obtained from a least square fitting of $GZ(\theta(t), \xi_c(t))$ and correspondingly $c_{om}=\Delta C_{0m}/(I_{44}+A_{44})$, $(m=1,3,5\ldots)$ and $c_{wml}=\Delta C_{wml}/(I_{44}+A_{44})$.

3. Linear filter technique

In this Section, a linear filter is introduced in order to model the effective wave amplitude process $\xi_c(t)$ whose governing spectrum is given by Eq. (11). The techniques based on the linear superposition procedures with deterministic spectral amplitude or stochastic spectral amplitude are simple and commonly used if the target spectrum is given. For the superposition technique with deterministic amplitudes, such as the Eqs. (5) and (8), the FFT technique can be applied for generating the time series with a significant reduction of computation time. However, it has to be noted that the quality of this simulation depends on the value of $\Delta\omega$ and the generated time series will smoothly repeat itself after the duration time $T=2\pi/\Delta\omega$. An alternative method is to sum components with stochastic amplitudes and the series repeats itself only after a long time. The drawback of this method is that the standard FFT algorithm could be unavailable and the generation of time series will be time consuming. On the other hand, Park et al. (2013) mentioned that caution is need for the linear superposition procedure since the parametric roll response is greatly sensitive to the method of discretization of the spectrum as well as the number of components in the linear superposition procedure.

Nevertheless, the above obstacles can be circumvented by introducing the filter technique. Spanos (1983, 1986) was the pioneer in applying the filter technique in order to approximate the wave elevation and the wave kinematics. Subsequently, the filter algorithms were widely used to model random processes and to evaluate the response of nonlinear systems in the field of ocean engineering (Alevras and Yurchenko, 2013; Francescutto and Naito, 2004; Su, 2012; Thampi and Niedzwecki, 1992). In general, the filter technique is applicable only for stationary stochastic processes. Therefore, the effective wave amplitude process can be adequately approximated by a suitable filter. The input of the filter is a Gaussian white noise and the corresponding output, also known as the filtered white noise can be applied in order to approximate the target random process with specific spectral characteristics.

Due to the simplicity and practicality of the linear filter approach, it has been widely used by the engineering community. In this study, a fourth-order linear filter is introduced to model the target spectrum (11) and approximate the effective wave amplitude process $\xi_c(t)$.

$$\begin{cases} dx_3 = (x_4 - \lambda_1 x_3)dt \\ dx_4 = (x_5 - \lambda_2 x_3)dt + \gamma_1 dW \\ dx_5 = (x_6 - \lambda_3 x_3)dt \\ dx_6 = -\lambda_4 x_3 dt \end{cases} \tag{16}$$

where x_3, x_4, x_5 and x_6 are variables introduced for the state-space representation and x_3 represents the filter output $\xi_c(t)$. $dW(t)=W(t+dt)-W(t)$ represents an infinitesimal increment of a standard Wiener process with $E\{dW(t)\}=0$, $E\{dW(t)dW(s)\}=0$ for $t\neq s$ and $E\{dW(t)^2\}=dt$.

The double-sided spectrum generated by Eq. (16) for the output x_3 will have the following form:

$$S_{4th}(\omega) = \frac{1}{2\pi}\frac{\gamma_1^2\omega^4}{[(\beta_1-\omega^2)^2 + (\alpha_1\omega)^2][(\beta_2-\omega^2)^2 + (\alpha_2\omega)^2]} \tag{17}$$

where, the parameters α_1, α_2, β_1, β_2 and γ_1 are the parameters of the fourth-order linear filter and the parameters λ_1, λ_2, λ_3, and λ_4 in Eq. (17) can be determined by the following relationship: $\lambda_1=\alpha_1+\alpha_2$, $\lambda_2=\beta_1+\beta_2+\alpha_1\alpha_2$, $\lambda_3=\alpha_1\beta_2+\alpha_2\beta_1$, $\lambda_4=\beta_1\beta_2$. In addition, α_1, α_2, β_1, β_2, γ_1 for the fourth-order filter are determined by a least-square algorithm which is utilized for fitting of the target spectrum. The characteristics of the filtered spectra, such as the bandwidth and the peak frequency can be adjusted by changing the values of these parameters.

It can be seen that the principles of the linear filter model (16) and the linear superposition schemes are different. The former method generate a Gaussian process by means of the input

Gaussian white noise and the linearity of the system (16), while the latter is based on the well-known central limit theorem that requires a discretization of the spectrum as well as a large number of harmonic components. The periodic repetition or the high numerical cost problem encountered when applying the linear superposition approaches is not encountered by the filter technique. Moreover, the filtered spectrum (17) is double-sided, while the target spectrum is physically single-sided and this difference must be considered in the practical simulation.

By combining the governing equation of the roll motion (14) with the fourth-order filter (16), the extended dynamic system is formed. Therefore, the roll motion for random longitudinal sea can be described by a 6D state-space equation.

$$\begin{cases} dx_1 = x_2 dt \\ dx_2 = \left(-b_{44}x_2 - b_{44c}x_2^3 - \sum_{m=1,3,5\cdots}^{N_\theta} \left(c_{0m} + \sum_{l=1}^{N_\xi} c_{wlm} x_3^l \right) \right) \cdot x_1^m \Big) d \\ dx_3 = (x_4 - \lambda_1 x_3) dt \\ dx_4 = (x_5 - \lambda_2 x_3) dt + \gamma_1 dW \\ dx_5 = (x_6 - \lambda_3 x_3) dt \\ dx_6 = -\lambda_4 x_3 dt \end{cases} \tag{18}$$

where $x_1 = \theta(t),\ x_2 = \dot{\theta}(t),\ x_3 = \xi_c(t)$.

4. Extreme response prediction

The dynamic system represented by the stochastic differential equation (SDE) (18) is a Markov system driven by Gaussian white noise. The advantage of the Markov dynamic system is that a host of accurate and useful response statistics can be obtained by solving the governing equation, i.e. the FP equation. However, for the nonlinear extended system (18), the so-called "curse of dimensionality" comes into play which means that difficulties associated with the numerical methods arise due to the fact that processing capacity as well as the storage needed for computation will increase dramatically with the dimension of the FP equations. Nevertheless, the straightforward MCS method, which estimates the response statistics by direct counting work could be a possible approach. However, the associated computational cost as well as the efficiency would be sacrificed when the direct MCS technique is applied in order to estimate the statistics of large roll response and the associated low levels of probability. In this Section, we describe the procedure based on the conventional MCS method for estimation of the empirical mean upcrossing rate and also elaborate the crucial role of this quantity in order to determine the extreme value distribution. An extrapolation scheme which takes advantage of the assumed regularity behavior of the mean upcrossing rate in the tail regions is then introduced in combination with the MCS method in order to predict the mean upcrossing rate in the far tail region which is hardly accessible by the traditional MCS method.

4.1. Mean upcrossing rate

The mean upcrossing rate is a key parameter for estimation of the large and extreme response statistics as well as for evaluation of the associated reliability of marine structures (Naess and Moan, 2012). As mentioned above, the standard MCS method can be applied in order to estimate the empirical mean upcrossing rate of the roll response in random longitudinal seas. For the dynamic system which is represented by Eq. (18), the corresponding MCS usually includes two parts: generate a sample of the random effective wave amplitude process and a numerical solution of the differential equation. The fourth-order Runge-Kutta approximation method is applied to the deterministic part of the SDE. It is combined with the Maruyama approximation for the stochastic part of the SDE (Naess and Moe, 2000), whereby the Maruyama approximation is of weak order one, there may seem to be a disparity in approximation orders of our numerical solution procedure. This approach is applied to solve the SDE (18) and time series of the roll response are then obtained.

In practice, large amplitude roll motion or even ship capsizing may occur when the simulation time T is long enough or the parametric roll response caused by the variation of the restoring moment is intense enough. Moreover, if the mean time to capsize is long enough, the dynamic system can be regarded as a highly reliable system (Roberts and Vasta, 2000) and the practical time-variant upcrossing rate $\nu^+(\zeta, t)$ can be approximated as a time-invariant parameter, i.e., the mean upcrossing rate, $\nu^+(\zeta)$ at a suitable reference point in time.

For a stationary process (in the present case of roll motion), the appropriate sample mean value of the upcrossing rate can be obtained from the time series of the roll response:

$$\hat{\nu}^+(\zeta) = \frac{1}{k} \sum_{i=1}^{k} \frac{n_i^+(\zeta; T_i)}{T_i} \tag{19}$$

where $n_i^+(\zeta; T_i)$ denotes the counted number of upcrossing of the level ζ within a time duration of length T_i for simulated time history no. i. The practical simulation time T_i is not fixed for each simulation, it is equal to the predetermined simulation time T if no capsizing occurs. Otherwise, it is the value of the termination time t_i for each case where capsizing occurs.

Moreover, the number of simulations, i.e. k, is selected according to the values of the upcrossing rates in the tail region and the length of the predetermined simulation time T. Usually, low upcrossing rates and short time periods T correspond to a large simulation number k. A fair approximation of the 95% confidence interval, $CI_{0.95}$, for the value of $\hat{\nu}^+(\zeta)$ can be expressed as:

$$CI_{0.95}(\zeta) = \left(\hat{\nu}^+(\zeta) - 1.96\frac{\hat{s}(\zeta)}{\sqrt{k}},\ \hat{\nu}^+(\zeta) + 1.96\frac{\hat{s}(\zeta)}{\sqrt{k}} \right) \tag{20}$$

where the empirical standard deviation $\hat{s}(\xi)$ in this particular case, is calculated by the expression:

$$\hat{s}(\zeta)^2 = \frac{1}{k-1} \sum_{i=1}^{k} \left(\frac{n_i^+(\zeta; T_i)}{T_i} - \hat{\nu}^+(\zeta) \right)^2 \tag{21}$$

Roll angles near or beyond the maximum of the still water restoring arm GZ_0 can be regarded as high-level responses. If the assumption of statistically independent upcrossing is valid for a certain level in this region, it is reasonable to assume that the random number of upcrossings in an arbitrary time interval of length T is approximately Poisson distributed. For high response levels, let $\Theta(T) = \max\{\theta(t):\ 0 \le t \le T\}$ denote the largest (or extreme) value of the roll angle process $\theta(t)$ over the time interval of length T. The cumulative distribution function (CDF) of $\Theta(T)$ under the Poisson assumption is approximately given in terms of the mean upcrossing rate by the following relationship for a stationary short-term sea state (Naess and Moan, 2012):

$$\text{Prob}(\Theta(T) \le \zeta) = exp(-\nu^+(\zeta) \cdot T) \tag{22}$$

Moreover, under the Poisson assumption, the reliability measure is usually expressed in terms of the probability that the roll angle process $\theta(t)$ exceeds the specific level ζ at least once during a time interval of length T. Therefore, the exceedance probability for a duration of exposure time T can be approximated by a widely used approach given as follows:

$$P_{MC}(\zeta; T) = 1 - \exp(-\nu^+(\zeta) \cdot T) \tag{23}$$

Eqs. (22) and (23) clearly indicate the crucial role of the mean upcrossing rate in determining the extreme value distribution. The exceedance probabilities for extreme values and evaluation of the CDF for the extreme responses have already been applied in McTaggart (2000) and Kim et al. (2014), respectively, by invoking asymptotic extreme value distributions. It can be seen that, the Poisson estimate, which is expressed Eqs. (22) and (23), can provide values for the above two aspects directly without resorting to the use of asymptotic distributions, whose validity is hard to verify.

The Poisson estimate is a good approximation and widely used in reliability engineering due to its simplicity and accuracy. In addition, relevant study with respect to its performance for random roll motion in Chai et al. (2015b) demonstrated that the Poisson estimate can provide satisfactory results for stochastic roll responses, except for the vessel characterized by extremely light roll damping. In such a case the ACER method can be applied to estimate the extreme value distribution (Naess and Moan, 2012).

4.2. Efficient monte Carlo simulation

The conventional (or standard) MCS method is not very efficient for estimating the mean upcrossing rate with respect to the far tail region. In this part, an efficient extrapolation scheme is introduced in order to provide an accurate and reasonable estimation of the extreme response with a dramatic reduction of the computation time. The combination of the MCS method and the extrapolation procedure is referred to as the efficient MCS method in this work.

The efficient extrapolation approach for the purpose of extreme response prediction derives from the fact that for the ships being considered, the mean upcrossing rate as a function of level ζ is in general highly regular in a specific way in the tail region. In fact, for a large class of stochastic process, the mean upcrossing rate tail (e.g. $\zeta \geq \zeta_0$) behaves similarly to $\exp\{-a(\zeta-b)^c\}$, where $a>0$, $b \leq \zeta_0$, and $c>0$ are suitable constants. Therefore, as discussed in detail in Naess and Gaidai (2008), it may be assumed that the mean upcrossing rate is approximated as:

$$\nu^+(\zeta) \approx q(\zeta) exp\{ -a(\zeta - b)^c\}, \quad \zeta \geq \zeta_0 \tag{24}$$

where the function $q(\zeta)$ is slowly varying compared with the exponential function $\exp\{-a(\zeta-b)^c\}$ for the tail values of ζ and the function $q(\zeta)$ can be replaced by a single constant q for large values of ζ.

In order to find the optimal values of parameters a, b, c, q, an optimized fitting on the log level is selected. These parameters can be determined by minimizing the following mean square error function,

$$F(q, a, b, c) = \sum_{j=1}^{M} \rho_j \left| \ln \hat{\nu}^+(\zeta_j) - lnq + a(\zeta_j - b)^c \right|^2 \tag{25}$$

where $\hat{\nu}^+(\zeta_j), j=1, \ldots, N$ denote a set of empirical mean upcrossing rates at different levels. ρ_j denotes a weight factor that puts more emphasis on the more reliable data points. The choice of weight factors is arbitrary to some extent. In this work, we use $\rho_j=(\ln CI^+(\zeta_j)-\ln CI^-(\zeta_j))^{-2}$, where CI^+ and CI^- are the bounds of the confidence interval determined by Eq. (20), combined with a Levenberg-Marquardt least squares optimization method (Gill et al., 1981). This method has usually worked well provided reasonable initial values for the parameters were chosen. It should be noted that there is a level ζ_j beyond which the weight factor ρ_j is no longer defined. Therefore, the summation in Eq. (25) has to stop before such a scenario happens. Also, the data of the empirical mean upcrossing rates should be preconditioned by establishing the tail maker ζ_0 in a sensible way.

Although the Levenberg-Marquardt method, as described above, generally works well, it can be transformed into a more simplified and transparent two-parameter optimization method. This is realized by considering Eq. (25) when the values of b and c are kept fixed. The optimization problem then reduces to a standard weighted linear regression problem. That is, with both b and c fixed, the optimal values of a and $\ln q$ are found using closed form weighted linear regression formulas in terms of ρ_j, $y_j = \ln \hat{\nu}^+(\zeta_j)$ and $x_j=(\zeta_j-b)^c$. The optimal values of a and q are given by the relations:

$$a^*(b, c) = -\frac{\sum_{j=1}^{N} \rho_j (x_j - \bar{x})(y_j - \bar{y})}{\sum_{j=1}^{N} \rho_j (x_j - \bar{x})^2} \tag{26}$$

and

$$\ln q^*(b, c) = \bar{y} + a^*(b, c)\bar{x} \tag{27}$$

where $\bar{x} = \sum_{j=1}^{N} \rho_j x_j / \sum_{j=1}^{N} \rho_j$ and $\bar{y} = \sum_{l=1}^{N} \rho_j y_j / \sum_{l=1}^{N} \rho_j$.

In order to calculate the final optimal set of parameters, the Levenberg-Marquardt method can now be applied to the function $\tilde{F} = F(q^*(b, c), a^*(b, c), b, c)$ to find the optimal values of b^* and c^*, and then the corresponding a^* and q^* can be calculated from Eqs. (26) and (27). For estimation of a confidence interval for a predicted value of the upcrosing rate function provided by the optimal curve, the empirical confidence band is reanchored to the optimal curve. The weight factors ρ_j and the Levenberg-Marquardt scheme mentioned above can also be applied to determine the optimal parameters for fitting to the boundary curves of the reanchored confidence band. This provides the optimal fitted bounding curves to the confidence band. Extrapolation of these bounding curves will determine an optimized confidence interval of the predicted value. As a final point, the predicted value is not very sensitive to the choice of tail maker ζ_0, provided it is chosen with some care.

As a result of the efficient extrapolation, which is based on the assumption of regularity of mean upcrossing rate in the tail region (i.e. no abrupt variations of the mean upcrossing rate for the system in the extrapolation region), the empirical estimation of the upcrossing rate with respect to the far tail region can be achieved with sufficient accuracy for most practical prediction purposes with much less computational efforts than using the standard MCS method directly.

5. Numerical results

In this Section, the performances of the linear filter technique and the efficient MCS method will be studied. Specifically, the feasibility of the linear filter approach, which is applied to model the random effective wave amplitude process, will be investigated. The rationality and efficiency of the enhanced MCS method based on the extrapolation technique for prediction of the extreme responses will be illustrated by numerical simulations. Moreover, the principle of the parametric roll in random seas and the effects of some parameters, such as the vessel speed on the stochastic roll response will also be discussed.

5.1. Random effective wave amplitude process

A RORO ship from Bulian (2006) is considered for the numerical simulation in the subsequent study. The main parameters of the vessel are given in Table 1 and Fig. 1 shows the body plan of the reference vessel. The restoring arm in still water $GZ_0(\theta)$, is presented in Fig. 2. In this Section, the ship is assumed to be moving with a speed of $V=2.5$ m/s in pure head seas. The values of

Table 1
List of ship parameters.

Parameters	Dimensional value
L	132.2 m
Δ	7.75×10^7 N
b_{44}	0.012 s^{-1}
b_{44q}	0.0
b_{44c}	1.06 s
C_{01}	0.865 m
ω_0	0.396 rad/s

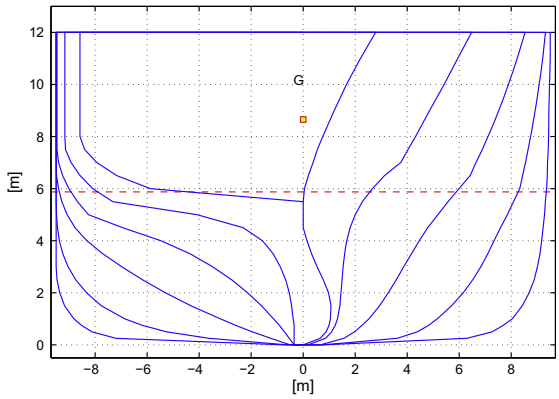

Fig. 1. Frames of the reference RORO ship (Bulian, 2006).

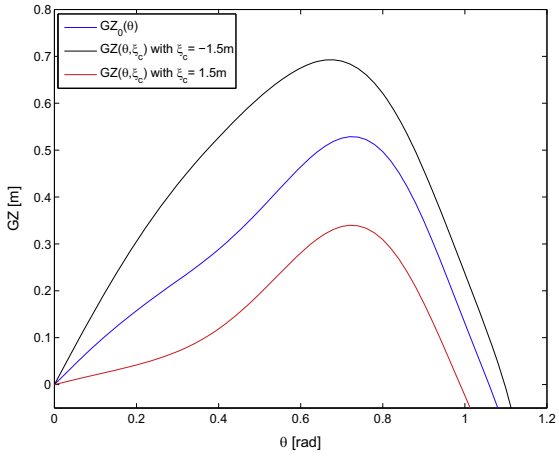

Fig. 2. GZ curves for different waves amidships: GZ_0 for still water; $\xi_c > 0$ for wave crest case; $\xi_c < 0$ for wave trough case.

damping coefficients, in principle, depend on vessel speed V, but herein constant coefficients are used (see Table 1), which are considered to be sufficiently representative for the range of speeds used in this study. Fig. 3 gives an example of irregular wave surface $\xi(x,t)$ with the corresponding equivalent (effective) wave approximation $\xi_{eff}(x,t)$. Based on the Grim's effective wave approximation (12), the time-varying restoring arm in random seas is fitted by means of a nonlinear polynomial Eq. (13) with respect to the heeling angle and the effective wave amplitude. The coefficient of determination (denoted as R^2), which indicates the goodness of fit for the GZ surface data (which are obtained by means of a standard hydrostatic software by using the nonlinear expression (13)) is 0.9995. The fitted GZ surface is plotted in Fig. 4 and GZ curves for waves with different amplitudes amidships can then be calculated by the nonlinear expression (13) where the coefficients are determined by means of the least square error method. Fig. 2 also shows the GZ curves for wave crest case ($\xi_c > 0$) and for wave trough case ($\xi_c < 0$). It is observed in Fig. 2 that the slope of the GZ curve with respect to the roll angle, i.e. the GM value, and the area under the GZ curve vary with the effective wave amplitude ξ_c. Generally, for the wave trough case, the GM value as well as the area under the GZ curve are greater than the still water values and those for the wave crest cases. This implies enhanced initial ship stability for the wave trough case and conversely, decrease of the initial ship stability for the wave crest condition.

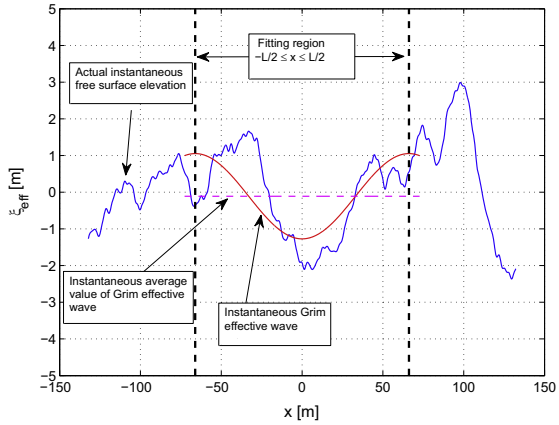

Fig. 3. Example of actual irregular wave surface $\xi(x,t)$ and the corresponding equivalent (effective) wave approximation $\xi_{eff}(x,t)$, modified P-M spectrum with H_s=4.0 and T_p=9.2 s.

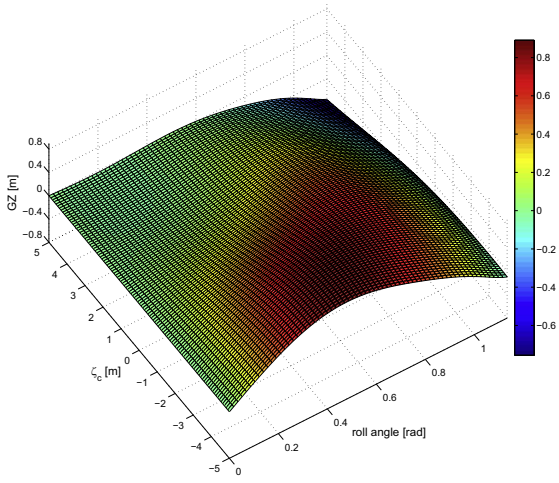

Fig. 4. Fitted GZ surface with the nonlinear expression (12).

In this work, the random stationary sea state is specified by the modified Pierson-Moskowitz spectrum, which is widely used for fully developed sea states (Naess and Moan, 2012). The sea spectrum is given as

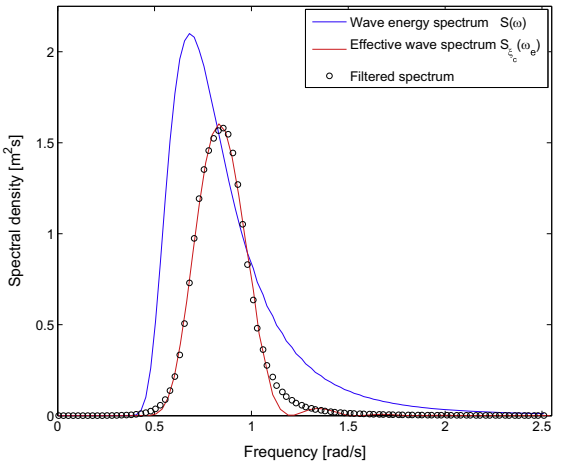

Fig. 5. Wave energy spectrum for the sea state with H_s=4.0 m, T_p=9.2 s, the corresponding encounter spectrum for the effective wave amplitude process $\xi_c(t)$ with vessel speed V=2.5 m/s in head seas and the filtered spectrum generated by the linear filter (16).

$$S(\omega) = \frac{5.058g^2H_s^2}{T_p^4\omega^5}\exp\left(-1.25\frac{\omega_p^4}{\omega^4}\right) \tag{28}$$

where H_s denotes the significant wave height, ω_p is the peak frequency (or the modal frequency) at which the wave spectrum $S(\omega)$ has its maximum, and T_p is the corresponding peak period. The peak frequency of the sea spectrum is selected to be the value which corresponds to a wave length equals to the Grim's reference length (i.e., $\omega_p = \sqrt{2\pi g/L} = 0.683$ rad/s) and the significant wave height H_s is chosen to be 4.0 m for the subsequent study.

The selected wave energy spectrum is presented in Fig. 5 and then the encounter spectrum for the effective wave amplitude process, i.e., the effective wave spectrum $S_{\xi_c}(\omega_e)$ (which is determined by Eq. (11) with the vessel speed V= 2.5 m/s) is also shown in Fig. 5. After determining the target spectrum $S_{\xi_c}(\omega_e)$, the parameters $\alpha_1, \alpha_2, \beta_1, \beta_2, \gamma_1$ in the fourth-order linear filter (17) are obtained by minimizing the square error between the filtered spectrum and the desired spectrum. The fitting result for the linear filter is shown in Fig. 5 and it can be readily seen that the spectrum obtained from the fourth order filter represents a good fitting. It is satisfactory in terms of band width, peak frequency and also the peak value. Even though there is a slight discrepancy between the target spectrum and the filtered spectrum near the frequency 1.2 rad/s, it would not impact the subsequent roll response since the parametric roll would not be induced by the frequencies within that region.

For the numerical implementation of the linear filter (16) in the time domain, the fourth-order Runge-Kutta-Maruyama (RKM) method is applied in order to solve the SDE (16) and an example of the random wave amplitude process is presented in Fig. 6. Moreover, the spectrum obtained by the FFT technique based on the time series of random wave amplitude process is introduced in order to compare with the theoretical filtered spectrum (17). The spectrum determined by the FFT technique is averaged over 50 h time series and the satisfactory agreement between the two spectra, which is shown in Fig. 7, verifies the feasibility of using the linear filter in time domain simulations for generation of the random input.

In addition, the Gaussian property of the random effective wave amplitude process $\xi_c(t)$, i.e., the output of the linear filter can be

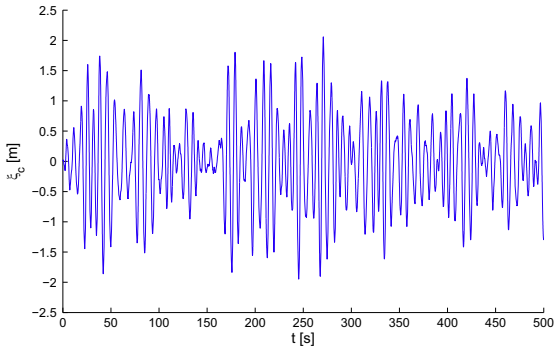

Fig. 6. Time series of the effective wave amplitude process $\xi_c(t)$ generated by the linear filter approach.

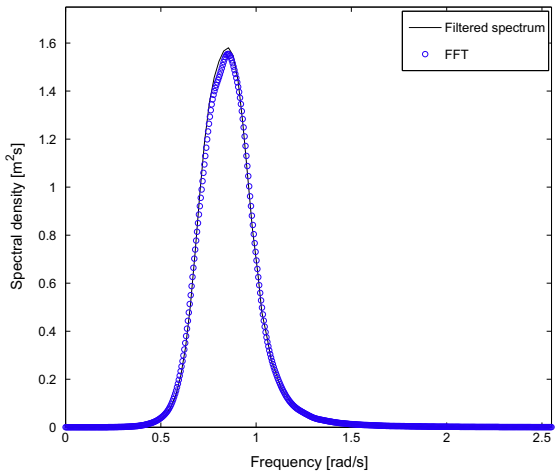

Fig. 7. Theoretical filtered spectrum and the spectrum generated by the FFT technique with time series of effective wave amplitude process.

used in order to verify the efficiency and accuracy of the extrapolated MCS method. The empirical upcrossing rate of the random effective wave amplitude process can be obtained based on direct counting (i.e. the MCS technique) and the practical simulation time T_i in Eq. (19) will be the same for each realization. The empirical upcrossing rate as well as the 95% confidence interval obtained by the direct MCS method are plotted in Fig. 8. Generally, the computation cost of the direct MCS for estimation of the mean upcrossing rate which is associated with probability level lower than 10^{-7} is formidable. Nevertheless, the extrapolation procedure described in Section 4.2 is applied in order to predict the upcrossing rate in the far tail region within a reasonable and acceptable computation cost.

Since the output of the linear filter (16) is a Gaussian process govern by the spectrum (17), the theoretical upcrossing of the process $\xi_c(t)$ is given by the following expression:

$$\nu^+(\zeta) = \frac{1}{2\pi}\frac{\sigma_2}{\sigma_1}\exp\left(-\frac{\zeta^2}{2\sigma_1^2}\right) \tag{29}$$

where σ_1 is the standard deviation of the Gaussian process $\xi_c(t)$ and it can be determined as: $\sigma_1^2 = \int_0^\infty S_{4th}(\omega)d\omega$ and σ_2 is the standard deviation for the stochastic process $d\xi_c(t)/dt$, which is given as $\sigma_2^2 = \int_0^\infty \omega^2 \cdot S_{4th}(\omega)d\omega$.

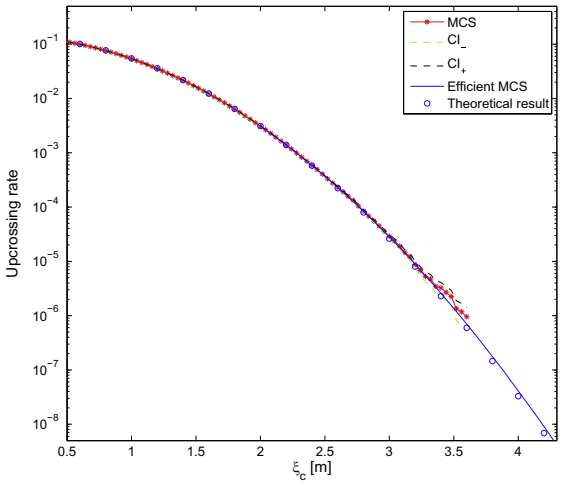

Fig. 8. Empirical mean upcrossing rate of the effective wave amplitude process $\xi_c(t)$ obtained by the direct MCS method with 95% confidence intervals based on 3000 h of time series, upcrossing rate obtained by the efficient MCS technique and the corresponding theoretical value.

The upcrossing rate obtained by the efficient MCS technique and the theoretical upcrossing rate of this Gaussian process $\xi_c(t)$ are also presented in Fig. 8. In addition, CI_- and CI_+ denote the lower and upper limits of the 95% confidence interval calculated by Eq. (20), respectively. Comparing with Eq. (29), the theoretical values of the parameters q, a, b, c for the upcrossing rates of the effective wave amplitude processes in the formula (24) can be obtained. Moreover, for different vessel speeds, the theoretical values of the parameters q, a, b, c and the corresponding values determined by the corresponding Levenberge-Marquardt optimization technique in the efficient MCS are shown in Table 2. On the basis of the satisfactory agreements of the upcrossing rate in Fig. 8 as well as the parameters in Table 2, the conclusion can be drawn that the efficient MCS method based on the extrapolation technique is able to provide a reliable estimation of the upcrossing rate for Gaussian processes in the far tail region within an acceptable computation time. Moreover, the good performances of the efficient MCS method for some nonlinear (non-Gaussian) processes have been reported in Naess and Gaidai (2008).

5.2. Selection of simulation time

In Bulian (2006), the stochastic linearization technique was used, with application to the damping and restoring terms of the nonlinear roll motion equation, in order to determine an approximation of the stochastic stability boundaries for the inception of parametric roll. However, when parametric roll is excited, large amplitude motions can arise and in such cases nonlinear effects associated with the restoring terms and the damping terms have a significant influence, particularly with respect to the high response levels (Chai et al., 2015b, 2016). Accordingly, these terms should be taken into account more explicitly.

The versatile MCS technique can be applied in order to address the above mentioned difficulty since it allows us to account for the effect of nonlinear damping and restoring terms directly in the time domain simulation. For a selected vessel speed, the high response levels for sea states near or beyond the corresponding stability boundary should be considered in practice. However, in relation to the time domain simulation, the computation cost and accuracy for a short-term sea state case would be important for its practical applications since they determine the computation time and accuracy associated with the subsequent prediction of long-term statistics prediction. These long-term statistics are based on response calculations for a number of short-term sea states as well as on the wave data (e.g. the scatter diagram for the sea states).

In this part, empirical estimation of the mean upcrossing rate of the roll response for the selected sea state (i.e., $H_s=4.0$ m and $T_p=2\pi/\omega_p=9.2$ s) with a vessel speed $V=2.5$ m/s as obtained by the efficient MCS technique will be presented. It was shown by Bulian (2006) and Vidic-Perunovic and Jensen (2009), that the SDOF model based on the Grim effective wave concept could tend to overestimate the roll response. In order to compensate this effect, in Bulian (2006) it was proposed to introduce a correction factor k_c in order to reduce the parametric excitation by correcting the effective wave spectrum as follows:

$$S_{\xi_c,k_c}(\omega) = k_c^2 \cdot S_{\xi_c}(\omega) \tag{30}$$

The effective wave amplitude process is accordingly corrected as:

$$\xi_{c,k_c}(t) = k_c \cdot \xi_c(t) \tag{31}$$

For the selected vessel, the correction factor k_c is taken to be 0.7 by comparison with the experimental data (Bulian, 2006). Correspondingly, the driving process for variation of the restoring term, x_3 in the dynamic system (18) will be the corrected effective wave amplitude process. Subsequently, roll responses can be obtained by solving the SDE (17) with several examples of roll response being shown in Fig. 9. In addition, it should be noted that the selection of empirical correction factor k_c depends on the broadness of the wave spectrum, for example, $k_c=0.8$ for the narrow-banded wave spectrum and $k_c=0.7$ for the current case with modified Pierson-Moskowitz spectrum (28). The value of k_c will influence the intensity of the subsequent roll response, this limitation may prevent the Grim effective wave model being employed at the early design process. Nevertheless, the simple Grim effective wave model is still recommended for the following quantitative study in this work. It can be seen in Fig. 9 that parametric roll occurs for the selected sea state and vessel speed. In order to overcome the fact that for parametrically excited roll motion, in some cases, too long single realizations would be necessary for obtaining sufficiently accurate statistical estimators

Table 2
Theoretical values of the parameters q, a, b, c in expression (24) for the mean upcrossing rates of the effective wave amplitude processes under different vessel speeds and the corresponding values determined by the Levenberge-Marquardt optimization method in the efficient MCS.

Parameters	$V=2.5$ m/s		$V=4.0$ m/s		$V=5.5$ m/s	
	Theoretical	Practical	Theoretical	Practical	Theoretical	Practical
q	0.142	0.133	0.153	0.154	0.166	0.173
a	0.955	1.005	0.955	0.971	0.955	0.890
b	0.000	0.040	0.000	0.005	0.000	−0.051
c	2.000	1.963	2.000	1.993	2.000	2.039

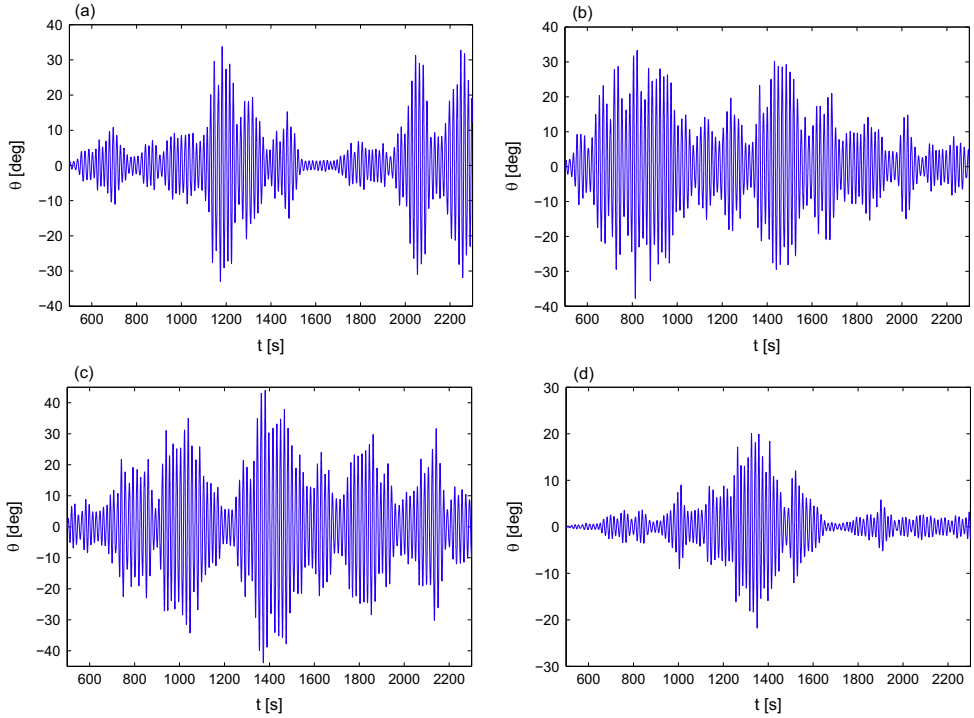

Fig. 9. Time series of the roll response for the sea state with H_s=4.0 m, T_p=9.2 s and vessel speed V=2.5 m/s.

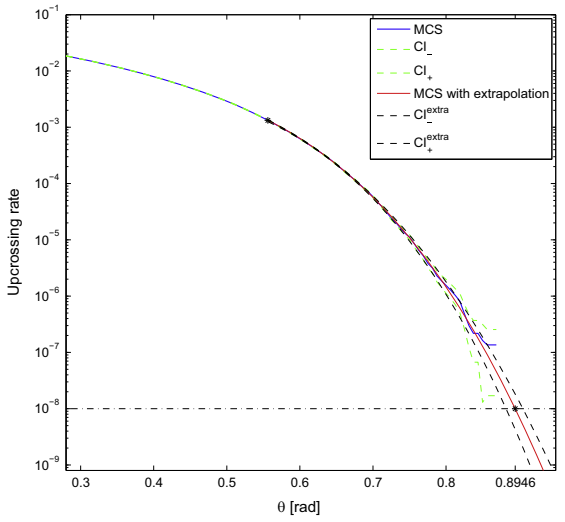

Fig. 10. Empirical mean upcrossing rate obtained by the direct MCS with 95% confidence interval based on 3334 realizations (10,000 h of response time histories) and the efficient MCS for the empirical upcrossing rate and confidence interval with the starting point ζ_0=0.556, q=0.0106, a=23.253, b=0.019, c=3.887. Sea state with H_s=4.0 m, T_p=9.2 s and vessel speed V=2.5 m/s.

(Bulian et al., 2006; Song et al., 2013), it is advisable, as an alternative, to perform multiple realizations. In the numerical simulation, therefore, 3334 realizations are generated for estimating the empirical mean upcrossing rate. Each realization has a duration of 11,300 s with the first 500 s being removed to eliminate the transient effect of the roll response. Fig. 10 shows the corresponding empirical mean upcrossing rate and the 95% confidence interval obtained by the direct MCS. The upcrossing rate in the far tail region as well as the corresponding confidence interval estimated by the efficient MCS technique (denoted as CI_{-}^{extra} and CI_{+}^{extra}) are also presented in Fig. 10. For a target crossing rate level of 10^{-8}, which requires formidable efforts for the conventional MCS technique, the roll response obtained by the proposed 10,000 h simulation and the efficient MCS based on the extrapolation procedure is predicted to be 0.8946 rad and the confidence interval is estimated to be (0.8821 0.9051).

As mentioned above, the reduction of simulation time would be important for the subsequent long-term prediction of extreme responses in practice. Therefore, the effort in the present part, which is devoted to illustrate that good accuracy can also be obtained by much shorter records of time-domain simulation, can provide valuable references for the practical applications. Fig. 11 shows the result of using only 100 h of simulated response time histories constituted by 200 realizations. Each realization lasts 2300 s and the results of the first 500 s are neglected as the former case with 10,000 h of simulation. The expected roll response for the crossing rate level of 10^{-8} for this case is obtained as 0.9343 rad and the confidence interval is estimated to be (0.8757 0.9828). Furthermore, similar calculations, such as the cases with 500 h and 2000 h of simulation, have been made to obtain the expected roll responses for the target crossing rate level of 10^{-8} as well as the confidence intervals which are given in Table 3. It can be seen from Table 3 and Figs. 10 and 11 that, the confidence interval becomes gradually narrower when the ensemble simulation time increase. Generally, more realizations and longer simulation time provide more accurate distributions. Nonetheless, it seems that for the selected case, the good agreement of the predicted

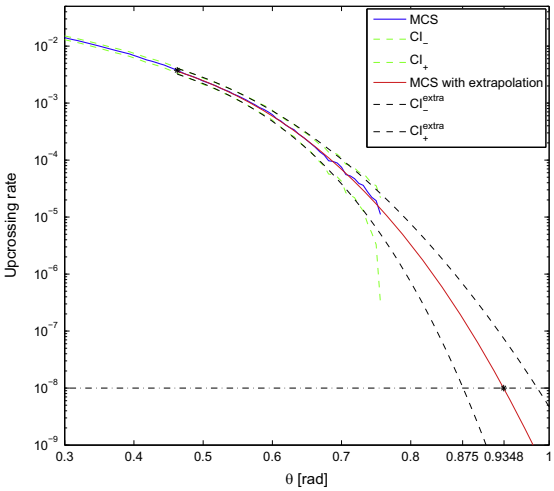

Fig. 11. Empirical mean upcrossing rate obtained by the direct MCS with 95% confidence interval based on 200 realizations (100 h of response time histories) and the efficient MCS for the empirical upcrossing rate and confidence interval with the starting point $\zeta_0=0.4625$, $q=0.011$, $a=27.515$, $b=0.075$, $c=3.167$. Sea state with $H_s=4.0$ m, $T_p=9.2$ s and vessel speed $V=2.5$ m/s.

Table 3
Expected roll responses for the target upcrossing rate level of 10^{-8} and the corresponding confidence intervals for the sea state with $H_s=4.0$ m, $T_p=9.2$ s and vessel speed $V=2.5$ m/s for different simulation time.

Simulation time (h)	Estimated value (rad)	$CI_{0.95}$
10,000	0.8946	(0.8821 0.9051)
2000	0.9223	(0.9074 0.9370)
500	0.9457	(0.8964 0.9699)
100	0.9343	(0.8757 0.9828)

responses presented in Figs. 10 and 11 demonstrates that 100 h simulation is available to provide good estimates of the extreme response and that the reduction of simulation time is feasible and reasonable. Moreover, the parameters and the starting value, ζ_0 used in the extrapolation scheme of the efficient MCS for the above two sets of data are given below.

5.3. Influence of vessel speed

It is well known that, for a selected sea state, the vessel speed determines the subsequent encountered wave spectrum (4) and the effective wave spectrum (11). For the head sea condition (and, in general, for conditions with encounter wave angle $90^\circ < \chi < 270^\circ$), the increase of the vessel speed reduces the peak value and increase the spectral bandwidth of the encountered wave spectrum and the corresponding effective wave spectrum. The influence of vessel speed on the effective wave spectrum is shown in Fig. 12 and the spectra generated by the linear filter (17) for different speeds are also presented.

For the regular wave scenario, when the encountered wave frequency is approximately twice that of the natural roll frequency ω_0 and when the corresponding wave length is on the order of the ship length, the principal parametric roll resonance occurs if the parametric excitation is large enough. Similarly, for random seas, the occurrence of parametric roll is correlated to the components of the effective wave amplitude process with frequencies in the critical frequency region near $2\omega_0$. According to Belenky et al. (2011), the critical frequency region, which is essential for

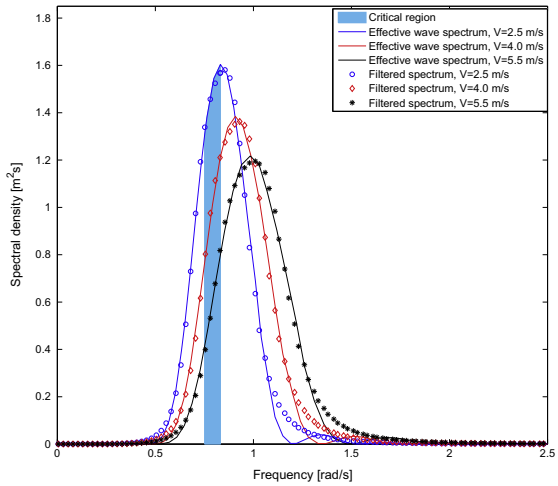

Fig. 12. Influence of the vessel speed V on the effective wave spectrum for the sea state with $H_s=4.0$ m, $T_p=9.2$ s, the corresponding filtered spectra and the critical frequency region ($1.9–2.1\omega_0$).

inducing the parametric roll, is selected to be 1.9–2.1 times that of the natural roll frequency ω_0. This empirical critical frequency region is indicated in Fig. 11 and it is seen that for the selected sea state and head sea condition, the increase in vessel speed results in weaker "energy" (i.e., the area under the effective wave spectrum) in the critical frequency region. Generally, for the head sea condition, roll damping would increase with the vessel speed and such an increment will decrease the stochastic roll response since the amplitudes of the roll motion are limited due to the presence of damping. In this work, the roll is assumed to be constant for different vessel speeds in order to concentrate on the investigation of the influence of parametric excitation energy in the critical frequency region on the roll response.

The empirical mean upcrossing rate of the roll response and the 95% confidence intervals obtained by the direct MCS method as well as the response tails and confidence intervals predicted by the efficient MCS technique for the selected seas state with vessel speeds $V=4.0$ m/s and $V=5.5$ m/s are presented in Figs. 13 and 14, respectively. The simulation time is determined to be 100 h and the procedure which is applied in order to get the required response statistics is similar to the case with vessel speed $V=2.5$ m/s mentioned in Section 5.2. The information related to the parameters and the starting values used in the extrapolation schemes of the efficient MCS for the above two cases are also mentioned in Figs. 13 and 14.

The estimated roll responses for the target crossing rate level of 10^{-8} and the corresponding confidence intervals are given in Table 3. It can be seen in Figs. 11, 13 and 14 as well as in Table 4 that the decrease of parametric excitation energy (i.e., the area under the effective wave spectrum in the critical frequency region) in the critical frequency region results in decreasing roll response. The occurrence of parametric roll in random seas is sensitive to the parametric excitation energy in this critical region and it can also be seen in Figs. 5 and 12 that the linear filter model (17) provides satisfactory approximation of the effective wave spectrum in the critical region. Hence, the slight discrepancies between the filtered spectrum and the effective wave spectrum in Fig. 11 would not influence the subsequent roll response since this discrepancy is far away from the critical frequency region. Furthermore, for some commercial ships (such as the container carrier), a number of other damages will occur at large angles and the ship could

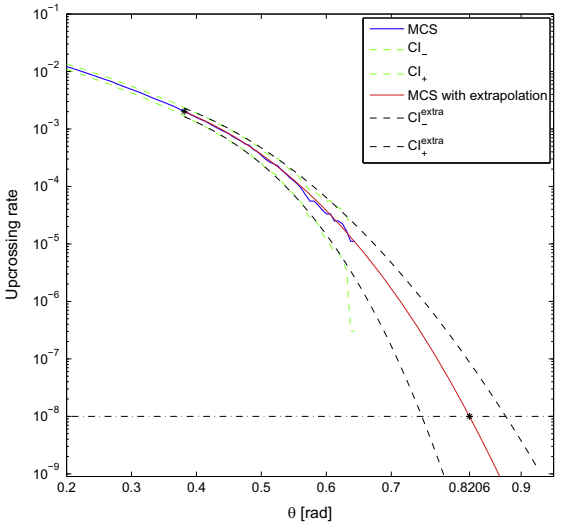

Fig. 13. Empirical mean upcrossing rate obtained by the direct MCS with 95% confidence interval based on 200 realizations (100 h of response time histories) and the efficient MCS for the empirical upcrossing rate and confidence interval with the starting point $\zeta_0=0.381$, $q=0.0071$, $a=27.4848$, $b=0.0427$, $c=2.8359$. Sea state with $H_s=4.0$ m, $T_p=9.2$ s and vessel speed $V=4.0$ m/s.

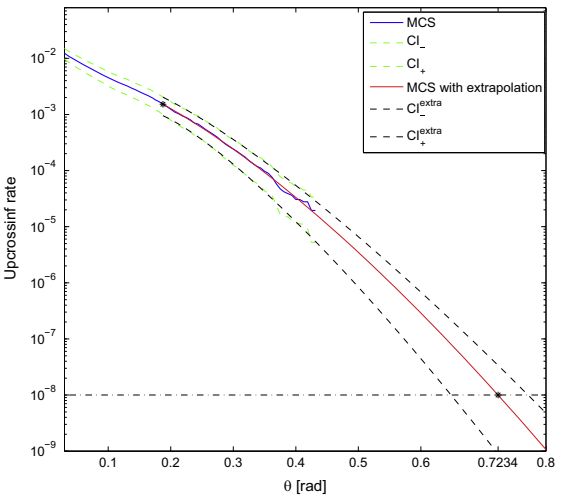

Fig. 14. Empirical mean upcrossing rate obtained by the direct MCS with 95% confidence interval based on 200 realizations (100 h of response time histories) and the efficient MCS for the empirical upcrossing rate and confidence interval with the starting point $\zeta_0=0.1875$, $q=0.0068$, $a=23.1275$, $b=0.0337$, $c=1.4629$. Sea state with $H_s=4.0$ m, $T_p=9.2$ s and vessel speed $V=5.5$ m/s.

Table 4
Expected roll responses for the target upcrossing rate level of 10^{-8} and the corresponding confidence intervals for the sea state with $H_s=4.0$ m, $T_p=9.2$ s for different vessel speeds.

Speed	Estimated value (rad)	$CI_{0.95}$
$V=2.5$ m/s	0.9343	(0.8757 0.9828)
$V=4.0$ m/s	0.8206	(0.7472 0.8763)
$V=5.5$ m/s	0.7234	(0.6481 0.7714)

probably start to fail before it reaches to the angle of vanishing stability. For such cases, the rationality of the applying the simple SDOF model (1) to describe the roll dynamics of the vessel and the regularity of the mean upcrossing rate in the tail region (presented in Figs. 10, 11, 13 and 14) could not be guaranteed. The above limitations for the mathematical model of the roll motion as well as for the efficient MCS method should be considered in practice.

Based on the observations and the discussions above, it can be confirmed that the occurrence of parametric roll in random seas is directly related to the parametric excitation energy in the critical frequency region near $2\omega_0$. When the parametric excitation energy in this region is large enough to overcome a threshold which is determined by the ship parameters (such as the damping and stiffness coefficients, etc.), the parametric roll phenomena with excessive roll motion in random seas would probably be observed. Moreover, it can be predicted that parametric roll in following seas would be more dangerous. Since the vessel speed in following seas will increase the peak value and decrease the bandwidth of the effective wave spectrum, this implies that parametric excitation energy will concentrate in a narrower frequency band than for the head sea cases. Dangerous effects of spectral narrowing with reference to ship motions have been discussed by Takaishi (1982). Once parametric roll occurs in following seas, the roll response could become serious due to the concentration of parametric excitation energy in the critical region. Moreover, the stochastic roll response is sensitive to the variation of energy in the critical region and reducing the parametric excitation energy in this region is a practical and effective way to decrease the stochastic roll response or even keep it absent from the parametric roll.

6. Conclusions

The main accomplishment of the present work is to study the parametric roll behavior in random longitudinal seas and to estimate the associate large or extreme roll response by means of probabilistic approaches.

Specifically, the mathematical model of roll motion was established on the basis of the Grim effective wave approximation which was introduced in order to model the variation of the restoring moment in random longitudinal seas. The linear filter technique and an efficient MCS method (based on the combination of a standard MCS approach and an extrapolation technique) were applied in order to approximate the effective wave amplitude process and estimate the extreme roll response, respectively. The feasibility and rationality of these two techniques has been shown by numerical simulations. Furthermore, the phenomenon of parametric roll in random seas as well as the effect of vessel speed on the stochastic roll response were studied. The parametric excitation energy in the critical region which is located near twice of the natural roll frequency has a great effect on the occurrence of parametric roll. The associated stochastic roll response is sensitive to the variation of parametric excitation energy in this critical region (i.e., variation of the restoring moment for certain frequencies in this region).

Based on the numerical simulations and the discussions above, it has been found that the efficient MCS technique gives a satisfactory estimation of the extreme roll response with a dramatic reduction of computation time. Moreover, for practical applications, the linear filter technique and the extrapolated MCS method can be applied for long-term stochastic predictions due to the satisfactory accuracy and efficiency.

Acknowledgments

The authors wish to thank Dr. Vadim Belenky and Dr. Leo Dostal for discussions in connection with the Grim effective wave model. The financial support from China Scholarship Council (CSC) (Grant no. 201306230077), affiliated with the Ministry of Education of the PR China, is greatly acknowledged.

References

Alevras, P., Yurchenko, D., 2013. Stochastic rotational response of a parametric pendulum coupled with an SDOF system. Probab. Eng. Mech. 37, 124–131.
Belenky, V., Yu, H.-C., Weems, K., 2011. Numerical procedures and practical experience of assessment of parametric roll of container carriers. Contemporary Ideas on Ship Stability and Capsizing in Waves, Springer, pp. 295–305.
Bulian, G., 2006. Development of Analytical Nonlinear Models for Parametric Roll and Hydrostatic Restoring Variations in Regular and Irregular Waves (Ph.D. Thesis). University of Trieste, Trieste, Italy.
Bulian, G., 2008. On an improved Grim effective wave. Ocean Eng. 35 (17), 1811–1825.
Bulian, G., Francescutto, A., Lugni, C., 2006. Theoretical, numerical and experimental study on the problem of ergodicity and 'practical ergodicity' with an application to parametric roll in longitudinal long crested irregular sea. Ocean Eng. 33 (8), 1007–1043.
Chai, W., Naess, A., Leira, B.J., 2015a. Filter models for prediction of stochastic ship roll response. Probab. Eng. Mech. 41, 104–114.
Chai, W., Naess, A., Leira, B.J., 2015b. Stochastic dynamic analysis and reliability of a vessel rolling in random beam seas. J. Ship Res. 59 (2), 113–131.
Chai, W., Naess, A., Leira, B.J., 2016. Stochastic roll response for a vessel with nonlinear damping models and steady heeling angles in random beam seas. Ocean Eng. 120, 202–211.
Chang, B., 2008. On the parametric rolling of ships using a numerical simulation method. Ocean Eng. 35 (5), 447–457.
Dostal, L., Kreuzer, E., Namachchivaya, N.S., 2012. Non-standard stochastic averaging of large-amplitude ship rolling in random seas. Proc. R. Soc. A: Math. Phys. Eng. Sci., 4146–4173.
Dostal, L., Kreuzer, E., 2014. Assessment of extreme rolling of ships in random seas. In: Proceedings of the ASME 2014 33rd International Conference on Ocean, Offshore and Arctic Engineering, American Society of Mechanical Engineers.
Ellermann, K., 2009. The motion of floating systems: nonlinear dynamics in periodic and random waves. J. Offshore Mech. Arct. Eng. 131 (4), 041104.
France, W.N., Levadou, M., Treakle, T.W., Paulling, J.R., Michel, R.K., Moore, C., 2003. An investigation of head-sea parametric rolling and its influence on container lashing systems. Mar. Technol. 40 (1), 1–19.
Francescutto, A., Naito, S., 2004. Large amplitude rolling in a realistic sea. Int. Shipbuild. Progress. 51 (2), 221–235.
Francescutto, A., Bulian, G., Lugni, C., 2004. Nonlinear and stochastic aspects of parametric rolling modeling. Mar. Technol. 41 (2), 74–81.
Gill, P.E., Murray, W., Wright, M.H., 1981. Practical optimization. Academic Press, London.
Grim, O., 1961. Beitrag zu dem Problem der Sicherheit des Schiffes im Seegang. Schiffbau-Versuchsanstalt.
Hua, J., Wang, W.-H., Chang, J.-R., 1999. A representation of GM-variation in waves by the Volterra system. J. Mar. Sci. Technol. 7 (2), 94–100.
Jensen, J.J., 2007. Efficient estimation of extreme non-linear roll motions using the first-order reliability method (FORM). J. Mar. Sci. Technol. 12 (4), 191–202.
Kim, D.-H., Belenky, V., Campbell, B.L., Troesch, A.W., 2014. Statistical Estimation of Extreme Roll in Head Seas, ASME 2014 33rd International Conference on Ocean, Offshore and Arctic Engineering. American Society of Mechanical Engineers, pp. V007T012A011-V007T012A011.
Kröger, H., 1986. Rollsimulation von schiffen im seegang. Schiffstechnik 33, 187–216.
McTaggart, K.A., 2000. Ship capsize risk in a seaway using fitted distributions to roll maxima. J. Offshore Mech. Arct. Eng. 122 (2), 141–146.
Moideen, H., Somayajula, A., Falzarano, J.M., 2014. Application of volterra series analysis for parametric rolling in irregular seas. J. Ship Res. 58 (2), 97–105.
Naess, A., Moe, V., 2000. Efficient path integration methods for nonlinear dynamic systems. Probab. Eng. Mech. 15 (2), 221–231.
Naess, A., Gaidai, O., 2008. Monte Carlo methods for estimating the extreme response of dynamical systems. J. Eng. Mech. 134 (8), 628–636.
Naess, A., Moan, T., 2012. Stochastic Dynamics of Marine Structures. Cambridge University Press.
Naess, A., Gaidai, O., Haver, S., 2007a. Efficient estimation of extreme response of drag-dominated offshore structures by Monte Carlo simulation. Ocean Eng. 34 (16), 2188–2197.
Naess, A., Gaidai, O., Teigen, P., 2007b. Extreme response prediction for nonlinear floating offshore structures by Monte Carlo simulation. Appl. Ocean Res. 29 (4), 221–230.
Park, D.-M., Kim, Y., Song, K.-H., 2013. Sensitivity in numerical analysis of parametric roll. Ocean Eng. 67, 1–12.
Paulling, J.R., 2011. Parametric rolling of ships–then and now. Contemporary Ideas on Ship Stability and Capsizing in Waves, Springer, pp. 347–360.
Peters, W., Belenky, V., Bassler, C., Spyrou, K., Umeda, N., Bulian, G., Altmayer, B., 2011. The second generation of intact stability criteria: an overview of development. SNAME Annual Meeting and Expo, Houston, TX. (16–18 November).
Roberts, J., Vasta, M., 2000. Markov modelling and stochastic identification for nonlinear ship rolling in random waves. Philos. Trans. R. Soc. Lond. Ser. A: Math. Phys. Eng. Sci. 358 (1771), 1917–1941.
Shin, Y., Belenky, V., Paulling, J., Weems, K., Lin, W., 2004. Criteria for parametric roll of large containerships in longitudinal seas. Trans.-Soc. Nav. Arch. Mar. Eng. 112, 14–47 (Discussion).
e Silva, S.R., Soares, C.G., 2013. Prediction of parametric rolling in waves with a time domain non-linear strip theory model. Ocean Eng. 72, 453–469.
Song, K.-H., Kim, Y., Park, D.-M., 2013. Quantitative and qualitative analyses of parametric roll for ship design and operational guidance. In: Proceedings of the Institution of Mechanical Engineers, Part M: Journal of Engineering for the Maritime Environment, vol. 227(2), pp. 177–189.
Spanos, P., 1983. ARMA algorithms for ocean wave modeling. J. Energy Resour. Technol. 105 (3), 300–309.
Spanos, P., 1986. Filter approaches to wave kinematics approximation. Appl. Ocean Res. 8 (1), 2–7.
Spanos, D., Papanikolaou, A., 2009. Benchmark study on numerical simulation methods for the prediction of parametric roll of ships in waves. Group 2 (9.66), 2.4–11.55.
Spyrou, K., 2000. Designing against parametric instability in following seas. Ocean Eng. 27 (6), 625–653.
Su, Z., 2012. Nonlinear Response and Stability Analysis of Vessel Rolling Motion in Random Waves Using Stochastic Dynamical Systems. Texas A&M University, Houston, USA.
Takaishi, Y., 1982. Consideration on the dangerous situations leading to capsize of ships in waves. In: Proceedings of the 2nd International Conference on Stability of Ships and Ocean Vehicles.
Thampi, S.K., Niedzwecki, J.M., 1992. Filter approach to ocean structure response prediction. Appl. Ocean Res. 14 (4), 259–271.
Tucker, M., Challenor, P.G., Carter, D., 1984. Numerical simulation of a random sea: a common error and its effect upon wave group statistics. Appl. Ocean Res. 6 (2), 118–122.
Umeda, N., Yamakoshi, Y., 1992. 6. Probability of Ship Capsizing due to Pure Loss of Stability in Quartering Seas. Nav. Arch. Ocean Eng. 30, 73–85.
Vidic-Perunovic, J., 2011. Influence of the GZ calculation method on parametric roll prediction. Ocean Eng. 38 (2), 295–303.
Vidic-Perunovic, J., Jensen, J.J., 2009. Parametric roll due to hull instantaneous volumetric changes and speed variations. Ocean Eng. 36 (12), 891–899.

Appendix B

Metocean information

Figure B1: Site of the NDBC buoy, No. 42058 in the Caribbean Sea.

Table B1: Empirical probability of occurrence of sea states at the location of the NDBC buoy, No. 42058 based on 9 years (2006-2014) of data.

Tp (s)		2.5	3.5	4.5	5.5	6.5	7.5	8.5	9.5	10.5	11.5	12.5	Total
Hs (m)	<0.5	0.000	0.000	0.030	0.139	0.100	0.172	0.078	0.018	0.000	0.000	0.000	**0.54**
	0.5	0.000	0.000	0.959	5.558	2.645	0.793	0.142	0.003	0.000	0.000	0.000	**10.10**
	1.0	0.000	0.000	0.202	6.846	10.559	1.405	0.148	0.006	0.003	0.000	0.000	**19.17**
	1.5	0.000	0.000	0.000	1.089	18.243	6.560	0.078	0.021	0.012	0.000	0.000	**26.00**
	2.0	0.000	0.000	0.000	0.075	3.996	19.458	0.745	0.006	0.021	0.000	0.000	**24.30**
	2.5	0.000	0.000	0.000	0.000	0.293	**8.683**	**5.450**	**0.015**	**0.045**	0.000	0.000	**14.49**
	3.0	0.000	0.000	0.000	0.000	0.015	**0.766**	**3.743**	**0.121**	**0.015**	0.000	0.000	**4.66**
	3.5	0.000	0.000	0.000	0.000	0.000	**0.024**	**0.422**	**0.262**	**0.000**	0.000	0.000	**0.71**
	4.0	0.000	0.000	0.000	0.000	0.000	**0.000**	**0.006**	**0.030**	**0.000**	0.000	0.000	**0.04**
	4.5	0.000	0.000	0.000	0.000	0.000	**0.000**	**0.000**	**0.000**	**0.000**	0.000	0.000	**0.00**
	5.0	0.000	0.000	0.000	0.000	0.000	0.000	0.000	0.000	0.000	0.000	0.000	**0.00**
	5.5	0.000	0.000	0.000	0.000	0.000	0.000	0.000	0.000	0.000	0.000	0.000	**0.00**
	6.0	0.000	0.000	0.000	0.000	0.000	0.000	0.000	0.000	0.000	0.000	0.000	**0.00**
Total		**0.00**	**0.00**	**1.19**	**13.71**	**35.85**	**37.86**	**10.81**	**0.48**	**0.10**	**0.00**	**0.00**	**100.00**

Table B2: Fitted distribution of sea states at the site of the NDBC buoy, No. 42058 based on 9 years (2006-2014) of data.

Tp (s)		2.5	3.5	4.5	5.5	6.5	7.5	8.5	9.5	10.5	11.5	12.5	Total
Hs (m)	< 0.5	0.000	0.000	0.000	0.000	0.000	0.000	0.000	0.000	0.000	0.000	0.000	**0.00**
	0.5	0.000	0.006	0.880	4.135	2.868	0.645	0.069	0.005	0.000	0.000	0.000	**8.61**
	1.0	0.000	0.000	0.055	5.590	13.398	3.346	0.196	0.004	0.000	0.000	0.000	**22.59**
	1.5	0.000	0.000	0.000	0.524	17.394	11.058	0.539	0.005	0.000	0.000	0.000	**29.52**
	2.0	0.000	0.000	0.000	0.001	3.435	18.129	1.832	0.013	0.000	0.000	0.000	**23.41**
	2.5	0.000	0.000	0.000	0.000	0.058	**7.143**	**4.259**	**0.066**	**0.000**	0.000	0.000	**11.53**
	3.0	0.000	0.000	0.000	0.000	0.000	**0.407**	**2.950**	**0.246**	**0.001**	0.000	0.000	**3.60**
	3.5	0.000	0.000	0.000	0.000	0.000	**0.003**	**0.367**	**0.267**	**0.005**	0.000	0.000	**0.64**
	4.0	0.000	0.000	0.000	0.000	0.000	**0.000**	**0.007**	**0.054**	**0.007**	0.000	0.000	**0.07**
	4.5	0.000	0.000	0.000	0.000	0.000	**0.000**	**0.000**	**0.002**	**0.002**	0.000	0.000	**0.00**
	5.0	0.000	0.000	0.000	0.000	0.000	0.000	0.000	0.000	0.000	0.000	0.000	**0.00**
	5.5	0.000	0.000	0.000	0.000	0.000	0.000	0.000	0.000	0.000	0.000	0.000	**0.00**
	6.0	0.000	0.000	0.000	0.000	0.000	0.000	0.000	0.000	0.000	0.000	0.000	**0.00**
Total		**0.00**	**0.01**	**0.94**	**10.25**	**37.15**	**40.73**	**10.22**	**0.66**	**0.02**	**0.00**	**0.00**	**100.00**

Appendix C

List of previous PhD thesis at Department of Marine Technology

Previous PhD theses published at the Departement of Marine Technology
(earlier: Faculty of Marine Technology)
NORWEGIAN UNIVERSITY OF SCIENCE AND TECHNOLOGY

Report No.	Author	Title
	Kavlie, Dag	Optimization of Plane Elastic Grillages, 1967
	Hansen, Hans R.	Man-Machine Communication and Data-Storage Methods in Ship Structural Design, 1971
	Gisvold, Kaare M.	A Method for non-linear mixed -integer programming and its Application to Design Problems, 1971
	Lund, Sverre	Tanker Frame Optimalization by means of SUMT-Transformation and Behaviour Models, 1971
	Vinje, Tor	On Vibration of Spherical Shells Interacting with Fluid, 1972
	Lorentz, Jan D.	Tank Arrangement for Crude Oil Carriers in Accordance with the new Anti-Pollution Regulations, 1975
	Carlsen, Carl A.	Computer-Aided Design of Tanker Structures, 1975
	Larsen, Carl M.	Static and Dynamic Analysis of Offshore Pipelines during Installation, 1976
UR-79-01	Brigt Hatlestad, MK	The finite element method used in a fatigue evaluation of fixed offshore platforms. (Dr.Ing. Thesis)
UR-79-02	Erik Pettersen, MK	Analysis and design of cellular structures. (Dr.Ing. Thesis)
UR-79-03	Sverre Valsgård, MK	Finite difference and finite element methods applied to nonlinear analysis of plated structures. (Dr.Ing. Thesis)
UR-79-04	Nils T. Nordsve, MK	Finite element collapse analysis of structural members considering imperfections and stresses due to fabrication. (Dr.Ing. Thesis)
UR-79-05	Ivar J. Fylling, MK	Analysis of towline forces in ocean towing systems. (Dr.Ing. Thesis)
UR-80-06	Nils Sandsmark, MM	Analysis of Stationary and Transient Heat Conduction by the Use of the Finite Element Method. (Dr.Ing. Thesis)
UR-80-09	Sverre Haver, MK	Analysis of uncertainties related to the stochastic modeling of ocean waves. (Dr.Ing. Thesis)
UR-81-15	Odland, Jonas	On the Strength of welded Ring stiffened cylindrical Shells primarily subjected to axial Compression
UR-82-17	Engesvik, Knut	Analysis of Uncertainties in the fatigue Capacity of

		Welded Joints
UR-82-18	Rye, Henrik	Ocean wave groups
UR-83-30	Eide, Oddvar Inge	On Cumulative Fatigue Damage in Steel Welded Joints
UR-83-33	Mo, Olav	Stochastic Time Domain Analysis of Slender Offshore Structures
UR-83-34	Amdahl, Jørgen	Energy absorption in Ship-platform impacts
UR-84-37	Mørch, Morten	Motions and mooring forces of semi submersibles as determined by full-scale measurements and theoretical analysis
UR-84-38	Soares, C. Guedes	Probabilistic models for load effects in ship structures
UR-84-39	Aarsnes, Jan V.	Current forces on ships
UR-84-40	Czujko, Jerzy	Collapse Analysis of Plates subjected to Biaxial Compression and Lateral Load
UR-85-46	Alf G. Engseth, MK	Finite element collapse analysis of tubular steel offshore structures. (Dr.Ing. Thesis)
UR-86-47	Dengody Sheshappa, MP	A Computer Design Model for Optimizing Fishing Vessel Designs Based on Techno-Economic Analysis. (Dr.Ing. Thesis)
UR-86-48	Vidar Aanesland, MH	A Theoretical and Numerical Study of Ship Wave Resistance. (Dr.Ing. Thesis)
UR-86-49	Heinz-Joachim Wessel, MK	Fracture Mechanics Analysis of Crack Growth in Plate Girders. (Dr.Ing. Thesis)
UR-86-50	Jon Taby, MK	Ultimate and Post-ultimate Strength of Dented Tubular Members. (Dr.Ing. Thesis)
UR-86-51	Walter Lian, MH	A Numerical Study of Two-Dimensional Separated Flow Past Bluff Bodies at Moderate KC-Numbers. (Dr.Ing. Thesis)
UR-86-52	Bjørn Sortland, MH	Force Measurements in Oscillating Flow on Ship Sections and Circular Cylinders in a U-Tube Water Tank. (Dr.Ing. Thesis)
UR-86-53	Kurt Strand, MM	A System Dynamic Approach to One-dimensional Fluid Flow. (Dr.Ing. Thesis)
UR-86-54	Arne Edvin Løken, MH	Three Dimensional Second Order Hydrodynamic Effects on Ocean Structures in Waves. (Dr.Ing. Thesis)
UR-86-55	Sigurd Falch, MH	A Numerical Study of Slamming of Two-Dimensional Bodies. (Dr.Ing. Thesis)
UR-87-56	Arne Braathen, MH	Application of a Vortex Tracking Method to the Prediction of Roll Damping of a Two-Dimension Floating Body. (Dr.Ing. Thesis)

UR-87-57	Bernt Leira, MK	Gaussian Vector Processes for Reliability Analysis involving Wave-Induced Load Effects. (Dr.Ing. Thesis)
UR-87-58	Magnus Småvik, MM	Thermal Load and Process Characteristics in a Two-Stroke Diesel Engine with Thermal Barriers (in Norwegian). (Dr.Ing. Thesis)
MTA-88-59	Bernt Arild Bremdal, MP	An Investigation of Marine Installation Processes – A Knowledge - Based Planning Approach. (Dr.Ing. Thesis)
MTA-88-60	Xu Jun, MK	Non-linear Dynamic Analysis of Space-framed Offshore Structures. (Dr.Ing. Thesis)
MTA-89-61	Gang Miao, MH	Hydrodynamic Forces and Dynamic Responses of Circular Cylinders in Wave Zones. (Dr.Ing. Thesis)
MTA-89-62	Martin Greenhow, MH	Linear and Non-Linear Studies of Waves and Floating Bodies. Part I and Part II. (Dr.Techn. Thesis)
MTA-89-63	Chang Li, MH	Force Coefficients of Spheres and Cubes in Oscillatory Flow with and without Current. (Dr.Ing. Thesis
MTA-89-64	Hu Ying, MP	A Study of Marketing and Design in Development of Marine Transport Systems. (Dr.Ing. Thesis)
MTA-89-65	Arild Jæger, MH	Seakeeping, Dynamic Stability and Performance of a Wedge Shaped Planing Hull. (Dr.Ing. Thesis)
MTA-89-66	Chan Siu Hung, MM	The dynamic characteristics of tilting-pad bearings
MTA-89-67	Kim Wikstrøm, MP	Analysis av projekteringen for ett offshore projekt. (Licenciat-avhandling)
MTA-89-68	Jiao Guoyang, MK	Reliability Analysis of Crack Growth under Random Loading, considering Model Updating. (Dr.Ing. Thesis)
MTA-89-69	Arnt Olufsen, MK	Uncertainty and Reliability Analysis of Fixed Offshore Structures. (Dr.Ing. Thesis)
MTA-89-70	Wu Yu-Lin, MR	System Reliability Analyses of Offshore Structures using improved Truss and Beam Models. (Dr.Ing. Thesis)
MTA-90-71	Jan Roger Hoff, MH	Three-dimensional Green function of a vessel with forward speed in waves. (Dr.Ing. Thesis)
MTA-90-72	Rong Zhao, MH	Slow-Drift Motions of a Moored Two-Dimensional Body in Irregular Waves. (Dr.Ing. Thesis)
MTA-90-73	Atle Minsaas, MP	Economical Risk Analysis. (Dr.Ing. Thesis)
MTA-90-74	Knut-Aril Farnes, MK	Long-term Statistics of Response in Non-linear Marine Structures. (Dr.Ing. Thesis)
MTA-90-75	Torbjørn Sotberg, MK	Application of Reliability Methods for Safety Assessment of Submarine Pipelines. (Dr.Ing.

		Thesis)
MTA-90-76	Zeuthen, Steffen, MP	SEAMAID. A computational model of the design process in a constraint-based logic programming environment. An example from the offshore domain. (Dr.Ing. Thesis)
MTA-91-77	Haagensen, Sven, MM	Fuel Dependant Cyclic Variability in a Spark Ignition Engine - An Optical Approach. (Dr.Ing. Thesis)
MTA-91-78	Løland, Geir, MH	Current forces on and flow through fish farms. (Dr.Ing. Thesis)
MTA-91-79	Hoen, Christopher, MK	System Identification of Structures Excited by Stochastic Load Processes. (Dr.Ing. Thesis)
MTA-91-80	Haugen, Stein, MK	Probabilistic Evaluation of Frequency of Collision between Ships and Offshore Platforms. (Dr.Ing. Thesis)
MTA-91-81	Sødahl, Nils, MK	Methods for Design and Analysis of Flexible Risers. (Dr.Ing. Thesis)
MTA-91-82	Ormberg, Harald, MK	Non-linear Response Analysis of Floating Fish Farm Systems. (Dr.Ing. Thesis)
MTA-91-83	Marley, Mark J., MK	Time Variant Reliability under Fatigue Degradation. (Dr.Ing. Thesis)
MTA-91-84	Krokstad, Jørgen R., MH	Second-order Loads in Multidirectional Seas. (Dr.Ing. Thesis)
MTA-91-85	Molteberg, Gunnar A., MM	The Application of System Identification Techniques to Performance Monitoring of Four Stroke Turbocharged Diesel Engines. (Dr.Ing. Thesis)
MTA-92-86	Mørch, Hans Jørgen Bjelke, MH	Aspects of Hydrofoil Design: with Emphasis on Hydrofoil Interaction in Calm Water. (Dr.Ing. Thesis)
MTA-92-87	Chan Siu Hung, MM	Nonlinear Analysis of Rotordynamic Instabilities in Highspeed Turbomachinery. (Dr.Ing. Thesis)
MTA-92-88	Bessason, Bjarni, MK	Assessment of Earthquake Loading and Response of Seismically Isolated Bridges. (Dr.Ing. Thesis)
MTA-92-89	Langli, Geir, MP	Improving Operational Safety through exploitation of Design Knowledge - an investigation of offshore platform safety. (Dr.Ing. Thesis)
MTA-92-90	Sævik, Svein, MK	On Stresses and Fatigue in Flexible Pipes. (Dr.Ing. Thesis)
MTA-92-91	Ask, Tor Ø., MM	Ignition and Flame Growth in Lean Gas-Air Mixtures. An Experimental Study with a Schlieren System. (Dr.Ing. Thesis)
MTA-86-92	Hessen, Gunnar, MK	Fracture Mechanics Analysis of Stiffened Tubular Members. (Dr.Ing. Thesis)

MTA-93-93	Steinebach, Christian, MM	Knowledge Based Systems for Diagnosis of Rotating Machinery. (Dr.Ing. Thesis)
MTA-93-94	Dalane, Jan Inge, MK	System Reliability in Design and Maintenance of Fixed Offshore Structures. (Dr.Ing. Thesis)
MTA-93-95	Steen, Sverre, MH	Cobblestone Effect on SES. (Dr.Ing. Thesis)
MTA-93-96	Karunakaran, Daniel, MK	Nonlinear Dynamic Response and Reliability Analysis of Drag-dominated Offshore Platforms. (Dr.Ing. Thesis)
MTA-93-97	Hagen, Arnulf, MP	The Framework of a Design Process Language. (Dr.Ing. Thesis)
MTA-93-98	Nordrik, Rune, MM	Investigation of Spark Ignition and Autoignition in Methane and Air Using Computational Fluid Dynamics and Chemical Reaction Kinetics. A Numerical Study of Ignition Processes in Internal Combustion Engines. (Dr.Ing. Thesis)
MTA-94-99	Passano, Elizabeth, MK	Efficient Analysis of Nonlinear Slender Marine Structures. (Dr.Ing. Thesis)
MTA-94-100	Kvålsvold, Jan, MH	Hydroelastic Modelling of Wetdeck Slamming on Multihull Vessels. (Dr.Ing. Thesis)
MTA-94-102	Bech, Sidsel M., MK	Experimental and Numerical Determination of Stiffness and Strength of GRP/PVC Sandwich Structures. (Dr.Ing. Thesis)
MTA-95-103	Paulsen, Hallvard, MM	A Study of Transient Jet and Spray using a Schlieren Method and Digital Image Processing. (Dr.Ing. Thesis)
MTA-95-104	Hovde, Geir Olav, MK	Fatigue and Overload Reliability of Offshore Structural Systems, Considering the Effect of Inspection and Repair. (Dr.Ing. Thesis)
MTA-95-105	Wang, Xiaozhi, MK	Reliability Analysis of Production Ships with Emphasis on Load Combination and Ultimate Strength. (Dr.Ing. Thesis)
MTA-95-106	Ulstein, Tore, MH	Nonlinear Effects of a Flexible Stern Seal Bag on Cobblestone Oscillations of an SES. (Dr.Ing. Thesis)
MTA-95-107	Solaas, Frøydis, MH	Analytical and Numerical Studies of Sloshing in Tanks. (Dr.Ing. Thesis)
MTA-95-108	Hellan, Øyvind, MK	Nonlinear Pushover and Cyclic Analyses in Ultimate Limit State Design and Reassessment of Tubular Steel Offshore Structures. (Dr.Ing. Thesis)
MTA-95-109	Hermundstad, Ole A., MK	Theoretical and Experimental Hydroelastic Analysis of High Speed Vessels. (Dr.Ing. Thesis)
MTA-96-110	Bratland, Anne K., MH	Wave-Current Interaction Effects on Large-Volume Bodies in Water of Finite Depth. (Dr.Ing. Thesis)
MTA-96-111	Herfjord, Kjell, MH	A Study of Two-dimensional Separated Flow by a Combination of the Finite Element Method and

		Navier-Stokes Equations. (Dr.Ing. Thesis)
MTA-96-112	Æsøy, Vilmar, MM	Hot Surface Assisted Compression Ignition in a Direct Injection Natural Gas Engine. (Dr.Ing. Thesis)
MTA-96-113	Eknes, Monika L., MK	Escalation Scenarios Initiated by Gas Explosions on Offshore Installations. (Dr.Ing. Thesis)
MTA-96-114	Erikstad, Stein O., MP	A Decision Support Model for Preliminary Ship Design. (Dr.Ing. Thesis)
MTA-96-115	Pedersen, Egil, MH	A Nautical Study of Towed Marine Seismic Streamer Cable Configurations. (Dr.Ing. Thesis)
MTA-97-116	Moksnes, Paul O., MM	Modelling Two-Phase Thermo-Fluid Systems Using Bond Graphs. (Dr.Ing. Thesis)
MTA-97-117	Halse, Karl H., MK	On Vortex Shedding and Prediction of Vortex-Induced Vibrations of Circular Cylinders. (Dr.Ing. Thesis)
MTA-97-118	Igland, Ragnar T., MK	Reliability Analysis of Pipelines during Laying, considering Ultimate Strength under Combined Loads. (Dr.Ing. Thesis)
MTA-97-119	Pedersen, Hans-P., MP	Levendefiskteknologi for fiskefartøy. (Dr.Ing. Thesis)
MTA-98-120	Vikestad, Kyrre, MK	Multi-Frequency Response of a Cylinder Subjected to Vortex Shedding and Support Motions. (Dr.Ing. Thesis)
MTA-98-121	Azadi, Mohammad R. E., MK	Analysis of Static and Dynamic Pile-Soil-Jacket Behaviour. (Dr.Ing. Thesis)
MTA-98-122	Ulltang, Terje, MP	A Communication Model for Product Information. (Dr.Ing. Thesis)
MTA-98-123	Torbergsen, Erik, MM	Impeller/Diffuser Interaction Forces in Centrifugal Pumps. (Dr.Ing. Thesis)
MTA-98-124	Hansen, Edmond, MH	A Discrete Element Model to Study Marginal Ice Zone Dynamics and the Behaviour of Vessels Moored in Broken Ice. (Dr.Ing. Thesis)
MTA-98-125	Videiro, Paulo M., MK	Reliability Based Design of Marine Structures. (Dr.Ing. Thesis)
MTA-99-126	Mainçon, Philippe, MK	Fatigue Reliability of Long Welds Application to Titanium Risers. (Dr.Ing. Thesis)
MTA-99-127	Haugen, Elin M., MH	Hydroelastic Analysis of Slamming on Stiffened Plates with Application to Catamaran Wetdecks. (Dr.Ing. Thesis)
MTA-99-128	Langhelle, Nina K., MK	Experimental Validation and Calibration of Nonlinear Finite Element Models for Use in Design of Aluminium Structures Exposed to Fire. (Dr.Ing. Thesis)
MTA-99-	Berstad, Are J., MK	Calculation of Fatigue Damage in Ship Structures.

129		(Dr.Ing. Thesis)
MTA-99-130	Andersen, Trond M., MM	Short Term Maintenance Planning. (Dr.Ing. Thesis)
MTA-99-131	Tveiten, Bård Wathne, MK	Fatigue Assessment of Welded Aluminium Ship Details. (Dr.Ing. Thesis)
MTA-99-132	Søreide, Fredrik, MP	Applications of underwater technology in deep water archaeology. Principles and practice. (Dr.Ing. Thesis)
MTA-99-133	Tønnessen, Rune, MH	A Finite Element Method Applied to Unsteady Viscous Flow Around 2D Blunt Bodies With Sharp Corners. (Dr.Ing. Thesis)
MTA-99-134	Elvekrok, Dag R., MP	Engineering Integration in Field Development Projects in the Norwegian Oil and Gas Industry. The Supplier Management of Norne. (Dr.Ing. Thesis)
MTA-99-135	Fagerholt, Kjetil, MP	Optimeringsbaserte Metoder for Ruteplanlegging innen skipsfart. (Dr.Ing. Thesis)
MTA-99-136	Bysveen, Marie, MM	Visualization in Two Directions on a Dynamic Combustion Rig for Studies of Fuel Quality. (Dr.Ing. Thesis)
MTA-2000-137	Storteig, Eskild, MM	Dynamic characteristics and leakage performance of liquid annular seals in centrifugal pumps. (Dr.Ing. Thesis)
MTA-2000-138	Sagli, Gro, MK	Model uncertainty and simplified estimates of long term extremes of hull girder loads in ships. (Dr.Ing. Thesis)
MTA-2000-139	Tronstad, Harald, MK	Nonlinear analysis and design of cable net structures like fishing gear based on the finite element method. (Dr.Ing. Thesis)
MTA-2000-140	Kroneberg, André, MP	Innovation in shipping by using scenarios. (Dr.Ing. Thesis)
MTA-2000-141	Haslum, Herbjørn Alf, MH	Simplified methods applied to nonlinear motion of spar platforms. (Dr.Ing. Thesis)
MTA-2001-142	Samdal, Ole Johan, MM	Modelling of Degradation Mechanisms and Stressor Interaction on Static Mechanical Equipment Residual Lifetime. (Dr.Ing. Thesis)
MTA-2001-143	Baarholm, Rolf Jarle, MH	Theoretical and experimental studies of wave impact underneath decks of offshore platforms. (Dr.Ing. Thesis)
MTA-2001-144	Wang, Lihua, MK	Probabilistic Analysis of Nonlinear Wave-induced Loads on Ships. (Dr.Ing. Thesis)
MTA-2001-145	Kristensen, Odd H. Holt, MK	Ultimate Capacity of Aluminium Plates under Multiple Loads, Considering HAZ Properties. (Dr.Ing. Thesis)
MTA-2001-146	Greco, Marilena, MH	A Two-Dimensional Study of Green-Water

		Loading. (Dr.Ing. Thesis)
MTA-2001-147	Heggelund, Svein E., MK	Calculation of Global Design Loads and Load Effects in Large High Speed Catamarans. (Dr.Ing. Thesis)
MTA-2001-148	Babalola, Olusegun T., MK	Fatigue Strength of Titanium Risers – Defect Sensitivity. (Dr.Ing. Thesis)
MTA-2001-149	Mohammed, Abuu K., MK	Nonlinear Shell Finite Elements for Ultimate Strength and Collapse Analysis of Ship Structures. (Dr.Ing. Thesis)
MTA-2002-150	Holmedal, Lars E., MH	Wave-current interactions in the vicinity of the sea bed. (Dr.Ing. Thesis)
MTA-2002-151	Rognebakke, Olav F., MH	Sloshing in rectangular tanks and interaction with ship motions. (Dr.Ing. Thesis)
MTA-2002-152	Lader, Pål Furset, MH	Geometry and Kinematics of Breaking Waves. (Dr.Ing. Thesis)
MTA-2002-153	Yang, Qinzheng, MH	Wash and wave resistance of ships in finite water depth. (Dr.Ing. Thesis)
MTA-2002-154	Melhus, Øyvin, MM	Utilization of VOC in Diesel Engines. Ignition and combustion of VOC released by crude oil tankers. (Dr.Ing. Thesis)
MTA-2002-155	Ronæss, Marit, MH	Wave Induced Motions of Two Ships Advancing on Parallel Course. (Dr.Ing. Thesis)
MTA-2002-156	Økland, Ole D., MK	Numerical and experimental investigation of whipping in twin hull vessels exposed to severe wet deck slamming. (Dr.Ing. Thesis)
MTA-2002-157	Ge, Chunhua, MK	Global Hydroelastic Response of Catamarans due to Wet Deck Slamming. (Dr.Ing. Thesis)
MTA-2002-158	Byklum, Eirik, MK	Nonlinear Shell Finite Elements for Ultimate Strength and Collapse Analysis of Ship Structures. (Dr.Ing. Thesis)
IMT-2003-1	Chen, Haibo, MK	Probabilistic Evaluation of FPSO-Tanker Collision in Tandem Offloading Operation. (Dr.Ing. Thesis)
IMT-2003-2	Skaugset, Kjetil Bjørn, MK	On the Suppression of Vortex Induced Vibrations of Circular Cylinders by Radial Water Jets. (Dr.Ing. Thesis)
IMT-2003-3	Chezhian, Muthu	Three-Dimensional Analysis of Slamming. (Dr.Ing. Thesis)
IMT-2003-4	Buhaug, Øyvind	Deposit Formation on Cylinder Liner Surfaces in Medium Speed Engines. (Dr.Ing. Thesis)
IMT-2003-5	Tregde, Vidar	Aspects of Ship Design: Optimization of Aft Hull with Inverse Geometry Design. (Dr.Ing. Thesis)
IMT-	Wist, Hanne Therese	Statistical Properties of Successive Ocean Wave

2003-6		Parameters. (Dr.Ing. Thesis)
IMT-2004-7	Ransau, Samuel	Numerical Methods for Flows with Evolving Interfaces. (Dr.Ing. Thesis)
IMT-2004-8	Soma, Torkel	Blue-Chip or Sub-Standard. A data interrogation approach of identity safety characteristics of shipping organization. (Dr.Ing. Thesis)
IMT-2004-9	Ersdal, Svein	An experimental study of hydrodynamic forces on cylinders and cables in near axial flow. (Dr.Ing. Thesis)
IMT-2005-10	Brodtkorb, Per Andreas	The Probability of Occurrence of Dangerous Wave Situations at Sea. (Dr.Ing. Thesis)
IMT-2005-11	Yttervik, Rune	Ocean current variability in relation to offshore engineering. (Dr.Ing. Thesis)
IMT-2005-12	Fredheim, Arne	Current Forces on Net-Structures. (Dr.Ing. Thesis)
IMT-2005-13	Heggernes, Kjetil	Flow around marine structures. (Dr.Ing. Thesis
IMT-2005-14	Fouques, Sebastien	Lagrangian Modelling of Ocean Surface Waves and Synthetic Aperture Radar Wave Measurements. (Dr.Ing. Thesis)
IMT-2006-15	Holm, Håvard	Numerical calculation of viscous free surface flow around marine structures. (Dr.Ing. Thesis)
IMT-2006-16	Bjørheim, Lars G.	Failure Assessment of Long Through Thickness Fatigue Cracks in Ship Hulls. (Dr.Ing. Thesis)
IMT-2006-17	Hansson, Lisbeth	Safety Management for Prevention of Occupational Accidents. (Dr.Ing. Thesis)
IMT-2006-18	Zhu, Xinying	Application of the CIP Method to Strongly Nonlinear Wave-Body Interaction Problems. (Dr.Ing. Thesis)
IMT-2006-19	Reite, Karl Johan	Modelling and Control of Trawl Systems. (Dr.Ing. Thesis)
IMT-2006-20	Smogeli, Øyvind Notland	Control of Marine Propellers. From Normal to Extreme Conditions. (Dr.Ing. Thesis)
IMT-2007-21	Storhaug, Gaute	Experimental Investigation of Wave Induced Vibrations and Their Effect on the Fatigue Loading of Ships. (Dr.Ing. Thesis)
IMT-2007-22	Sun, Hui	A Boundary Element Method Applied to Strongly Nonlinear Wave-Body Interaction Problems. (PhD Thesis, CeSOS)
IMT-2007-23	Rustad, Anne Marthine	Modelling and Control of Top Tensioned Risers. (PhD Thesis, CeSOS)
IMT-2007-24	Johansen, Vegar	Modelling flexible slender system for real-time simulations and control applications
IMT-2007-25	Wroldsen, Anders Sunde	Modelling and control of tensegrity structures.

		(PhD Thesis, CeSOS)
IMT-2007-26	Aronsen, Kristoffer Høye	An experimental investigation of in-line and combined inline and cross flow vortex induced vibrations. (Dr. avhandling, IMT)
IMT-2007-27	Gao, Zhen	Stochastic Response Analysis of Mooring Systems with Emphasis on Frequency-domain Analysis of Fatigue due to Wide-band Response Processes (PhD Thesis, CeSOS)
IMT-2007-28	Thorstensen, Tom Anders	Lifetime Profit Modelling of Ageing Systems Utilizing Information about Technical Condition. (Dr.ing. thesis, IMT)
IMT-2008-29	Refsnes, Jon Erling Gorset	Nonlinear Model-Based Control of Slender Body AUVs (PhD Thesis, IMT)
IMT-2008-30	Berntsen, Per Ivar B.	Structural Reliability Based Position Mooring. (PhD-Thesis, IMT)
IMT-2008-31	Ye, Naiquan	Fatigue Assessment of Aluminium Welded Box-stiffener Joints in Ships (Dr.ing. thesis, IMT)
IMT-2008-32	Radan, Damir	Integrated Control of Marine Electrical Power Systems. (PhD-Thesis, IMT)
IMT-2008-33	Thomassen, Paul	Methods for Dynamic Response Analysis and Fatigue Life Estimation of Floating Fish Cages. (Dr.ing. thesis, IMT)
IMT-2008-34	Pákozdi, Csaba	A Smoothed Particle Hydrodynamics Study of Two-dimensional Nonlinear Sloshing in Rectangular Tanks. (Dr.ing.thesis, IMT/ CeSOS)
IMT-2007-35	Grytøyr, Guttorm	A Higher-Order Boundary Element Method and Applications to Marine Hydrodynamics. (Dr.ing.thesis, IMT)
IMT-2008-36	Drummen, Ingo	Experimental and Numerical Investigation of Nonlinear Wave-Induced Load Effects in Containerships considering Hydroelasticity. (PhD thesis, CeSOS)
IMT-2008-37	Skejic, Renato	Maneuvering and Seakeeping of a Singel Ship and of Two Ships in Interaction. (PhD-Thesis, CeSOS)
IMT-2008-38	Harlem, Alf	An Age-Based Replacement Model for Repairable Systems with Attention to High-Speed Marine Diesel Engines. (PhD-Thesis, IMT)
IMT-2008-39	Alsos, Hagbart S.	Ship Grounding. Analysis of Ductile Fracture, Bottom Damage and Hull Girder Response. (PhD-thesis, IMT)
IMT-2008-40	Graczyk, Mateusz	Experimental Investigation of Sloshing Loading and Load Effects in Membrane LNG Tanks Subjected to Random Excitation. (PhD-thesis, CeSOS)
IMT-2008-41	Taghipour, Reza	Efficient Prediction of Dynamic Response for Flexible amd Multi-body Marine Structures. (PhD-

		thesis, CeSOS)
IMT-2008-42	Ruth, Eivind	Propulsion control and thrust allocation on marine vessels. (PhD thesis, CeSOS)
IMT-2008-43	Nystad, Bent Helge	Technical Condition Indexes and Remaining Useful Life of Aggregated Systems. PhD thesis, IMT
IMT-2008-44	Soni, Prashant Kumar	Hydrodynamic Coefficients for Vortex Induced Vibrations of Flexible Beams, PhD thesis, CeSOS
IMT-2009-45	Amlashi, Hadi K.K.	Ultimate Strength and Reliability-based Design of Ship Hulls with Emphasis on Combined Global and Local Loads. PhD Thesis, IMT
IMT-2009-46	Pedersen, Tom Arne	Bond Graph Modelling of Marine Power Systems. PhD Thesis, IMT
IMT-2009-47	Kristiansen, Trygve	Two-Dimensional Numerical and Experimental Studies of Piston-Mode Resonance. PhD-Thesis, CeSOS
IMT-2009-48	Ong, Muk Chen	Applications of a Standard High Reynolds Number Model and a Stochastic Scour Prediction Model for Marine Structures. PhD-thesis, IMT
IMT-2009-49	Hong, Lin	Simplified Analysis and Design of Ships subjected to Collision and Grounding. PhD-thesis, IMT
IMT-2009-50	Koushan, Kamran	Vortex Induced Vibrations of Free Span Pipelines, PhD thesis, IMT
IMT-2009-51	Korsvik, Jarl Eirik	Heuristic Methods for Ship Routing and Scheduling. PhD-thesis, IMT
IMT-2009-52	Lee, Jihoon	Experimental Investigation and Numerical in Analyzing the Ocean Current Displacement of Longlines. Ph.d.-Thesis, IMT.
IMT-2009-53	Vestbøstad, Tone Gran	A Numerical Study of Wave-in-Deck Impact usin a Two-Dimensional Constrained Interpolation Profile Method, Ph.d.thesis, CeSOS.
IMT-2009-54	Bruun, Kristine	Bond Graph Modelling of Fuel Cells for Marine Power Plants. Ph.d.-thesis, IMT
IMT 2009-55	Holstad, Anders	Numerical Investigation of Turbulence in a Sekwed Three-Dimensional Channel Flow, Ph.d.-thesis, IMT.
IMT 2009-56	Ayala-Uraga, Efren	Reliability-Based Assessment of Deteriorating Ship-shaped Offshore Structures, Ph.d.-thesis, IMT
IMT 2009-57	Kong, Xiangjun	A Numerical Study of a Damaged Ship in Beam Sea Waves. Ph.d.-thesis, IMT/CeSOS.
IMT 2010-58	Kristiansen, David	Wave Induced Effects on Floaters of Aquaculture Plants, Ph.d.-thesis, CeSOS.

IMT 2010-59	Ludvigsen, Martin	An ROV-Toolbox for Optical and Acoustic Scientific Seabed Investigation. Ph.d.-thesis IMT.
IMT 2010-60	Hals, Jørgen	Modelling and Phase Control of Wave-Energy Converters. Ph.d.thesis, CeSOS.
IMT 2010- 61	Shu, Zhi	Uncertainty Assessment of Wave Loads and Ultimate Strength of Tankers and Bulk Carriers in a Reliability Framework. Ph.d. Thesis, IMT/ CeSOS
IMT 2010-62	Shao, Yanlin	Numerical Potential-Flow Studies on Weakly-Nonlinear Wave-Body Interactions with/without Small Forward Speed, Ph.d.thesis,CeSOS.
IMT 2010-63	Califano, Andrea	Dynamic Loads on Marine Propellers due to Intermittent Ventilation. Ph.d.thesis, IMT.
IMT 2010-64	El Khoury, George	Numerical Simulations of Massively Separated Turbulent Flows, Ph.d.-thesis, IMT
IMT 2010-65	Seim, Knut Sponheim	Mixing Process in Dense Overflows with Emphasis on the Faroe Bank Channel Overflow. Ph.d.thesis, IMT
IMT 2010-66	Jia, Huirong	Structural Analysis of Intect and Damaged Ships in a Collission Risk Analysis Perspective. Ph.d.thesis CeSoS.
IMT 2010-67	Jiao, Linlin	Wave-Induced Effects on a Pontoon-type Very Large Floating Structures (VLFS). Ph.D.-thesis, CeSOS.
IMT 2010-68	Abrahamsen, Bjørn Christian	Sloshing Induced Tank Roof with Entrapped Air Pocket. Ph.d.thesis, CeSOS.
IMT 2011-69	Karimirad, Madjid	Stochastic Dynamic Response Analysis of Spar-Type Wind Turbines with Catenary or Taut Mooring Systems. Ph.d.-thesis, CeSOS.
IMT - 2011-70	Erlend Meland	Condition Monitoring of Safety Critical Valves. Ph.d.-thesis, IMT.
IMT – 2011-71	Yang, Limin	Stochastic Dynamic System Analysis of Wave Energy Converter with Hydraulic Power Take-Off, with Particular Reference to Wear Damage Analysis, Ph.d. Thesis, CeSOS.
IMT – 2011-72	Visscher, Jan	Application of Particla Image Velocimetry on Turbulent Marine Flows, Ph.d.Thesis, IMT.
IMT – 2011-73	Su, Biao	Numerical Predictions of Global and Local Ice Loads on Ships. Ph.d.Thesis, CeSOS.
IMT – 2011-74	Liu, Zhenhui	Analytical and Numerical Analysis of Iceberg Collision with Ship Structures. Ph.d.Thesis, IMT.
IMT – 2011-75	Aarsæther, Karl Gunnar	Modeling and Analysis of Ship Traffic by Observation and Numerical Simulation. Ph.d.Thesis, IMT.

Imt – 2011-76	Wu, Jie	Hydrodynamic Force Identification from Stochastic Vortex Induced Vibration Experiments with Slender Beams. Ph.d.Thesis, IMT.
Imt – 2011-77	Amini, Hamid	Azimuth Propulsors in Off-design Conditions. Ph.d.Thesis, IMT.
IMT – 2011-78	Nguyen, Tan-Hoi	Toward a System of Real-Time Prediction and Monitoring of Bottom Damage Conditions During Ship Grounding. Ph.d.thesis, IMT.
IMT- 2011-79	Tavakoli, Mohammad T.	Assessment of Oil Spill in Ship Collision and Grounding, Ph.d.thesis, IMT.
IMT- 2011-80	Guo, Bingjie	Numerical and Experimental Investigation of Added Resistance in Waves. Ph.d.Thesis, IMT.
IMT- 2011-81	Chen, Qiaofeng	Ultimate Strength of Aluminium Panels, considering HAZ Effects, IMT
IMT- 2012-82	Kota, Ravikiran S.	Wave Loads on Decks of Offshore Structures in Random Seas, CeSOS.
IMT- 2012-83	Sten, Ronny	Dynamic Simulation of Deep Water Drilling Risers with Heave Compensating System, IMT.
IMT- 2012-84	Berle, Øyvind	Risk and resilience in global maritime supply chains, IMT.
IMT- 2012-85	Fang, Shaoji	Fault Tolerant Position Mooring Control Based on Structural Reliability, CeSOS.
IMT- 2012-86	You, Jikun	Numerical studies on wave forces and moored ship motions in intermediate and shallow water, CeSOS.
IMT- 2012-87	Xiang ,Xu	Maneuvering of two interacting ships in waves, CeSOS
IMT- 2012-88	Dong, Wenbin	Time-domain fatigue response and reliability analysis of offshore wind turbines with emphasis on welded tubular joints and gear components, CeSOS
IMT- 2012-89	Zhu, Suji	Investigation of Wave-Induced Nonlinear Load Effects in Open Ships considering Hull Girder Vibrations in Bending and Torsion, CeSOS
IMT- 2012-90	Zhou, Li	Numerical and Experimental Investigation of Station-keeping in Level Ice, CeSOS
IMT- 2012-91	Ushakov, Sergey	Particulate matter emission characteristics from diesel enignes operating on conventional and alternative marine fuels, IMT
IMT- 2013-1	Yin, Decao	Experimental and Numerical Analysis of Combined In-line and Cross-flow Vortex Induced Vibrations, CeSOS

IMT-2013-2	Kurniawan, Adi	Modelling and geometry optimisation of wave energy converters, CeSOS
IMT-2013-3	Al Ryati, Nabil	Technical condition indexes doe auxiliary marine diesel engines, IMT
IMT-2013-4	Firoozkoohi, Reza	Experimental, numerical and analytical investigation of the effect of screens on sloshing, CeSOS
IMT-2013-5	Ommani, Babak	Potential-Flow Predictions of a Semi-Displacement Vessel Including Applications to Calm Water Broaching, CeSOS
IMT-2013-6	Xing, Yihan	Modelling and analysis of the gearbox in a floating spar-type wind turbine, CeSOS
IMT-7-2013	Balland, Océane	Optimization models for reducing air emissions from ships, IMT
IMT-8-2013	Yang, Dan	Transitional wake flow behind an inclined flat plate-----Computation and analysis, IMT
IMT-9-2013	Abdillah, Suyuthi	Prediction of Extreme Loads and Fatigue Damage for a Ship Hull due to Ice Action, IMT
IMT-10-2013	Ramìrez, Pedro Agustìn Pèrez	Ageing management and life extension of technical systems- Concepts and methods applied to oil and gas facilities, IMT
IMT-11-2013	Chuang, Zhenju	Experimental and Numerical Investigation of Speed Loss due to Seakeeping and Maneuvering. IMT
IMT-12-2013	Etemaddar, Mahmoud	Load and Response Analysis of Wind Turbines under Atmospheric Icing and Controller System Faults with Emphasis on Spar Type Floating Wind Turbines, IMT
IMT-13-2013	Lindstad, Haakon	Strategies and measures for reducing maritime CO2 emissons, IMT
IMT-14-2013	Haris, Sabril	Damage interaction analysis of ship collisions, IMT
IMT-15-2013	Shainee, Mohamed	Conceptual Design, Numerical and Experimental Investigation of a SPM Cage Concept for Offshore Mariculture, IMT
IMT-16-2013	Gansel, Lars	Flow past porous cylinders and effects of biofouling and fish behavior on the flow in and around Atlantic salmon net cages, IMT
IMT-17-2013	Gaspar, Henrique	Handling Aspects of Complexity in Conceptual Ship Design, IMT
IMT-18-2013	Thys, Maxime	Theoretical and Experimental Investigation of a Free Running Fishing Vessel at Small Frequency of Encounter, CeSOS
IMT-19-2013	Aglen, Ida	VIV in Free Spanning Pipelines, CeSOS

IMT-1-2014	Song, An	Theoretical and experimental studies of wave diffraction and radiation loads on a horizontally submerged perforated plate, CeSOS
IMT-2-2014	Rogne, Øyvind Ygre	Numerical and Experimental Investigation of a Hinged 5-body Wave Energy Converter, CeSOS
IMT-3-2014	Dai, Lijuan	Safe and efficient operation and maintenance of offshore wind farms ,IMT
IMT-4-2014	Bachynski, Erin Elizabeth	Design and Dynamic Analysis of Tension Leg Platform Wind Turbines, CeSOS
IMT-5-2014	Wang, Jingbo	Water Entry of Freefall Wedged – Wedge motions and Cavity Dynamics, CeSOS
IMT-6-2014	Kim, Ekaterina	Experimental and numerical studies related to the coupled behavior of ice mass and steel structures during accidental collisions, IMT
IMT-7-2014	Tan, Xiang	Numerical investigation of ship's continuous- mode icebreaking in leverl ice, CeSOS
IMT-8-2014	Muliawan, Made Jaya	Design and Analysis of Combined Floating Wave and Wind Power Facilities, with Emphasis on Extreme Load Effects of the Mooring System, CeSOS
IMT-9-2014	Jiang, Zhiyu	Long-term response analysis of wind turbines with an emphasis on fault and shutdown conditions, IMT
IMT-10-2014	Dukan, Fredrik	ROV Motion Control Systems, IMT
IMT-11-2014	Grimsmo, Nils I.	Dynamic simulations of hydraulic cylinder for heave compensation of deep water drilling risers, IMT
IMT-12-2014	Kvittem, Marit I.	Modelling and response analysis for fatigue design of a semisubmersible wind turbine, CeSOS
IMT-13-2014	Akhtar, Juned	The Effects of Human Fatigue on Risk at Sea, IMT
IMT-14-2014	Syahroni, Nur	Fatigue Assessment of Welded Joints Taking into Account Effects of Residual Stress, IMT
IMT-1-2015	Bøckmann, Eirik	Wave Propulsion of ships, IMT
IMT-2-2015	Wang, Kai	Modelling and dynamic analysis of a semi-submersible floating vertical axis wind turbine, CeSOS
IMT-3-2015	Fredriksen, Arnt Gunvald	A numerical and experimental study of a two-dimensional body with moonpool in waves and current, CeSOS
IMT-4-2015	Jose Patricio Gallardo Canabes	Numerical studies of viscous flow around bluff bodies, IMT

IMT-5-2015	Vegard Longva	Formulation and application of finite element techniques for slender marine structures subjected to contact interactions, IMT
IMT-6-2015	Jacobus De Vaal	Aerodynamic modelling of floating wind turbines, CeSOS
IMT-7-2015	Fachri Nasution	Fatigue Performance of Copper Power Conductors, IMT
IMT-8-2015	Oleh I Karpa	Development of bivariate extreme value distributions for applications in marine technology,CeSOS
IMT-9-2015	Daniel de Almeida Fernandes	An output feedback motion control system for ROVs, AMOS
IMT-10-2015	Bo Zhao	Particle Filter for Fault Diagnosis: Application to Dynamic Positioning Vessel and Underwater Robotics, CeSOS
IMT-11-2015	Wenting Zhu	Impact of emission allocation in maritime transportation, IMT
IMT-12-2015	Amir Rasekhi Nejad	Dynamic Analysis and Design of Gearboxes in Offshore Wind Turbines in a Structural Reliability Perspective, CeSOS
IMT-13-2015	Arturo Jesùs Ortega Malca	Dynamic Response of Flexibles Risers due to Unsteady Slug Flow, CeSOS
IMT-14-2015	Dagfinn Husjord	Guidance and decision-support system for safe navigation of ships operating in close proximity, IMT
IMT-15-2015	Anirban Bhattacharyya	Ducted Propellers: Behaviour in Waves and Scale Effects, IMT
IMT-16-2015	Qin Zhang	Image Processing for Ice Parameter Identification in Ice Management, IMT
IMT-1-2016	Vincentius Rumawas	Human Factors in Ship Design and Operation: An Experiential Learning, IMT
IMT-2-2016	Martin Storheim	Structural response in ship-platform and ship-ice collisions, IMT
IMT-3-2016	Mia Abrahamsen Prsic	Numerical Simulations of the Flow around single and Tandem Circular Cylinders Close to a Plane Wall, IMT
IMT-4-2016	Tufan Arslan	Large-eddy simulations of cross-flow around ship sections, IMT

IMT-5-2016	Pierre Yves-Henry	Parametrisation of aquatic vegetation in hydraulic and coastal research,IMT
IMT-6-2016	Lin Li	Dynamic Analysis of the Instalation of Monopiles for Offshore Wind Turbines, CeSOS
IMT-7-2016	Øivind Kåre Kjerstad	Dynamic Positioning of Marine Vessels in Ice, IMT
IMT-8-2016	Xiaopeng Wu	Numerical Analysis of Anchor Handling and Fish Trawling Operations in a Safety Perspective, CeSOS
IMT-9-2016	Zhengshun Cheng	Integrated Dynamic Analysis of Floating Vertical Axis Wind Turbines, CeSOS
IMT-10-2016	Ling Wan	Experimental and Numerical Study of a Combined Offshore Wind and Wave Energy Converter Concept
IMT-11-2016	Wei Chai	Stochastic dynamic analysis and reliability evaluation of the roll motion for ships in random seas, IMT